

José Alexandre Gouveia Henriques

## BEHAVIOUR OF JOINTS: SIMPLE AND EFFICIENT STEEL-TO-CONCRETE JOINTS

Dissertação apresentada para o grau de Doutor  
na Especialidade de Construção Metálica e Mista

2013



UNIVERSIDADE DE COIMBRA





**FCTUC DEPARTAMENTO DE ENGENHARIA CIVIL**  
FACULDADE DE CIÊNCIAS E TECNOLOGIA  
UNIVERSIDADE DE COIMBRA



Institute for Sustainability and  
Innovation in Structural Engineering



Universidade do Minho  
Escola de Engenharia



Research Fund  
for Coal & Steel

# **Behaviour of joints: Simple and efficient steel-to-concrete joints**

Dissertação científica na especialidade de Construção Metálica e Mista

**Autor**

**José Alexandre Gouveia Henriques**

**Orientador**

**Prof. Doutor Luís Alberto Proença Simões da Silva**

**Co-orientador**

**Prof. Maria Isabel Brito Valente**

**ISISE, Departamento de Engenharia Civil – Universidade de Coimbra**

**Coimbra, 2013**



To my son  
Théo



## RESUMO

A utilização de sistemas estruturais combinando elementos de diferente natureza, como seja paredes de betão armado com vigas e pilares metálicos ou mistos, apresenta-se como uma solução competitiva onde se retira partido da eficiência estrutural de cada tipo de elemento. Este tipo de solução requer ao projectista um conhecimento multidisciplinar onde o principal obstáculo reside na ligação entre os elementos de diferente natureza como são as ligações parede de betão armado com viga metálica/mista. Neste tipo de ligação, a principal problemática reside na ausência de configurações e modelos simplificados para dimensionamento que facilitem a avaliação das suas propriedades e a sua realização.

Ao longo das últimas décadas, o desenvolvimento do método das componentes permitiu demonstrar a eficiência da metodologia na avaliação do comportamento de ligações metálicas e mistas. Consequentemente, a sua extensão a ligações estruturais aço-betão revela-se conveniente e requer a integração de “novas” componentes associadas aos modos de ruptura que despontam no elemento de betão armado. Assim, torna-se necessário a caracterização e inclusão destas componentes nos modelos globais de avaliação do comportamento da ligação.

Foi com o intuito de responder a esta problemática que se desenrolou um projecto Europeu de investigação (RFCS). Neste, estudaram-se várias configurações de forma a responder às diferentes exigências estruturais. Do envolvimento do autor no projecto, desenvolveu-se a presente tese. O seu principal objectivo é a abordagem transversal às ligações estruturais aço-betão, utilizando uma configuração desenvolvida no projecto. Na versão “mais completa”, a configuração seleccionada permite realizar uma ligação entre viga mista e parede de betão armado, conferindo continuidade parcial ou total (ligação semi-continua/continua). Contudo, a flexibilidade da configuração permite a adaptação para soluções com diferentes exigências estruturais, ou seja, ligação rotulada.

Na presente tese efectua-se uma abordagem sequencial, evoluindo da configuração mais simples para a mais completa, com caracterização numérica e analítica de componentes e ligações. A validação experimental é feita sempre que possível com a contribuição da

literatura e dos resultados da campanha experimental do referido projecto. Assim, propõe-se modelos numéricos e analíticos que permitem avaliar o comportamento de uma ligação entre viga mista e parede de betão armado independentemente da idealização estrutural pretendida: rotulada, semi-continua ou continua.

Por fim, é efectuado um estudo simplificado ao nível do comportamento estrutural global onde se pretende investigar as exigências estruturais a que estão submetidas as ligações estudadas. A análise considera um conjunto de pórticos planos (solução mista aço-betão) onde se incorpora o comportamento das ligações e se extraem os requisitos para diferentes estados limites.

## **Palavras-Chave**

Ligações estruturais aço-betão, Comportamento das ligações, Método das componentes, Modelação numérica, Curva momento-rotação



## ABSTRACT

The use of the structural systems combining members of different nature, such as reinforced concrete walls with steel/composite beams and columns, presents a competitive solution benefiting from the structural efficiency of each type of member. This type of solution requires to the designer multidisciplinary knowledge where the main obstacle lies in the joints between members of different nature, as are the reinforced concrete wall to steel/composite beam joints. In such joints, the main problem is the lack of solutions for easy execution and simplified models for evaluation of their properties.

Over the past decades, the development of the component method has demonstrated the effectiveness of the methodology in assessing the behaviour of steel and composite joints. Consequently, its extension to structural steel-concrete joints is convenient and requires the integration of "new" components associated with the failures modes that develop in the reinforced concrete member. Thus, it becomes necessary to characterize and to include these components in global models for evaluation of the joint behaviour.

Aiming at the study of steel-to-concrete joints, the RFCS project entitled "New market chances for steel structures by innovative fastening solutions" was developed. In the project, three joint configurations were investigated for different structural requirements. The present thesis is also the outcome of the author's involvement in this project. Its main objective is a transversal approach to structural steel-to-concrete joints using a configuration developed within the referred project. In its "complete" version, the joint configuration provides a semi-continuous/continuous solution to connect a composite beam to a reinforced concrete wall. Though, the adaptability of the configuration allows its modification to perform under different structural requirements, as pinned joint.

In this thesis a sequential approach is carried out, evolving from the simplest configuration to the "most complete", with numerical and analytical characterization of the components, connections and joints. The experimental validation is performed whenever possible with the contribution of the results available in the literature and produced in the experimental campaign of the referred project. Thus, analytical and numerical models are proposed for characterization of the behaviour of joints between composite beam and reinforced

concrete wall independently of the structural idealization: pinned, semi-continuous and continuous.

Finally, at the structural level, a simplified study is performed to investigate the performance requirements of the steel-to-concrete joints. The analysis considers the structural calculation of three portal frames (mixed steel-concrete solution) which incorporate the behaviour of joints. The structural requirements for the different limit states are extracted and compared with the properties of the approached joints.

**Keywords:**

Structural steel-to-concrete joints, Behaviour of joints, Component method, Numerical modelling, Moment-rotation curve

## ACKNOWLEDGMENTS

The present thesis is the outcome of several years of research activity at the University of Coimbra involving the contribution of many persons with whom I interacted. To all I would like to express my sincere gratitude.

First of all, I would like to thank to Professor Luís Simões da Silva, the promoter of this thesis, for his guidance, support and advices. He gave me conditions to make possible the achievement of this work, offering me the opportunity to participate actively in a RFCS project, an enriching experience at a high European level.

My gratitude goes also to Professor Isabel Valente who, as co-supervisor, dedicated part of her time to analyse and discuss the present work. Her encouragement and critique were valuable.

Then, my acknowledgements go to all the colleagues of the RFCS research project “InFaSo” that through several project meetings shared their knowledge and experiences. But mainly, special thanks to Ana Ozbolt and Professor Ulrike Kuhlmann, for the experimental data provided, for receiving me in Stuttgart and for the many discussions during my stay there.

A word of gratitude to all colleagues of the research group of “Mecânica Estrutural”, at the University of Coimbra, that in one way or another had some contribution to this work. Though, a special word goes to: i) Professor Rui Simões, for his availability to answer my doubts and to share his experience; ii) André Tenchini and Rui Matos, who shared with me the office, where in many discussions my doubts were also theirs; iii) Rui Saldanha and Sara Gomes, colleagues from the “concrete” group, who helped me interpreting the complexity of the concrete behaviour.

A special thanks to my family and friends for their encouragement and for understanding my frequent absence during many weekends of work. Finally, my strong gratitude goes to Cécile, my wife and great friend in life, who encouraged me when I was demotivated, who

always believed this work would come to an end, and for being at my side having her family and her country distant. Merci.

# TABLE OF CONTENTS

RESUMO .....	i
ABSTRACT .....	iii
ACKNOWLEDGMENTS .....	v
TABLE OF CONTENTS .....	vii
NOTATIONS .....	xiii

<b>I. General introduction.....</b>	<b>I.1</b>
I.1 Introduction .....	I.3
I.2 Steel-to-concrete joints and the RFCS research project <i>InFaSo</i> .....	I.6
I.2.1 Definition of steel-to-concrete joints.....	I.6
I.2.2 Overview of the European RFCS research project <i>InFaSo</i> .....	I.6
I.3 Objectives and scope .....	I.10
I.4 Thesis outline .....	I.11
<b>References .....</b>	<b>I.13</b>

<b>II. Study of the behaviour of steel-to-concrete beam-to-wall joints .....</b>	<b>II.1</b>
II.1 Introduction .....	II.3
II.2 Literature review and background .....	II.11
II.2.1 Analysis and modelling of joints.....	II.11
II.2.1.1 Steel and composite joints .....	II.11
II.2.1.2 Reinforced concrete joints.....	II.16
II.2.1.3 Steel-to-concrete joints .....	II.18
II.2.2 Characterization of the joint components.....	II.23
II.2.2.1 Relevant steel/composite components .....	II.23
II.2.2.2 “New” components related to anchorage in concrete .....	II.29
II.2.2.2.1 Identification of the “new” components.....	II.29
II.2.2.2.2 Behaviour of headed anchors in tension.....	II.31
II.2.2.2.3 Behaviour of headed anchors in shear .....	II.39
II.2.2.2.4 Behaviour of headed anchors in combined tension and shear.....	II.40

II.2.2.3	Components in a strut-and-tie model.....	II.42
II.2.3	Recent developments within the RFCS research project <i>InFaSo</i> .....	II.44
II.2.3.1	Experimental and analytical characterization of the “new” components .....	II.44
II.2.3.2	Experimental and analytical characterization of anchor plate connections ...	II.48
II.2.3.3	Experimental characterization of the composite beam to reinforced concrete wall joint .....	II.51
II.3	Anchor plate connection.....	II.56
II.3.1	Anchor plate subject to compression .....	II.56
II.3.1.1	Introduction.....	II.56
II.3.1.2	Numerical modelling.....	II.57
II.3.1.2.1	Finite element program and modelling tools .....	II.57
II.3.1.2.2	Validation of numerical tool.....	II.61
II.3.1.2.3	Numerical modelling of anchor plate to pure compression .....	II.64
II.3.1.3	Analytical modelling.....	II.72
II.3.1.3.1	Sophisticated modelling.....	II.72
II.3.1.3.2	Simplified modelling: Adaptation of the T-stub in compression.....	II.80
II.3.1.4	Validation and calibration of the analytical models .....	II.89
II.3.1.4.1	Reference case.....	II.89
II.3.1.4.2	Parametric variation .....	II.91
II.3.2	Anchor plate subject to shear.....	II.95
II.3.2.1	Introduction.....	II.95
II.3.2.2	Numerical analysis .....	II.96
II.3.2.2.1	Numerical tools .....	II.96
II.3.2.2.2	Validation of the numerical model for anchor plate subject to shear .....	II.98
II.3.2.2.3	Discussion on the numerical simulations of the anchor plate subject to shear .....	II.102
II.3.2.3	Analytical model to characterize the connection behaviour.....	II.105
II.3.2.3.1	Components activated in the connection .....	II.105
II.3.2.3.2	Component based analytical model.....	II.108
II.3.2.3.3	Assessment of the accuracy of the analytical model .....	II.110

II.3.3	Anchor plate subject to combined shear and compression .....	II.111
II.3.3.1	Introduction.....	II.111
II.3.3.2	Numerical analysis of the anchor plate under combined shear and compression .....	II.111
II.4	Joint Link.....	II.114
II.4.1	Introduction .....	II.114
II.4.2	Numerical modelling basis of analytical modelling.....	II.115
II.4.2.1	Description of the numerical model.....	II.115
II.4.2.1.1	General.....	II.115
II.4.2.1.2	Reinforced concrete numerical modelling.....	II.116
II.4.2.1.3	Validation of the reinforcement-concrete bond-slip modelling.....	II.118
II.4.2.2	Elastic analysis of the joint link .....	II.119
II.4.2.2.1	Wall response to joint loading.....	II.119
II.4.2.2.2	Identification of load path and critical regions .....	II.122
II.4.2.3	Non-linear analysis of the Joint Link.....	II.125
II.4.2.3.1	Introduction .....	II.125
II.4.2.3.2	Reference case.....	II.126
II.4.2.3.3	Parametric variations.....	II.130
II.4.3	Analytical modelling of the Joint Link.....	II.133
II.4.3.1	Idealized model.....	II.133
II.4.3.1.1	Conception and principles .....	II.133
II.4.3.1.2	Characterization of the components and determination of Joint Link properties .....	II.135
II.4.3.2	Application of the analytical model.....	II.140
II.5	Moment-resisting composite beam to reinforced concrete wall joint.....	II.142
II.5.1	Introduction .....	II.142
II.5.2	Numerical model.....	II.142
II.5.2.1	Description of the finite element model .....	II.142
II.5.2.1.1	Identification of the joint components to be simulated.....	II.142
II.5.2.1.2	Description of the numerical tools.....	II.143
II.5.2.1.3	Benchmark example for calibration of the joint components modelling .....	II.144

II.5.2.1.4 Description of the numerical model developed to simulate the composite beam to reinforced concrete wall joint.....	II.155
II.5.2.2 Validation and calibration of the finite element model for the composite beam to reinforced concrete wall joint.....	II.160
II.5.2.2.1 Validation through comparison of results in terms of moment-rotation curves (M- $\Phi$ ) .....	II.160
II.5.2.2.2 Assessment of the quality of the numerical model for experimental parameters other than the M- $\Phi$ curve.....	II.162
II.5.2.3 Further analysis of the joint through exploitation of the finite element model .....	II.167
II.5.2.3.1 Participation of joint components .....	II.167
II.5.2.3.2 Load on shear connectors of the composite beam and position of the 1st shear connector.....	II.168
II.5.2.3.3 Shear load path .....	II.169
II.5.2.4 Sensitivity of the joint behaviour to some parametric variations .....	II.170
II.5.2.4.1 Parametric study .....	II.170
II.5.2.4.2 Discussion and analysis on the results .....	II.173
II.5.2.4.2.1 Steel class of the longitudinal reinforcement bars.....	II.173
II.5.2.4.2.2 Thickness of the steel bracket .....	II.173
II.5.2.4.2.3 Thickness of the anchor plate .....	II.174
II.5.2.4.2.4 Joint configuration variant: two rows of longitudinal reinforcement bars .....	II.175
II.5.3 Analytical component base model.....	II.177
II.5.3.1 Joint Model .....	II.177
II.5.3.2 Characterization of the activated components.....	II.178
II.5.3.2.1 Longitudinal steel reinforcement in the slab .....	II.178
II.5.3.2.2 Slip of the composite beam .....	II.181
II.5.3.2.3 Other joint components.....	II.184
II.5.3.3 Joint assembly and determination of the joint properties.....	II.185
II.5.3.4 Validation of the analytical model.....	II.188
II.6 Concluding remarks .....	II.192
<b>References .....</b>	<b>II.196</b>



<b>III. Behaviour of mixed steel-concrete structures: influence of the joint modelling and requirements to steel-to-concrete joints .....</b>	<b>III.1</b>
III.1 Introduction.....	III.3
III.2 Background.....	III.4
III.2.1 Structural analysis including the joint behaviour.....	III.4
III.2.2 Definition of case studies .....	III.8
III.2.2.1 Description of the reference building structures .....	III.8
III.2.2.2 Performed calculations .....	III.11
III.2.2.3 Description of the structural models .....	III.12
III.2.2.3.1 Geometric and mechanical properties of members .....	III.12
III.2.2.3.2 Joint properties .....	III.17
III.2.2.3.3 Loading conditions.....	III.19
III.2.2.3.4 Sub-structures finite element models .....	III.19
III.3 Analysis and discussion of results .....	III.21
III.3.1 Calculation results .....	III.21
III.3.1.1 Load combination for Service Limit State (SLS) .....	III.21
III.3.1.2 Load combination for Ultimate Limit State (ULS).....	III.25
III.3.1.3 Load combination for Accidental Action: exceptional event of loss of a column .....	III.26
III.4 Comparative analysis with the studied steel-to-concrete joints .....	III.32
III.4.1 General Considerations.....	III.32
III.4.2 Comparison and discussion of results .....	III.33
III.4.3 Improvement of the joints performance.....	III.34
III.5 Concluding remarks.....	III.36
<b>References .....</b>	<b>III.37</b>
<b>IV. General conclusions and perspectives.....</b>	<b>IV.1</b>
IV.1 Conclusions .....	IV.3
IV.2 Open questions and further research interests .....	IV.8
IV.3 Personal contributions.....	IV.11
<b>References .....</b>	<b>IV.14</b>



# NOTATIONS

## Lowercases

$a$	Distance of the first shear connector to joint face
$a_a$	Shoulder width
$b$	Width of the equivalent rectangular cross section
$b_{ap}$	Anchor plate width
$b_c$	Concrete block width
$b_{cp}$	Contact plate width
$b_{eff}$	Effective width of the equivalent T-Stub in compression flange
$b_{eff,rb}$	Effective width of the concrete around steel reinforcement bars
$b_{rb}$	Distance between the outer longitudinal reinforcement bars
$c$	Bearing width of the equivalent rigid anchor plate
$c_1$	Anchor edge distance in direction of loading
$c_{cr,N}$	Minimum anchor edge distance to avoid influence of edges on concrete cone resistance
$d$	Displacement
$d_a$	Diameter of the anchor shaft
$d_{ah}$	Diameter of the anchor head
$d_{h,C-T}$	Horizontal component of the deformation between compression and tension components
$d_{h,JL}$	Horizontal component of the deformation of the Joint Link
$d_{h,top,limit}$	Maximum top floor displacement
$d_i^{MP1-MP2}$	Deformation between measuring points 1 and 2 at load increment $i$
$d_i^{strut}$	Deformation of the concrete strut at load increment $i$
$d_{rb}$	Diameter of the steel reinforcement bar
$d_s$	Distance between the longitudinal reinforcing bars and the centroid of the steel beam section
$d_{shr}$	Diameter of the steel hanger reinforcement bars
$e_{1,l}$	End distance on the left hand side
$e_{1,r}$	End distance on the right hand side

$e_2$	Edge distance
$e_N$	Eccentricity between the anchorage loading and the centroid of the anchorage
$e_V$	Eccentricity of the shear load to the centroid of the anchor plate
$f_{b0}/f_{c0}$	Ratio of initial equibiaxial compressive yield stress to initial compressive yield stress for concrete damage plasticity model (Abaqus)
$f_{bm}$	Mean bond strength
$f_{c,200}$	Concrete compression strength measured on cube with 200mm edge length
$f_{cd}$	Design concrete cylinder compressive strength
$f_{ck}$	Characteristic concrete cylinder compressive strength
$f_{ck,cub}$	Characteristic concrete cube compressive strength
$f_{cm}$	Mean concrete compressive strength
$f_{ctm}$	Mean concrete tensile strength
$f_{ctk}$	Characteristic concrete tensile strength
$f_{Ed}$	Design stress
$f_j$	Amplified concrete compressive bearing strength due to confinement effect
$f_y$	Yield strength
$f_{yd}$	Design yield strength
$f_{yk}$	Characteristic yield strength
$f_{sry}$	Yield strength of the steel reinforcement bar
$f_{srym}$	Mean yield strength of the steel reinforcement bar
$f_u$	Ultimate strength
$f_{uk}$	Characteristic ultimate strength
$h$	Depth of the column
$h$	Depth of the equivalent cross-section
$h_b$	Height of the steel beam cross-section
$h_c$	Thickness of the concrete flange or block
$h_{c,eq}$	Equivalent concrete block height
$h_{ef}$	Embedment depth
$h_r, h_s$	Distance between of the bolt row $r$ to the centre of compression
$h_{sc}$	Height of the shear connector including the head
$h_{slab}$	Slab thickness

$k$	Tension-shear interaction factor for anchorage under combined loading
$k_1$	Embedment depth factor for evaluation of the pry-out resistance of an anchorage
$k_a$	Form factor at porous edge sections
$k_a$	Anchorage stiffness
$k_A$	Cross-section depending form factor
$k_{ab}$	Ratio of second stress invariant on the tensile meridian for concrete damage plasticity model (Abaqus)
$k_c$	Concrete cone component softening stiffness
$k_{eq,c}$	Equivalent stiffness coefficient of the compression components
$k_{eq,t}$	Equivalent stiffness coefficient of the tension components
$k_i$	Stiffness coefficient of component $i$
$k_{nn}, k_{ss}, k_{tt}$	Stiffness coefficients for normal and local shear directions in the traction-separation model (Abaqus)
$k_{RSi}$	Stiffness of the rotational spring $i$
$k_{SC}$	Stiffness of a shear connector
$k_{slip}$	Reduction factor of the stiffness coefficient of the longitudinal reinforcement
$k_{sr}$	Longitudinal reinforcement stiffness coefficient
$k_{T-Stub}$	Stiffness coefficient of the equivalent T-Stub in compression
$k_{zi}$	Stiffness of the extensional spring $i$
$l$	Length of the beam in hogging bending adjacent to the joint
$l_0^{MP1-MP2}$	Initial distance between measuring points 1 and 2
$l_i^{MP1-MP2}$	Distance between measuring points 1 and 2 at load increment $i$
$l_i^{strut}$	Length of the concrete strut at load increment $i$
$l_1$	Anchorage length of the hanger reinforcement
$l_{ap}$	Length of the anchor plate
$l_{as}$	Length of the anchor shaft
$l_{b,net}$	Anchorage length of a reinforcement bar beyond the node in a strut-and-tie
$l_c$	Length of the concrete block
$l_{cp}$	Length of the contact plate
$l_{eff}$	Effective length of the equivalent T-Stub in compression flange
$l_{sb}$	Length of the steel bracket

$m$	Pressing relation factor
$n_s$	Number of legs of the hanger reinforcement within the concrete cone
$p_1$	Anchors spacing in the direction of load transfer
$p_k$	Critical bearing strength of the concrete over the anchor head
$r$	Reinforcement bar bend radius
$s, s_1$	Anchors spacing
$s_0$	Spacing between the contact plate and steel bracket
$s_{cr,N}$	Minimum anchors spacing to form isolated concrete cones in an anchorage
$s_{rb}$	Spacing between steel reinforcement bars within the effective slab width
$t_{ap}$	Anchor plate thickness
$t_{cp}$	Contact plate thickness
$t_f, t_{fb}$	Thickness of the flange
$t_n, t_s, t_t$	Nominal tractions in the normal and local shear directions for the traction-separation model (Abaqus)
$t_{sb}$	Thickness of the steel bracket
$t_w$	Web thickness
$u$	Displacement
$u_x, u_y, u_z$	Spatial displacement components
$v$	vertical displacement measured at the top of the failing column
$w_{crack}$	Concrete crack “opening”
$x$	Distance to origin (position of springs)
$x$	Distance to neutral axis
$x_c$	Dimension of the component concrete block in compression
$y_i^{MP1}, y_i^{MP2}$	Coordinate of the measuring points in Y axis at load increment $i$
$z$	Lever arm of the tension bolt row
$z_0$	Vertical distance between the uncracked concrete flange and the uncracked unreinforced composite section
$z_i^{MP1}, z_i^{MP2}$	Coordinate of the measuring points in Z axis at load increment $i$
$z_{V,bear}$	Position of the bearing component of the shear resistance
$z_{C-T}$	Lever arm between compression and tension forces
$z_m$	Distance between the resultant tensile force acting on the anchorage and centroid of the compressive reaction on the anchor plate

## Uppercases

$A$	Cross-section area
$A_{c,N}^0$	Concrete cone projected area of an anchor
$A_{c,i}$	Equivalent area of concrete-plate contact
$A_{c,N}$	Concrete cone projected area of an anchorage
$A_{comp}$	Area of concrete in compression (component concrete block in compression under the anchor plate)
$A_{cp}$	Cross-section area of the contact plate in the interface plane with the beam end-plate
$A_{eff}$	Effective area of the anchor plate in compression
$A_{eff,cp}$	Effective area of the steel contact plate
$A_{eff,S}$	Effective are of the anchor plate in compression for stiffness calculation
$A_h$	Surface area of the anchor head in bearing against the concrete
$A_{pl-con}$	Area of the plate-concrete contact surface
$A_s$	Anchor shaft cross-section area
$A_{sb-ap}$	Cross-section area of the steel bracket in the interface with anchor plate
$A_{shr}$	Cross-section area of one leg of reinforcement within the concrete cone
$A_{sr}$	Cross-section area of longitudinal reinforcement within the effective width of the slab
$A_{N1}$	Cross-section area of the diagonal concrete strut at node N1
$A_{N2}$	Cross-section area of the diagonal concrete strut at node N2
$C$	Compression force
$C_1$	Headed anchors factor for pull-out resistance
$E$	Elasticity modulus (Young's modulus)
$E_c$	Concrete elasticity modulus (Young's modulus)
$E_{cm}$	Secant modulus of elasticity of the concrete
$E_s$	Steel elasticity modulus (Young's modulus)
$E_{sr}$	Steel reinforcement bar elasticity modulus (Young's modulus)
$E_{st}$	Strain hardening modulus
$F$	Force
$F_a$	Anchorage resistance
$F_c$	Compression component of a bending moment load

$F_{cp}$	Resistance of contact plate component
$F_{c,fb,Rd}$	Resistance of the beam flange and web in compression component
$F_{c,i}$	Compression force in compression strut
$F_{c,Rd}$	Basic component design resistance
$F_{eq,c}$	Equivalent resistance of the compression row
$F_{eq,t}$	Equivalent resistance of the tension row
$F_i$	Force on component i
$F_{r,N1}$	Resistance of the concrete strut at node N1
$F_{r,N2}$	Resistance of the concrete strut at node N2
$F_{slip}$	Resistance of the slip of the composite beam component
$F_{sr}$	Resistance of the steel longitudinal reinforcement bar in tension component
$F_{sru}$	Reinforcement bar force at ultimate stress
$F_{sry}$	Reinforcement bar force at yield stress
$F_t$	Tension component of a bending moment load
$F_{t,i}$	Tension force in tension tie
$F_{tr,Rd}$	Design tension resistance of bolt row r
$F_{C-T}$	Binary force
$F_{C-T,JL}, F_{JL}$	Resistance of the Joint Link component in the direction binary force generated by the bending moment applied to the joint
$F_{SC}$	Load on shear connectors
$G_f$	Fracture energy
$I$	Second moment area of the cross-section
$I_a$	Second moment area of the steel beam cross-section
$I_b$	Second moment area of the beam cross-section
$I_s$	Second moment area of the stub representing the panel in shear
$I_L$	Second moment area of the stub representing the connection
$K_c$	Homogenization of composite section factor
$K_{s,ini}$	Steel anchor initial stiffness
$K_{SC}$	Stiffness related to the shear connection
$L_b$	Beam length
$L_{bond-slip}$	Length of interaction surface where the bond-slip model is considered



$L_t$	Length of the reinforcement from joint face to first crack in the concrete slab (“introduction” or “transmission” length)
$M$	Bending moment
$M_{ap,R}$	Anchor plate bending moment resistance
$M_{b,pl,Rd}$	Beam plastic bending moment resistance
$M_{cb,max}$	Maximum bending moment capacity of the composite beam cross-section
$M_{c,pl,Rd}$	Column plastic bending moment resistance
$M_{Fc}$	Bending moment at the centroid of the anchor plate due to the compression component of a bending moment load
$M_{ext}$	External bending moment
$M_j$	Joint bending moment
$M_{j,max}$	Joint maximum bending moment
$M_{j,Ed}$	Joint design bending moment
$M_{j,Rd}$	Joint bending moment resistance
$M_{j,u}$	Joint ultimate bending moment
$M_{int}$	Internal bending moment
$M_{pl}$	Plastic bending moment
$M_{RSi}$	Bending moment at rotation spring $i$
$M_T$	Torsion moment
$M_V$	Bending moment at the centroid of the anchor plate generated by a shear load with eccentricity
$M_{V,small\ ecc.}$	Bending moment at the centroid of the anchor plate generated by a shear load with high eccentricity
$M_{V,small\ ecc.}$	Bending moment at the centroid of the anchor plate generated by a shear load with small eccentricity
$M_y$	Bending moment corresponding to the first fibers to yield within the cross-section
$N$	Axial force
$N$	Number of shear connectors distributed over the length $l$
$N_{Ed}$	Design axial load
$N_f$	Number of shear connectors required to have full interaction
$N_j$	Axial load in the joint
$N_{j,tens}$	Axial tension load in the joint

$N_{p,k}$	Pull-out characteristic resistance of an anchorage
$N_{Rd}$	Design tension resistance
$N_{s,k}$	Characteristic tension resistance steel anchor
$N_{shr,k}$	Characteristic tension resistance of the steel hanger reinforcement bars
$N_u$	Ultimate tension resistance
$N_{u,1}$	Ultimate resistance of an reinforced anchorage with yielding of the hanger reinforcement
$N_{u,2}$	Ultimate resistance of an reinforced anchorage with anchorage failure of the hanger reinforcement
$N_{u,c}$	Ultimate concrete cone resistance
$N_{ub,k}$	Characteristic anchorage resistance of one leg of hanger reinforcement
$N_{uc,k}$	Concrete cone characteristic resistance of an anchorage
$N_{us,k}$	Steel anchor ultimate characteristic resistance
$N_{uc,k}^0$	Concrete cone resistance of an isolated anchor
$N_{u,max}$	Ultimate resistance of reinforced anchorage (modified concrete cone)
$P_{Rk}$	Characteristic value of the shear resistance of a single connector
$R_{d,c}$	Design resistance of concrete block in compression
$R_v$	Vertical reaction force
$RS_i$	Rotational spring i
$S_1, S_2, S_3$	Characteristic slip values for the bond-slip model
$S_{ap,c,ini}$	Anchor plate in compression initial stiffness
$S_c$	Rotational spring representing the joint modelling
$S_{c,ini}$	Basic component initial stiffness
$S_j$	Joint rotational stiffness
$S_{j,ini}$	Joint initial rotational stiffness
$S_{r,L}$	L-springs representing the connecting zone in the joint modelling
$S_{r,S}$	S-springs representing the panel zone in the joint modelling
$T$	Tension force
$T_1$	Tension force on anchor 1
$T_2$	Tension force on anchor 2
$V$	Shear force
$V_1$	Shear force on anchor 1

$V_2$	Shear force on anchor 2
$V_3$	Shear force on anchor 3
$V_4$	Shear force on anchor 4
$V_{ap,R}$	Shear resistance of the anchor plate
$V_{bear}$	Bearing component of the shear resistance
$V_{bottom}$	Shear load transferred by the anchor plate
$V_f$	Friction component of the shear resistance
$V_{Ed}$	Design shear load
$V_j$	Shear load in the joint
$V_{Rd}$	Design shear resistance
$V_u$	Ultimate shear resistance
$V_{ucp,K}$	Characteristic pry-out resistance of an anchorage
$V_{us,K}$	Characteristic shear resistance of a steel anchor

### Lowercase Greek letters

$\alpha$	Angle between load applied to an anchorage and its shear component
$\alpha_a$	Factor to take into account the influence of the hanger reinforcement bar hook
$\alpha_i$	Rotation at degree of freedom $i$
$\alpha_p$	Experimental parameter for the pull-out failure deformation model
$\alpha_{sV}$	Experimental coefficient that traduces the ratio between the tensile and shear strength of the anchor
$\alpha_s$	Experimental parameter for the hanger reinforcement deformation model
$\beta$	Transformation parameter
$\beta_j$	Foundation joint material coefficient
$\beta_t$	Factor that takes into account the short-term loading
$\delta_a$	Anchorage deformation
$\delta_c$	Deformation of the concrete cone component
$\delta_{c+s}$	Deformation of the assembly concrete cone with steel hanger reinforcement
$\delta_i$	Elongation of spring $i$
$\delta_{max}$	Maximum beam deflection

$\delta_n, \delta_s, \delta_t$	Displacement related to the nominal strains in the traction-separation model (Abaqus)
$\delta_{p1}, \delta_{p2}, \delta_{p3}$	Deformation of the pull-out failure component
$\delta_s$	Deformation of the steel hanger reinforcement bars component
$\delta_{s,y}$	Deformation of the steel hanger reinforcement bars component at yield strength
$\delta_u$	Ultimate deformation
$\delta_{u,1SC}$	Ultimate deformation of the first shear connector
$\delta_{u,slip}$	Ultimate slip
$\delta_u^{ss,tt}$	Slip at ultimate bond strength for bond-slip model
$\delta_{ub}$	Deformation of the hanger reinforcement at anchorage failure of the hanger reinforcement
$\delta_{\tau,max}^{ss,tt}$	Slip at maximum bond strength for bond-slip model
$\epsilon$	Strain
$\epsilon_1$	Strain on anchor 1
$\epsilon_2$	Strain on anchor 2
$\epsilon_{ab}$	Flow potential eccentricity for concrete damage plasticity model (Abaqus)
$\epsilon_c$	Concrete strain at concrete compressive strength
$\epsilon_{c2}$	Concrete strain at reaching the maximum compressive strength
$\epsilon_{cu}$	Ultimate compressive strain in the concrete
$\epsilon_{cu2}$	Ultimate compressive strain in the concrete
$\epsilon_n, \epsilon_s, \epsilon_t$	Nominal strains in the traction-separation model (Abaqus)
$\epsilon_{sr}$	Steel reinforcement bar strain
$\epsilon_{sr1}$	Strain in the reinforcement at the onset of concrete cracking
$\epsilon_{srmu}$	Ultimate strain of the reinforcement bar embedded in concrete
$\epsilon_{sru}$	Ultimate strain of the reinforcement bar
$\epsilon_{srmy}$	Yield strain of the steel reinforcement bar embedded in concrete
$\epsilon_{sry}$	Yield strain of the steel reinforcement bar
$\epsilon_{st}$	Strain at the beginning of the strain hardening range (yield plateau limit)
$\epsilon_{true}$	Logarithmic strain
$\epsilon_u$	Steel ultimate strain
$\epsilon_y$	Yield strain

$\eta$	Joint stiffness modification coefficient
$\theta$	Angle between elements of a strut and tie model
$\lambda$	Load factor
$\mu$	Joint stiffness ratio
$\mu_{ab}$	Viscosity parameter for concrete damage plasticity model (Abaqus)
$\mu_f$	Friction coefficient
$\upsilon$	Factor for admissible stress in a concrete strut
$\xi$	Parameter related to deformation of the shear connection
$\rho$	Percentage of reinforcement in reinforced concrete slab
$\sigma$	Stress
$\sigma_{adm}$	Admissible stress
$\sigma_{cp,n}$	Stresses in the contact plate in direction of the thickness
$\sigma_{sr1}$	Reinforcement stress
$\sigma_{sr1}$	Reinforcement stress at the onset of concrete cracking
$\sigma_{sm}$	Reinforcement stress at the formation of last concrete crack
$\sigma_{true}$	True stress
$\sigma_{AP,VonMises}$	Von Mises stresses on anchor plate
$\sigma_{Wall, Min Prinp}$	Minimum principal stresses on the concrete wall
$\tau$	Bond stress
$\tau_f$	Ultimate bond strength
$\tau_{max}$	Maximum bond strength
$\tau_{sb}$	Tangential stresses in the steel-bracket
$\tau_{sm}$	Average bond stress
$\psi_{ab}$	Dilatation angle for concrete damage plasticity model (Abaqus)

### Uppercase Greek letters

$\Delta$	Deformation
$\Delta_{c,u}$	Basic component ultimate deformation
$\Delta d_{wall-slab}$	Slab-wall separation
$\Delta_{eq,t}$	Equivalent deformation of the tension components

$\Delta_{eq,c}$	Equivalent deformation of the compression components
$\Delta_{jL}$	Deformation of the joint link component
$\Delta l$	Elongation
$\Delta_{slip}$	Deformation of the slip of composite beam component
$\Delta_{sru}$	Deformation of reinforcement bar at ultimate strain
$\Delta_{sry}$	Deformation of reinforcement bar at yield strain
$\Delta\varepsilon_{sr}$	Reinforcement strain increase within the concrete crack
$\Phi$	Rotation
$\Phi$	Reinforcement bar diameter
$\Phi_{ap}$	Anchor plate rotation
$\Phi_j$	Joint rotation
$\Phi_{j,Mmax}$	Joint rotation at maximum joint bending moment
$\Phi_{j,u}$	Joint ultimate rotation
$\Phi_r$	Diameter of the longitudinal reinforcement bars
$\Psi_{ec,N}$	Factor to take into account the influence of anchorage loading eccentricity on the concrete cone resistance
$\Psi_{m,N}$	Factor to take into account the influence of a compressive region near the anchorage on the concrete cone resistance
$\Psi_{re,N}$	Factor to take into account the influence of closed space reinforcement near the anchorage on the concrete cone resistance
$\Psi_{s,N}$	Factor to take into account the influence of a close edge on the concrete cone resistance
$\Psi_{supp}$	Factor to take into account the influence of the hanger reinforcement on the concrete cone resistance
$\Psi_{ucr,N}$	Factor to take into account the influence of the concrete condition (cracked or un-cracked) on the concrete cone resistance

# *I. General introduction*





## I.1 Introduction

In the past, there were separate views in construction and engineers generally had to choose between concrete and steel structures. Composite structures have opened the way for more efficient solutions through judicious combinations of both materials. Consequently, the use of composite members, such as beams, slabs and columns, has become a common practice. In such members, the main function of concrete, besides its natural application in slabs, is to improve the performance of these structural elements in compression. Thus, composite members are inevitably related to steel design, and a separation remains between reinforced concrete and steel/composite structures. However, in many cases the use of mixed steel-concrete structures is the most competitive solution. The concept of mixed structure is based on using different materials for different members according to their best structural performance. Clear examples of this are reinforced concrete (RC) for foundations staircases/lift cores; and steel/composite for columns, slabs or beams. This type of construction presents significant advantages, with structural and economic benefits, giving more efficient solutions to employ in office, commercial and car parks multi-storey buildings when compared with more traditional steel or concrete solutions. Optimized solutions can be obtained in terms of structural performance, weight of the structure, erection time and therefore cost. Typical examples of the efficiency of this practice are the Millennium Tower in Vienna (Stahlbau, 1999) and many multi-storey buildings constructed in the U.K.

The evolution of standards for construction has followed the same separate mentality. Reinforced concrete structures and steel-concrete composite structures are analysed considering separate design codes. When dealing with design of mixed structures, engineers are faced with two distinct realities: design of members and design of joints. If for the first, the European codes (*EC2*, *EC3* and *EC4*) fulfil engineers' needs, for the latter, when steel/composite members have to be connected to reinforced concrete members, a lack of guidance is evident. Current solutions consist on the development of creative models, defined for particular or exceptional situations, based in methods used for steel and concrete (Stark and Hordijk, 2001). However, the complexity of such models makes the design of joints the main challenge involving three expertise fields: i) steel connections; ii) anchorage in concrete (using fasteners or reinforcement bars); and iii) concrete. In all three, extensive background exists reflecting decades of dedicated independent research.

For the design of steel and composites joints, the component method is nowadays a consensual approach, with proven efficiency, that is able to evaluate the nonlinear response of steel/composite joints. This approach, firstly developed for steel joints and later extended to composite joints, is now common practice in Europe. In (EN 1993-1-8, 2005) the method is prescribed and several joint configurations may be analysed accordingly. In (EN 1994-1-1, 2004) the extension to composite joints is made adding the transmission of forces achieved through the composite slab and strengthening of several components due to the embedment of steel components in concrete.

The anchorage in concrete is a key part of a steel-to-concrete joint; however, it is not in the design habits of “steel” designers. In the past recent years, considerable research work has been performed in this field, as it is proven by the varied solutions available to connect steel to concrete parts. The knowledge on this field is well expressed in several design guides and standards, such as: CEB Design Guide (CEB, 1997), ETAG 001 (EOTA, 1997), ACI 318 (ACI, 2001), fib Design Guideline (fib, 2007), CEN Technical Specifications (CEN/TS, 2007), (Eligehausen *et al.*, 2006). Though, the design philosophy is based on a capacity design, evaluating the resistance of the anchorage and disregarding its deformation.

In what regards to reinforced concrete part of the joints in a mixed steel-concrete structure, the so-called discontinuity regions (D-region) are “generated” in the reinforced concrete member. In such regions, the strain distribution is significantly nonlinear. Due to the inapplicability of the truss models for such complex regions, a rational approach has been developed known as strut-and-tie models (STM). This approach simplifies the design with some loss of accuracy; however, it is a preferable methodology than a practice based on detailing, experience and good practice (Schlaich *et al.*, 1987). The use of strut-and-tie models has been certified within the years and now the approach is prescribed by the code (EN 1992-1-1, 2004) for the design of reinforced concrete members where a non-linear strain distribution is expected, such as supports, near concentrated loads, etc.

Clearly, the lack of background knowledge is not an issue for an efficient analysis of joints in mixed steel-concrete structures. The main obstacle relies in the absence of unifying different approaches that can be integrated in Eurocodes’ methodology and design practice of engineers. The design philosophy of anchorage in concrete may be seen on the “side” of the concrete where its analysis is performed “separately” from the analysis of the structure, as it is the case with RC joints. For steel/composite joints, the past decades have introduced design procedures that include the joint behaviour and therefore, the joint is characterized in a complete way, where not only capacity is relevant but also deformability. Understandably, in concrete structures, due to the stiffness of the joints, this is not an important issue. When dealing with mixed steel-concrete structures, the analysis here performed stands on the steel point of view and a complete characterization of the joint is sought. Consequently, the extension of the component method is envisaged. The joint model should include all its active parts and be capable to reproduce its behaviour in terms of strength, stiffness and deformation capacity. Comprehensibly, this requires some effort from the concrete “side” to improve current approaches. Though, joints between steel and concrete members have already been approached in the past, as is the case of column bases (Heron, 2008), the approach remained separated. The concrete part is regarded separately by the concrete “side”, as prescribed by the steel code (EN 1993-1-8, 2005). Furthermore, beam to wall joints, in mixed steel-concrete structures, are completely disregarded.

Although the fabrication and erection issues are not part of the present thesis, one must point out that, besides the design purposes, the execution of the joints is an important aspect in such type of structures. Compatibility of tolerances has to be achieved. As known, steel and concrete constructions have tolerances of different order. Consequently, the joint

configuration has to be sufficiently “flexible” to accommodate these differences. This enhances the need of easy handle solutions to produce and erect, preserving structural requirements such as load capacity and ductility, sustained by simplified design methods.

Recently, an European RFCS (Research Fund for Coal and Steel) research project entitled “New market chances for steel structures by innovative fastening solutions” (Project N° RFSR-CT-2007-00051 – acronym: *InFaSo*) (Kuhlmann *et al.*, 2012) was dedicated to the analysis of joints in mixed steel-concrete structures. At an European level, for such type of joints, this was a first step regarding the development of simplified design models that assemble all active parts, with special emphasis on the anchorage in concrete. The present thesis reflects the author participation on this research project, as a member of the research group of steel and composite structures at the Civil Engineering Department of the University of Coimbra. Although different types of joints were analysed within the project work programme, the present thesis is mainly focused on the study of the behaviour of composite beam to reinforced concrete wall joints in mixed steel-concrete structures. For the proposed topic, the investigation includes experimental, numerical and analytical approaches.

## I.2 Steel-to-concrete joints and the RFCS research project *InFaSo*

### I.2.1 Definition of steel-to-concrete joints

In order to make a clear difference between steel-to-concrete joints and composite steel-concrete joints, a definition of these two types of joints seems appropriate. These types of joints have in common steel and concrete as base materials; however, their contribution to the joint behaviour, especially the concrete, is considered in a different form. In composite steel-concrete joints, all supported and supporting members (Fig. I.1-a) are made of steel or composite (steel-concrete). Horizontal members are always connected to vertical members through the steel parts, using welds and bolts. In some cases, the slab longitudinal reinforcement may be used to transfer further load to the vertical members. Failure of the joint originates in these steel parts and concrete is only considered to provide reinforcement to several steel components, affecting their resistance and stiffness. Composite joints are common practice amongst steel designers and rules for the design may be found in (EN 1994-1-1, 2004). In steel-to-concrete joints (Fig. I.1-b), the nature of the joining members is different. In general and within the scope of the present thesis, a steel or composite beam is supported by reinforced concrete column or wall. Column bases should be included in this type of joints. Till now, these are the sole steel-to-concrete joints approached by codes, either in (EN 1993-1-8, 2005) or in (EN 1994-1-1, 2004). In steel-to-concrete joints, connections are made between steel and concrete parts. Consequently, besides the steel failure modes, concrete failure modes have to be taken into account. So far, steel and composite codes refer to (EN 1992-1-1, 2004) for the verification of the concrete parts disregarding their influence on the joint behaviour.

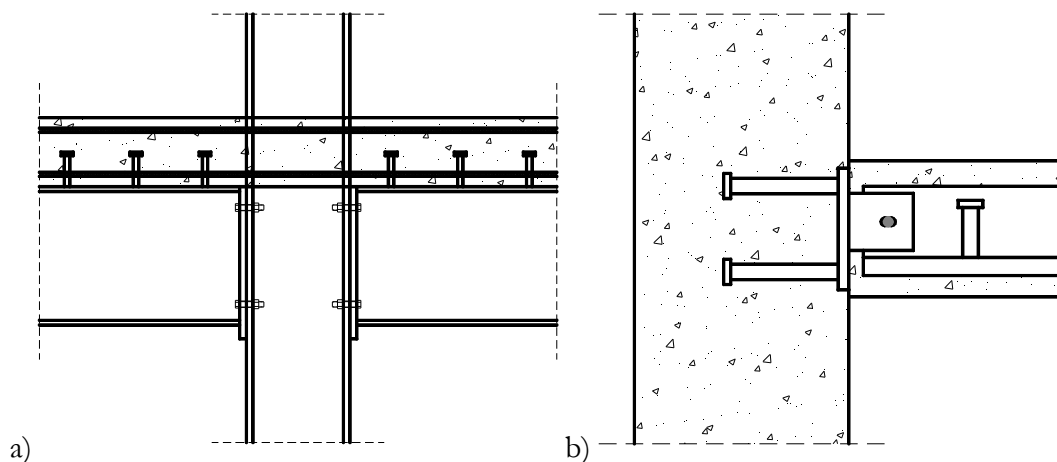


Fig. I.1: a) Typical double sided composite joint; b) Steel-to-concrete joint developed for the Millennium tower building in Vienna (Stahlbau, 1999)

### I.2.2 Overview of the European RFCS research project *InFaSo*

In most of the European countries, concrete dominates the market as building material. In order to reverse the situation, the research project *InFaSo* envisaged the promotion and encouragement of a wider use of steel through the implementation of more efficient and

economic structural solutions, as mixed steel-concrete structures. For structural reasons, foundations, and often stair cases and lift cores, have to be made of concrete in multi-storey buildings. Consequently, because of the gap between design of fastening in concrete and steel design and missing standardize joint solutions; it is easier for engineers to conceive the complete structure in concrete. Being this gap one of the obstacles for the implementation of mixed steel-concrete structural solutions, the project targeted the analysis/study of joints between steel/composite members and reinforced concrete members. Thus, the main expected outcome was the proposal of standardized steel-to-concrete joint solutions that combine the flexibility and adaptability of steel with fastening technology. This includes joint solutions of easy fabrication and erection, able to fulfil the structural requirements in terms of strength and/or ductility, sustained by simple and efficient design models. As an efficient approach, the extension of the component method to steel-to-concrete joints was envisaged. The integration of the concrete components, related to the fastening solutions (pre-installed or post-installed), into the method philosophy was foreseen. According to the structural needs, three types of joints were considered: steel beam to reinforced concrete wall; composite beam to reinforced concrete wall; and column bases (Fig. I.3).

To achieve the project objectives, four main tasks were defined and the work programme was divided into eight Work Packages (WP). The four tasks, coordinated by a superior task, followed a logic of action at different levels, by considering: i) the component behaviour; ii) the joint behaviour; iii) the structural behaviour; iv) construction rules and handbooks. The project organization and the dependencies between WP's are illustrated in Fig. I.2. WP 1 represents the coordination task that supervises all other tasks and assures their implementation. Within WP 1, existing and new proposals for steel-to-concrete joints configurations were assembled and catalogued. Out of the collected joints configurations, one for each type of joint was selected to be studied and characterized. WP 2 and WP 3 considered the work at the component level. Existing components models were gathered and the requirement developments identified. In the latter, regarding the application of the component approach, the components involving essentially the anchorage in concrete were of concern. In this way, experimental work was performed in WP 3, in order to form the basis of components characterization activated in anchorage in concrete. At the joint level, experimental work (WP 4) on the selected joint configurations was executed. The joint behaviour was characterized in terms of force-deformation ( $F-d$ ) or moment-rotation ( $M-\Phi$ ) curves and the interaction between components was checked. The theoretical characterization was accomplished in WP 5 through the development of joint component models. These models considered the assembly of all activated components within the whole joint. The experimental basis developed within WP 4 was fundamental for their conception and validation. Then, in order to evaluate the joint requirements regarding the behaviour of the whole structure, structural calculations (WP 6) were performed. A parametrical study using an office of building type, subjected to different type of actions (Service Limit State - SLS, Ultimate Limit State - ULS, Seismic Actions, Robustness), was considered. Finally, the practical output of the project was accomplished preparing

construction rules (WP 7), design guidance and electronic tools (WP 8). These two final WP's reflected the experience gained with the completion of the previous WP's.

Amongst the collected joint configurations, the ones illustrated in Fig. I.3 were chosen for deeper investigation. The three solutions consider the use of an anchor plate that is pre-installed in the concrete members. For the moment resisting joint, extra connection is achieved with reinforcement bars. The performed study was concentrated on the use of headed anchors welded to a steel plate (Anchor Plate). However, similar performance can be achieved using post-installed anchors, as undercut anchors. In this way, all analysed solutions involved the use of fastening technology, accomplishing the main objective of the project. Then, on the "steel" side of the joint, connection can be implemented by using fin plate (Fig. I.3-a), steel bracket (Fig. I.3-b) or column end plate with threaded bolts (Fig. I.3-c). The present thesis focuses on the joint solution to connect a composite beam to a reinforced concrete wall (Fig. I.3-b). Therefore, more detailed description of this configuration is given later, on Part II.

The project achievements are reported in detail in (Kuhlmann *et al.*, 2012). These can be summarized as follows:

- Elaboration of catalogue with several joint configurations for the different types of steel-to-concrete joints dealt within the project;
- Experimental and analytical characterization of the joint components activated in anchorage in concrete, mainly anchorage using headed anchors;
- Experimental and analytical characterization of the three selected joint configurations, three group of tests were performed and component model proposed for each joint configuration;
- Joint requirements in terms of resistance, stiffness and ductility regarding the structural behaviour under SLS, ULS, Seismic Action and Robustness;
- Design guidance and electronic tools for steel-to-concrete joints.

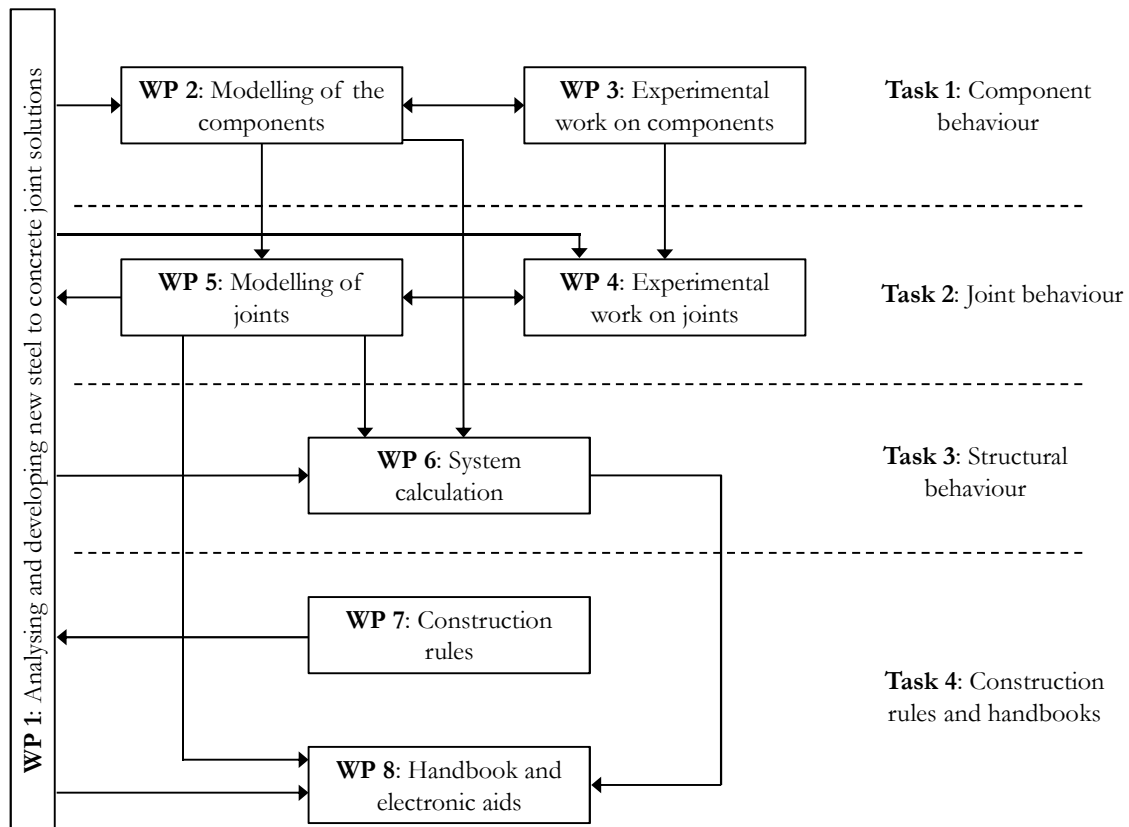


Fig. I.2: Organization of the *InFaSo* research project (Kuhlmann *et al.*, 2012)

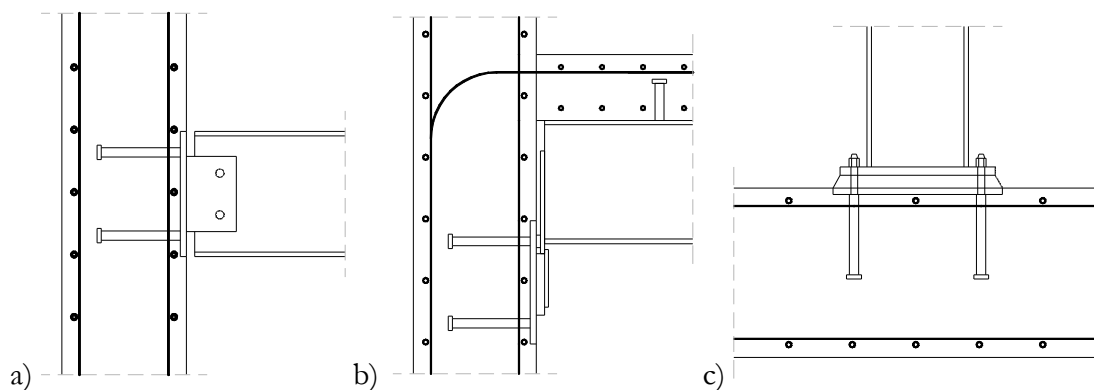


Fig. I.3: Joint configurations studied within the *InFaSo* research project: a) Steel beam to reinforced concrete wall; b) Composite beam to reinforced concrete wall; c) Column base

The relevance given in the present thesis to the research project *InFaSo* has two main reasons: first, the present thesis is a consequence of the contribution to the project; and second, relevant background was produced within the project which allow approaching the subject in a global manner. For example, characterizing only a component would be already an extensive work. In this way, important experimental and analytical developments achieved within the project are used in the development, application and validation of the analytical or numerical joint models discussed in this thesis. A detailed discussion of the project achievements, from other authors, relevant for the presented work, is given in literature review section of Part II of the present thesis.

### I.3 Objectives and scope

The purpose of this work is to investigate the behaviour of joints between steel/composite members and reinforced concrete members, focusing on those consisting of beam-to-wall joints studied within the research project *InFaSo*. The main objectives are to develop reliable numerical and analytical models, to examine the joints properties, namely: strength, stiffness and deformation capacity. Subsequently, simplified design models, following the (EN 1993-1-8, 2005) philosophy for the design of joints, are foreseen.

This thesis covers analytical, numerical and experimental aspects related to the behaviour of steel-to-concrete joints. In the analytical part, emphasis is placed on the proposal of appropriate models that can reproduce accurately and efficiently the response of steel-to-concrete joints. To this end, an extension of the component approach is proposed. Consequently, each activated component is characterized in terms of strength, stiffness and deformation, as required by the method. At the component level, the integration of the components activated with the anchorage in concrete is essential. For design purposes, simplification of the proposed models is performed.

On the numerical side, models are developed at the component, joint and structural level. The two first allow complementing the experimental tests and provide a deeper exploitation of the component and joint mechanics. The latter are used to derive requirements for the steel-to-concrete joints regarding the structural behaviour to SLS, ULS and accidental actions, as seismic loading.

Finally, the experimental tests on steel-to-concrete beam-to-wall joints, carried out as part of the collaborative research project *InFaSo*, are utilised in part for validation of analytical and numerical procedures, as well as to highlight important behavioural aspects.



## I.4 Thesis outline

The present thesis consists of four parts. The first part is introductory. The second part is the core of the thesis where the behaviour of steel-to-concrete joints is discussed. The third part is complementary and regards the structural calculations to derive joint requirements. And the fourth part is the closure with general conclusions and recommendations for further research interests.

Part I is divided in four chapters giving an introduction to this thesis. The importance and motivation for approaching the subject are discussed in chapter 1. In chapter 2, the European RFCS research project *InFaSo* is introduced and its relevance for the present work is enhanced. Chapter 3 presents the main objectives and scope of this thesis. And the present chapter provides the organization of this thesis.

Part II consists of six chapters. In chapter 1, the studied steel-to-concrete beam-to-wall joint is presented and the different configurations regarding the structural demands are discussed. Furthermore, the joint mechanics are analysed. Chapter 2 provides a general literature review of the component method and joint models basis for steel-to-concrete joints. The latter includes steel, composite and reinforced concrete joint modelling. Regarding the extension to steel-to-concrete joints, the required developments are identified. A literature review at the components level is also included with special focus on the anchorage in concrete. Important developments for the present work, achieved within the European RFCS research project *InFaSo*, are also included in this chapter. Chapter 3 deals with anchor plate connection. This may be part of a moment resisting joint or be the joint solution. Accordingly, analytical component based models are presented for different work conditions. The derivation and validation of these models include the development of numerical models. In chapter 4, a strut-and-tie model for the part of the joint within the reinforced concrete member, here denominated as Joint Link, is presented. In the absence of experimental data that specifically deals with this part of the joint, the analytical developments are based essentially on the existing models and numerical calculations. In chapter 5, the complete moment resisting joint is approached. A numerical model for this joint is presented and validated with the experimental data of the *InFaSo* research project. Based on the numerical and experimental observations, a component based model is proposed for the moment resisting joint which assembles the anchor plate and the joint panel with other activated components. Finally, in chapter 6, some concluding remarks are withdrawn.

Part III is divided in five chapters. In chapter 1, an introduction to the structural calculations performed and the type of building structures considered is provided. In chapter 2, a brief literature review on the joint modelling in the structural analysis is performed and the selected study cases presented. The structural calculations results are discussed in chapter 3. Then, regarding the steel-to-concrete joints, structural requirements are obtained. In chapter 4, using the structural calculation results, a comparative analysis between joint structural requirements and joint properties is done. Part III ends with a final chapter providing some concluding remarks.

Finally, part IV is divided in three chapters. Global conclusions of the thesis are given in the first chapter. In chapter 2, recommendations for further research are summarized. In chapter 3, the personal contributions to the presented developments are highlighted.

## References

- (ACI, 2001) American Concrete Institute – ACI. ACI 318: ACI Standard 318. Building Code Requirements for Structural Concrete, Detroit, 2001.
- (CEB, 1997) Comité Euro-International du Béton – CEB. CEB Design Guide: Design of Fastenings in Concrete, Lausanne, 1997.
- (CEN/TS, 2007) European Organization for Standardization – CEN. CEN Technical Specification (TS): Design of fastenings for use in concrete, Part 1: General, Part 2: Headed Fasteners, Part 3: Anchor Channels, Part 4: Post-installed Fasteners – Mechanical Systems, Part 5: Post-installed Fasteners – Chemical Systems, Brussels, 2007.
- (Eligehausen *et al.*, 2006) Eligehausen, R., Mallee, R., Silva, J. F., Anchorage in Concrete Construction, Ernst &Sohn, Berlin, 2006.
- (EN 1992-1-1, 2004) European Committee for Standardization – CEN. EN 1992-1-1. Eurocode 2: Design of concrete structures. Part 1-1: General rules and rules for buildings, Brussels, 2004.
- (EN 1993-1-8, 2005) European Committee for Standardization – CEN. EN 1993-1-8. Eurocode 3: Design of steel structures. Part 1-8: Design of joints, Brussels, 2005.
- (EN 1994-1-1, 2004) European Committee for Standardization – CEN. EN 1994-1-1. Eurocode 4: Design of composite steel and concrete structures. Part 1-1: General rules and rules for buildings, Brussels, 2004.
- (EOTA, 1997) European Organization for Technical Approval – EOTA. ETAG 001: Guideline for European Technical Approval of Anchors (metal anchors) for use in concrete. Part 1, 2 and 3 and annexes A, B, and C, Brussels, 1997.
- (fib, 2007) Federation International du Béton – fib. fib Guide for the Design of fastenings in Concrete: Part 1: General, Part 2: Post-installed Anchors – Mechanical, Part 3: Post-installed Anchors – Bonded Anchors and Rebar Systems, Part 4: Headed Anchors, Part 5: Anchor Channels, Lausanne, 2007.
- (Heron, 2008) Heron, Special issue: Steel Column Bases, 53(1/2), 2008.
- (Kuhlmann *et al.*, 2012) Kuhlmann, U, Eligehausen, R, Wald, F, da Silva, L, Hofmann, J, “New market chances for steel structures by innovative fastening solutions”, Final report of the RFCS project *InFaSo*, project N° RFSPR-CT-2007-00051, Brussels, 2012.
- (Schlaich *et al.*, 1987) Schlaich, J., Schäfer, K., Jennewein, M., “Toward a Consistent Design of Structural Concrete”, PCI Journal, 32(3), pp. 74-150, 1987.
- (Stark and Hordijk, 2001) Stark, J., Hordijk, D. A., “Where structural steel and concrete meet”, International Symposium on “Connections between steel and concrete”, University of Stuttgart, ed. Eligehausen R., Stuttgart, pp. 1-11, 2001.
- (Stahlbau, 1999) Stahlbau Magazine, 68(8), Ernst &Sohn, Berlin, 1999.



## *II. Study of the behaviour of steel-to-concrete beam-to-wall joints*



## II.1 Introduction

The behaviour of steel-to-concrete beam-to-wall joints is discussed in the present part of this thesis. As referred in Part I, the composite beam to reinforced concrete wall joint is chosen to approach the subject. This joint was developed to provide a semi-continuous solution, allowing therefore transference of bending moment between supported and support members. In its original configuration, the joint depicted in Fig. II.1 may be divided in two parts: i) upper part, connection between reinforced concrete slab and wall; ii) bottom part, connection between steel beam and reinforced concrete wall. In the upper part, the connection is achieved extending and anchoring the longitudinal reinforcement bars of the slab (*a*) into the wall. Slab and wall are expected to be concreted in separate stages and therefore, the continuity between these members is only provided by the longitudinal reinforcement bars. In the bottom part, the fastening technology is implemented to connect the steel beam to the reinforced concrete wall. Thus, a steel plate (*b*) is anchored to the reinforced concrete wall using headed anchors (*c*), pre-installation system. The plate is embedded in the concrete wall with aligned external surfaces. Then, on the external face of the plate, a steel bracket (*d*) is welded. A second plate is also welded to this steel bracket but is not aligned in order to create a “nose”. The steel beam with an extended end plate (*f*) sits on the steel bracket, and the extend part of the end plate and steel bracket “nose” perform an interlock connection avoiding the slip of the steel beam out of the steel bracket. A contact plate (*g*) is placed between beam end plate and anchor plate, at the level of the beam bottom flange. Finally, although several types of anchors are nowadays available in the market, only the use of headed anchors is considered in the present thesis.

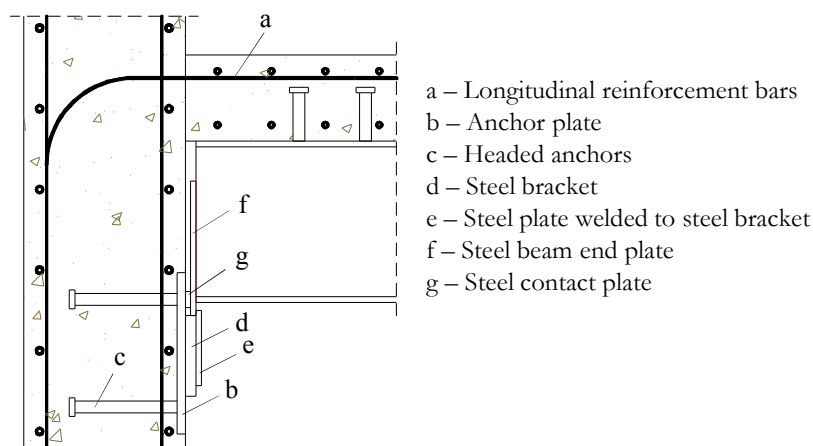


Fig. II.1: Composite beam to reinforced concrete wall joint configuration according to (Kuhlmann *et al.*, 2012)

In the described format, the joint is foreseen for moment resisting frames. Often, structures where the lateral restraining system is full effective are classified as non-sway and joints designed as pinned. For such structural systems, the present joint configuration can be readapted without modifying significantly the connection between steel and concrete parts. In this way, connecting the same types of members, the initial joint configuration can

drift to other configurations, as simple joints. The versatility of the joint is illustrated in Fig. II.2. Three working situations are possible: i) semi-continuous with medium/high capacity to hogging bending moment, shear and axial compression; ii) pinned for high shear and axial compression; iii) pinned for high shear and axial tension. In the first version, due to the apparent weakness of the “nose” system, it can be perceived that the sagging bending moment capacity is very limited and strongly dependent of the “nose” resistance. For the same reason, the resistance to axial tension load should be much reduced. Therefore, the application to reverse loading cases, as seismic actions demand, is restricted. For this purpose, a different layout should be developed which is out of the scope of the present thesis. In what concerns to the pinned versions of the joint, at the same time they can be regarded as part of the moment resisting joint or as joint for itself. Pinned joint A (ii) results from the semi-continuous joint (i) where no connection exists between slab and wall. Consequently, in terms of erection, this is a very “flexible” solution; however, for the above reasons; the joint should not be subject to axial tension. The latter joint solution (iii) differs on the steel beam to anchor plate connection where a fin plate is used. In this case, the tension capacity is improved and due to the symmetry of the joint, a cyclic loading may be applied. Although these observations concerning the capacity of the two pinned solutions to transfer axial loading, their main objective is to work as pinned joint transferring shear loads and allowing the “free” rotation of the joint.

As mentioned, the semi-continuous version (i) of the joint configuration has a limited performance to loading situations where the bottom part of the joint should transfer tension. Furthermore, the consideration of combined axial load and bending moment is not in the scope of the present thesis. Therefore, the joint is analysed only under hogging bending moment and shear loading. As for steel and composite joints, the high stiffness of the joint to the shear load should not affect the deformability of the joint under bending moment. In such joints, critical components should be verified to combined actions, e.g. bolts under combined tension and shear. Here, the longitudinal reinforcement contribution to the shear resistance should be low because of the stiffness of the bottom zone to shear load and because of its high contribution to the tension component of the joint under bending moment. For these reasons, the shear on the longitudinal reinforcement should be residual and its verification may be disregarded.



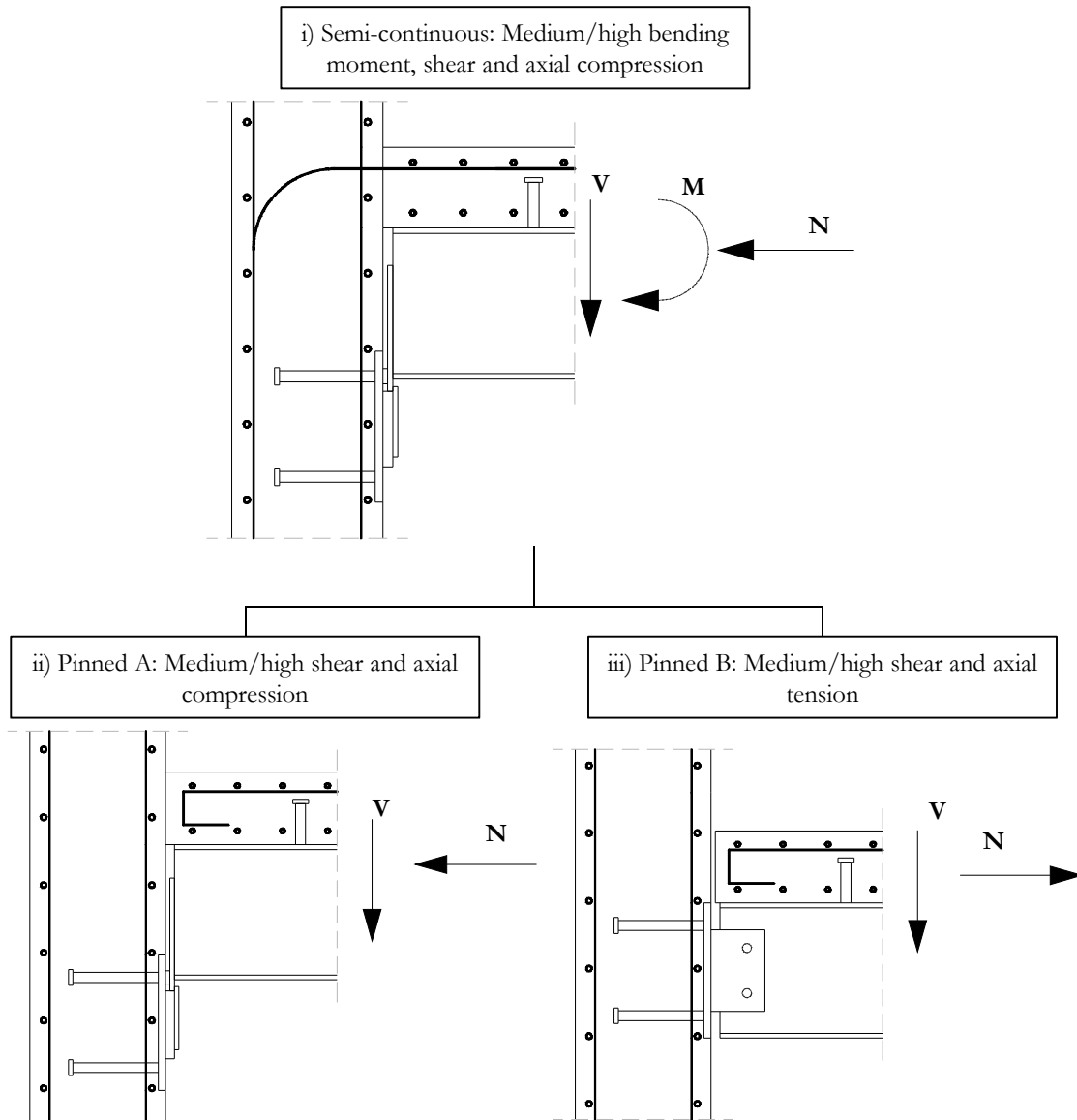


Fig. II.2: Steel-to-concrete joint solutions using similar joint configurations

To understand the behaviour of the joint under bending moment and shear loading, the mechanics of the joint is identified and the assumed stress flow is schematically represented in Fig. II.3. In the upper zone, only tension is transferred through the longitudinal reinforcement. Likewise, in this region, no shear and no tension is assumed to be transferred, from slab to wall, through the concrete, as the small bond developed is neglected. In the bottom zone, the shear load is transferred from the steel beam to the reinforced concrete wall using the following path: a) from the beam end-plate to steel bracket through contact pressure; b) from the anchor plate to the reinforced concrete wall through friction, between plate and concrete, and through bearing, between shank of the headed anchors and concrete. Still at the bottom zone, compression is transferred to the reinforced concrete wall through the contact plate between the beam end-plate and the anchor plate. Then, on the reinforced concrete wall, the high tension and compression loads introduced by the joint achieve equilibrium and flow to supports.

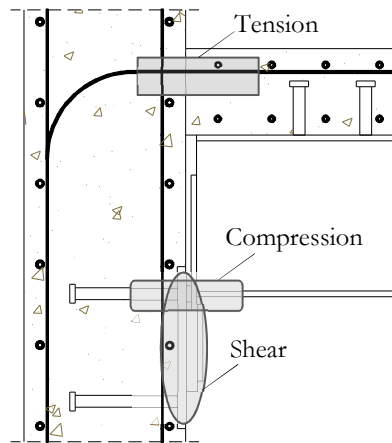


Fig. II.3: Stress flow on the semi-continuous joint under bending moment and shear loading

At the bottom zone of this joint, the connection between steel and concrete is similar to the pinned solutions. Though, because of the bending of the joint, high compression is introduced into the wall through this zone. Consequently, the loading conditions of the anchor plate differ from semi-continuous joint to the pinned joints. In the first case, the anchor plate is simultaneously subject to: a) compression load, introduced by the beam bottom flange; b) shear load, according to above all shear load flows through this part of the joint; c) secondary bending moment, due to the shear load applied to the anchor plate with eccentricity. The described loading conditions are illustrated in Fig. II.4. Although, a separate analysis of the joint to shear and bending moment loading is foreseen, one must notice that the secondary bending action ( $M_V$ ) has a “direct” influence on the anchor plate subject to compression. This bending action induces tension on the upper anchor row where the compression load is introduced. In this way, the shear has opposite effect to compression load on the anchor plate.

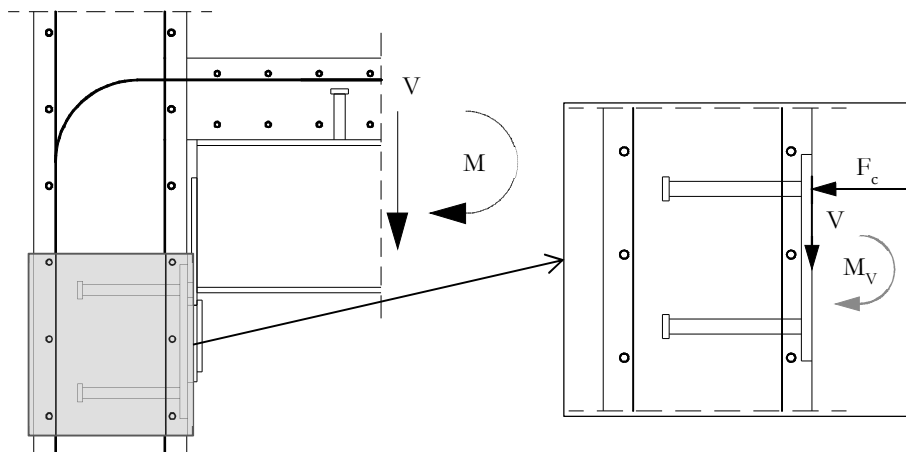


Fig. II.4: Loading conditions of the anchor plate on the semi-continuous joint under hogging bending moment and shear loading

A simplified analysis of the global joint configuration shows that the compression component of the bending moment on the joint, has a considerably higher effect on the anchor plate than the secondary bending moment due to the shear load on the joint. Based on the geometry of the reference specimen of the tests performed in (Kuhlmann *et al.*,

2012), a relation between  $F_c$  and  $V$  may be obtained. Then, reducing the system of forces to the centroid of the plate, the bending moment due to shear ( $M_V$ ) and due to compression ( $M_{F_c}$ ) may be compared. In Fig. II.5 is plotted the comparison between these bending moments. For the bending moment due to the shear load with eccentricity two lines are shown. These represent the envelope for this action according to the maximum and minimum eccentricity of the shear load considered in (Kuhlmann *et al.*, 2012). As it can be seen, the shear load has a residual effect in comparison to the compression load and consequently, its action may be neglected in the analysis of the semi-continuous joint under bending moment.

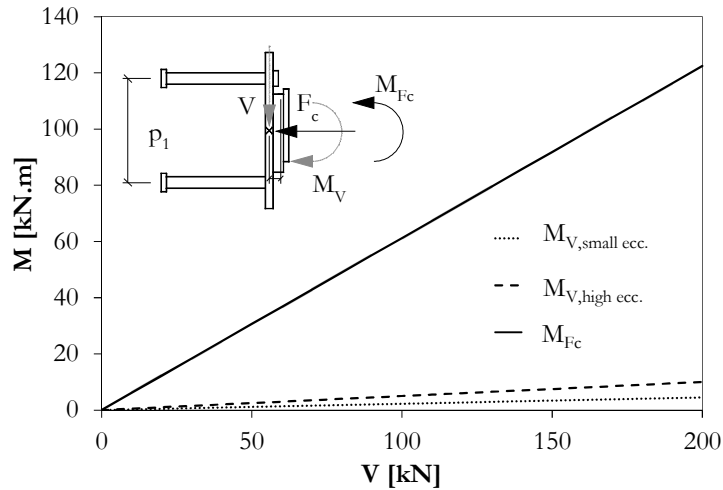


Fig. II.5: Evaluation of the effect of the shear load on the anchor plate under compression within the semi-continuous joint

In what respects to the pinned versions of the joint, for the present thesis, only the connection between anchor plate and wall is of interest. The steel-to-steel connection, independently of the system used, is not in its scope. In these joints, the shear load is the main action on the joint. In such conditions, the secondary bending moment is a relevant action on the anchor plate and cannot be neglected. Independently of steel-to-steel connection used, the mechanics of these pinned solutions is similar. In Fig. II.6 is schematically represented the mechanic of load transfer between anchor plate and reinforced concrete wall. In these joints, because of the relevance of the secondary bending moment, the consequent stress flow is also included. The shear load is transferred through: a) bearing between anchors shanks and concrete; b) friction between plate and concrete; c) bearing between plate edge and concrete. Similar load path is considered in the semi-continuous joint under shear. The secondary bending moment generates tension and compression forces that are transferred through the anchor rows and plate-to-concrete contact, respectively.

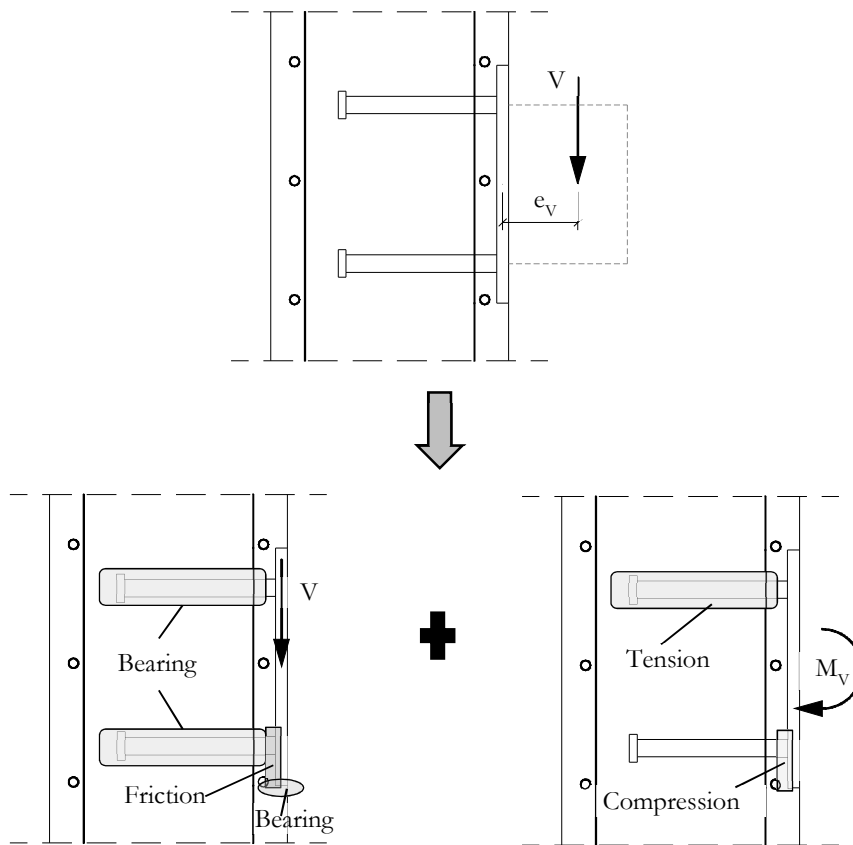


Fig. II.6: Stress flow on the pinned joints under shear loading

The proposal of simple and efficient models for the analysis of the above steel-to-concrete joints is an objective of the present thesis. As known, the component method is an approach for the design and analysis of steel and composite joints with proven efficiency, and is able to evaluate the nonlinear response of these joints. Therefore, in the present, the extension of the component method to steel-to-concrete joints is foreseen. This approach has been firstly developed for steel joints and later extended to composite joints, and is now a common practice in Europe. The basic principle of the approach consists in determining the complex non-linear response of the joint through its subdivision into different parts that contribute to one or more of its structural properties. These parts are denominated as basic joint components. This philosophy allows designers to take options more efficiently, as the contribution of each component can be optimized according to the limiting components. A joint component depends on the type of loading. Accordingly, three groups of components are usually identified: tension, compression and shear. In (EN 1993-1-8, 2005) the method is prescribed and a large number of joint configurations may be analysed accordingly. In (EN 1994-1-1, 2004) the extension to composite joints is made adding the transmission of forces achieved by the composite slab and considering the strengthen of several components due to the embedment in concrete. As a first step in its extension, the components activated in the steel-to-concrete joints are identified. These are listed in Table II.1 and their localization shown in Fig. II.7. Note that the number attributed to the joint components is set for the present thesis and disregards the usual numbering in (EN 1993-1-8, 2005). Barely all components are activated in the semi-

continuous joint, though several have a minor contribution to the joint response. For example components 7, 8, 9 and 10 should have a small influence in this joint as their activation does not result from a direct action/load but because of the anchor plate under compression load, at the level of the upper anchor row, which deforms the bottom and top edges in the opposite direction of loading. Due to the presence of the anchor row at the bottom part, this should act similarly to a prying force and consequently, the anchor row is activated in tension. However, it should be unnatural to observe a failure of the joint due to these components. On the other hand, in the pinned joint, these components have a higher significance as they are activated in different conditions. The activation results directly from the action of the shear load with eccentricity and therefore, depending on the dimension of the eccentricity, they can be critical for the response of the joint. In the same zone of these tension components, an additional component is identified which consists in the hanger reinforcement. This is a common solution to increase strength and ductility of an anchorage in tension. Although it can be used in the semi-continuous joint, because of the above reasons, its application is only reasonable in the case of the pinned joints. Component 11, here denominated as “Joint Link”, is only considered in case of the semi-continuous joint because the level of tension and compression is considerably high when compared to the pinned joints. At the joint scale, the first may have a global effect on the member while in the latter the effect should be local. In this way, this component represents the equilibrium of stresses in the reinforced concrete wall zone adjacent to the joint. Here, tension and compression stresses should be identified.

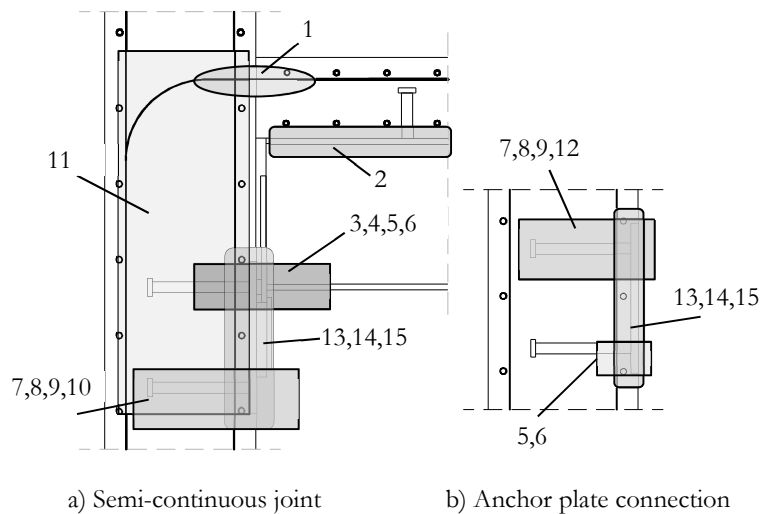


Fig. II.7: Localization of the identified joint components

The steel-to-concrete joints, aim of the present thesis, have been exposed and their analysis is performed in subsequent chapters. Thus, a literature review on the joint modelling, components characterization and on the most relevant developments within the research project *InFaSo* (Kuhlmann *et al.*, 2012) is presented in chapter two. This form the basis for the joint models proposed. In chapter three, the simple joint versions are analysed and later integrated in the analysis of the complete joint (semi-continuous). Because of its nature, the joint link is approached separately in chapter four and a model for its inclusion in the complete joint is proposed. In chapter five, the complete joint is discussed assembling the

main developments achieved in the previous chapters and adding the joint components activated in the tension zone. Lastly, in chapter six, the main concluding remarks are given at the end of this part.

Table II.1: List of components activated in the steel-to-concrete joints under analysis

<b>Component ID</b>	<b>Basic joint component</b>	<b>Type/Zone</b>	<b>Activated in joint</b>
1	Longitudinal steel reinforcement bar in the slab	Tension	Semi-continuous joint
2	Slip of composite beam	Tension	Semi-continuous joint
3	Beam web and flange	Compression	Semi-continuous joint
4	Steel contact plate	Compression	Semi-continuous joint
5	Anchor plate in bending under compression	Compression	Semi-continuous joint Pinned joint A and B
6	Concrete in compression	Compression	Semi-continuous joint Pinned joint A and B
7	Headed anchor in tension	Tension	Semi-continuous joint Pinned joint A and B
8	Concrete cone	Tension	Semi-continuous joint Pinned joint A and B
9	Pull-out of anchor	Tension	Semi-continuous joint Pinned joint A and B
10	Anchor plate in bending under tension	Tension	Semi-continuous joint Pinned joint A and B
11	Joint link	Tension and Compression	Semi-continuous joint
12	Hanger reinforcement	Tension	Pinned joint A and B
13	Plate-concrete friction	Shear	Semi-continuous joint Pinned joint A and B
14	Headed anchor in shear	Shear	Semi-continuous joint Pinned joint A and B
15	Concrete pry-out	Shear	Semi-continuous joint Pinned joint A and B

## II.2 Literature review and background

### II.2.1 Analysis and modelling of joints

#### II.2.1.1 Steel and composite joints

In steel and composite construction, the joints between members are key parts of the structure with highly complex behaviour due to material nonlinearities and geometrical discontinuities. Historically, assessing the behaviour of joints was seen as a difficult task and their behaviour was assumed in the structural analysis as perfect hinges or fully continuous. This dichotomy reflected the joint response to bending moment loading, either fully flexible with no capacity to transfer bending moment, or fully rigid with full bending moment resistance. However, in the majority of the cases their real behaviour relies between these extreme concepts. Earlier, this reality was shown by a great number of experimental investigations but the main concern of the researchers was to guarantee the required resistance of the joint (Jaspart, 1991), and no relevance was given to the deformability. The concept of semi-rigid joints appeared later (Bjordhove *et al.*, 1990) and the influence of the joint behaviour on the structural analysis was demonstrated (Jaspart, 1991). Considering the real behaviour of the joint became not only a matter of structural interest but also an economic issue. Semi-rigid joints allowed saving material and simplifying the execution of joints. For all these reasons, in the past three decades the behaviour of steel and composite joints has become subject of series of researches and numerous works have been performed worldwide covering different approaches (experimental, numerical, analytical), configurations (single and double sided, weak axis, I/H profiles to tubular, etc.) and actions (monotonic, cyclic, fire, robustness, etc.). Although all this extensive research activity has taken place in the past, the study of the behaviour of joints is still an unfinished work, as is the example of the need to predict the 3D behaviour of the joints (Simões da Silva, 2008).

The response of a steel or composite beam-to-column joint is typically given in terms of moment-rotation ( $M-\Phi$ ) curves as illustrated in Fig. II.8 and may be described as follows:

- Initial linear elastic range (*I*);
- Non-linear range with plastic deformations (*II*);
- Strain hardening branch (*III*) up to the ultimate bending moment  $M_{j,u}$ ;
- The existence and extend of this strain hardening branch depends on the part of the joint limiting its resistance and defining its deformation capacity  $\Phi_{j,u}$  (high ductility, limited ductility, brittle).

The execution of experimental tests is the most reliable form of characterizing the joint properties. Though, for design purposes, this is not a practical and feasible procedure. In this way, the analytical characterization has always been in the concerns of the practical oriented researches. Several analytical models have been proposed in the past (Jaspart and Maquoi, 1992), where the component method has become the most consensual approach and is nowadays in the design habits of practical engineers. This approach, first developed

to steel joints, had its first developments with the work of (Zoetemeijer, 1974) on bolted beam-to-column connections. In the beginning of the nineties, the efficiency and accuracy of the approach was highly recognized and implemented in the European code (EN 1993-1-8, 2005). Later, the development of analytical models for composite joints (Tschammernegg *et al.*, 1998) and column bases (Wald *et al.*, 1998), led to its extension and inclusion in the (EN 1994-1-1, 2004).

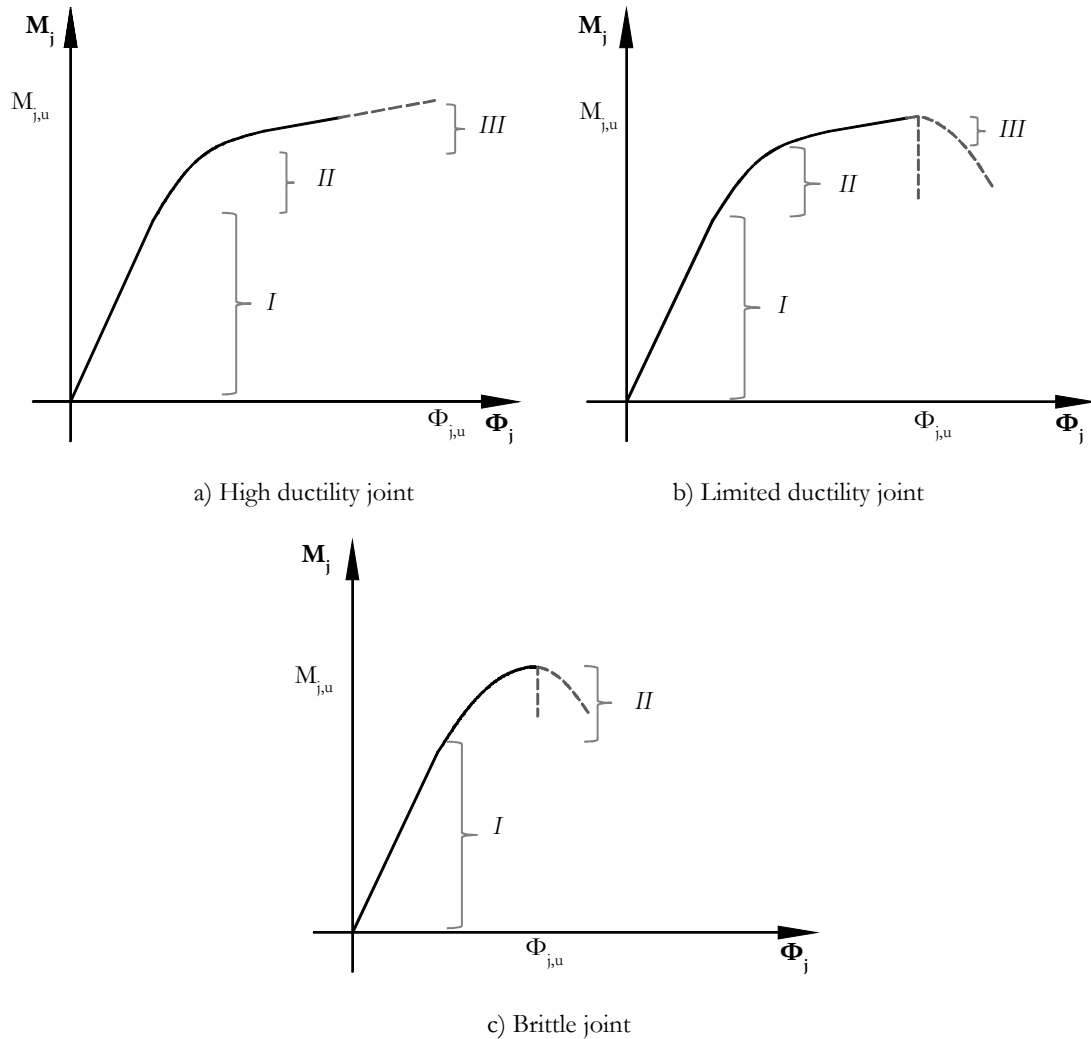


Fig. II.8: Characteristic  $M$ - $\Phi$  curves of steel and composite joints

The basic principle of the component method consists in determining the complex non-linear joint response through the subdivision into simple parts. The joint is then regarded as a set of individual basic components that contribute to its structural behaviour. A joint component depends on the type of loading. Accordingly, three groups are usually identified: tension, compression and shear. Additionally, a second division may be done according to their location: panel zone or connecting zone. In Fig. II.9 is represented the double sided composite joint which illustrates these two definitions.



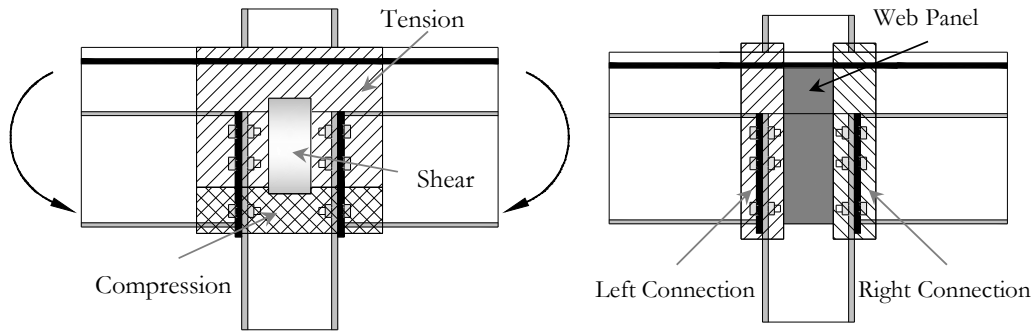


Fig. II.9: Division of a joint into groups and zones

In the component method, components are modelled by means of translational springs with non-linear force-deformation ( $F-d$ ) response that are exposed to internal forces instead of stresses. The joint mechanics can then be represented by means of spring mechanical models assembling all activated components. In this way, for each joint configuration and loading conditions (monotonic, cyclic, fire), it is common to idealize a spring mechanical model. In Fig. II.10 the Innsbruck sophisticated model proposed by (Tschemmerneegg *et al.*, 1998) for a double sided composite joint is given as example. The model is an extension of the component model for steel joints to composite joints with inclusion of additional components to deal with composite behaviour. In Table II.2, each spring that represents a specific part of the joint (basic components) is identified. In the model, a rigid separation bar between the panel zone and the connecting zone guarantees the straight deformation of the column front which was observed in tests. According to (Huber, 1999), in the case of extended end-plates, this rigid separation should only be extended according to the proportion between the stiffness of end-plate and connecting elements. Spring n°13 also deserves a comment; this spring is only active if unbalanced forces are applied on left and right hand sides. This spring represents the redirection of these unbalanced forces to the column web.

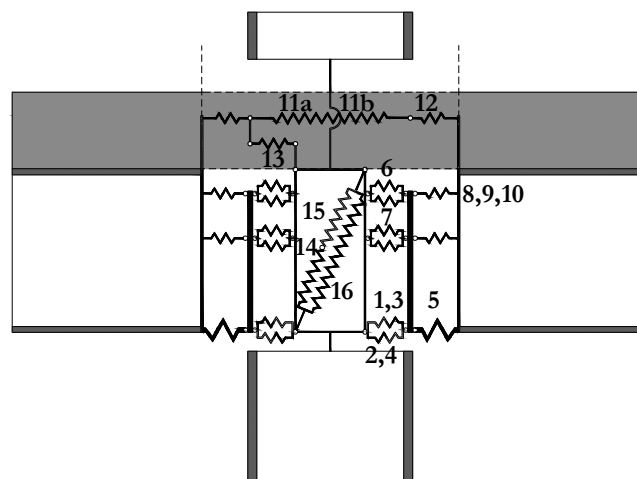


Fig. II.10: Innsbruck component model for double sided composite joint (Tschemmerneegg *et al.*, 1998)

The above types of models allow obtaining the complete  $M-\Phi$  curve characterizing the joint response. Because of the components interplay, their assembly becomes iterative. Simplifications have been proposed (Weynand *et al.*, 1996) which avoid an iterative

assembly; e.g.: interplay between tension and compression components within web panel zone is prevented. The simplifications adopted (consciously) introduce errors, however these have been observed to be acceptable and the advantages are reflected in the component assembly, which becomes easier, analytical instead of iterative. This model is the basis of the design procedure prescribed in (EN 1994-1-1, 2004). According with, the joint properties are defined in terms of rotational stiffness ( $S_j$ ), bending moment resistance ( $M_{j,Rd}$ ) and rotation capacity ( $\Phi_{j,u}$ ). In what regards to stiffness and resistance, the code allows a quantitative assessment; however, for the deformation capacity only qualitative evaluation can be performed, where sufficient or insufficient joint rotation capacity may be assumed for a plastic design.

Table II.2: List of components identified in the Innsbruck model for double sided composite joints

Spring number	Joint component	Region	Zone
1	Column web in compression	Compression	Connecting zone
2	Inner Stiffening due to concrete encasement		
3	Column flange in compression		
4	Outer stiffening due to concrete encasement		
5	Beam flange in compression		
6	Column web panel in tension	Tension	
7	Additional reinforcement		
8	Column flange in bending		
9	End-plate in bending		
10	Bolts in tension		
11	Steel reinforcement		
12	End slip of composite beam		
13	Redirection force through concrete		
14	Column web panel in shear	Shear	Panel zone
15	Column web in bending		
16	Compressed concrete strut		

At the component level, the accurate characterization is essential for the performance of the described models. The limiting component governs the joint response and an incorrect evaluation may change an expected ductile behaviour to a brittle behaviour. The evaluation of the joint basic components can be performed through experimental tests, numerical and/or analytical models, and should be expressed in terms of  $F-d$  curves. The evaluation of the basic joint components is addressed later in the present chapter.

To summarize, the application of the component method requires the following steps:

- Identification of the joint basic components;
- Characterization of the structural properties of each component;
- Assembly of the components into a joint model and determination of the joint properties.

As prescribed by the code (EN 1993-1-8, 2005), the joint properties obtained with application of the component method are the joint rotational stiffness ( $S_j$ ) and the joint design bending moment resistance ( $M_{j,Rd}$ ). These may be obtained as follows.

$$M_{j,Rd} = \sum_r b_r F_{tr,Rd} \quad (\text{II.1})$$

$$S_j = \frac{E \bar{\alpha}^2}{\mu \sum_i \bar{k}_i} \quad (\text{II.2})$$

Where:  $F_{tr,Rd}$  is the design tension resistance of bolt-row  $r$ ;  $b_r$  is the distance from bolt-row  $r$  to the centre of compression;  $r$  is the bolt-row number;  $E$  is the Young's modulus;  $\bar{\alpha}$  is the lever arm of the tension bolt-row, in the case of more than one this should be an equivalent lever arm;  $\bar{k}_i$  is the stiffness coefficient for all components activated within the joint; and  $\mu$  is a stiffness ratio.

The above expression is also valid for composite joint, where the layers of longitudinal reinforcement bars in the composite slab are assumed as bolt-rows. Setting the stiffness ratio  $\mu$  equal to 1, the initial joint rotational stiffness may be obtained. According to the type of global analysis to be performed, the behaviour of the joint may be assumed as elastic or plastic. For the elastic analysis, if the expected acting bending moment ( $M_{j,Ed}$ ) on the joint is smaller than 2/3 of the joint design bending moment resistance ( $M_{j,Rd}$ ), the initial joint rotational stiffness ( $S_{j,ini}$ ) may be used. In the other cases a modified rotational stiffness ( $S_{j,ini}/\eta$ ) should be considered. For a plastic analysis, one of the following three options may be assumed: i) bilinear, where the joint rotational stiffness is ( $S_{j,ini}/\eta$ ) and considered up to  $M_{j,Rd}$ ; ii) trilinear, where the initial joint rotational stiffness ( $S_{j,ini}$ ) is assumed up to 2/3 of  $M_{j,Rd}$  followed by second linear branch up to  $M_{j,Rd}$ ; iii) nonlinear, which considers a linear elastic branch up to 2/3 of  $M_{j,Rd}$  and then a nonlinear range obtained using expression (II.2) with a varying stiffness ratio according to (EN 1993-1-8, 2005). Then, when the design bending moment resistance ( $M_{j,Rd}$ ) is attained, a plateau may be assumed according to the governing component.

Finally, the application of the component method is illustrated in Fig. II. 11 by comparing the experimental result of a composite beam-to-column joint tested at the Faculty of Sciences and Technology of the University of Coimbra (Simões da Silva *et al.*, 2001) with the component analytical model according to (EN 1994-1-1, 2004). For the component method the commercial software COP 2 (Feldmann + Weynand GmbH, 2011) was used. Because this is a design calculation software, the results were corrected regarding the safety

factors and the real mechanical properties ( $f_y$ ). The three curves that may be considered in a plastic analysis are presented. These were obtained from the main joint properties calculated as described before. In terms of rotation capacity, the plateau represented is illustrative, according to (EN 1994-1-1, 2004) only a qualitative evaluation may be performed.

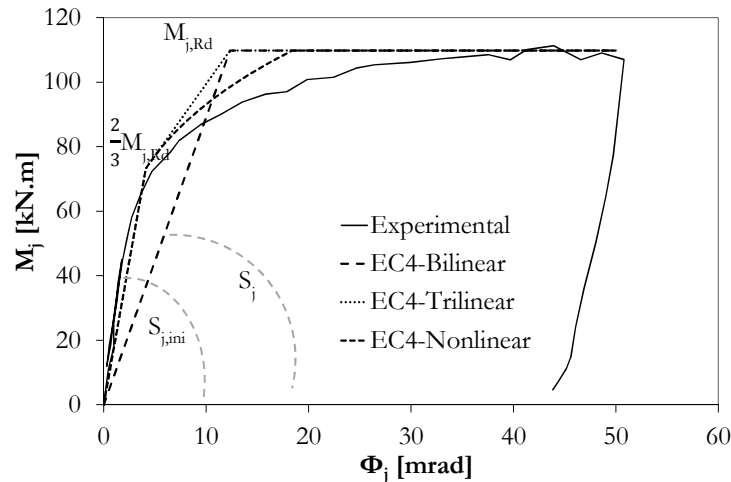


Fig. II. 11: Application of the component method to a composite joint and comparison with experimental tests (Simões da Silva *et al.*, 2001)

### II.2.1.2 Reinforced concrete joints

In reinforced concrete structures, joints are identified as D-regions where geometrical and mechanical discontinuities exist. In such joints, the main concern is in terms of capacity so that the resistance of the members is guaranteed. Because of the inherent high stiffness, its deformability is negligible and in the structural analysis joints are assumed as fully rigid. In this way, a full continuity is obtained if the joint resistance is at least equal to the resistance of the weakest member it connects. In order to avoid an inadequate capacity of the joint, efficient reinforcement detailing is required. In the past, the design of D-regions, and in particular reinforced concrete joints, was sustained by practice experience and no analytical method was used (Schlaich *et al.*, 1987). To fill this gap an approach has been derived known as strut-and-tie modelling (STM). With this method, a rational design concept for D-regions, extendable to any part of the reinforced concrete member (Schlaich and Schäffer, 1991), was established. The acceptance of this approach is proved by its inclusion in design codes, first in the Model Code 90 (CEB-FIP, 1993) and later in the Eurocode 2 (EN 1992-1-1, 2004). Its suitability for problems involving reinforced concrete is evidenced with its application in composite joints (EN 1994-1-1, 2004), when considering the redirection of the unbalanced loading from the slab to the column.

The strut-and-tie method is a rational approach that simplifies the complex structural member into a truss model and considers all loading effects ( $M$ ,  $N$ ,  $V$ , and  $M_T$ ) simultaneously. The method uses the lower bound of plasticity: equilibrium of the structure under a system of external loads and yield condition not violated anywhere in the structure (Narayanan and Beeby, 2005).

The basic concept of the method consists in the definition of a truss model that contains:

- Compression members – concrete struts;
- Tension members – steel reinforcement and concrete ties;
- Connection members – nodes;

Several models may be developed for the same problem. There is no unique solution and the process to define the best model may be iterative. However, in the best model, struts and ties should be located according to the direction of principal compressive and tensile forces (following the stress paths). In addition, the number of members and deformations should be minimized (principle of minimum strain energy). For the definition of such model, linear elastic finite element calculations can be very useful. According to (Narayanan and Beeby, 2005), angles between strut and ties should generally be greater than  $45^\circ$ . A more flexible criterion is given by (Kunz, 2009) where the angle of an inclined compression strut with the horizontal direction should be between  $30^\circ$  and  $60^\circ$ . In Fig. II.12-a) a STM for a single span beam is illustrated. In such models, struts are usually represented by dashed lines and ties by continuous lines. In this example, bottom compression strut and longitudinal reinforcement are used to resist bending moment while diagonal struts and vertical stirrups transfer shear to the supports. Nodes are the regions where tension and compression members join. Accordingly, four types of nodes may be identified:

- CCC – only struts are connected at the node;
- CCT – one of the connected members is a tie;
- CTT – two or more ties are connected;
- TTT - only ties are connected.

In Fig. II.12-b) are identified the types of nodes for the single span beam example. In this case, no TTT node type exists.

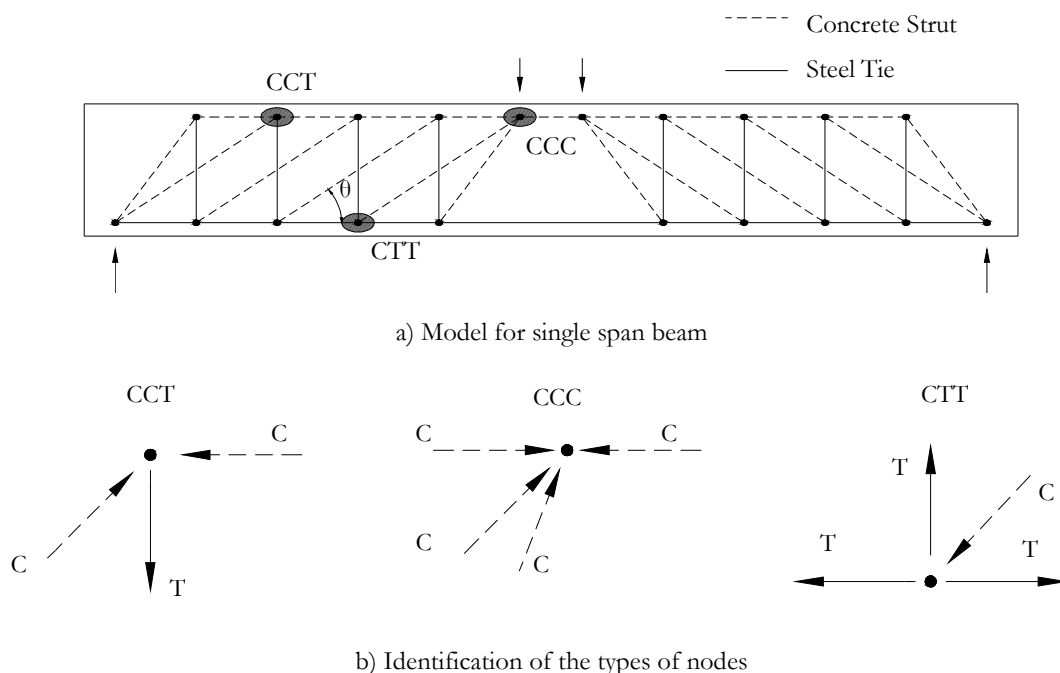


Fig. II.12: Example of STM in reinforced concrete structures (Schlaich *et al.*, 1987)

In the available literature, proposed models for beam-to-column joints in concrete structures may be found. Several of these models are illustrated in Fig. II.13. The differences between models depend mainly on the following: type of joint (single or double sided); dimension of the connecting members; and type of loading (opening or closing bending moments). Due to the similarity between these joints and the steel-to-concrete joint under study, these models are a suitable basis for the conception of a model for the joint link.

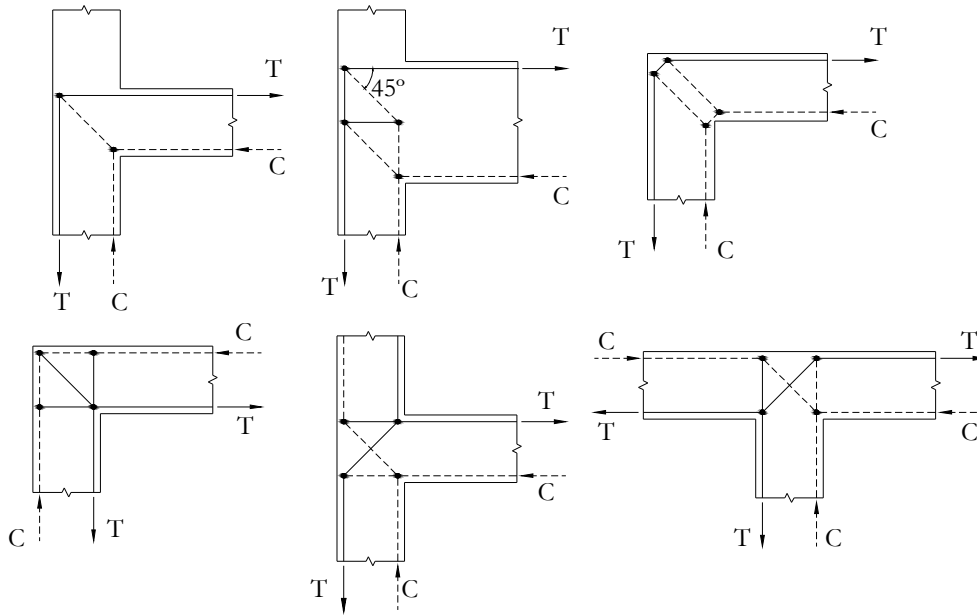


Fig. II.13: Strut-and-tie models developed for beam-to-column joints in concrete structures (Schlaich *et al.*, 1987), (Schlaich and Schäffer, 1991) and (Liang, 2006)

Finally, it should be mentioned that STMs are mostly used for design purposes in Ultimate Limit States. Only resistance is evaluated, the equilibrium is respected within model elements and no strain compatibility is required (fib, 2008). For these reasons, no evaluation of deformation is obtained with such models. Furthermore, as the stresses are limited to the yield capacity of the materials, deformations are in elastic domain and should be therefore reduced. The application of the STM for the joint link of the semi-continuous joint has the purpose of guaranteeing its structural safety and introducing directly the loads through the supporting member.

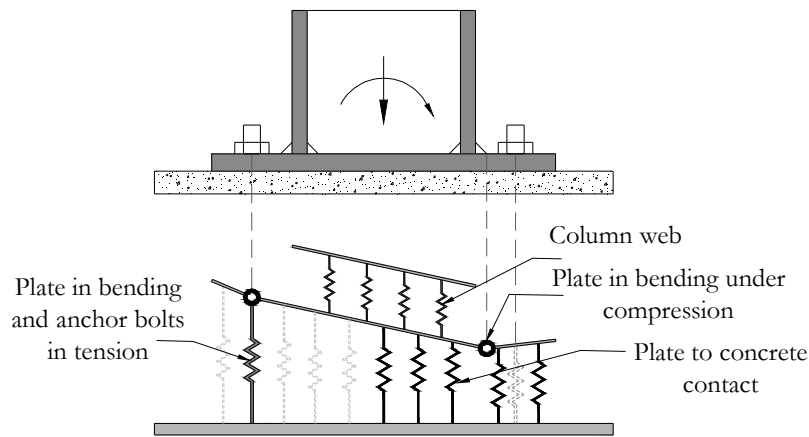
### II.2.1.3 Steel-to-concrete joints

As for the above types of joints, steel-to-concrete joints are a part of the structure where geometrical and material discontinuities can be found. In addition, connection is performed between members of different nature. To this end, the use of anchors is essential. Nowadays, a large variety of anchors are available in the market. These can be cast-in place or post-installed solutions and the transmission of load can be achieved through one or more of the following mechanisms: mechanical interlock, friction and bond. The anchors mechanical response is fundamental to the performance of the steel-to-concrete joint, under service and ultimate loads. According to the principles of the component method,

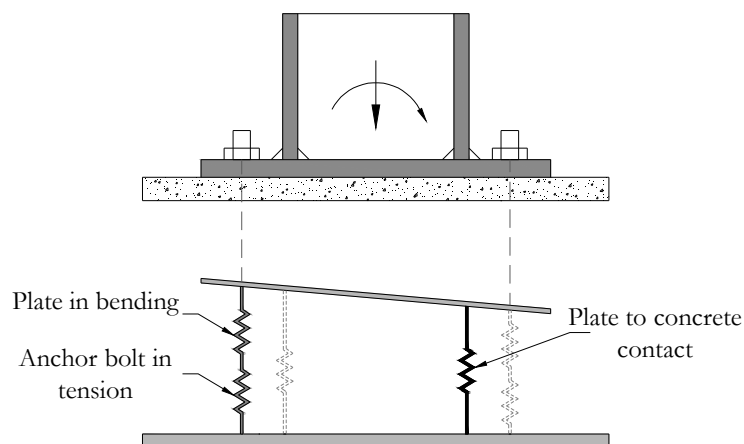
these anchors involve the activation of several components, whose behaviour is approached in the next chapter.

Although the developments on column bases have been obtained within the framework of steel joints, they should be classified as steel-to-concrete joints. This can be seen as the first approach to extend the component method to steel-to-concrete joints. However, it was not achieved in a complete manner, as the concrete part, which may have a decisive role on the response of the joint, was “left” to the concrete designer, as prescribed by the code (EN 1993-1-8, 2005). In this way, there is no unified approach and the joint has to be analysed in two stages.

For the analysis of column bases, two component based models stand out from the past developments (Heron, 2008). These are illustrated in Fig. II.14. The sophisticated model proposed by (Guisse *et al.*, 1996) is a complex 2D non-linear spring model which reflects in detail the mechanic of the column base. The model, developed based on a series of experimental tests, takes into account the non-linear behaviour of each component (Fig. II.14-a) where an iterative procedure allows describing correctly the connection behaviour. The activated components are represented considering two types of springs: extensional and rotational. The first are used for the tension and compression components, as the anchor bolts plus base plate in tension and the concrete in compression, respectively. The second represents the base plate in bending and is activated when the extended part of the plate in compression zone is subject to contact (plastic deformation of the plate in compression). The application of the model and the comparison with experimental tests (Jaspart and Vandegans, 1998) showed to be accurate. Divergence begins only for high deformation. However, the complexity of the model showed to be inappropriate for practical use. This led to the proposal (Wald *et al.*, 1996) of the simplified model presented in Fig. II.14-b) which is prescribed in the current version of code (EN 1993-1-8, 2005). In this model, the compression under the column web is neglected. Two groups of extensional springs in each side of the column are considered. One group represents the tension components and the other the compression ones. The location of the springs, and the consequent definition of the lever arm, is obtained considering: the centre of compression under the compressed column flange and the centre of tension at the anchor bolt. In the case of more than one row in tension, the centre of tension should be defined according to their stiffness, as for steel beam-to-column joints. The model is not fully in line with the real behaviour; however, it is accurate enough to assume the centre of compression under the column flange. Comparisons with experimental tests carried out by (Vandegans, 1997) and (Wald *et al.*, 2008) showed good results. In addition, the simplification assumed avoids an iterative procedure, as in the model proposed by (Guisse *et al.*, 1996).



a) Sophisticated component model for column bases (Guisse *et al.*, 1996)



b) Simplified component model for column bases (Wald *et al.*, 1996)

Fig. II.14: Component models for column bases

Still regarding to column bases, it should be mentioned that the presence of high axial load (tension or compression) affects the joint response. Therefore, the analytical determination of the joint properties is more complex than in case of beam-to-column joints where axial loading may often be neglected. In this way, the joint bending moment resistance and rotational stiffness are determined differently of (II.1) and (II.2), respectively. In the analysis of column bases, several cases have to be considered which take into account the following: type of axial loading, activated components (only compression/tension; left tension and right compression and vice-versa), and eccentricity. In (EN 1993-1-8, 2005) expressions to determine both bending moment resistance and rotational stiffness are given for all possible situations.

Column bases are not the only type of steel-to-concrete joints commonly used in construction. In many multi-storey buildings which combine steel/composite members with reinforced concrete walls, connection between these two types of members is achieved using what can be designated as anchor plates. An anchor plate consists in a steel plate fastened to a reinforced concrete member using any type of anchors. In the case of column bases, the most common type of anchors is the anchor bolt. This cast-in place



solution consists in a reinforcement bar, partially or completely threaded, installed in the concrete block with a hook or a wash plate to guarantee the anchorage. The base plate, welded to the column, is then fixed with the use of nuts. In the case of the beam-to-wall joints, different types of anchors are used which can rely on cast-in or post-installed solutions. Within the different types of anchors available, a common solution is the use of headed anchors. As referred in §II.1, here only this type of anchors welded to the plate are considered. Then in the external part of the anchor plate, a fin plate or a steel bracket is used to support the beam.

Besides the conception differences, the analysis and design of base plates and anchor plates is performed differently. Firstly, anchor plates in beam-to-wall joints are not approached in the steel and composite design codes. This type of connection has always been concern of “concrete” engineering, more precisely in the fastening technology. Secondly, the design of anchor plates disregards deformation (assumed to be small) and relies in the determination of the loads acting on the anchors. In beam-to-wall joints, the common loading of the anchor plate is shear and bending moment. Depending on the horizontal loads acting on the building, axial loads may or not be neglected. According to the European design guides and standards (CEB, 1997), (EOTA, 1997) and (CEN/TS 1992-4, 2009), the distribution of loads can be determined with elastic theory or with non-linear methods. Table II.3 summarizes the main assumptions of each method. Fig. II.15 illustrates the load distribution to consider accordingly; obviously, not all cases are considered. The elastic analysis provides a simplified and conservative approach, however, sufficiently accurate in most practical cases (Eligehausen et al., 2006). Afterwards, the anchors are designed according to the loads they have to carry. This matter is dealt later in the next section.

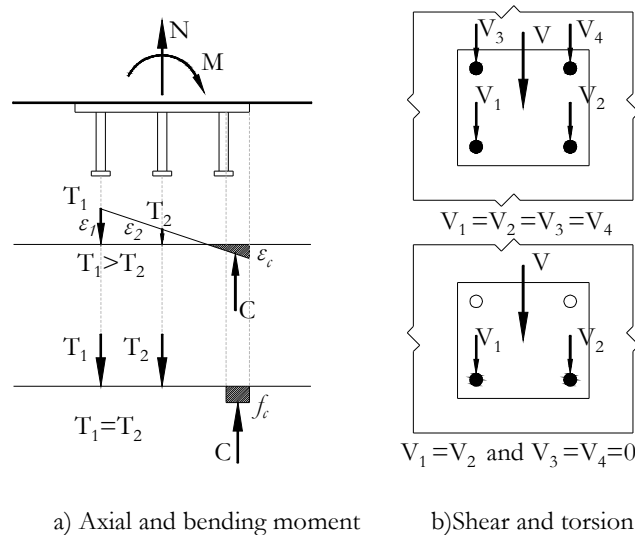


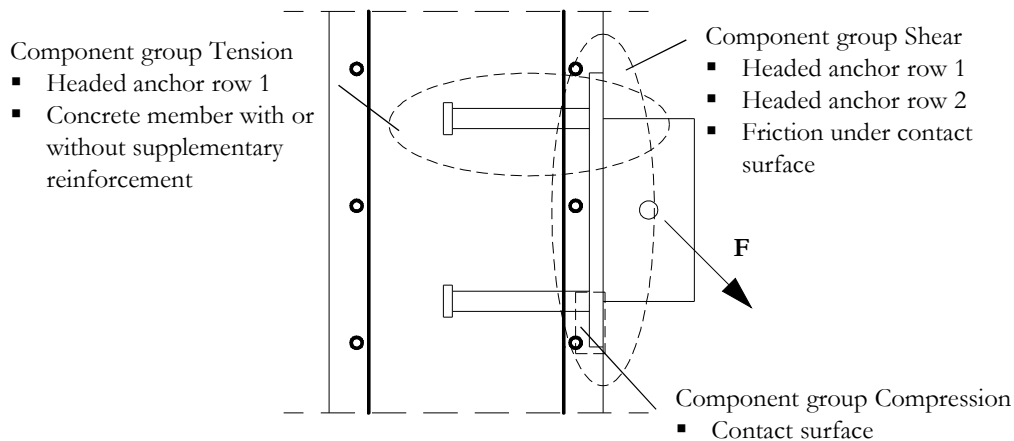
Fig. II.15: Distribution of loads in anchor plate

Table II.3: Main assumptions for the analysis of anchor plates

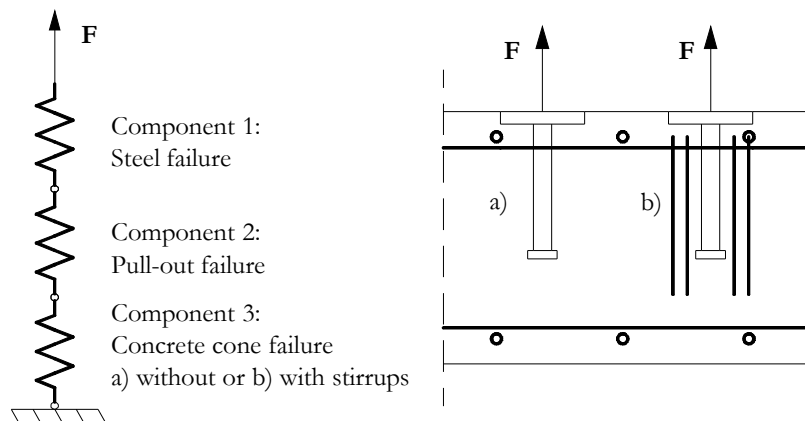
Loading Type of Analysis	Axial + Bending moment	Shear + Torsion
Elastic	<ul style="list-style-type: none"> <li>▪ Rigid plate (<math>f_{Ed} \leq f_{yd}</math>)</li> <li>▪ Bernoulli hypothesis of plane sections</li> <li>▪ Equal stiffness of all anchors</li> <li>▪ In the compression zone anchors do not contribute to the tension resistance</li> <li>▪ Steel and concrete remain linear elastic</li> <li>▪ Anchors displacements neglected</li> </ul>	<ul style="list-style-type: none"> <li>▪ For high edge distance, all anchors are assumed with equal shear stiffness</li> <li>▪ For anchors close to an edge, those near the edge carry the applied load</li> <li>▪ For shear load with eccentricity, equilibrium conditions should be applied</li> </ul>
Plastic	<ul style="list-style-type: none"> <li>▪ Failure should be governed by steel part</li> <li>▪ Minimum concrete resistance, <math>R_{d,c} \geq 1,25 R_{d,s} \frac{f_{yk}}{f_{yk}}</math></li> <li>▪ <math>f_{yk} \leq 800 \text{ N/mm}^2</math>; <math>\frac{f_{yk}}{f_{yk}} \leq 0,8</math>; <math>\epsilon_u \leq 12\%</math></li> <li>▪ The steel anchors may be assumed stressed up to their design resistance</li> <li>▪ Rectangular stress block is considered in the compressive zone</li> <li>▪ Location of the compressive zone varies according to the stiffness of the plate</li> </ul>	<ul style="list-style-type: none"> <li>▪ Shear resistance is taken by the anchors under the compression zone</li> <li>▪ If required, anchors under tension may be assigned to resistance to shear loads, where shear tension interaction should be verified</li> <li>▪ The shear resistance of the tensioned anchors should be limited</li> </ul>

The extension of the component method to anchor plate connections allows the integration of these types of connections, especially of the fastening technology, in the same design philosophy of the steel and composite joints. The principles of the component method have been applied to anchor plate connections by (Kuhlmann and Rybinski, 2007) as illustrated in Fig. II.16-a). The components activated on the steel-concrete connection are identified. Each failure mode associated to the anchorage in concrete is defined as a basic component. Especially those related to the concrete may be assumed as “New” components. In Fig. II.16-b) is shown the proposed mechanical model to represent the group of tension components. These components are identified as working in series where the weakest component defines the load capacity of the group. In order to achieve the complete characterization of the connection, the “New” basic components need to be characterized in terms of force-deformation behaviour as required by the component method. This has not been in the main concerns of the fastening technology yet. Therefore, the first step required to extend the component method is the complete characterization of the components activated within the anchorage in concrete. Toward

this end, first developments have been produced within the *InFaSo* research project (Kuhlmann *et al.*, 2012). These are presented in a later section of the present chapter.



a) Components groups of an anchor plate with two rows of headed anchors



b) Spring model of component group loaded by tension forces

Fig. II.16: Extension of the component method to anchor plate connections (Kuhlmann and Rybinski, 2007)

## II.2.2 Characterization of the joint components

### II.2.2.1 Relevant steel/composite components

One of the advantages of the component method is that the analysis of an individual component may be done independently of the type of joint. The task of assembling their behaviour is then for designers, according to the joint configuration. In Eurocode 3 (EN 1993-1-8, 2005) a list of components that may be found in the most common joint configurations is given and guidance for their evaluation is provided. The majority of these components are related to steel parts, except for the concrete in compression in column bases. In Eurocode 4 (EN 1994-1-1, 2004) the referred list is complemented by adding the components especially related to the composite joints, as the longitudinal steel reinforcement in tension and the steel contact plate in compression. In addition, the embedment of the steel parts in concrete, within the composite member, is considered.

According to the principles of the method, the behaviour of the basic components is characterized by strength, stiffness and deformation capacity (Fig. II.17). Concerning the strength and stiffness, former research works, e.g. (Zoetemeijer, 1974), (Jaspart, 1991), (Weynand *et al.*, 1996), (Wald *et al.*, 1998), led to the actual Eurocode specifications and almost all listed components are approached; however, regarding the ductility, a lack of information is still noticed. In the current version of code (EN 1993-1-8, 2005), ductility is expressed qualitatively. For few components, the deformation capacity is defined according to the sufficient or insufficient rotation capacity available for a plastic analysis. In Table II.4 is given a list of the relevant components for steel-to-concrete joints under study that may be found in the codes, as well as the clauses where specifications for their evaluation may be checked.

The application of a global plastic analysis requires the evaluation of the rotation capacity, not only for members, but also for joints. Because the behaviour of a joint is controlled by the behaviour of its components, the available rotation capacity of a joint depends on the available deformation capacity of its components. As it can be observed in Table II.4, the code provides specifications regarding the rotation capacity for barely any of the listed components. Only for the slip of the composite beam one may assume that the deformation capacity is limited by the deformation capacity of the shear connection. In (Kuhlmann *et al.*, 1998) and (Simões da Silva *et al.*, 2002) three different ductility classes have been proposed: components with high ductility (very high or nearly unlimited deformation capacity); components with limited ductility (limited deformation capacity, and softening response after maximum resistance); and brittle components (no deformation capacity, linear elastic behaviour up to failure). The various steel components were then assigned to a ductility class. From the performed classification, only the beam web and flange in compression is of interest for the present type of joints which has been classified as a component with limited ductility.

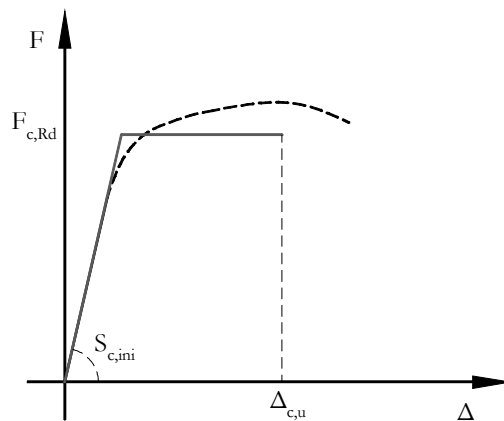


Fig. II.17: Behavioural characterization of basic components as required by the component method

Table II.4: List of components relevant for the present study in (EN 1993-1-8, 2005) and in (EN 1994-1-1, 2004)

Component	Resistance	Stiffness	Deformation Capacity
Anchor bolts in tension*	EC3-1-8 (6.2.6.12)	EC3-1-8 (6.3.2)	No information
Anchor bolts in shear*	EC3-1-8 (6.2.2)	No information	No information
Base plate in bending including compression	EC3-1-8 (6.2.6.10)	EC3-1-8 (6.3.2)	No information
Base plate in bending including tension	EC3-1-8 (6.2.6.11)	EC3-1-8 (6.3.2)	No information
Beam flange and web in compression	EC3-1-8 (6.2.7)	EC3-1-8 (6.3.2)	No information
Concrete in compression including grout	EC3-1-8 (6.2.6.9)	EC3-1-8 (6.3.2)	No information
T-stub in compression	EC3-1-8 (6.2.5)	-	-
Longitudinal reinforcement in tension	EC4-1-1 (8.4.2.1)	EC4-1-1 (Annex A – A.2.1.1)	No information
Steel contact plate in compression	EC4-1-1 (8.4.2.2)	EC4-1-1 (A2.1.2)	No information
Slip of composite beam	EC4-1-1(6.6) Defined by the level of interaction	EC4-1-1 (Annex A – A.3)	EC4-1-1(6.6) Deformation capacity of shear connectors

\*The tension and shear resistance of the steel headed anchors should be analogously determined as for anchor bolts; this is dealt in the next section.

In the semi-continuous joint configuration, the longitudinal steel reinforcement bar is the single component that is able to transfer tension forces from the beam to the wall. In addition, the experimental investigations realized within the *InFaSo* research project (Kuhlmann *et al.*, 2012) reveal the importance of this component on the joint response. For this reason, the accuracy of the joint model to predict the joint response will much depend on the level of accuracy introduced in the modelling of this component. For the remaining components, a simplified approach, as performed by the codes (EN 1993-1-8, 2005) and (EN 1994-1-1, 2004), should be satisfactory.

The behaviour of the longitudinal steel reinforcement according to (EN 1994-1-1, 2004) may be assumed bi-linear, elasto-perfectly-plastic. In terms of resistance, the longitudinal steel reinforcement may be stressed up to its design yield strength. It is assumed that all the reinforcement within the effective width of the concrete flange is used to transfer forces. Regarding the deformation of the component, the code provides stiffness coefficients for

two composite joint configurations, single and double-sided joints. This stiffness coefficient depends essentially on the elongation length of the longitudinal reinforcement contributing to its deformation. In terms of deformation capacity, depending on the steel ductility class, higher or lower deformation capacity may be obtained. To ensure ductility for a plastic distribution of forces, reinforcement bars ductility of class B or C (Demonceau, 2008), according (EN 1992-1-1, 2004), should be used.

Though the code limits the resistance of the longitudinal reinforcement to its yield strength, as a material with strain-hardening, higher stresses are attained in the reinforcement bars. The load capacity is then proportional to the ultimate strength instead of the yield strength. Furthermore, because reinforcement is embedded in concrete and because of the bond between the two materials, yielding is only achieved after cracking of the concrete. Rupture of the steel longitudinal reinforcement bars will then occur between these cracks. In terms of deformation, the bond between bars and concrete also affects its behaviour. For these reasons, in order to improve the model of the component, the behaviour of the steel longitudinal reinforcement bars embedded in concrete should be assumed differently from the bare steel bar as in (EN 1994-1-1, 2004). In (ECCS, 1999) the simplified stress-strain relationship of the embedded reinforcing steel, based on the model prescribed by the Model Code (CEB-FIP, 1993), is proposed to improve the component model. Assuming a constant area of reinforcement and defining the elongation length, the force-deformation curve may be derived from this stress-strain relationship. The determination of the force-deformation curve may, in this way, be described as follows and illustrated as in Fig. II.18.

While the concrete is uncracked, the stiffness of the longitudinal reinforcement is considerably high when compared with bare steel. Cracks form in the concrete when mean tensile strength of the concrete  $f_{ctm}$  is achieved. The stress in the reinforcement at the beginning of cracking ( $\sigma_{sr1}$ ) is then determined as follows.

$$\sigma_{sr1} = \frac{f_{ctm} k_c}{\rho} \left[ 1 + \rho \frac{E_s}{E_c} \right] \quad (II.3)$$

Where:  $f_{ctm}$  is the tensile strength of the concrete;  $E_s$  and  $E_c$  are the Young Modulus of the steel reinforcement bar and concrete, respectively;  $k_c$  is a factor which allows using the properties of the steel beam section (homogenization of composite section) and may be determined as in (II.4);  $\rho$  is the ratio between the area of steel reinforcement and the area of concrete flange as expressed in (II.5).

$$k_c = \frac{1}{1 + \frac{b_c}{2z_0}} \quad (II.4)$$

$$\rho = \frac{A_{sr}}{A_c} \quad (II.5)$$

Where:  $A_c$  is the area of the effective concrete slab;  $A_{sr}$  is the area of longitudinal reinforcement within the effective slab width;  $b_c$  is the thickness of the concrete flange and  $z_0$  is the vertical distance between the centroid of the uncracked concrete flange and uncracked unreinforced composite section, calculated using the modular ratio for short-term effects,  $E_s/E_c$ .

After the first crack occurs, an increase on the reinforcement strain ( $\Delta\varepsilon_{sr}$ ) is observed, at the crack location. The increase of the stress up to  $\sigma_{srn}$  defines the formation of the last crack. Then, after cracking stabilization, the steel reinforcement behaves as bare steel bar recovering the proportionality ( $E_{sr}$ ) between stress and strain up to yielding of the steel reinforcement bar. However, due to the tension stiffening between cracks, strain at yielding is smaller than in the case of bare steel. This range of the behaviour of the embedded reinforcement bar may be defined as follows.

$$\Delta\varepsilon_{sr} = \frac{f_{ctm} k_c}{E_s \rho} \quad (II.6)$$

$$\varepsilon_{sr1} = \frac{\sigma_{sr1}}{E_s} - \Delta\varepsilon_{sr} \quad (II.7)$$

$$\sigma_{srn} = 1,3\sigma_{sr1} \quad (II.8)$$

$$\varepsilon_{srny} = \frac{\sigma_{sr} - \sigma_{sr1}}{E_s} + \varepsilon_{sr1} + \Delta\varepsilon_{sr} \quad (II.9)$$

The ultimate strain is determined as expressed in (II.10), where the tension stiffening is also taken into account. The factor  $\beta_t$  ( $=0,4$ ) takes into account the short-term loading; and for high-ductility bars,  $\delta$  is taken equal to 0,8.

$$\varepsilon_{srnu} = \varepsilon_{sry} - \beta_t \Delta\varepsilon_{sr} + \delta \left( 1 - \frac{\sigma_{sr1}}{f_{sry}} \right) (\varepsilon_{srn} - \varepsilon_{sry}) \quad (II.10)$$

Where:  $\varepsilon_{sry}$  and  $f_{sry}$  are the yield strain and stress of the bare steel reinforcement bars, respectively;  $\varepsilon_{srn}$  is the ultimate strain of the bare steel reinforcement bars.

Assuming the area of reinforcement constant, the force-deformation curve may be derived from the stress-strain curve. However, in what concerns the deformation, the main problem relies in the elongation length to be used. According to (ECCS, 1999), the deformation is determined as follows.

$$\Delta \leq \Delta_{sry}: \quad \Delta = \varepsilon (b + L_t) \quad (II.11)$$

$$\rho < 0,8\%: \quad \Delta_{srn} = 2L_t \varepsilon_{srnu}$$

$$\rho \geq 0,8\% \text{ and } a < L_t: \quad \Delta_{srn} = (b + L_t) \varepsilon_{srnu} \quad (II.12)$$

$$\rho \geq 0,8\% \text{ and } a > L_t: \quad \Delta_{srn} = (b + L_t) \varepsilon_{srnu} + (a - L_t) \varepsilon_{srny}$$

In the above expression,  $L_r$  is defined as the “introduction” or “transmission” length and may be determined as expressed in (II.13). This parameter represents the length of the reinforcement from the wall face up to the first crack zone which should form close to the joint. The major contribution to the joint rotation should be within this zone and within the column depth ( $h$ ). In the case of the composite beam to reinforced concrete wall joint under analysis, this length ( $h$ ) is assumed from the wall face to the beginning of the hook of the longitudinal bar. The parameter  $a$  is the distance of the first shear connector to the joint. As explained below, in the case of high percentage of reinforcement, the deformation of the longitudinal reinforcement bar is assumed up to the first shear connector in the composite beam.

$$L_r = (k_e f_{dm} \Phi) / (4 \tau_{sm} \rho) \quad (\text{II.13})$$

Where:  $\tau_{sm}$  is the average bond stress which may be obtained as follows.

$$\tau_{sm} = 1,8 f_{dm} \quad (\text{II.14})$$

If the percentage of reinforcement is small, almost all deformation should be considered in the transmission zone, as expressed in (II.12). In case of higher percentage of reinforcement the elongation length increases, increasing the deformation capacity of the component and consequently the joint rotation capacity. The elongation length is then defined by: the reinforcement length within the wall before anchorage of the reinforcement ( $h$ ); the position of the main crack; and the position of the first shear connector ( $a$ ). The effect of the position of the first shear connector on the rotation capacity of composite joints was tested in (Schäffer, 2005). In this study, an increase of rotation capacity with the increase of the distance  $a$  was observed. According to (ECCS, 1999), the rupture of the reinforcement will occur within the transmission length. However; the remaining part of the elongation length contributes to the deformation capacity. The strain in the remaining part of the elongation length is conservatively assumed to be, at maximum, the reduced yield strain ( $\varepsilon_{sy}$ ) of the embedded reinforcement.

Finally, in (II.15) and (II.16) are expressed the evaluation of the component force and deformation, where the reinforcement stresses and strain should be evaluated as described above.

$$F = \sigma A_{sr} \quad (\text{II.15})$$

$$\Delta = \varepsilon l \quad (\text{II.16})$$

Note that in expression (II.16) the elongation length ( $l$ ) to consider is equal to sum of the  $L_r$  with  $h$ . Only in the determination of the ultimate deformation capacity, the length of the reinforcement bar is considered higher than this value, as expressed in (II.12).

In Fig. II.18-a) are represented the stress-strain relationship for the bare steel bar and embedded bar. The main difference is observed while the concrete is uncracked. The fact



that the bar is embedded is reflected in a stiffer response and lower ultimate deformation. In Fig. II.18-b) are shown the force deformation curves characterizing the behaviour of the longitudinal steel reinforcement bar according to both approaches, (EN 1994-1-1, 2004) and (ECCS, 1999). Remark that the sophisticated approach (ECCS, 1999) allows assuming higher resistance and estimating the deformation capacity of the component.

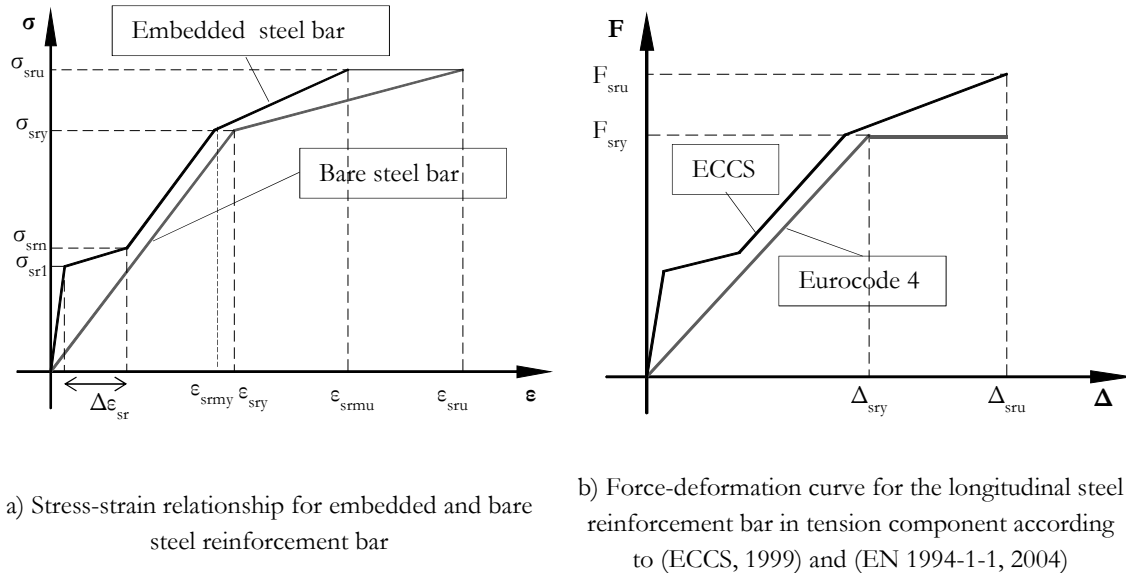


Fig. II.18: Behaviour of the component longitudinal steel reinforcement bar in tension

## II.2.2.2 “New” components related to anchorage in concrete

### II.2.2.2.1 Identification of the “new” components

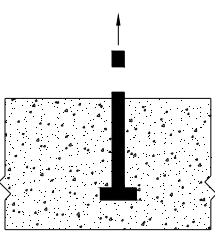
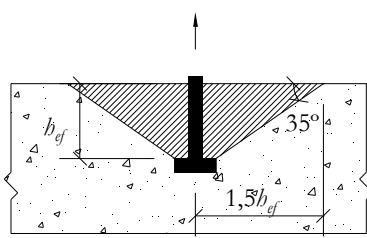
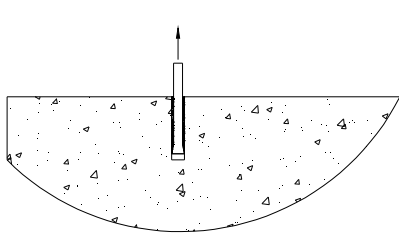
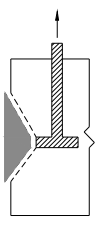
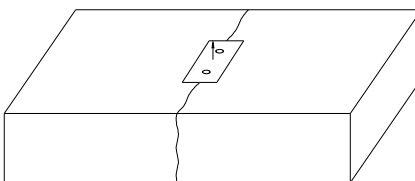
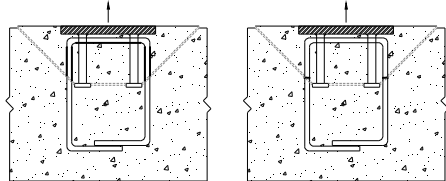
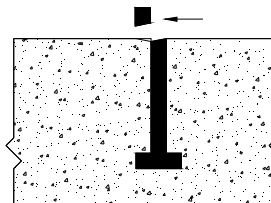
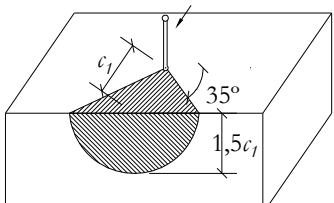
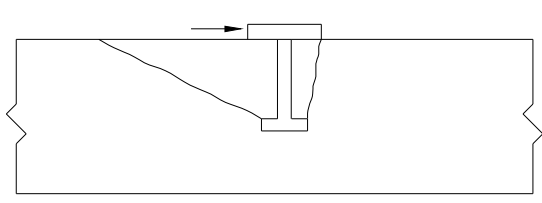
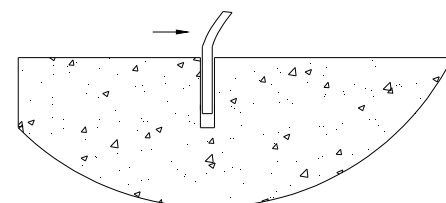
Steel-to-concrete connections introduce into the problem “new” components that are not yet taken into account by the codes (EN 1993-1-8, 2005) and (EN 1994-1-1, 2004). These regard the anchorage in concrete of the steel parts and involve the concrete material, as a possible critical part of the joint.

To perform the anchorage in concrete many different solutions have been developed in the past decades and are today well documented in several design guides as: CEB Design Guide (CEB, 1997), ETAG 001 (EOTA, 1997), ACI 318 (ACI, ACI 318: ACI Standard 318. Building code requirements for structural concrete, 2001), fib Design Guide (fib, 2007), CEN Technical Specification (CEN/TS 1992-4, 2009). The choice of the appropriate solution is then up to the engineer. Though, a variety of systems is available, the joint solutions dealt within this thesis only concern the use of headed anchors. This is a cast-in place solution which transfers the tension loads to the concrete through mechanical interlock. The small bond and friction that may develop within the anchor shaft is neglected. In (EN 1993-1-8, 2005), anchor bolts are used to perform the steel-to-concrete connection in column bases. This is the type of anchors that steel engineers are familiar with; however, they are not a common solution for beam-to-wall joints. Furthermore, in the code, the behaviour of the anchorage in concrete is reduced to the steel part of the anchorage and the concrete verification is “left” for the concrete designer.

In order to unify approaches, it is now required the complete integration of the anchorage behaviour in the component approach concept by considering the additional components activated. Applying its principles, these represent the different failure modes associated to the anchorage in concrete. The response of an anchorage in concrete depends on the type of solicitation. The anchor may be subjected to: tension, shear and combined tension and shear. Accordingly, two groups of failure modes are identified (see Table II.5). The identification of these modes is based on extensive experimental work performed in the past decades, as documented in (Eligehausen *et al.*, 2006). Besides the type of loading, the behaviour of the anchorage depends on the condition of the concrete member: cracked or uncracked. Like in reinforced concrete, hanger reinforcement may be used to increase resistance and ductility of an anchorage in concrete. It may be provided in form of stirrups or hairpins which should be located in the load transfer zone of the anchorage and properly anchored in the surrounding concrete. In practice, this type of reinforcement is only applicable to cast-in-place anchors. It may be used in both situations, anchors in tension or in shear. In the present work, only the hanger reinforcement is considered.

In Table II.5 are represented all possible failure modes for the different type of loading and installation conditions. However, for the joints under analysis only the following will be considered: i) Tension loading - steel failure, concrete cone failure, pull-out failure and yielding or anchorage failure of the hanger reinforcement; ii) Shear loading – steel failure and pry-out failure. Because of the concrete member dimensions, the type of anchors and the edge distances, the other modes of failure are disregarded.

Table II.5: Identification of the components activated in an anchorage in concrete

<b>Anchorage in Tension</b>		
		
Steel failure	Concrete cone failure	Pull-out/Pull-through
		
Local blow-out failure	Splitting failure	Yielding or anchorage failure of the reinforcement
<b>Anchorage in Shear</b>		
		
Steel failure	Concrete edge failure	
		
Pry-out failure	Pull-out failure	

#### II.2.2.2.2 Behaviour of headed anchors in tension

In the literature, the evaluation of all possible failure modes may be found. For the present thesis, only the headed anchors welded to anchor plate, installed distant from the concrete member edges, were considered. Accordingly, only the relevant failure modes are approached hereafter. Note that, safety factors are neglected.

a) Steel failure

The shaft of the steel anchor fails in tension. Depending on the type of steel, this is normally a ductile failure. In the (CEN/TS 1992-4, 2009), the characteristic resistance is limited by the conventional yield capacity of the shaft of the steel anchor and is determined as follows.

$$N_{s,k} = A_s f_{yk} \quad (\text{II.17})$$

In (Eligehausen *et al.*, 2006) the resistance is assumed up to the rupture of the anchor shaft and therefore its ultimate resistance is determined using the ultimate strength of the steel.

$$N_{us,k} = A_s f_{uk} \quad (\text{II.18})$$

In terms of deformation, up to the yield capacity of the anchor shaft, the behaviour may be assumed as linear elastic where the component stiffness is proportional to: the length of the anchor ( $l_{a,s}$ ), between head and plate; the cross-section of the anchor shaft; and the steel Young modulus.

$$K_{s,ini} = \frac{E_s A_s}{l_{a,s}} \quad (\text{II.19})$$

b) Concrete cone failure

The concrete cone failure is the most characteristic mode of failure of an anchorage in concrete subject to tension. It consists of a cone-shaped fracture surface that forms in the concrete, as illustrated in Fig. II.19. The full tensile capacity of the concrete is used. It may happen with an isolated anchor or with a group of anchors. This type of failure may occur in the case of: close spaced anchors, anchor near edge, low anchor embedment depth or small tensile capacity of the concrete.

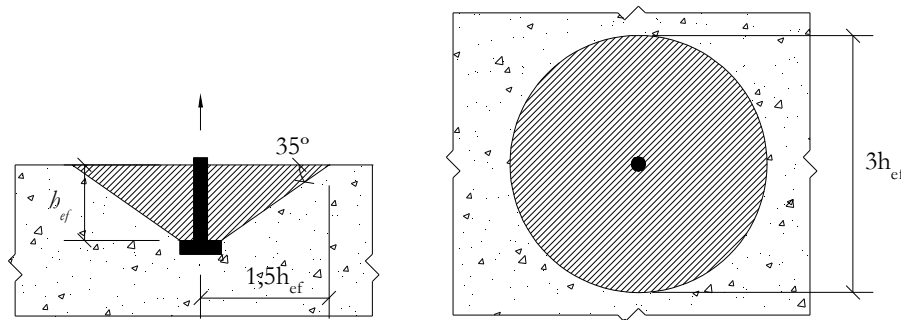


Fig. II.19: Concrete cone failure of an anchor subject to tension

In normal conditions (sufficient edge distance, anchors properly installed, sufficient embedment depth, strong steel anchor, etc) this is the type of failure that should be observed. Many authors (Eligehausen, Sawade, Ozbolt, Bazant) studied this type of failure and a method known as the CC-Method has been developed to determine the load

capacity. This is now the common practice which is prescribed by the European guides and standards as: CEB Design Guide (CEB, 1997), ETAG 001 (EOTA, 1997), fib Design Guide (fib, 2007), CEN Technical Specification (CEN/TS 1992-4, 2009). In the US, the ACI 349 design guide (ACI, 1998) prescribes a similar method that considers the failure surface with a slope of 45°. The new ACI 318-08 considers an angle of 35°. (Farrow and Klingner, 1995), (Farrow *et al.*, 1996), (Klingner *et al.*, 1998) compared the ACI method and the CC-Method with a large number of tests results. They conclude that CC-Method predicts the concrete cone capacity more accurately than the 45° cone Method prescribed by the former ACI code. Thus, the evaluation of the failure load according to the CC-Method is here described.

The concrete cone failure may be developed individually for each anchor if the spacing is sufficiently large to avoid the overlapping of the cones. Or, in the case of close anchors, a common cone forms and the failure load is smaller than the sum of the individual anchors capacity.

The resistance of a single anchor with large edge distance is given by equation (II.20),

$$N_{uc,k}^0 = k' b_{ef}^{1,5} f_{ck}^{\rho,5} \quad (II.20)$$

where:  $k'$  is a factor that takes into account the concrete tensile capacity, the surface area of the concrete cone failure and the size effect. This factor depends on the type of anchor. In the case of headed anchors the following values are proposed: 15,5 [ $N^{0,5}/mm^{0,5}$ ] (Eligehausen *et al.*, 2006); 9,0 [ $N^{0,5}/mm^{0,5}$ ] (CEB, 1997); and 11,9 [ $N^{0,5}/mm^{0,5}$ ] (CEN/TS 1992-4, 2009). In (II.20)  $b_{ef}$  is the embedment depth (Fig. II.19) and  $f_{ck}$  is the characteristic concrete cylinder compressive strength in the case of the CEB and CEN TS. In the case of formulae provided in (Eligehausen *et al.*, 2006),  $f_c$  represents the concrete cube compressive strength at the time of the test. For the latter, this resistance is obtained in concrete cubes with 200mm side ( $f_{c,200}$ ). Because of the design purposes, the values provided by (CEB, 1997) and (CEN/TS 1992-4, 2009) are conservative. If the mean load capacity of the concrete cone failure is required, the values proposed by (Eligehausen *et al.*, 2006) should be used in (II.20).

According to a slope of 35°, the individual concrete cone forms if the anchors spacing  $s$  is bigger than  $3b_{ef}$ , characteristic spacing ( $s_{cr,N}$ ). Otherwise, a common concrete cone should be considered and the ultimate failure load determined as follows.

$$N_{uc,k} = \frac{A_{c,N}}{A_{c,N}^0} N_{uc,K}^0 \quad (II.21)$$

The ratio  $A_{c,N}/A_{c,N}^0$  represents the geometrical influence of anchor spacing ( $s$ ) and edge distance on the concrete cone ( $c$ ).  $A_{c,N}^0$  is the projected area of concrete cone idealized as a pyramid of height  $b_{ef}$  and base length  $s_{cr,n} = 3b_{ef}$  ( $\rightarrow A_{c,N}^0 = 9b_{ef}^2$ ).  $A_{c,N}$  is the real projected area of concrete cone that is limited by the overlapping of the concrete cones of adjacent anchors ( $s < s_{cr,N}$ ) as well as by the edges of the concrete member ( $c < c_{cr,N}$  – minimum edge

distance to allow the complete formation of the concrete cone). Two examples on how to determine  $A_{cr,N}$  are presented in Fig. II.20. Other examples may be found in design guides as the CEB design guide (CEB, 1997).

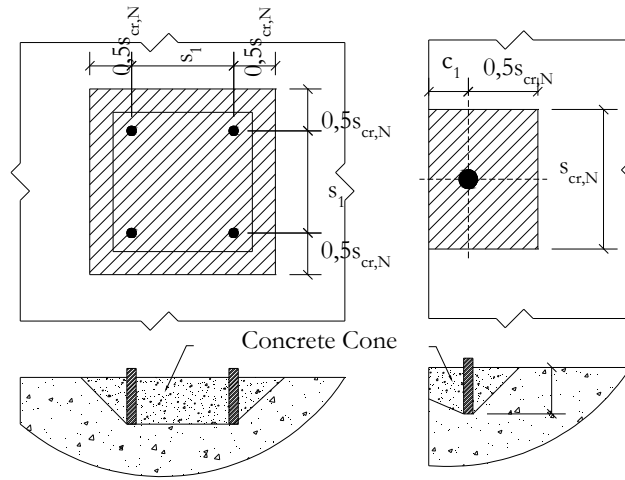


Fig. II.20: Examples for the definition of  $A_{cr,N}$

In certain situations, because of limited dimensions of the concrete member, anchors are installed close to the edges. It has been observed that for edge distances smaller than  $1,5h_{ef}$  ( $c_1 < 1,5h_{ef}$ ) the concrete cone cannot be formed completely and consequently the resistance is reduced. In order to take into account the loss of resistance due to a close edge, the factor  $\Psi_{s,N}$  defined in (II.22), should be added in (II.21),

$$\Psi_{s,N} = 0,7 + 0,3 \frac{c_1}{c_{cr,N}} \leq 1,0 \quad (\text{II.22})$$

where  $c_1$  is the real edge distance and  $c_{cr,N}$  is the edge distance required to form a concrete cone ( $=1,5h_{ef}$ ). In the case of more than one close edge, the smaller distance should be used.

In (II.21) it is considered a concentric loading however, eccentric load applications or bending moments may occur in practical situations. Thus, the factor  $\Psi_{ec,N}$  to account for the load eccentricity should be applied.

$$\Psi_{ec} = \frac{1}{1 + 2 \frac{e_N}{s_{cr,N}}} \leq 1,0 \quad (\text{II.23})$$

The parameter  $e_N$  is the distance between the resultant tensile force and the geometrical centroid of the tension-loaded anchors. In the case of eccentricity in two directions, two factors should be calculated for each direction using (II.23) and applied simultaneously in (II.21).

In the case that the anchor plate is subject to bending moment, the fact that part of the concrete is under compressive stresses may have a positive influence. The smaller the distance between the resultant of the tensile and compressive forces, the greater is the

increase in the load required to originate the concrete cone failure. In (CEB, 1997) and (CEN/TS 1992-4, 2009), this positive effect is not taken into account. The consideration of this effect into the evaluation of the concrete cone resistance is proposed in (Eligehausen and Fichtner, 2003) through the factor  $\Psi_{m,N}$  defined in (II.24).

$$\left\{ \begin{array}{l} \Psi_{m,N}=1,0 \text{ for } \frac{z_m}{h_{ef}} \geq 1,5 \\ \Psi_{m,N}=\frac{2,5}{1+\frac{z_m}{h_{ef}}} \text{ for } \frac{z_m}{h_{ef}} < 1,5 \end{array} \right. \quad (\text{II.24})$$

The lever arm  $z_m$  is calculated in accordance with the elastic theory. However, in the case of anchors situated close to an edge, this factor should be neglected if the tension part is closer to the edge (failure mechanism is dominated by the crack running towards the edge).

When the concrete member reinforcement is located close to an anchorage with small spacing, an overlap of bond stresses has been observed. In addition, the reinforcement acts as a discontinuity and reduces the volume of concrete available to transfer tensile forces. To consider these effects, (Eligehausen *et al.*, 1989) derived an additional factor. This factor is also prescribed by the design guides and standards (CEB, 1997), (EOTA, 1997) and (CEN/TS 1992-4, 2009).

$$\left\{ \begin{array}{l} \Psi_{re,N}=0,5+\frac{h_{ef}[\text{mm}]}{200} \leq 1,0 \\ \text{[if } s < 150\text{mm for any diameter or } s < 100\text{mm for } d_{sr} < 10\text{mm}] \\ \Psi_{re,N}=1,0 \\ \text{[if } s \geq 150\text{mm for any diameter or } s \geq 100\text{mm for } d_{sr} \leq 10\text{mm}] \end{array} \right. \quad (\text{II.25})$$

Several authors (Rehm *et al.*, 1988), (Eligehausen and Ozbolt, 1992), (Eligehausen and Balogh, 1995) and (Zhang, 1997) performed tests on anchors installed in cracked concrete and verified that headed anchors, in such conditions, presented an average reduction of load capacity, in comparison to uncracked condition. According with, this reduction must be attributed to the interruption of the stress field associated with the cracks. In order to take into account the concrete state, cracked or uncracked, another factor ( $\Psi_{cr,N}$ ) should be applied to (II.21). In the case of using the expression based on mean values, as proposed by (Eligehausen *et al.*, 2006), this factor should be 0,75 in the case of cracked concrete and 1,0 in the case of uncracked concrete. In the (CEN/TS 1992-4, 2009), this factor is taken equal to 1,0 if the concrete is in cracked state and 1,4 in the uncracked condition. In addition, according to this standard, in cracked condition, the factor  $k'$  in (II.20) should be taken as 8,5 instead of 11,9.

Finally, taking into account all the presented factors, expression (II.26) estimates the concrete cone failure load.

$$N_{uc,k} = \frac{A_{c,N}}{A_{c,N}^0} \Psi_{s,N} \Psi_{ec,N} \Psi_{m,N} \Psi_{re,N} \Psi_{ucr,N} N_{uc,k}^0 \quad (\text{II.26})$$

In what concerns to the deformation of this component, no information is available in the literature. In the *InFaSo* research project (Kuhlmann *et al.*, 2012) an empirical formulae has been proposed. This is discussed later in the §II.2.3.1.

c) Pull-out failure

In the pull-out failure the concrete over the anchors head is crushed. Such failure may happen when the mechanical interlock is insufficient (e. g. small anchor head). The anchorage resistance is achieved through the contact stresses generated over the head pressed against the concrete. According to the CEB Design Guide (CEB, 1997), is obtained a function of the allowable pressure stresses in concrete over the anchors head and is expressed as follows.

$$N_{p,k} = p_k A_b \quad (\text{II.27})$$

Where:  $A_b$  the area of the head pressed against the concrete ( $\pi/4(d_{ab}^2 - d_a^2)$ ) and  $p_k$  the critical pressure developed at failure. According to the design guide,  $p_k$  may take the following values:  $p_k = 11 f_{ck}$  for uncracked concrete;  $p_k = 7,5 f_{ck}$  for cracked concrete.

In terms of deformation the codes are absent of information. An empirical model was proposed by (Furche, 1994) which demonstrated reliable results. Accordingly, the deformation of the component is dependent of the load on the anchor, the surface of the anchor head under pressure and the concrete strength. The derived deformation model is expressed in (II.28). The calibration of this model required the introduction of several test parameters which consider the geometrical properties of the anchors. In the *InFaSo* research project (Kuhlmann *et al.*, 2012) this model has been used and a parameter was added to calibrate the model with the performed tests. This is discussed later in §II.2.3.1.

$$d = \frac{k_a k_A}{C_1} \left( \frac{N}{A_b f_{c,200}} \right)^2 \quad (\text{II.28})$$

With

$$a_a = 0,5(d_b - d) \quad (\text{II.29})$$

$$k_a = \sqrt{5/a_a} \geq 1 \quad (\text{II.30})$$

$$k_A = 0,5 \sqrt{d^2 + m(d_b^2 - d^2)} - 0,5d_b \quad (\text{II.31})$$

Where:  $k_a$  is a form factor at porous edge sections;  $a_a$  is the shoulder width;  $k_A$  is cross-section depending form factor;  $m$  is the pressing relation ( $m=9$  for headed anchors);  $C_1$  is the factor for headed anchors ( $=600$  in uncracked concrete;  $=300$  in cracked concrete);  $N$



the applied load to the anchorage;  $d_{ab}$  is the diameter of the anchor head;  $d_a$  is the diameter of the anchor shaft.

d) Yielding or anchorage failure of the hanger reinforcement

The hanger reinforcement should be located in the load transfer zone of the fastening and properly anchored in the surrounding concrete, as illustrated in Fig. II.21. It may be used in both situations, anchors in tension or in shear. In both loading cases, the reinforcement is activated in tension. For the present joints, only in the case of the anchor in tension is considered. In such conditions, the reinforcement is used to improve the behaviour of the anchorage upon to concrete cone failure.

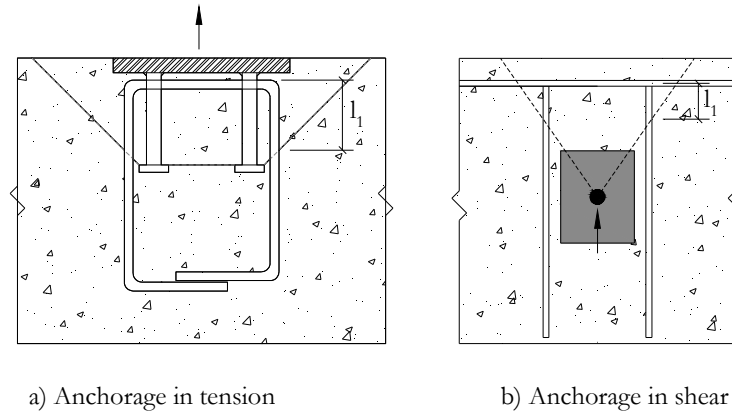


Fig. II.21: Examples of the application of the hanger reinforcement in anchorage in concrete

In the current approach the activation of the reinforcement occurs upon the development of the concrete cone. Therefore, conservatively it is assumed that the applied load is only resisted by the reinforcement and the concrete resistance should be ignored. Two failure modes may be observed: anchorage failure or yielding of the reinforcement. According to (EN 1992-1-1, 2004), the resistance of one leg of reinforcement, in the concrete cone, may be determined as follows.

$$N_{ub,k} = \pi d_{shr} l_1 f_{bm} / \alpha_a \leq A_{shr} f_{yk} \quad (\text{II.32})$$

Where:  $d_{shr}$  is the diameter of hanger reinforcement,  $l_1$  is the anchorage length (see Fig. II.21),  $f_{bm}$  is the mean bond strength ( $=2,25 f_{ctm}$ ),  $f_{ctm}$  is the average concrete tensile strength ( $0,3 f_c^{2/3}$ ),  $\alpha_a$  is a factor to take into account the influence of hook ( $=0,7$ ),  $A_{shr}$  is the cross-section area of one leg of hanger reinforcement and  $f_{yk}$  is the characteristic yield strength of hanger reinforcement ( $\leq 500 \text{ N/mm}^2$ ). A similar expression may be found in the CEB Design Guide (CEB, 1997). However,  $1/\alpha_a$  is replaced by a factor 2 which takes into account the hook effect and the confinement provided by the concrete on the bond resistance of the reinforcement bar. In the case the concrete cover  $c$  is bigger or equal than  $10d_{shr}$ , the code allows the increase of  $N_{ub,k}$  by a factor of 1,5.

Expression (II.32) considers simultaneously the contribution of the bond and the hook effect in the resistance of the hanger reinforcement in the concrete cone. Consequently, both components of resistance are proportional to the length of the hanger reinforcement.

However, as observed experimentally in (Raposo, 2006), these should be separated, as the hook effect should not be influenced by the length of the hanger reinforcement. An expression to determine the resistance of the hanger reinforcement in the concrete cone considering separately the contribution of these two components (bond and hook effect) was proposed in (Kuhlmann and Immiger, 2003) and (Kuhlmann and Rybinski, 2005),

$$N_{u,b} = N_{u,b1} + N_{u,b2} \leq A_{sb} f_{yk} \quad (\text{II.33})$$

where:  $N_{u,b1}$  is the resistance obtained through the hook effect and  $N_{u,b2}$  is the bond resistance, and may be determined with (II.34) and (II.35), respectively.

$$N_{u,b1} = 0,4 A_{sb} f_{yk} \sqrt{\frac{\beta_w}{30}} \quad (\text{II.34})$$

$$N_{u,b2} = \pi d_s l_1 \tau_u \quad (\text{II.35})$$

In (II.34) and (II.35),  $l_1$  corresponds to the average length of the group of reinforcement inside the concrete cone;  $\beta_w$  is a factor that includes the concrete compression resistance determined as  $1,31f_{ck} + 5$  [MPa];  $\tau_u$  is a variable obtained by  $2,1\tau_t$ , being  $\tau_t$  the steel-to-concrete bond stress; all the other involved parameters have been described above.

In the experimental tests reported by (Henriques *et al.*, 2013) was observed that the current approach, to evaluate the improvement of the anchorage resistance due to the use of reinforcement, underestimates the experimental values of anchors installed in concrete members with surface reinforcement. The use of hanger reinforcement activated the surface reinforcement of the concrete member and, in average; the experimental ultimate load was 30% above the estimated load. The response of two of the tested specimens is shown in Fig. II.22. The response of the anchorage without reinforcement is very stiff up to its load capacity, after the concrete cone is completely formed and the cracks achieve the surface of the concrete member. As consequence, an abrupt loss of resistance is noticed. Load stabilizes when the resistance is provided by the friction and mechanical interlock within the cracks interface. In the case of the specimen with same geometric and material properties but with hanger reinforcement, the initial stiffness is similar, but the resistance and the deformation capacity increase. In what concerns the analytical predictions, expressions (II.26) and (II.32) have been used for the case without and with hanger reinforcement (HR), respectively. For the material properties, the mean values were considered. In the case without hanger reinforcement, the approximation is excellent, demonstrating the accuracy of the approach. However, in the case with hanger reinforcement the applied approach is quite limited. An improvement of the current model for an anchorage with hanger reinforcement has been proposed within the *InFaSo* research project (Kuhlmann *et al.*, 2012). This model will be presented later in §II.2.3.1.

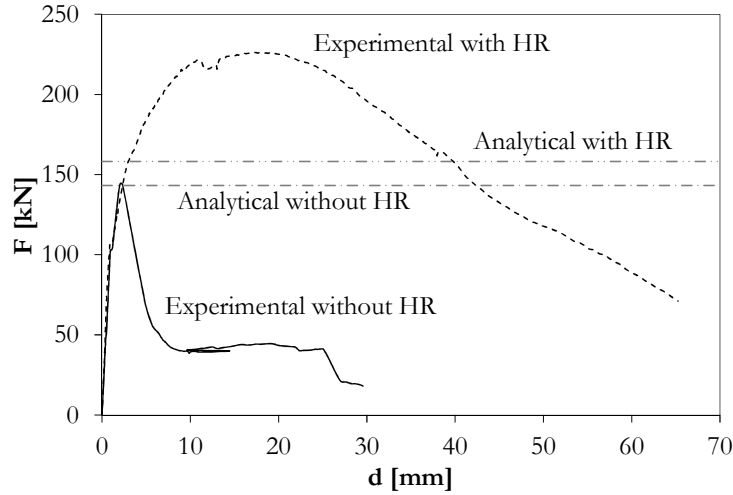


Fig. II.22: Experimental load-deformation of anchorage in tension with and without hanger reinforcement (Henriques *et al.*, 2013), and comparison with analytical models

### II.2.2.2.3 Behaviour of headed anchors in shear

According to the geometric properties and type of anchors used in the joint configurations under analysis, from the possible failure modes presented in Table II.5, for an anchorage in shear, only the steel failure of the anchor shaft and the pry-out failure should be considered. Again, only headed anchors welded to anchor plate are used and no safety factors are included in the presented expressions.

#### a) Steel failure

The steel failure of a fastener occurs when the shear capacity of the connector is exceeded. This type of failure happens mainly when the embedment depth and the edge/spacing distance are sufficiently large to avoid other types of failure. The spalling of the concrete surface may be observed before the steel failure.

The shear load applied to an anchor may be with or without lever arm. Accordingly, the resistance of the anchor is determined differently. Here, only the case without lever arm is of interest. In a shear-loaded anchor, there is a complex interaction of shear, tension and bending stresses. At the moment, no general theoretical approach to calculate the steel failure associated to this complex interaction has been proposed. Thus, a more reasonable approach is experimentally based,

$$V_{us,k} = a_{sV} A_s f_{uk} \quad (II.36)$$

where:  $A_s$  is the net/gross section area of the anchor/stud at the shear plane,  $f_{uk}$  is the characteristic ultimate steel strength and  $a_{sV}$  is a coefficient derived experimentally that traduces the ratio between the tensile and shear strength of the anchor. Many researchers have derived experimental values for  $a_{sV}$ . The generality of published result proposes 0,7 for headed studs welded to base plates.

## b) Pry-out failure

In the case of a small anchor, loaded in shear, arises the possibility of failure by pry-out fracture in the concrete. The pry-out failure is originated by the shear load that develops bearing stresses in the concrete. With the increase of the load, the surface of the concrete is crushed or spalled. The centroid of resistance ( $V_{bear}$ ) is then shifted to a location deeper in the concrete. Simultaneously, the plate rotates and loses contact in the load side leading to an eccentricity of the applied load. The resulting bending moment generates a compressive force  $C$  between the plate and the concrete and tensile force in the stud. When the tensile force exceeds the tensile capacity that can be activated by the stud in the concrete, a fracture surface is formed at the head of the stud and projected in a conical way behind it, as illustrated in Table II.5. In anchor groups a single pry-out fracture may form. The concrete pry-out failure load is proportional to the concrete cone breakout and may be calculated as follows.

$$V_{up,k} = k_1 N_{uc,k} \quad (II.37)$$

In (Eligehausen and Lehr, 1993) was observed that  $k_1$  is dependent on the embedment depth and suggested following values: 2,0 for  $h_{ef} \geq 60mm$ , < 2,0 for  $h_{ef} < 60mm$ . The CEB Design Guide (CEB, 1997) recommends  $k_1$  equal to 1,0 for  $h_{ef}$  smaller than 60mm. In the other cases, the value of 2,0 is also recommend. The same prescriptions are provided in (CEN/TS 1992-4, 2009).  $N_{uc,k}$  is analogously determined as for the concrete cone failure load for anchors in tension using expression (II.26).

### II.2.2.2.4 Behaviour of headed anchors in combined tension and shear

In many situations the load applied to the anchor is oblique (Fig. II.23). This is the case of a shear load applied with eccentricity, where the originated bending moment induces also tension in an anchor row that transfer part of the shear load. Under these combined actions, the behaviour of the anchor is in between the response to pure tension and to pure shear loading. Associated to this type of loading, the following combined failures may be observed:

- The steel anchor fails in tension and in shear; such failure may happen in the case of an anchor installed with large embedment depths and edges distances.
- The concrete fails due to tension and the steel failure is caused by shear; may be observed in anchors with average embedment depth and large edge distance; and with the increase of the angle  $\alpha$ , steel failure  $\rightarrow$  concrete failure.
- The concrete fails in tension and in shear; this case occurs when anchors are installed with small embedment depths and edge distances.
- The steel fails in tension and the concrete in shear; in order to observe such failure the diameter of the anchor should be small and installed with large embedment depth near to an edge.

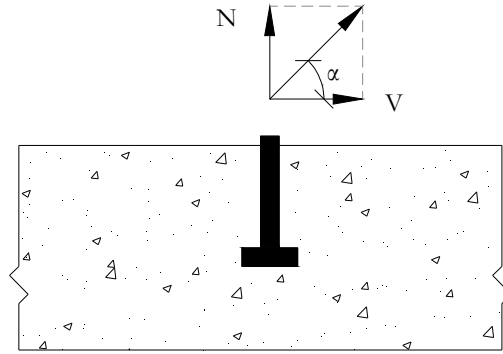


Fig. II.23: Anchor subject to combined shear and tension

The usual evaluation of tests to determine the failure load of anchors submitted to combined tension and shear is done through interaction diagrams ( $N/N_u - V/V_u$ ). In (Bode and Hanenkamp, 1985), the following tri-linear interaction relationship is proposed.

$$\begin{cases} \text{For } V/V_u \leq 0,2 \rightarrow N/N_u = 1,0 \\ \text{For } N/N_u \leq 0,2 \rightarrow V/V_u = 1,0 \\ \text{else} \quad \quad \quad \frac{N}{N_u} + \frac{V}{V_u} = 1,2 \end{cases} \quad (\text{II.38})$$

Where:  $N$  is the tension component of failure load under combined tension and shear,  $V$  is the shear component of failure load under combined tension and shear,  $N_u$  is the mean tension failure load and  $V_u$  is the mean shear failure load.

The evaluation of a group of tests, to determine the failure load of anchors submitted to combined tension and shear, is presented in (Zhao and Eligehausen, 1992). The following interaction curve is suggested to approximate the tests results.

$$\left(\frac{N}{N_u}\right)^k + \left(\frac{V}{V_u}\right)^k \leq 1,0 \quad (\text{II.39})$$

Where:  $k$  is a factor determined by regression analysis. Table II.6 presents some of the values found in the literature for this interaction formula.

Table II.6: Values of  $k$  for interaction formula depending on the failure modes, source (Eligehausen *et al.*, 2006)

ACI (1990); Cook, Klingner (1989)	$K = 1.0$
McMackin, Slutter, Fischer (1973); Meinheit, Heidrink (1985), Johnson, Lew (1990)	$K = 5/3$
Shaik, Whayoung (1985)	$K = 2.0$

The values of  $k$  depend on the failure modes observed (remember combination of failures described before). Taking  $k$  equal to 1,0 provides conservative values for all failure combinations, while the value 2,0 provides none conservative values for all cases except for

steel failure in shear and in tension. In (Eligehausen *et al.*, 2006) the value of 5/3 is suggested which provides reasonable results for the common case: concrete failure in tension and steel failure in shear. In the CEB Design Guide (CEB, 1997),  $k$  may be taken equal to 2,0 in the case of steel failure, while in the other cases 1,5 should be assumed. As a simplified and conservative recommendation, the guide suggests the value of 1,0 independently of the failure mode.

In the case of using reinforcement to take tension and shear forces, the CEB Design Guide (CEB, 1997) prescribes the following interaction formulae.

$$\left(\frac{N_{Ed}}{N_{Rd}}\right)^{2/3} + \left(\frac{V_{Ed}}{V_{Rd}}\right)^{2/3} \leq 1,0 \quad (\text{II.40})$$

Finally, in Fig. II.24 are plotted the described interaction formulae.

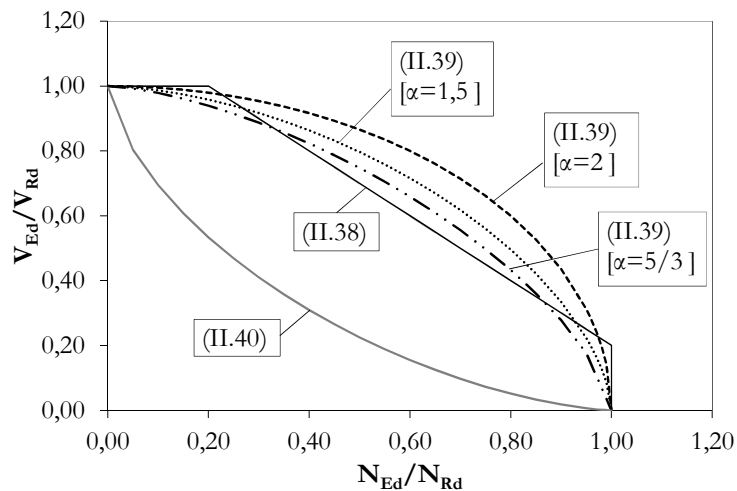


Fig. II.24: Interaction models for an anchorage subject to combined shear and tension loading

### II.2.2.3 Components in a strut-and-tie model

By performing an analogy with the component method, struts, ties and nodes are the components in the STM. Consequently, the resistance of the model is defined by the limiting component. Reinforcement ties are one-dimensional elements, while concrete struts and ties are two- (or three-) dimensional, as the stresses tend to spread in between two adjacent nodes. The dimension of strut and nodes is derived from the dimension of load application and reaction zones. Depending on the stress field, the concrete strut shape may vary: a) “fan-shaped”; b) “bottled-shaped”; c) “prism-shaped”. These are illustrated in Fig. II.25. Steel reinforcement cross-section is obtained according to the tie force to transfer and its yield strength. In what respects to nodes, “smeared” and “continuous” should be distinguished. In the first case, wide stresses fields join each other, and in the latter case, reinforcing bars are closely distributed. The geometry of the node depends on the forces applied and on the dimension of the elements converging to the nodes. The anchorage of a reinforcement bar in a node, starts at the beginning of the node and is extended beyond the node ( $l_{b,node}$ ). In Fig. II.26 are shown three possible node typologies that

may be found in (CEB-FIP, 1993) and (Schlaich and Schäffer, 1991). Additional configurations can be found in the same references.

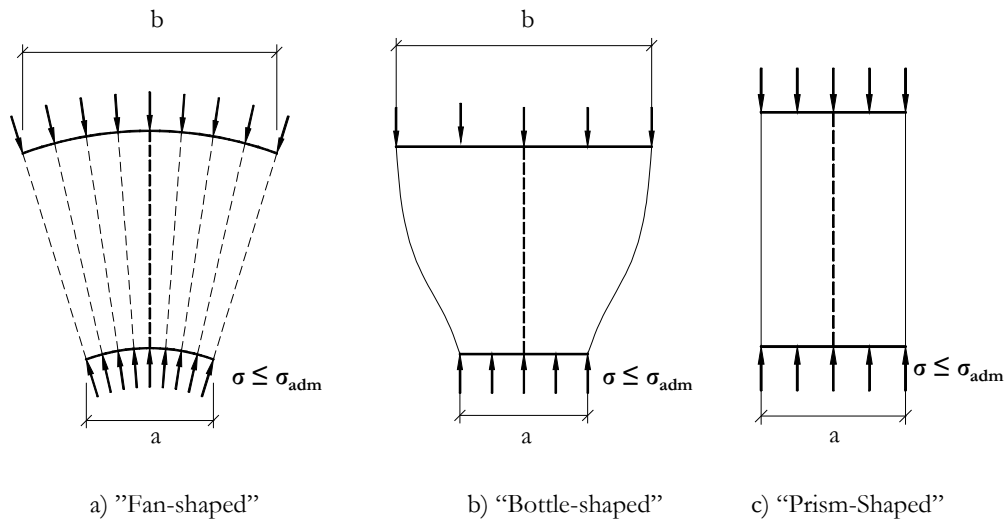


Fig. II.25: Concrete strut shape according to the stress field

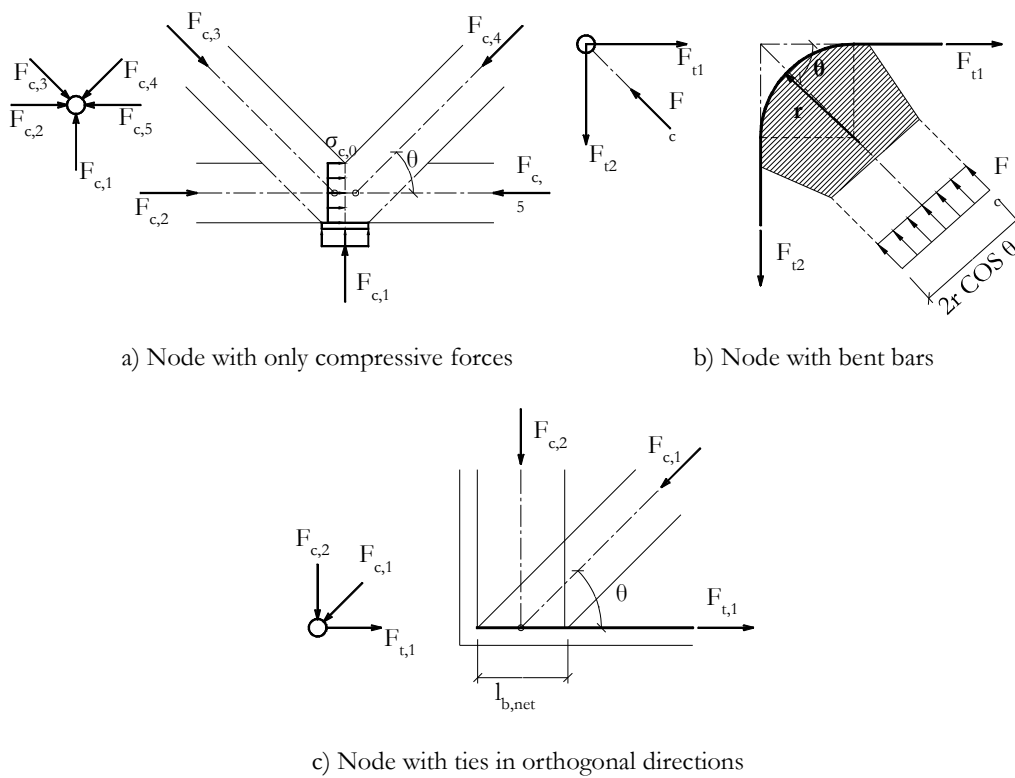


Fig. II.26: Examples of node typologies in strut-and-tie models, (CEB-FIP, 1993) and (Schlaich and Schäffer, 1991)

In what regards to the admissible stresses, for the majority of cases, recommendations are given in the code (EN 1992-1-1, 2004). These are summarized in Table II.7. Situations not considered in the code are added. This is the case of concrete ties. In some cases, although the difficulty to develop design criteria for the concrete ties, equilibrium may only be satisfied if tensile stresses may be accepted in places where reinforcement cannot be provided. According to (Schlaich *et al.*, 1987), the tensile resistance of the concrete should

only be used for equilibrium forces and where no collapse is expected. For the compression members, the admissible stresses vary according to type of transverse stresses they are subjected to. For the nodes, the type of members, converging to the node, are decisive to determine the allowable stresses.

Table II.7: Allowable stresses in strut-and tie models according to (EN 1992-1-1, 2004)

Model Element	Type	Admissible Stresses ( $\sigma_{adm}$ )
Strut	With transverse compression	$f_{cd}$
	With transverse tension	$0,6\nu f_{cd}$ with $\nu = 1 - f_{sk}/250$
	With skew cracks with extraordinary width*	$0,4f_{cd}$
Tie	Concrete*	$f_{cd}$
	Steel reinforcement	$f_{yd}$
Node	CCC	$\nu f_{cd}$
	CCC (triaxially compressed)	$3\nu f_{cd}$
	CCT	$0,85 \nu f_{cd}$
	CTT	$0,75 \nu f_{cd}$
	TTT	$0,75 \nu f_{cd}$

\*Not considered in the code. Reference used is (Schlaich *et al.*, 1987).

## II.2.3 Recent developments within the RFCS research project *InFaSo*

### II.2.3.1 Experimental and analytical characterization of the “new” components

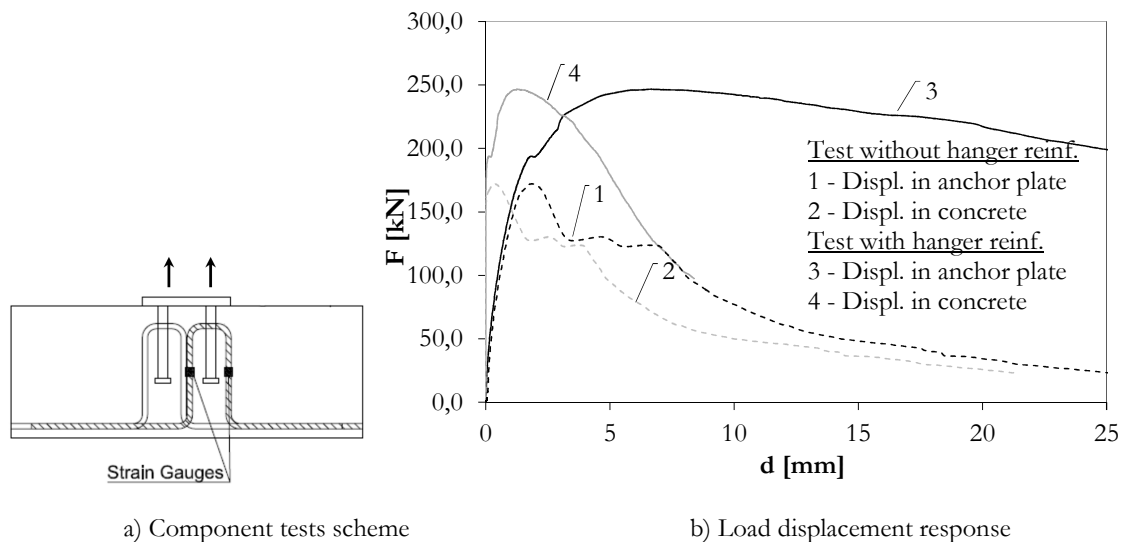
The experimental and analytical work on the “new” components activated in steel-to-concrete joints, performed within the *InFaSo* research project (Kuhlmann *et al.*, 2012), had the main objective to fill the identified gap in terms of the behavioural characterization of these components; the determination of the force-deformation response as required by the component method.

The experimental programme on components was concentrated on the anchorage in concrete. Several groups of tests were performed. The following parameters were varied: i) type of fastener, headed anchors or undercut anchors; ii) type of loading, tension and combined shear and tension; iii) concrete state, always cracked state (anchor is installed in the crack plane); iv) use of hanger reinforcement, with and without hanger reinforcement;



v) position of the hanger reinforcement, close or distant to the anchors. Here, only the tests with headed anchors in tension are discussed.

For the pure tension tested specimens, the general test procedure is illustrated in Fig. II.27-a). The relative load-displacements curves for two specimens, one without and one with hanger reinforcement are shown in Fig. II.27-b). The curves show the typical response of this type of anchorage. For each test, two curves are obtained, one representing the displacements measured in the anchor plate and the other the displacements measured in the concrete. The latter allows identifying the contribution of the concrete cone component to the global deformation of the anchorage. In what concerns the use of hanger reinforcement, the results demonstrate that this type of reinforcement increases both the resistance and the deformation capacity of the anchorage, as discussed before. The use of strain gauges (Fig. II.27-a), allowed obtaining the force in the hanger reinforcement component and consequently quantifying its contribution.



a) Component tests scheme

b) Load displacement response

Fig. II.27: Experimental work on components performed in (Kuhlmann *et al.*, 2012)

The described experimental tests are used for the development of analytical models to characterize the “new” components, not only in terms of resistance but also in terms of deformation. The proposed analytical models were developed at the Institute of Construction Materials of the University of Stuttgart. A detailed description of these models may be found in (Kuhlmann *et al.*, 2012) and (Berger *et al.*, 2011). The proposed analytical expressions for the different components activated are presented in Table II.8. The response of each component may be described as follows:

- Concrete cone failure: Up to maximum load ( $N_{u,d}$ ), the behaviour is assumed fully rigid. Then, a descending branch is observed. As a simplification, this range of the load-deformation curve is simplified assuming a linear relation between load and deformation. This is considered by a negative stiffness ( $k_c$ ) calibrated with tests. This stiffness was obtained in function of the embedded depth ( $b_{ef}$ ), the concrete resistance ( $f_{c,200}$ ), the number and disposition of the anchors ( $A_{c,N}/A_{c,N}^0$ ), as it was found for the resistance evaluation. In addition an empirical coefficient is

introduced in this model. The value proposed is limited to the range of tests performed.

- Pull-out failure: According to the model proposed in (Furche, 1994) the deformation of this component is obtained in every load step and the response is non-linear. The Furche's model was calibrated for the performed tests (Kuhlmann *et al.*, 2012) which considered the number of anchors and the introduction of an experimental parameter ( $\alpha_p$ ).
- Hanger reinforcement: the behaviour is assumed non-linear and proportional to the load in the legs. The deformation expression contains a factor 2 that takes into account the contribution of the deformation from the concrete cone and concrete member. The deformation of this component is only relevant after the formation of the concrete cone crack intersecting the hanger reinforcement leg. As for the above components, an empirical parameter ( $\alpha_v$ ) is considered whose validity is limited to the range of tests performed.
- Assembly: In Table II.8 only the equations for the case with hanger reinforcement are presented. According to (Berger *et al.*, 2011), a new mode of failure was identified. This consisted in the development of a crack surface that goes from the anchor head up to the top of the hanger reinforcement. Then, a new cone is formed from the hanger reinforcement to the concrete surface where the crack angle is 35°. The new mode of failure provides a maximum value for the resistance of anchorage with hanger reinforcement ( $N_{u,max}$ ). However, depending on the position of the hanger reinforcement, its yielding or the anchorage failure may be observed. According to the limiting capacity of the hanger reinforcement, yielding or anchorage failure,  $N_{u,1}$  or  $N_{u,2}$  should be compared with  $N_{u,max}$ . Consequently, the capacity of the group is then limited by the minimum of the resistances ( $N_{u,i}$  and  $N_{u,max}$ ). In terms of deformation, as the hanger reinforcement acts in “parallel” with the concrete cone, an expression is proposed to consider the deformation of these two components ( $\delta_{v+y}$ ). The total deformation of the anchorage is obtained adding the contribution of other activated components. For the case without hanger reinforcement, as the components are assumed working in series, the weakest component defines the resistance of the group and deformation is obtained adding the contribution of all activated components.

In Fig. II.28 is illustrated the application of the model to a case where hanger reinforcement is used. The quality of the results is very interesting. Although, the validity of the proposed analytical models are limited to the range of the tests performed within the *InFaSo* research project (Kuhlmann *et al.*, 2012), this is a very important contribution towards the extension of the component method to steel-to-concrete joints, namely the characterization of the components activated within an anchorage in concrete subject to tension loading.

Table II.8: Analytical models for the components activated in an anchorage in concrete propose by (Berger *et al.*, 2011)

Component	Analytical evaluation	New parameters
Concrete Cone	$\delta_c = 0 \rightarrow N = N_{u,c} \text{ as in (II.26)}$ $\delta_c > 0 \rightarrow N = N_{u,c} + \delta_c k_c$ $k_c = a_c \sqrt{b_{eff}} \sqrt{f_{cc,200}} \frac{A_{c,N}}{A_{c,N}^0}$	$k_c$ – stiffness of the descending branch $\alpha_c$ – test parameter which is currently -537
Pull-out	$N_{p,k} \text{ as in (II.27)}$ $0 \leq N \leq N_{u,c} \rightarrow \delta_{p1} = a_p \frac{k_u k_{u,A}}{C_1} \left( \frac{N}{A_{bf,cc,200} n} \right)^2$ $N_{u,c} < N \leq N_u \rightarrow \delta_{p2} = \frac{a_p k_u k_{u,A}}{C_1 A_b^2 n^2 f_{cc,200}^2} (2N^2 - N_{u,c}^2)$ <p>If failure is yielding of the hanger reinforcement and hanger reinforcement encloses the concrete reinforcement</p> $\delta_{p3} > \delta_{p2} \rightarrow \delta_{p3} = \delta_{p2} + \frac{N_u - N}{1000}$ <p>If failure is concrete cone or anchorage failure of the hanger reinforcement</p> $\delta_{p3} = \delta_{p2}$	$\alpha_p$ – test parameter which is currently 0,25
Hanger Reinforcement	$N_{s,k} \text{ as in (II.32)}$ $\delta_s = \frac{2N^2}{\alpha_s f_{c,200} n_s^2 d_{shr}^4}$	$\alpha_s$ – test parameter which is currently 12100 $n_s$ – the number of legs in the concrete cone
Assembly of components	<p>Resistance with hanger reinforcement (new proposal)</p> $N_u = \text{Min}\{N_{u,max}; N_{u,1} \text{ or } N_{u,2}; N_{p,k}\}$ $N_{u,max} = \Psi_{supp} N_{u,c}$ $N_{u,1} = N_{shr,k} + N_{u,c} + \delta_{sy} k_c$ $N_{u,2} = N_{ub,k} + N_{u,c} + \delta_{ub} k_c$ $\Psi_{supp} = 2,5 - \frac{x}{b_{eff}} \geq 1,0$ <p>Deformation of component concrete cone with hanger reinforcement</p> $\delta_{c+s} = \frac{\left( \sqrt{k_c (N - N_{u,c}) + 0,125 a f_{cc,200}^4 n_s^2 - \sqrt{a_s} / 8} \sqrt{f_{cc,200}^2 n_s} \right)^2}{k_c^2}$	$x$ – distance between the anchor and the crack of the concrete cone on the surface considering the crack to develop from the stirrup to the concrete surface with an angle of 35°, check (Berger <i>et al.</i> , 2011)  <i>Remark:</i> the deformation of the component Concrete Cone with hanger reinforcement is only valid for loads above $N_{u,c}$ up to this value, a rigid response is assumed.

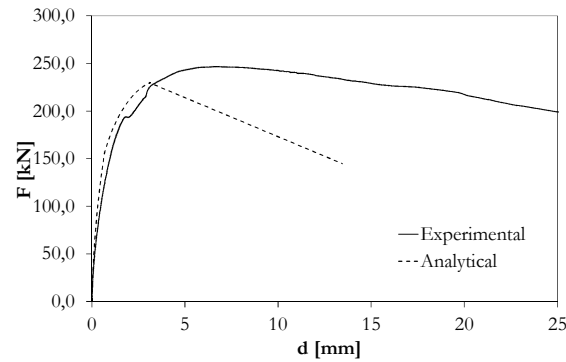


Fig. II.28: Comparison between the experimental results of anchorage with hanger reinforcement with the analytical model proposed in (Kuhlmann *et al.*, 2012)

### II.2.3.2 Experimental and analytical characterization of anchor plate connections

The experimental tests performed within the project *InFaSo* consisted in testing an anchor plate with welded headed anchors installed in a reinforced concrete wall. This is the connection foreseen for the pinned solution of the joint under study which has been illustrated in Fig. II.2. The tests were performed at the Institute for Structural Design of the University of Stuttgart and are described in detail in (Kuhlmann *et al.*, 2012). Here, only a brief summary of the test results and of the analytical model developed to evaluate the joint properties is provided.

The experimental programme was focused on the steel-to-concrete connection. A stiff anchor plate with two rows of headed anchors was connected to a reinforced concrete wall. The stiff anchor plate was used so that the concrete components were fully activated. The load was applied to the anchor plate with eccentricity. This eccentricity was varied. The joints were tested mainly in cracked concrete with and without hanger reinforcement. The cracks were installed perpendicular to the applied load and crossing the anchor row that should be activated in tension due to the eccentricity of the shear load. Furthermore, the disposition and the length of the headed anchors were varied. The test layout is illustrated in Fig. II.29 and the complete test programme is presented in Table II.9.

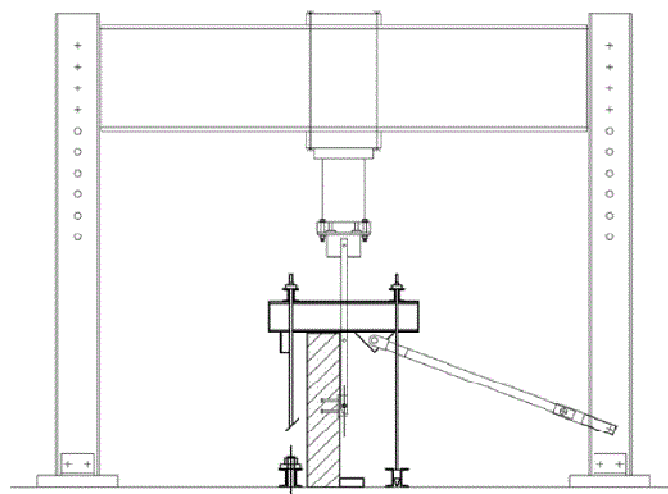


Fig. II.29: Anchor plate test layout performed within the *InFaSo* research project (Kuhlmann *et al.*, 2012)

Table II.9: Anchor plate test programme (Ozbolt *et al.*, 2011)

Test specimen	Eccentricity [mm]	Anchorage length $h_{ef}$ [mm]	Hanger reinforcement	Concrete condition	Disposition of anchors (rows x columns)
B0-BS	53	160	-	uncracked	2x3
B1-BS	53	160	-	cracked	2x3
B1-BS-R	53	160	Yes	cracked	2x3
B2-C	139	160	-	cracked	2x3
B2-C-R	139	160	Yes	cracked	2x3
R1-C	139	160	-	cracked	2x2
R1-C-R	139	160	Yes	cracked	2x2
R2-C	139	210	-	cracked	2x3
R2-C-R	139	210	Yes	cracked	2x3

In all tests, failure was attained with concrete cone failure and/or pry-out failure. The simultaneous development of these two modes of failure is due to the loading conditions of the anchor plate, shear load and secondary bending moment. According to the level of the eccentricity, one of the failures modes becomes more relevant. In Fig. II.30 a comparison of the load-rotation behaviour of four tested specimens is shown. The load represents the shear force applied to the anchor plate and the plate rotation was determined considering the displacements at the upper and bottom anchor row. Comparing the results of the specimens with hanger reinforcement (B1-BS-R and B2-C-R) with those without hanger reinforcement (B1-BS and B2-C) an increase of resistance and ductility of the joints is observed. In what respects to the effect of the eccentricity, in the test specimens with higher eccentricity, the maximum shear load was considerably smaller (up to  $\approx 50\%$ ). In these cases, the tension concrete component governed the behaviour of the joint due to the higher tension introduced to the anchor row on the tension side of the joint. For smaller eccentricities the joint behaviour was governed by the shear failure (concrete pry-out).

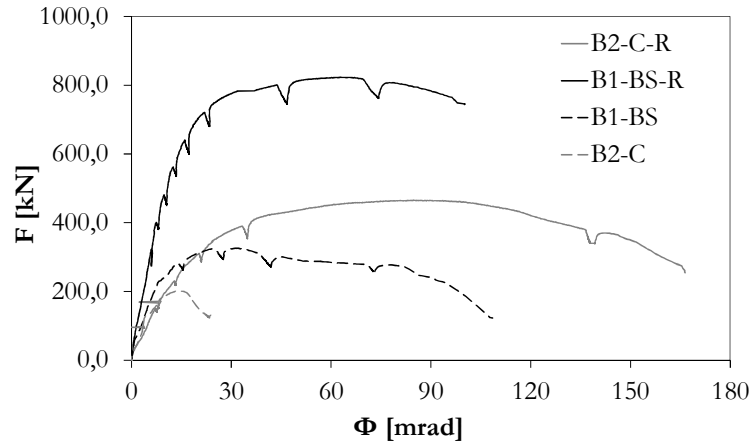
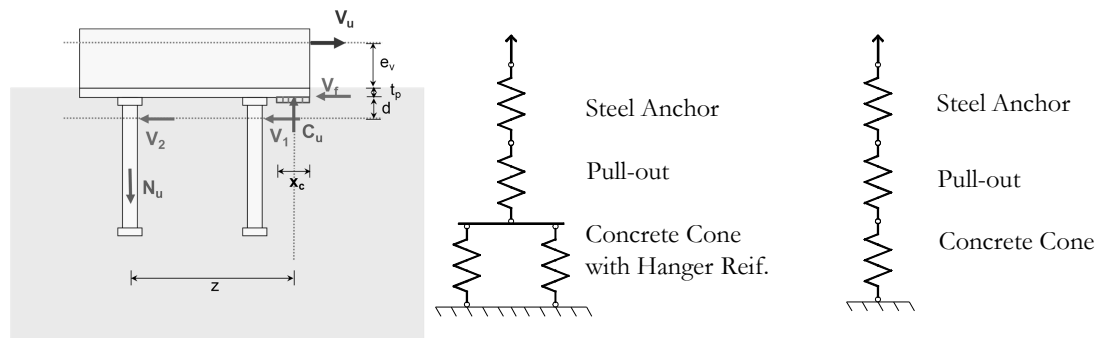


Fig. II.30: Comparison between load-rotation curves of test specimens with and without stirrups (Ozbolt *et al.*, 2011)

The focus of the experimental work was on the concrete components therefore, the developed mechanical model mainly consists of the components at the concrete side of the joint. The use of stiff anchor plate and stiff cam/fin plate allowed neglecting their behaviour, as they did not play a role. In Fig. II.31-a) is illustrated the internal loading of the joint to equilibrate the external shear load  $V_u$ . Due to the eccentricity of the latter, a secondary bending moment develops and consequently the tension components are activated on the non-loaded side of the plate (left side according to Fig. II.31-a). In Fig. II.31-b) are represented the tension components to be considered in the model of the joint. As referred before, each component represents the possible failure modes associated to the anchorage in concrete. The contribution of hanger reinforcement is considered by adding a spring parallel to the concrete cone component. For the compression zone a rectangular stress block is assumed under the loaded side of the steel plate, see Fig. II.31-a). The stresses in the concrete are limited to  $3f_{cm}$ , as proposed in (CEN/TS 1992-4, 2009). This approach requires an iterative process, as the area of the compression zone is dependent on the tension load and at the same time on the factor  $\Psi_{m,N}$  (remember expression (II.24)). The latter, is dependent on the inner lever arm  $\xi$  and therefore on the tension load. Based on this, the inner moment carried by the joint due to the shear force can be calculated.

The shear resistance is evaluated considering the sum of the shear resistance of the fasteners and the friction between the concrete surface and the anchor plate. The resistance due to friction  $V_f$  is proportional to the compression load on the bottom part and to the coefficient  $\mu_f$  for friction between steel and concrete, which may be assumed equal to 0,4 according to (Cook and Klinger, 1992). The resistance of the fasteners is dependent of two possible failure modes due to shear: Steel failure of the anchors shafts and Pry-out failure. Then, the shear load, subtracted by the friction resistance, is distributed amongst anchor rows depending on the failure mode of the tensioned anchor row. If the stress on these anchors, induced by the tension loading, is above the yield capacity of the steel of the anchors shaft, their shear stiffness should be small and all remaining shear load is assumed to be transferred at the bottom anchor row. Otherwise, an equal distribution of the remaining shear load is considered. Furthermore, the interaction between tension and shear

at the tensioned anchor row has to be considered. This interaction is assumed to reduce shear capacity of this anchor row.

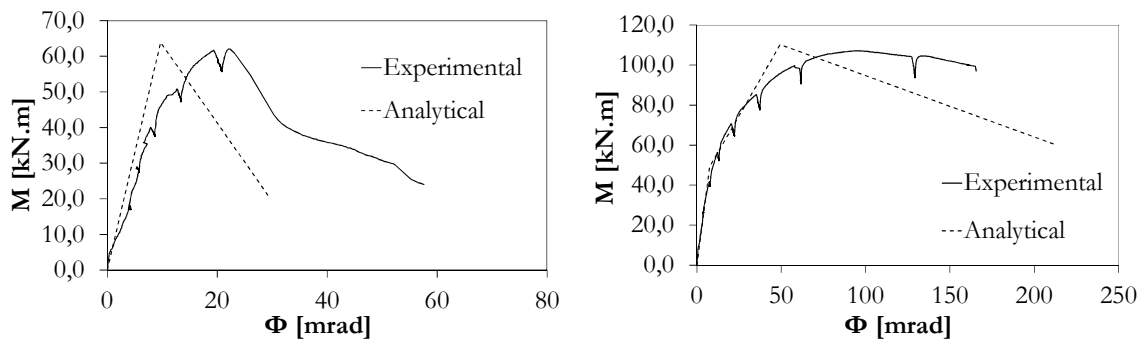


a) Schematic representation of the joint loading

b) Model for tension components

Fig. II.31: Analytical modelling of the anchor plate connection subject to shear load with eccentricity proposed in (Ozbolt *et al.*, 2011)

The comparison of the developed component model with the respective experimental results is shown in Fig. II.32. For this purpose, two specimens are used, one without and one with hanger reinforcement. These curves compare the moment-rotation behaviour of the anchor plate subject to shear. In the experimental tests, the bending moment is calculated considering the eccentricity of the shear load to the centroid of the shear resistance. In the analytical model the inner bending moment was determined using the model described above. The presented moment-rotation curves demonstrate a good agreement between results. It can be seen that the model can predict the contribution of the hanger reinforcement, for the resistance and ductility, in a satisfying way. In terms of resistance, the average approximation of the results, either for the case without hanger reinforcement or the case with hanger reinforcement, is very good. A maximum deviation of 4% is observed.



a) Test without hanger reinforcement

b) Test with hanger reinforcement

Fig. II.32: Moment-rotation curve comparing experimental and analytical results for the anchor plate subject to shear with eccentricity performed within the *InFaSo* research project (Kuhlmann *et al.*, 2012)

### II.2.3.3 Experimental characterization of the composite beam to reinforced concrete wall joint

The composite beam to reinforced concrete wall joint configuration studied within the *InFaSo* research project (Kuhlmann *et al.*, 2012) has been described in §II.1 and illustrated

in Fig. II.1. Within the project, experimental tests were performed and an analytical model was proposed. The latter had a strong contribution of the author and as an input of this thesis requires a detailed discussion. This model has been improved and is presented in §II.5. Thus, in the present section only the experimental tests are summarized. A detailed discussion of the tests and of the analytical model, proposed within the project, may be found in (Kuhlmann *et al.*, 2012).

The test programme comprised a total of six tests. Three were performed at the Institute for Structural Design of University of Stuttgart (USTUTT) and the other three at the Faculty of Civil Engineering of the Czech Technical University in Prague (CTU). The reference test specimen configuration consists of a cantilever composite beam supported by a reinforced concrete wall (Fig. II.33-a). The geometry of the test specimens was varied within each group of three tests. One specimen had the same geometric properties and therefore was common to both groups. Besides this common test specimens, the variation of geometry differed from one institution to another. In Stuttgart, the variation consisted of the percentage of reinforcement in the slab and the disposition of the shear studs ( $a$  – distance of the first shear stud to the joint face) in the composite beam. In Prague, the geometric parameters, thickness of the anchor plate and the steel bracket, were varied. The varied geometric and material properties within the different test specimens are summarized in Table II.10 and in Table II.11, respectively. The test procedure relied on applying a concentrated load at the free-end of the cantilever beam with a hydraulic jack up to failure. The tests were static monotonic. The reinforced concrete wall was fixed at bottom and top. In Fig. II.33-b) the test layout is shown. The tests were performed using control of displacements.

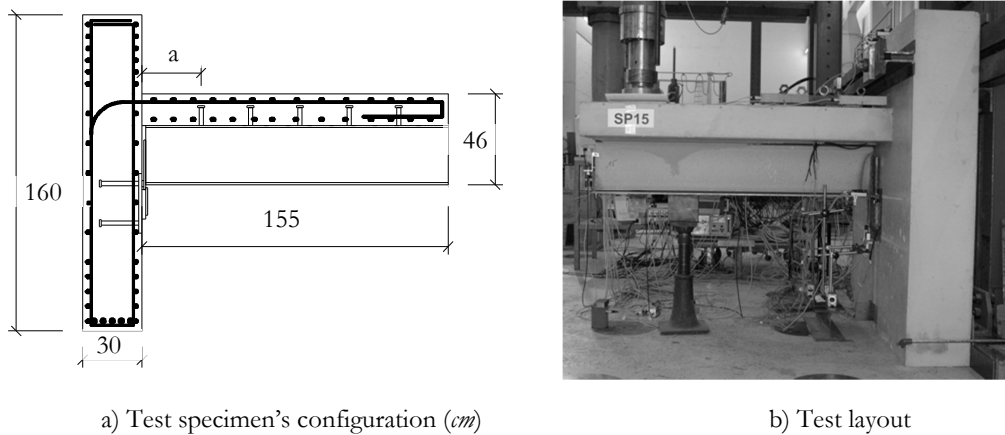


Fig. II.33: Experimental tests on composite beam to reinforced concrete wall joint (Henriques *et al.*, 2011)



Table II.10: Geometric properties of the experimental tests on composite beam to reinforced concrete wall joint (Henriques *et al.*, 2011)

	Stuttgart tests			Prague tests		
Test ID	SP13	SP14	SP15	P15-20	P15-50	P10-50
$t_{ap}$ [mm]	15	15	15	15	15	10
$t_{sb}$ [mm]	20	20	20	20	50	50
$\Phi_r$ [mm]	16	12	16	16	16	16
$a$ [mm]	500	270	270	270	270	270

In all tests failure was attained with rupture of one of the longitudinal steel reinforcement bars in tension. This made the longitudinal steel reinforcement in tension the component governing the behaviour of the joint. In Fig. II.34, the moment-rotation curves of all tested specimens are presented. In Fig. II.35 is shown a test specimen after failure. A ductile failure is confirmed by the rotation capacity achieved in all tests. The Prague tests demonstrated that the variations of the anchor plate and steel bracket geometry did not affect significantly the results. As for the Stuttgart tests, the behaviour of the joint was completely governed by the longitudinal steel reinforcement. The variation of the percentage of reinforcement in the Stuttgart tests resulted in an obvious variation of the resistance; showing an increase between SP14 and the other tests SP13 and SP15 of about 80%. In what concerns the effect of the position of the shear studs  $a$ , as observed in (Schäffer, 2005), there is an influence on the deformation capacity of the joint. The comparison between test specimen SP13 and SP15 reveals that higher ultimate rotation is obtained with higher value of  $a$ . This result is consistent with the experimental observations in (Schäffer, 2005). For smaller values of  $a$ , the cracks concentrate near the joint face resulting in a smaller elongation length contributing to the joint rotation. The slip in the shear connection of the composite beam was measured at 4 sections along the beam length. Higher slip was observed closer to the joint, and with the increase of the distance to the joint the slip diminished.

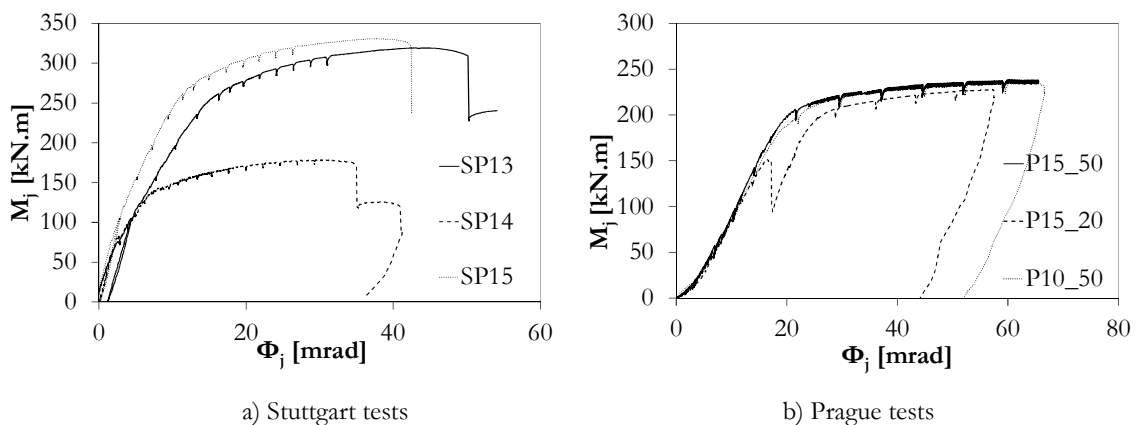


Fig. II.34: Moment-rotation curves of the tests on composite beam to reinforced concrete wall joint performed within the *InFaSo* research project (Kuhlmann *et al.*, 2012)

Table II.11: Mean values of the material properties of the experimental tests on composite beam to reinforced concrete wall joint (Kuhlmann *et al.*, 2012)

Test ID	Concrete Wall [ $f_{ck,cub}$ ]	Concrete Slab [ $f_{ck,cub}$ ]	Steel Long rebars ( $f_y$ ; $f_u$ ; $\varepsilon_y$ ; $\varepsilon_u$ )	Steel Headed Anchors ( $f_y$ , $f_u$ )	Steel Plates ( $f_y$ , $f_u$ )	Steel Profile ( $f_y$ , $f_u$ )
SP13	73,5MPa	71,3MPa	520MPa; 673,11MPa; 2,62‰; 73,58‰	460MPa; 562MPa	427MPa; 553MPa	380MPa; 539MPa
SP14	71,6MPa	66,1MPa	540MPa; 679,27MPa; 3,14‰; 81,89‰	Same as SP13	Same as SP13	Same as SP13
SP15	70,3MPa	69,9MPa	Same as SP13	Same as SP13	Same as SP13	Same as SP13
P15-50	83,3MPa	73,0MPa	Same as SP13	Same as SP13	Same as SP13	Same as SP13
P10-50	83,3MPa	73,0MPa	Same as SP13	Same as SP13	Same as SP13	Same as SP13
P15-20	71,4MPa	62,5MPa	Same as SP13	Same as SP13	Same as SP13	Same as SP13

Finally, though in both group of tests the main geometric characteristics, namely the percentage of slab reinforcement (except for test specimen SP14) and respective material properties, and the observed failure were the same, it was with surprise that the tests performed in Prague presented lower moment capacity than those performed in Stuttgart. No experimental observation provided a justification for such difference. One acceptable hypothesis consists in the fact that the test specimens for the tests in Prague presented less reinforcement than initially foreseen. Without the possibility of analysing the test specimens after the tests, this question was left without answer. Comparing all moment-rotation curves, it is noticed that in Prague tests also the initial stiffness was lower than in the tests performed in Stuttgart, as shown in Fig. II.36. Comparing test specimen P15-50 and SP15 (same geometric and material properties) one can observe that the deviation is of about 30%, which is above an acceptable value. Furthermore, comparing SP15-50 with SP14, only a decrease of 20% in the specimen resistance is obtained. The decrease of percentage of longitudinal reinforcement is about 44%. This shows an unreasonable loss of efficiency of the longitudinal reinforcement for two test specimens with similar material and geometrical properties, and similar experimental observations, as the failure mode. Comparing test specimen SP15 with SP14, the decrease of resistance is of 46% which is very close to the reduction in the percentage of reinforcement. This is a more reasonable

result. For these reasons, the tests performed in Prague are excluded later on when validating the numerical and analytical models developed within this thesis.

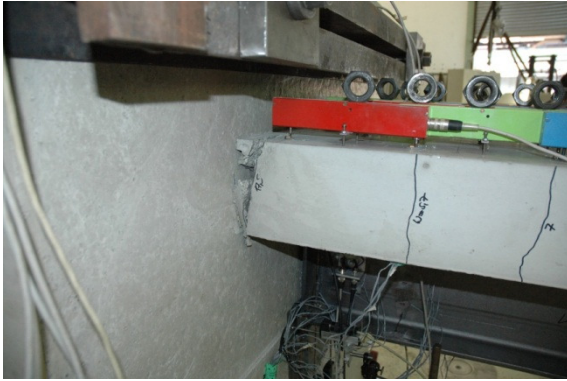


Fig. II.35: Test specimen SP14 at failure (Kuhlmann *et al.*, 2012)

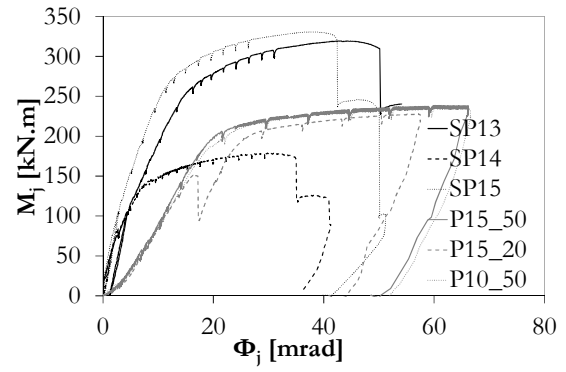


Fig. II.36: Moment-rotation curve comparing Stuttgart and Prague tests (Kuhlmann *et al.*, 2012)

## II.3 Anchor plate connection

### II.3.1 Anchor plate subject to compression

#### II.3.1.1 Introduction

In the present section, a detailed analysis of the anchor plate connection under similar conditions to those within the semi-continuous joint configuration is presented. Considering the limited information available from the experimental tests, this is a required input for the behavioural characterization of the complete joint. Thus, in order to provide a comprehensive analysis of its mechanics, the anchor plate is “extracted” from the complete joint and studied as an isolated connection.

The working conditions of the anchor plate within the semi-continuous joint configuration under analysis have been described in §II.1. Accordingly, the anchor plate connection is here subjected to pure compression and the shear load neglected, as illustrated in Fig. II.37. No specific experimental tests, considering the anchor plate in such circumstances, were produced within the *InFaSo* research project (Kuhlmann *et al.*, 2012) or found in the available literature. The problem is then here investigated using only finite element modelling.

The main outcome of the present section is the numerical and analytical models to characterize the response of the anchor plate connection within the complete joint. Analogously to column bases, the problem can be seen as the component plate in bending under compression with headed anchors on the non-loaded side of the plate. In (EN 1993-1-8, 2005), the referred component may be represented by a T-stub in compression which is a simplified model with practical interest. However, this model cannot take into consideration the effect of the headed anchors on the non-loaded side. Therefore, a sophisticated modelling of the anchor plate in compression reproducing their effect is envisaged. Because of the similarities, the proposed model is based on the sophisticated model for columns bases proposed in (Guisse *et al.*, 1996) performing the required adaptations. Finally, for practical use, a modification of the T-stub in compression is foreseen to incorporate the component in the complete joint model.

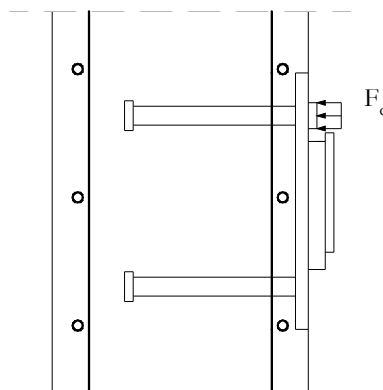


Fig. II.37: Anchor plate subject to pure compression

## II.3.1.2 Numerical modelling

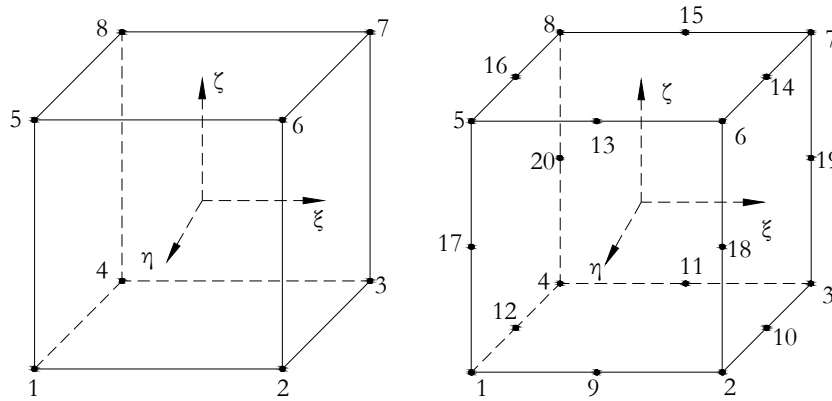
### II.3.1.2.1 Finite element program and modelling tools

The numerical tool used is the non-linear finite element package (Abaqus, 2011). The software provides a complete and flexible solution for a large range of problems. The number and the variety of finite elements available in the ABAQUS library are quite large. Geometric and material non-linearities can be included in the analysis. Different numerical techniques are available allowing the resolution of the non-linear problem using implicit or explicit methods. Regarding the mesh, the software offers both automatic and manual meshing techniques. Because of its application to a wide range of engineering problems, a complete description is outside of the scope of the thesis. More detailed information about the program may be found in (Abaqus, 2011).

The anchor plate in compression is a three dimensional problem therefore, the numerical model developed used solid elements and geometrical and material non-linearities were taken into account. Furthermore, concrete-plate and concrete-anchor interactions were treated in numerical simulations as contact problems. A brief description of the most relevant modelling tools used in the numerical simulations of the anchor plate is given below.

#### a) Finite elements

The ABAQUS finite elements library provides a varied number and type of finite elements suitable for a wide range of engineering problems. Amongst these, the continuum stress/displacement 3D solid finite elements of linear (Fig. II.38-a) and quadratic (Fig. II.38-b) order are of interest for the present application. For both, a version with reduced and full integration is available. Table II.12 provides a summary of the main characteristics of these elements. The selection of one element or the other depends on the application. For plasticity-controlled type of problems, in which the elements have to reproduce yield lines, i.e. discontinuities in the strain field, the first-order elements are likely to be the most successful, because some components of the displacement solution can be discontinuous at the element edges (Abaqus, 2011). The 8-node full integration element can exhibit shear locking in bending dominated problems while the reduced integration version may suffer from hour glassing when the mesh is coarse. In the first case, the response may become too stiff while in the latter a flexible result may be obtained. In order to avoid these numerical difficulties, the use of reduced integration elements with finer meshes may be the solution. Hence, the 8-node element with reduced integration was chosen for the general numerical simulations. A sensitivity analysis was performed with respect to the element type in order to calibrate the use of the first order elements with reduced integration.



a) Linear order solid element with 8 nodes b) Quadratic order solid element with 20 nodes

Fig. II.38: 3D solid finite elements selected for numerical calculations

Table II.12: Main properties of the finite elements selected for numerical calculations

Finite elements	Main properties
C3D8R	<p>8 nodes</p> <p>1 integration point</p> <p>3 degrees of freedom per node</p> <p>Hourglassing problems (zero strain in integration point)</p>
C3D8	<p>8 nodes</p> <p>8 integration points</p> <p>3 degrees of freedom per node</p> <p>Shear lock problems (unrealistic high shear strains)</p>
C3D20R	<p>20 nodes</p> <p>8 integration points</p> <p>3 degrees of freedom per node</p> <p>Hourglassing problems (zero strain in integration point)</p>
C3D20	<p>20 nodes</p> <p>27 integration points</p> <p>3 degrees of freedom per node</p> <p>High time consuming</p>

#### b) Interactions

In the anchor plate problem two types of interactions are considered. First, because the welds between steel parts are neglected, plates are connected to each other considering a rigid connection between contacting surfaces. In ABAQUS, this type of interaction is denominated as Tie Constraint and is based on a Master-Slave surface interaction. The

degrees of freedom of the Master surface enforce the displacements on the degree of freedoms of the Slave surface. No sliding is allowed between surfaces. The Tie constraint is also useful for mesh refinement purposes, as it allows creating a discontinuity in the mesh without losing the mechanical continuity.

The second type of interaction regards “real” contact problems between steel and concrete parts. In this case, the interaction is modelled using the “hard” contact without friction model for the normal direction. This contact model is also based in a Master-Slave surface interaction. In the normal direction, when in contact, any pressure can be transmitted and a zero-penetration is enforced or minimized. On the other hand, if no contact exists, no pressure exists. In Fig. II.39-a) is illustrated the behaviour of the model selected to solve the contact problem in the normal direction. In the tangential direction, the behaviour is assumed frictionless. In this way, if master and slave surfaces are in contact and pressure is developed, no shear stress develops and the surfaces are free to slip. The assumed behaviour is shown in Fig. II.39-b). Friction models are available in (Abaqus, 2011) however, for the particular case of the anchor plate, the friction forces are negligible and therefore, the contact model is simplified in order to minimize convergence problems and the required calibrations.

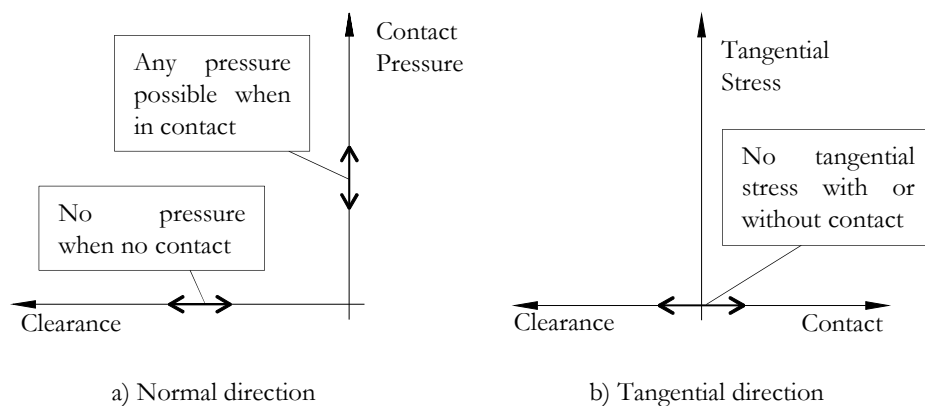


Fig. II.39: Contact model

### c) Constitutive models

The constitutive laws used to model the mechanical behaviour of the materials, concrete and steel, are the Concrete Damage Plasticity and the Isotropic Material, respectively.

The behaviour of concrete may be modelled in ABAQUS using one of the following constitutive models: Concrete Smeared Cracking; Concrete Damage Plasticity; Drucker-Prager. According to (Gil and Bayo, 2008), the Concrete Damage Plasticity was chosen because it is simpler to model and more stable for the numeric calculation. The Concrete Damage Plasticity constitutive model is defined by a uniaxial compression and tension response (Fig. II.40), where five constitutive parameters are needed to identify the shape of the flow potential surface and the yield surface (Jankowiak and Lodygwoki, 2005). In the analysis of the anchor plate under pure compression, the constitutive response assumed for the concrete in compression is Parabola-Rectangle diagram for stress-strain relation as prescribed by the (EN 1992-1-1, 2004). As from the test reports only the usual parameters

are reported (compression strength and Young's modulus), the concrete uniaxial compressive behaviour is obtained by applying expression (II.41), as specified in (EN 1992-1-1, 2004).

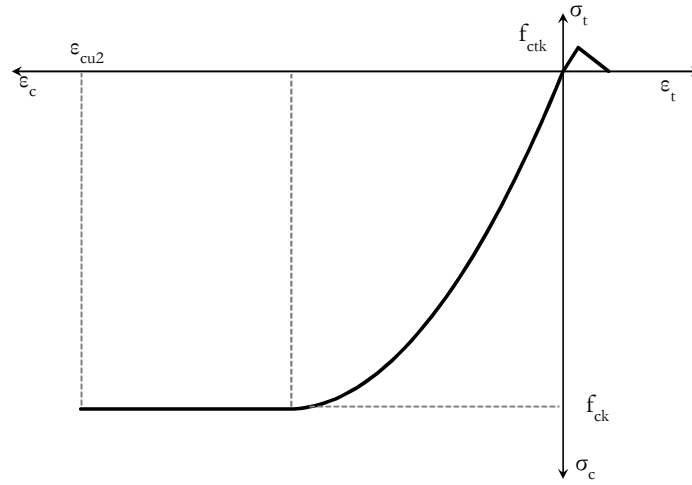


Fig. II.40: Uniaxial response of the concrete considered in (Abaqus, 2011) for the analysis of the anchor plate under pure compression

$$\sigma_c = f_{ctk} \left[ 1 - \left( 1 - \frac{\varepsilon_c}{\varepsilon_{c2}} \right)^n \right] \quad \text{for } 0 \leq \varepsilon_c \leq \varepsilon_{c2} \quad (\text{II.41})$$

$$\sigma_c = f_{ctk} \quad \text{for } \varepsilon_{c2} < \varepsilon_c \leq \varepsilon_{cu2}$$

Where:  $\sigma_c$  is the concrete stress;  $f_{ctk}$  is the characteristic concrete cylinder compressive strength;  $n$  is an exponent depending of the concrete class and may be obtained in (EN 1992-1-1, 2004);  $\varepsilon_c$  is the concrete strain;  $\varepsilon_{c2}$  is the compressive strain at the peak stress  $f_{ctk}$ ; and  $\varepsilon_{cu2}$  is the ultimate compressive strain of the concrete.

In tension, the behaviour is assumed elastic up to the onset of cracking and then followed by tension stiffening. Tension stiffening may be introduced in the calculations by means of a Stress-Cracking Strain curve, a Stress-Displacement curve or Fracture Energy. The latter is used in the present models. However, this parameter was not provided in test reports. Thus, according to (fib, 2010), the fracture energy ( $G_f$ ) is estimated as expressed in (II.42). Finally, for the five constitutive parameters ( $\psi_{ab}$  – dilatation angle;  $\varepsilon_{ab}$  – flow potential eccentricity;  $f_{b0}/f_{c0}$  – ratio of initial equibiaxial compressive yield stress to initial compressive yield stress;  $k_{ab}$  – is the ratio of the second stress invariant on the tensile meridian,  $q(\text{TM})$ , to that on the compressive meridian,  $q(\text{CM})$ , at initial yield for any given value of the pressure invariant  $p$  such that the maximum principal stress is negative  $\sigma_{p,max} < 0$ ;  $\mu_{ab}$  – viscosity parameter) required to complete the definition of the constitutive model, in the absence of experimental information, the default values according to (Abaqus, 2011) presented in Table II.13 are used.

$$G_f = 73 f_{cm}^{0,18} \quad (\text{II.42})$$



Table II.13: Constitutive parameters to complete the definition of the Concrete Damage Plasticity for concrete in (Abaqus, 2011)

$\psi_{ab}$	$\varepsilon_{ab}$	$f_{b0}/f_{c0}$	$k_{ab}$	$\mu_{ab}$
38°	0,1	1,16	0,67	0

To model the behaviour of structural steel, the classical isotropic material law that implements the von Mises plasticity model (isotropic yielding) is used. This model uses the von Mises yield surface to define isotropic yielding. Then, a perfect plastic or isotropic hardening behaviour may be considered. In the case of the anchor plate connection, all steel parts are modelled using an elasto-perfectly-plastic response.

d) Numerical strategy for resolution of the non-linear problem

To solve the non-linear problem, the modified Riks method (Static Riks) is chosen amongst the techniques available in (Abaqus, 2011). This method allows solving geometrically nonlinear static problems showing negative stiffness in the load displacement response.

II.3.1.2.2 *Validation of numerical tool*

In the absence of specific experimental tests on anchor plates subject to pure compression, the numerical models are the main source of data to analyse the connection behaviour and to derive an analytical model. Consequently, the reliability of the numerical modelling has to be guaranteed. The validation of the numerical model, namely type of elements and constitutive models, is here envisaged using experimental data available in the literature. The response of the anchor plate in compression should be governed by the concrete under the load application zone and by the deformation of the plate defining the level of load achieving the anchor row on the non-loaded side. Thus, the following affects the connection behaviour: i) concrete compressive strength and deformation; ii) concrete-plate contact surface; iii) stiffness of the plate, controlling the load on the anchor row on the non-loaded side. In this way, experimental tests on T-stub in compression and T-stub in tension are used for validation of the numerical tool. In the first, the concrete modelling is assessed. In the latter, the plastic model for the steel is evaluated.

The experimental tests on T-stub in compression were performed in Prague and detailed information on the selected specimens may be found in (Sokol and Wald, 1997). In these tests, none of the specimens tested in compression was taken up to failure therefore mainly the initial stiffness can be compared. In all tests the same size of concrete block (550x550x550mm<sup>3</sup>) was used. Two types of tests were performed which consider the variation of the dimensions of the T-stub flange: test type I - 200x300x10mm<sup>3</sup>; test type II – 335x100x12mm<sup>3</sup>. In addition to the geometric differences, also the loading system varied. The two test types are illustrated in Fig. II.41, where the cylinder represents the hydraulic jack. The numerical models developed in ABAQUS are 3D using the type of finite elements, constitutive laws and interactions described above. Two types of elements (TI/II-C3D8R and TI/II-C3D20R) were tested and the results are shown in Fig. II.42. The

curves represent the force-deformation response and compare experimental with numerical results. For the test type I it can be observed that there is a very good agreement between experimental and numerical results independently the type of element used. According to the numerical model the resistance is considerably above the 600kN; however, the test was stopped at approximately 600kN without failure of the specimen. In this way, the model accuracy cannot be verified above this load. In what concerns to test type II, the quality of the approximation is lower but still acceptable. Though, it should be noticed that for the same type of concrete, at about 200kN, a considerable loss of stiffness occurs. From the tests report no justification was given to this observation. Numerically, at approximately this loading level, the steel bar representing the T-stub web achieves its yield capacity. Consequently, the response was governed by this part of the T-stub. Finally, it should be mentioned that convergence of results is obtained with two numerical models with different type of elements. Consequently, the use of first order elements with reduced integration is validated.

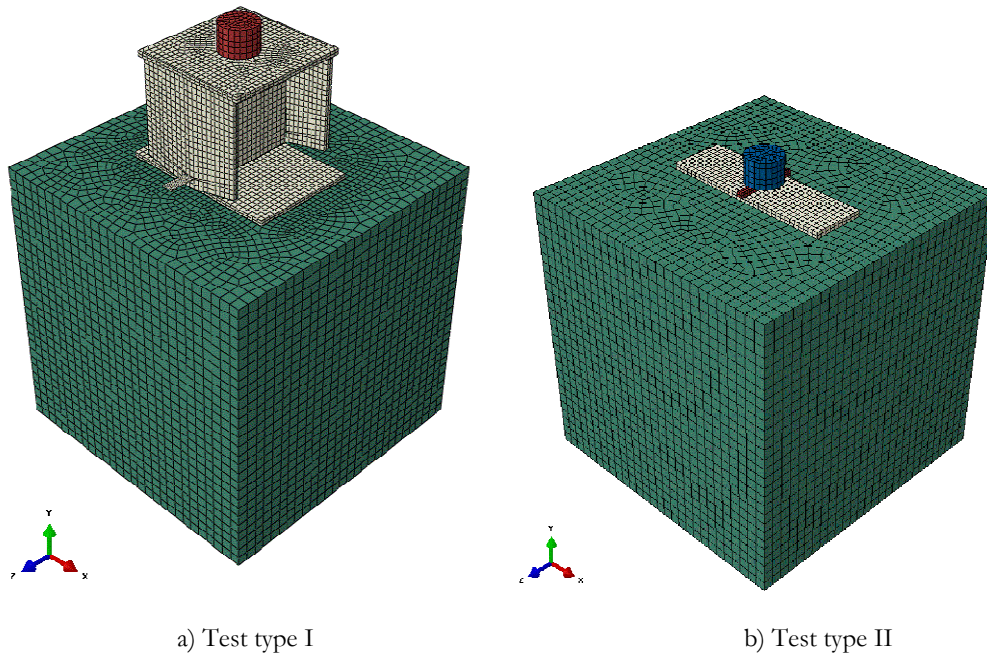


Fig. II.41: Numerical models on the T-stub in compression

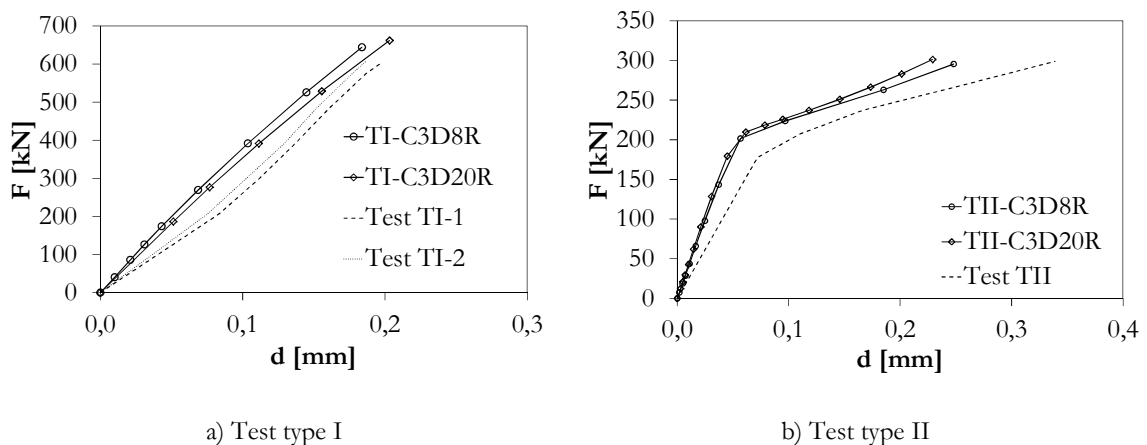


Fig. II.42: Comparison between experimental and numerical results for the T-stub in compression

For validation of the plastic model of the steel parts, one of the tests on T-stub in tension reported in (Bursi and Jaspart, 1997) was selected. The T-stub is produced from an IPE 300 and the bolts are non-preloaded, as illustrated in Fig. II.43-a). Detailed information on the geometric and material properties of the test specimen may be checked in (Bursi and Jaspart, 1997). The true stress-logarithmic strain properties of the materials were used and are depicted in Fig. II.44. Fig. II.43-b) illustrates the numerical model developed. Profiting from the geometry of the problem, only one quarter of the specimen is considered. Two models are developed, one considering the use of first order elements (TS-C3D8R) and another that uses second order elements (TS-C3D20R). Experimentally, failure that results from relevant flange yielding was observed. However, inelastic deformations were also registered in the bolts. This indicates that the failure is between mode 1 and mode 2. The load-deformation curve that compares experimental and numerical results is shown in Fig. II.45-a). The deformation corresponds to the variation of the distance  $d$  ( $\Delta d$ ). The results show a good agreement between tests and numerical models. A small deviation is observed in the plastic region which may be attributed to the bolt tightening not considered in the numerical model. Fig. II.45-b) illustrates the deformation of the T-stub and the elements “actively yielding” for a load of approximately 170kN. The formation of the plastic hinges in the flange is clearly identified. These occur in two parallel “lines”, one passing through the bolt and adjacent to the T-stub web. These results are in line with the experimental observations and attest the accuracy of the numerical modelling. The two models with different type of elements, first and second order elements, demonstrate the convergence of the numerical results.

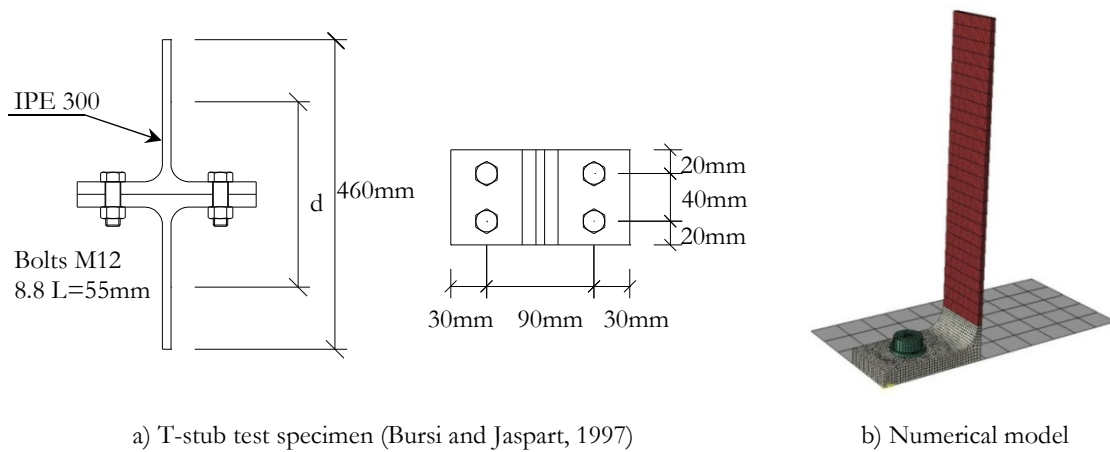


Fig. II.43: FE model to assess the plastic model for steel plates

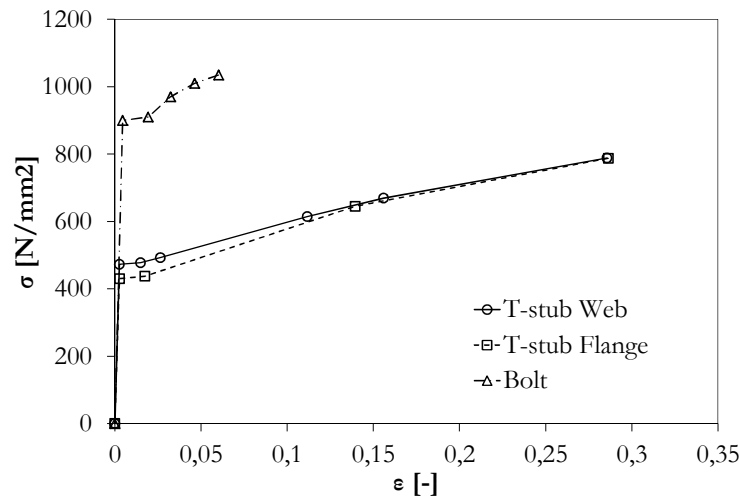
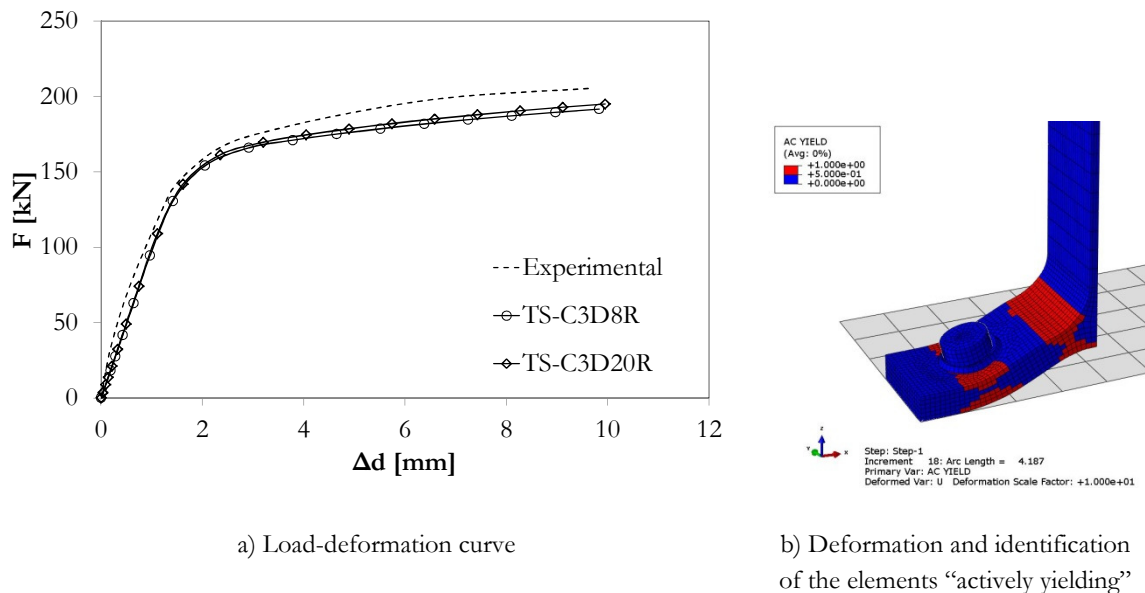


Fig. II.44: Material properties of the test specimen for T-stub in tension tests (Bursi and Jaspart, 1997)



a) Load-deformation curve

b) Deformation and identification of the elements “actively yielding”

Fig. II.45: Results of the T-stub in tension numerical calculations

### II.3.1.2.3 Numerical modelling of anchor plate in pure compression

A reference numerical model of the anchor plate under the loading conditions depicted in Fig. II.37 was developed to exploit the problem mechanics and to ground the formulation of the analytical model. The geometric properties of this reference case are illustrated in Fig. II.46 and given in Table II.14. A concrete block with infinite edge distance was considered to eliminate any edge effect. The anchor plate configuration considered was similar to the anchor plate foreseen for the bottom part of the semi-continuous joint. In this way, two rows of headed anchors were welded to one face of the steel plate. On the opposite face, a contact plate was aligned with one of the anchor rows and a steel bracket positioned, as in the complete joint, increasing the anchor plate stiffness. No reinforcement was assumed in the concrete block. The compression load was applied to the contact plate. In what regards to the materials mechanical behaviour, concrete and steel are modelled as

described in §II.3.1.2.1. In Table II.14 are included the main mechanical properties assumed in this reference case.

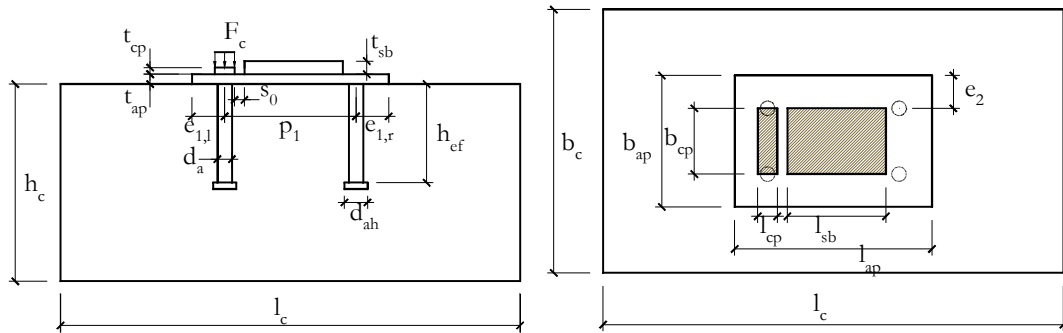


Fig. II.46: Geometry of the reference case for the analysis of the anchor plate subject to pure compression

Table II.14: Geometric and mechanical properties of the reference case for the analysis of the anchor plate subject to pure compression

<b>Concrete block</b>	$h_c$	$l_c$	$b_c$	$f_{cm}$	$E_{cm}$	$\varepsilon_{cu}$	
	[mm]	[mm]	[mm]	[N/mm <sup>2</sup> ]	[N/mm <sup>2</sup> ]	[%]	
	300	800	1000	33	31000	3,5	
<b>Anchor plate</b>	$t_{ap}$	$l_{ap}$	$b_{ap}$	$f_y$	$E$		
	[mm]	[mm]	[mm]	[N/mm <sup>2</sup> ]	[N/mm <sup>2</sup> ]		
	10	300	250	355	210000		
<b>Contact plate and steel bracket</b>	$t_{cp}$	$l_{cp}$	$b_{cp}$	$t_{sb}$	$l_{sb}$	$f_y$	$E$
	[mm]	[mm]	[mm]	[mm]	[mm]	[N/mm <sup>2</sup> ]	[N/mm <sup>2</sup> ]
	10	30	150	30	140	355	210000
<b>Anchors</b>	$n$	$d$	$d_b$	$h_{ef}$	$f_y$	$E$	
		[mm]	[mm]	[mm]	[N/mm <sup>2</sup> ]	[N/mm <sup>2</sup> ]	
	2	22	35	150	355	210000	
<b>Other geometric parameters</b>	$e_{1,l}$	$e_{1,r}$	$p_1$	$e_2$	$s_0$		
	[mm]	[mm]	[mm]	[mm]	[mm]		
	50	50	200	50	10		

In the numerical model, finite elements of first order with reduced integration (C3D8R) were used in all parts. In what respects to interactions, the steel parts were rigidly connected using the tie option therefore avoiding the modelling of the welds. For the concrete-plate and concrete-anchors interactions the hard-contact without friction model, was used. Besides the material non-linearities, also geometric non-linearities were taken into account in the calculations. No initial geometrical imperfections or residual stresses

were considered. The support conditions were applied to the bottom surface of the concrete block (opposite to the edge where the anchor plate was installed) and considered the restriction of the three degrees of freedom of the nodes in this surface. Profiting from the symmetry of the problem, additional boundary conditions were considered, as only half specimen was modelled. These additional boundary conditions restrain the degree of freedom of the nodes at the plane of symmetry, in its perpendicular direction. The strategy adopted for the loading consisted in imposing displacements at the top surface of the contact plate in the direction towards the concrete block. This strategy enforces a better conditioning of the tangent stiffness matrix and, as a result, a faster convergence (Bursi and Jaspart, 1997). The described numerical model is illustrated Fig. II.47. Finally, note that the anchor row on the compression side of the connection was ignored has its effect on the response was considered negligible. Preliminary numerical calculations regarding this issue demonstrated that the presence of the anchor on the loaded side (compression side) increased the resistance up to 6% and the initial stiffness variation was below 3%. Consequently, neglecting this anchor would simplify the analytical modelling.

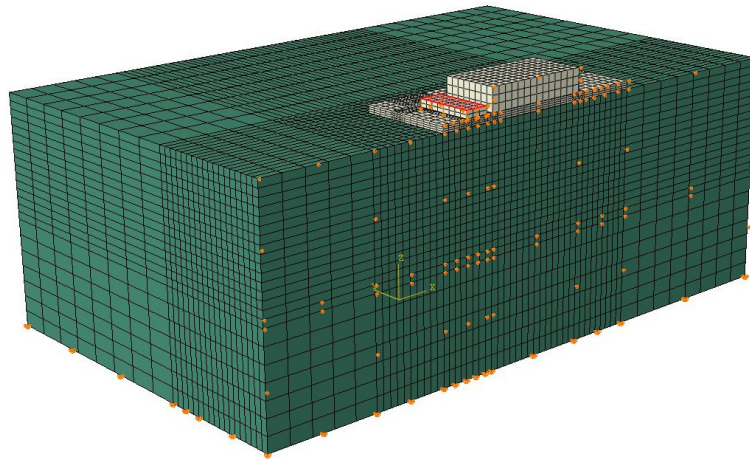


Fig. II.47: Numerical model of the reference case for analysis of the anchor plate subject to pure compression

A sensitivity study regarding the mesh refinement was performed in order to select the most efficient mesh dimension. Regarding this issue, the concrete block was of main concern as the number of elements for the steel parts is residual in comparison with the concrete block. The executed models are described in Table II.15. The mesh under the anchor plate was the main subject of investigation due to the higher stress gradient in comparison with other regions of the block. In Fig. II.48 are compared the obtained force-deformation curves. The force represents the total load applied to the contact plate, and the deformation the displacement in the concrete-plate interface, at the centroid of contact plate, in the same direction of the loading. The curves show that the response of the connection in terms of stiffness is not affected by the different meshes, as all curves are barely superposed. However, in what concerns the ultimate deformation, and consequently the ultimate load achieved, the numerical calculations are sensitive to the mesh quality. Though in all models, the concrete in compression governs the behaviour, as the calculations stop when the limit compressive strain is reached, the models with lower average aspect ratio achieve higher deformations. In fact, within a rational range of

dimensions, the aspect ratio is more relevant than the dimension itself. Giving the quality of the approximation and taking into account the efficiency of the calculation, namely time consumption, the mesh of the model AP-Mesh1 was selected to be the subsequent models. Understandably, this was slightly modified according to the geometry of the case under analysis.

Table II.15: Description of the models used in the mesh sensitivity study of anchor plate subject to pure compression

Model	Description
AP-Mesh1	Under the anchor plate in the loaded side, the elements of hexahedral shape have an approximate size of $10 \times 10 \times 10 \text{ mm}$ . Also in this region, the average aspect ratio is 1,10. In overall concrete block, the highest aspect ratio is 4,64 in the regions with minor relevance to the problem. Approximate number of elements 33000 (only concrete block).
AP-Mesh2	Under the anchor plate on the loaded side, the elements of hexahedral shape have an approximate size of $5 \times 5 \times 3,75 \text{ mm}$ . The average aspect ratio is 1,45. The highest aspect ratio is 12,19 in the regions with minor relevance to the problem. Approximate number of elements 123000 (only concrete block).
AP-Mesh3	Under the anchor plate on the loaded side, the elements of hexahedral shape have an approximate size of $15 \times 10 \times 10 \text{ mm}$ . The average aspect ratio is 1,60. The highest aspect ratio is 4,60 in the regions with minor relevance to the problem. Approximate number of elements 25200 (only concrete block).
AP-Mesh4	Under the anchor plate on the loaded side, the elements of hexahedral shape have an approximate size of $5 \times 5 \times 5 \text{ mm}$ . The average aspect ratio is 1,05. The highest aspect ratio is 7,65 in the regions with minor relevance to the problem. Approximate number of elements 130400 (only concrete block).
AP-Mesh5	Under the anchor plate on the loaded side, the elements of hexahedral shape have an average size of the elements sides of $7,5 \times 7,5 \times 7,5 \text{ mm}$ . The average aspect ratio is 1,05. The highest aspect ratio is 3,58 in the regions with minor relevance to the problem. Approximate number of elements 75100 (only concrete block).

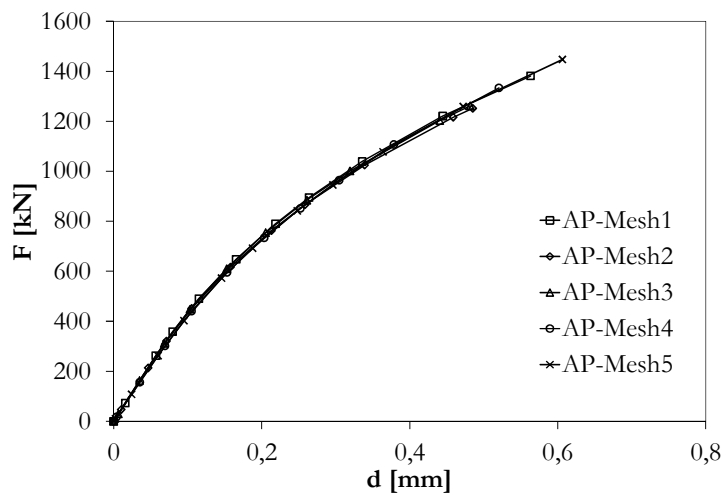


Fig. II.48: Load-deformation curve of models used in the mesh sensitivity study of anchor plate subject to pure compression

Fig. II.48 shows that the response of the anchor plate to pure compression is non-linear being the force-deformation curve governed by the behaviour of concrete in compression. However, the load capacity of the connection depends on the plate-concrete contact surface where the stiffness of the anchor plate plays a role. Fig. II.49 shows the deformation of the anchor plate at approximately 1400kN of applied load. The displacements in the load direction, at each node, are differentiated by colours. The part of the plate under the contact plate remains almost straight. As in a T-stub in compression, the others parts of plate work as cantilever beams, where the loading is proportional to the contact pressure between plate and concrete. On the non-loaded side of the connection, the anchor row restrains the uplifting of plate reversing its deformation. Because of the steel bracket welded to the plate, the reverse section is observed at the edge of the latter.

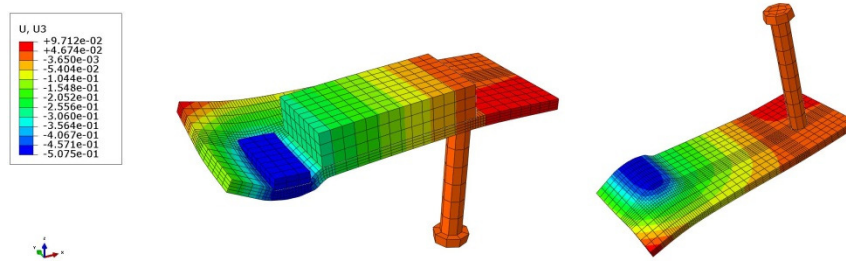


Fig. II.49: Deformation of the anchor plate subject to pure compression (*mm*)

In the numerical model, the failure of the connection was identified when the most deformed concrete element achieved the ultimate strain. In the case of the concrete this value was set equal to 3,5‰, as defined in (EN 1992-1-1, 2004). This element was located in the concrete block in the region under the loaded part of the plate as shown in Fig. II.50-a). Note that only plastic component of strains are plotted. The value of 2,53‰ is the limit plastic strain the concrete elements can experience. The failure in concrete block was desired, as the steel was modelled with high deformation capacity. In terms of stresses, Fig. II.50-b) shows that there is a concentration of stresses under loaded part degrading with the distance to this region in all directions (depth, width and length of the concrete block). In fact, as the load application area is small in comparison to the dimensions of the concrete block, the regions surrounding the loading zone provide confinement to the most loaded elements inducing these into a triaxial state of compression. This has a positive effect, as the concrete stresses under such conditions can exceed the uniaxial compressive stress. In Fig. II.50-b) the compressive stresses clearly exceed the maximum value considered in the uniaxial behaviour of  $30\text{N}/\text{mm}^2$ .



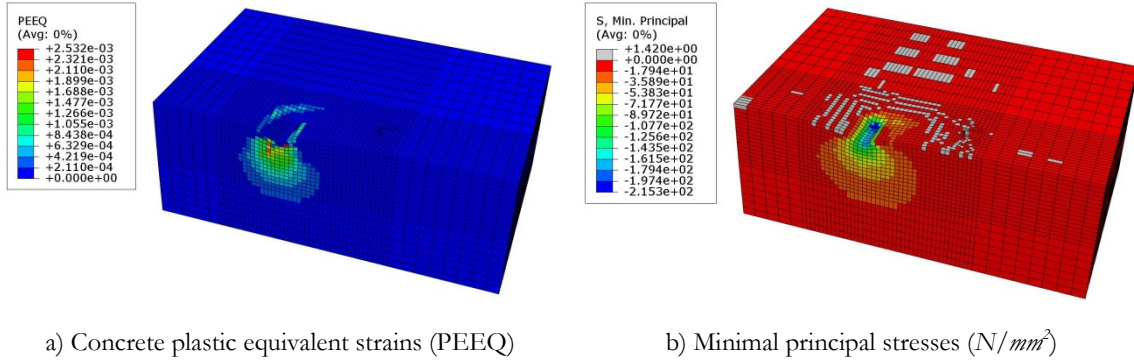
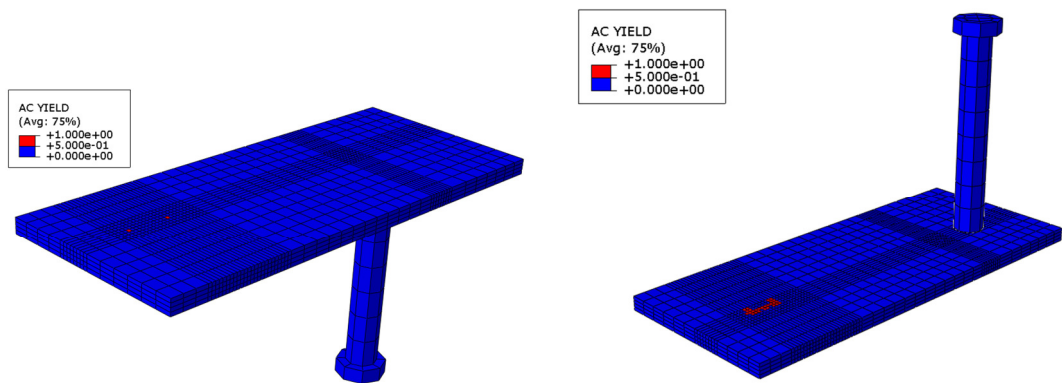


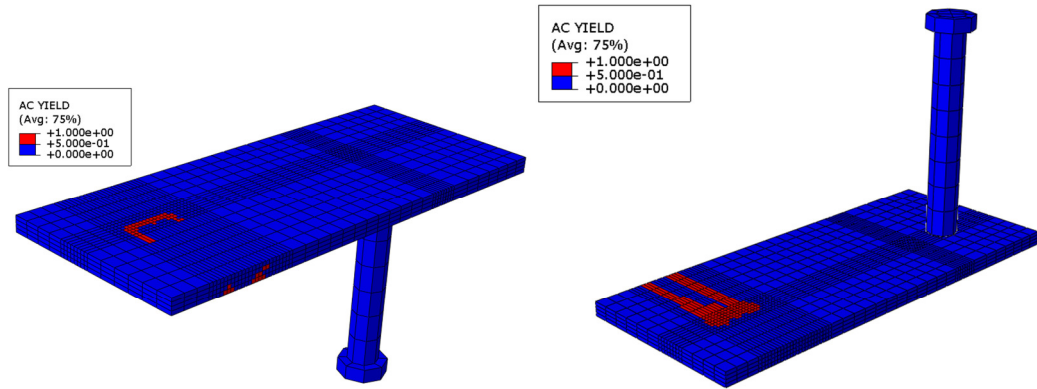
Fig. II.50: Concrete block deformation and stresses

Plastic deformations were also observed in the plate. These occur around the contact plate edges and are due to the plate bending, like in a T-stub in compression. Fig. II.51 shows the elements actively yielding at different load steps. The yielding of the plate initiated around the contact plate, starting along the edge, in the direction of plate length, and spreads towards the edge of symmetry, along the width. It was also noticed that these plastic deformations started at the bottom part and developed to the top with increase of the loading. At the edge of the steel console, in the non-loaded side, no plastic deformations were observed. Though, because of the restraining force produced by the anchor row, an inflexion on the plate deformation occurs. Consequently, higher stresses developed, as shown in Fig. II.52.

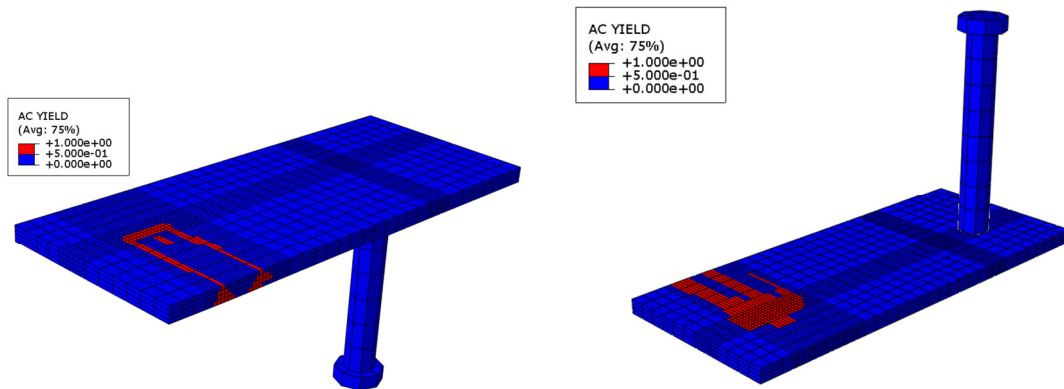


a)  $F \approx 625kN$

b)  $F \approx 865kN$



c)  $F \approx 1055 \text{ kN}$



d)  $F \approx 1380 \text{ kN}$

Fig. II.51: Evolution of yielding within the anchor plate

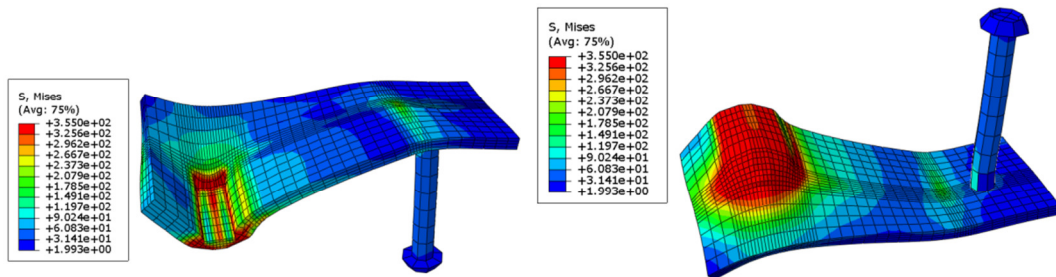


Fig. II.52: Distribution of von Mises stresses within the anchor plate at  $F=1380 \text{ kN}$  (deformation scale factor  $\times 100$ )

As stated, the presence of the anchor row on the non-loaded side of the plate acts as a restraining force to the “free” deformation of the plate. This effect was quantified determining the load on the anchor calculated using the pressure measured at the anchors head. Remind that the friction between shaft and concrete was neglected in the interaction model. Fig. II.53 shows the ratio between load on the headed anchors and the analytical resistance of the anchorage in function of the total load applied to the connection. The maximum resistance of the anchor row was determined analytically considering the contribution of three components (remember Table II.1): i) steel anchor shaft; ii) concrete cone failure; iii) pull-out failure. The resistance of these components was calculated as described in §II.2.2.2. A maximum of 10% of the anchor capacity was activated. This

confirms that failure of this connection through the anchorage on the non-loaded side is unexpected.

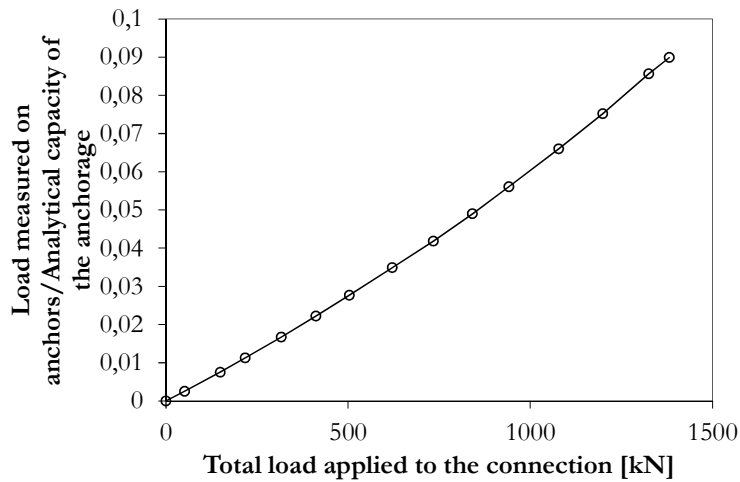


Fig. II.53: Percentage of activation of the anchorage capacity in function of the total load applied to the connection

The effect of the anchor row on the non-loaded side is beneficial to the connection as it increases the effective concrete-plate contact surface and therefore the resistance. In terms of deformation, the anchor row adds stiffness to the plate. A numerical model of the connection without any anchor was simulated to verify the described effect. Fig. II.54 shows the force-deformation curves comparing the effect of the anchor row on the non-loaded side. An increase of about 20% in the resistance of the connection attests the beneficial effect of the anchor row. In terms of initial stiffness, the anchors on the non-loaded side are not significantly influent. Evidently, on the non-loaded side of the plate, the influence is relevant. The plate is “free” to deform presenting an almost straight shape from the hinge formed on the edge of the contact plate up to the free edge on the non-loaded side. Consequently, lower stresses develop on the edge of the steel bracket, as observed in the case with anchors on this side of the connection.

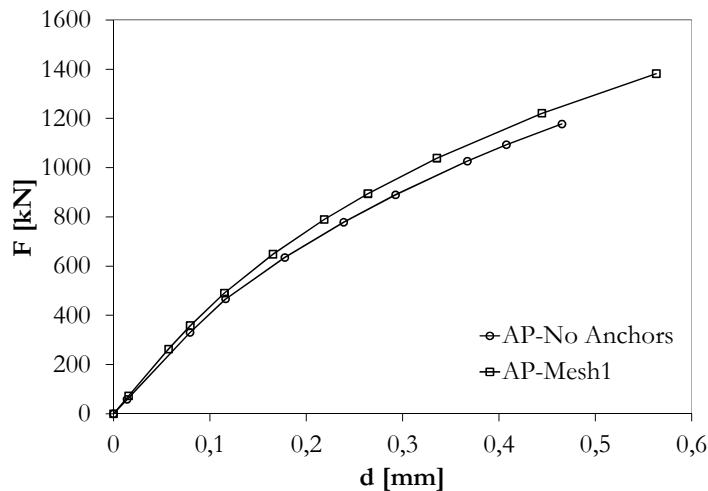


Fig. II.54: Force-deformation curve comparing the effect of the anchor row on the non-loaded side

### II.3.1.3 Analytical modelling

#### II.3.1.3.1 Sophisticated modelling

Based on the previous numerical analysis and on the same principles of the model for column bases proposed in (Guisse *et al.*, 1996), a sophisticated spring mechanical model for the anchor plate connection subject to pure compression was idealized. This is represented in Fig. II.55 and considers the following: i) series of extensional springs for the concrete in compression under the plate; ii) three rotational springs located at the sections of the plate where numerically was observed significant bending of the plate; iii) three extensional springs in the positions of anchor row on the non-loaded side of the connection. These springs represent the components activated within the connection. According to Table II.1, components 5 to 10 were considered, as identified in Fig. II.55. Though the level of sophistication of the model, note that this is an in plane model neglecting the 3D behaviour of the connection. The effects of the three-dimensionality of the connection were approximated in the components (springs) behaviour as simplified as possible.

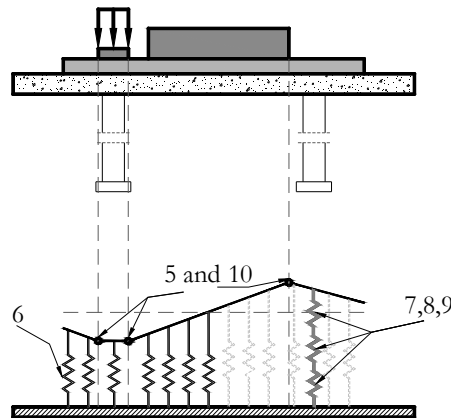


Fig. II.55: Spring mechanical model proposed to reproduce the anchor plate connection subject to pure compression

In the characterization of the components, the following is proposed:

- a) Concrete in compression (Component 6)

The concrete in compression component depends on the plate-to-concrete contact and therefore its complexity. As the concrete only contributes when in compression, the extent of the region under compression has to be identified at each load step. This will depend on the loading and on the flexibility of the system. For this reason the component is represented by series of spring. The more springs are used the better is the approximation for the location of the boundary of no contact section.

For determination of the component properties is important to define the dimension under the plate where stresses are admissible. Fig. II.56 illustrates the “effective” dimensions of the plate. In the present model was assumed that all the length ( $l_{ap}$ ) of the plate may be under compression stresses. The development of stresses on the farthest edges from the loaded area depends on the flexibility of the plate which is taken into consideration in the

model using the rotational springs. For the width, similarly to the (Guisse *et al.*, 1996) model, two zones were distinguished: i) within the contact plate length ( $l_p$ ); ii) and outside the contact plate length. In the first case was used the concept of equivalent rigid plate requiring the determination of the bearing width “ $c$ ”, as defined in (EN 1993-1-8, 2005) for T-stub in compression. In the latter zone, all the plate width was assumed. Note that along the width of the described zones stresses are assumed constant. Finally, the thick dashed lines in Fig. II.56 represent the location of the rotational springs.

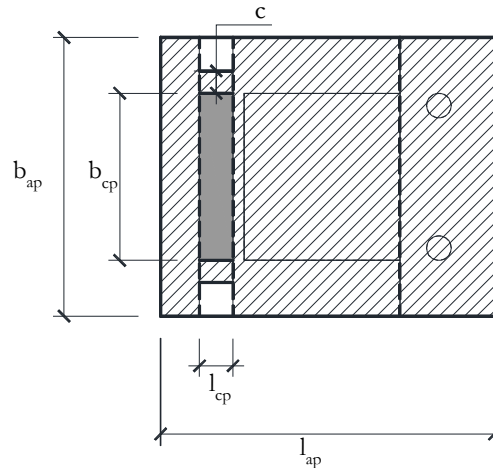


Fig. II.56: Effective plate dimensions considered in the sophisticated model for the anchor plate connection subject to pure tension

In order to reproduce the behaviour of the concrete in compression the mathematical expression proposed by (Guisse *et al.*, 1996) was used. This is based on constitutive stress-strain relation of second order (Parabolic). However, instead of the nominal strength of the concrete ( $f_{ck}$ ), because of the beneficial effect of the confinement on the load bearing zone, an amplified bearing strength ( $f_j$ ) was considered, as in the T-stub in compression model according with (EC3-Part 1.8). In this model, the maximum bearing strength of the concrete is achieved at an ultimate strain  $\varepsilon_{cu}$  and followed by a plateau. Here, the concrete is assumed to fail when the ultimate strain ( $\varepsilon_{cu}$ ) was reached, as in the numerical model presented in the previous section. In order to convert the stress-strain curve into a force-deformation curve, the concrete-to-plate contact zone was discretized through the use of a series of springs. Each spring represents an equivalent area of contact ( $A_{ci}$ ) where the stresses were assumed constant. Then, for the deformation of the spring, an equivalent concrete height ( $h_{c,eq}$ ) was determined where the strain was assumed constant. The resulting force-deformation relation is expressed in (II.43). For more detailed information on the model please check (Guisse *et al.*, 1996).

$$F_i = \left[ \frac{f_j E_c \varepsilon_{cu}}{\varepsilon_{cu}^2} \left( \frac{\delta_i}{h_{c,eq}} \right)^2 + E_c \left( \frac{\delta_i}{h_{c,eq}} \right) \right] A_{ci} \quad (\text{II.43})$$

Where:  $F_i$  is the force in the spring  $i$  of equivalent area of concrete-plate contact ( $A_{ci}$ );  $E_c$  is the Young's modulus of the concrete; and  $\delta_i$  is the elongation of the spring.

In (II.43) the equivalent concrete height ( $h_{c,eq}$ ) is an important parameter which governs the deformability of the component. In the model proposed in (Guisse *et al.*, 1996), the total height of the concrete block was assumed. Taking into account that the model assumes a constant strain within  $h_{c,eq}$ , this overestimates the concrete deformation. The numerical modelling demonstrated that there is a decreasing gradient of strains with the concrete height, remember Fig. II.50-a). In (Guisse *et al.*, 1996), the components governing the behaviour of the column base were the tension components, namely the steel parts, where high deformation capacity was available. Consequently, the referred assumption had an insignificant influence on the global response of the joint. Though, in the present study, the concrete in compression governs the connection response and therefore a more accurate estimation is required. In order to simplify the procedure, a series of numerical simulations were performed considering a plate, without anchors, loaded against a concrete block (pure T-stub), similar to test illustrated in Fig. II.41-b). These simulations took into account the variation of the following geometrical parameters: concrete member height ( $h_c$ ), the loading plate dimensions ( $l_p$  and  $b_p$ ) and the thickness of the anchor plate ( $t_{ap}$ ). Then, an expression was derived to determine the equivalent concrete height ( $h_{c,eq}$ ) equalizing the ultimate deformation obtained in the numerical with analytical calculation. The latter is simply obtained through multiplication of the ultimate concrete strain ( $\varepsilon_{cu}$ ) by the equivalent concrete height ( $h_{c,eq}$ ). In Fig. II.57 is shown the influence of the analysed parameters. As the equivalent concrete height ( $h_{c,eq}$ ) is directly related with the concrete member height ( $h_c$ ), the results are analysed in function of the ratio ( $h_{c,eq}/h_c$ ). It can be concluded that the dimensions of the loading plate may be neglected, while the concrete member height and the thickness of the plate affect the equivalent concrete height. Thus, the equivalent concrete height ( $h_{c,eq}$ ) defined as expressed in (II.44). Though, the loading plate dimensions ( $b_p$  and  $l_p$ ) are not included in derived expressions, note that a minimum edge distance between loading plate and main plate should be kept. This recommendation avoids the concentration of stresses that may be observed if the edges of these plates are too close. The confinement effect is significantly reduced if the highly loaded concrete is near the edge of the main plate.

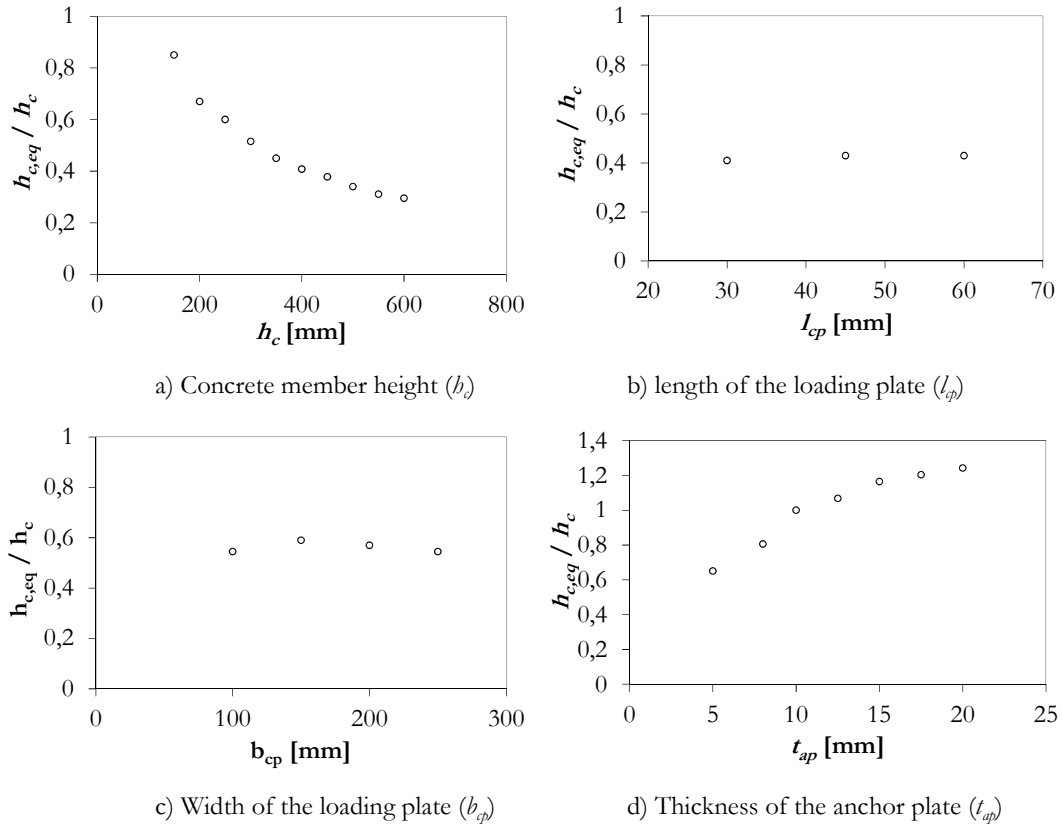


Fig. II.57: Variation of the ratio  $h_{c,eq}/h_c$  with the analysed parameters

$$h_{c,eq} = 12,13 h_c^{0,235} t_{ap}^{0,485} \tag{II.44}$$

Finally, in Fig. II.58 is shown the concrete force-deformation curve obtained with application of (II.43). The presented force-deformation curve was obtained using the geometrical and the mechanical properties of the reference case given in Table II.14. In this example, the effective area of concrete to obtain the spring properties considers was assumed unitary.

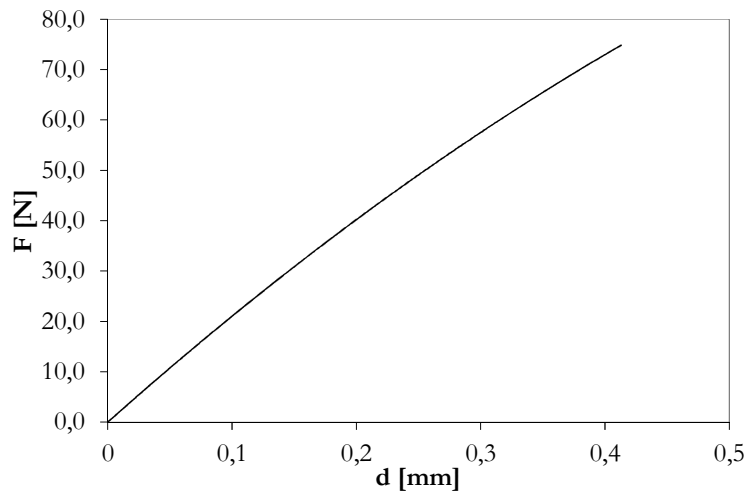


Fig. II.58: Force-deformation response for concrete in compression component within the anchor plate connection

b) Anchorage in tension (Components 7, 8, 9)

The anchorage in tension has for itself the contribution of three components: i) steel failure of the anchors shaft; ii) concrete cone failure; iii) pull-out failure. Note that in this case the edge effects are neglected, as the plate is installed with high edges distances. The analytical characterization of the behaviour of these three individual components has been presented in §II.2.2 and in §II.2.3. Subsequently, the behaviour of the anchorage in tension is determined from the assembly of the referred components, assumed to work in series, as expressed in (II.45) and (II.46). According with, the resistance and deformation capacity is governed by the weakest component. However, for the latter, the other components contribution is also taken into account. The properties of the individual components and of the resulting equivalent component are illustrated in Fig. II.59. For the presented force-deformation curves, the properties of the reference case used in the numerical analysis were considered.

$$F_{a,max} = \text{Min}(N_{us,k}; N_{p,k}; N_{u,c}) \quad (\text{II.45})$$

$$\delta_a = \sum \delta_i(F_a) \quad (\text{II.46})$$

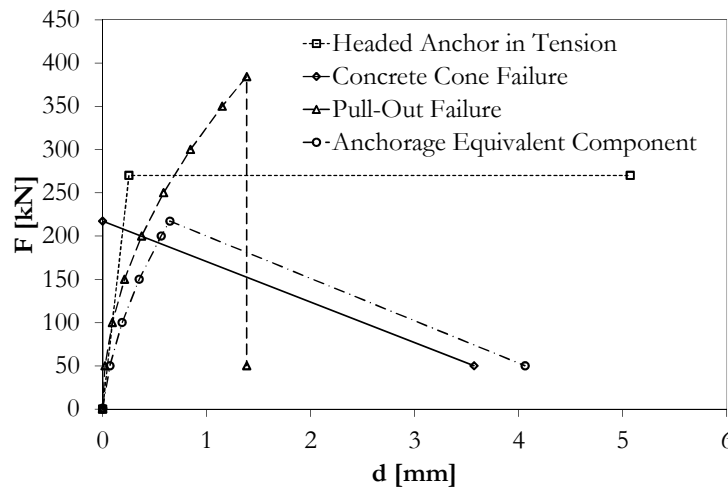


Fig. II.59: Force-deformation curve characterizing the behaviour of the components activated in anchorage subject to tension

c) Plate in bending under compression and tension (Components 5 and 10)

The behaviour of the plate in bending component is derived from the moment-rotation curve of a rectangular cross-section subject to bending moment. The total width of the plate is considered to contribute to the section resistance. No hardening is assumed and therefore the maximum resistance is limited to the yield strength ( $f_y$ ) of the steel plate. Accordingly, the maximum bending moment corresponds to the complete yielding of the cross-section. The several stages of the stress distribution within the cross-section are illustrated in Fig. II.60 and may be described as follows: i) linear elastic up to the yield of the extreme fibers of the steel plate cross-section where the bending moment ( $M_y$ ) is determined according to (II.47); ii) non-linear response up to maximum bending moment



( $M_{pl}$ ) calculated as in (II.48); iii) plateau up to ultimate rotation ( $\Phi_u$ ). The rotation (curvature) of the cross-section was always determined within the elastic portion of the cross-section, and the ultimate rotation ( $\Phi_u$ ) was assumed to be infinite, as the plate in bending was not the desired mode of failure. The cross-section rotation (curvature), before complete yielding, was determined as expressed in (II.49). Fig. II.61 shows the  $M-\Phi$  curve for the plate in bending component applying the model to the reference case (Fig. II.46 and Table II.14). These are the properties later assigned to the rotational springs representing component 5 and 10.

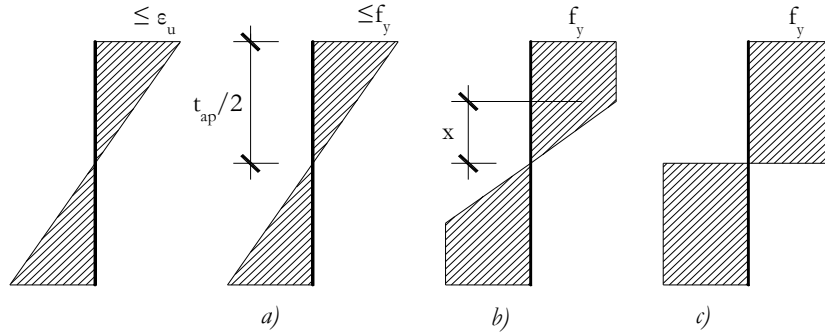


Fig. II.60: Diagram of evolution of stresses within the anchor plate cross-section

$$M_y = \frac{f_y b_{ap} t_{ap}^2}{6} \quad (II.47)$$

$$M_{pl} = \frac{f_y b_{ap} t_{ap}^2}{4} \quad (II.48)$$

$$\Phi = \frac{\epsilon_y}{x} \quad (II.49)$$

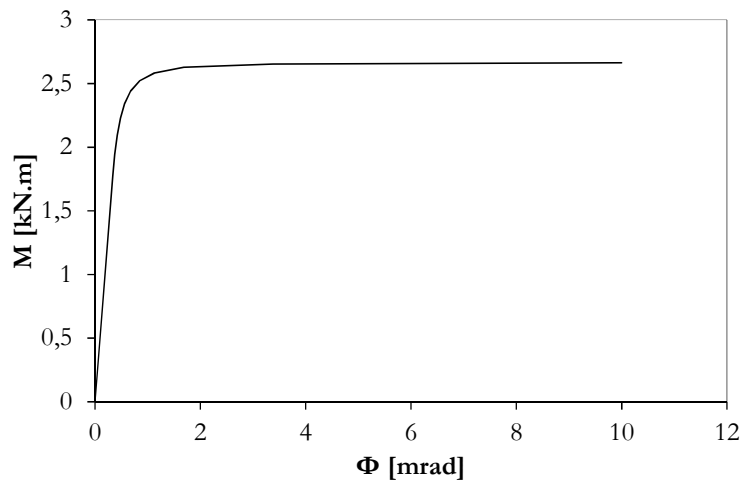


Fig. II.61: Moment-rotation curve characterizing the behaviour of the plate in bending component

d) Model assembly

At last, the model assembly was formulated in order to obtain the properties of the anchor plate connection subject to pure compression. The assembly of the model is illustrated in Fig. II.55 and followed the same formulation as the model proposed in (Guisse *et al.*, 1996). The mechanical model for the anchor plate illustrated and discretised in Fig. II.62. Accordingly, the following assumptions are basis in the formulation of the model assembly:

- Forces and displacements are positive downwards while rotations are positive in the anticlockwise direction;
- Four zones are identified and delimited by the edges of the anchor plate and the rotational springs;
- Four degrees of freedom are considered:  $u$ , vertical displacements;  $\alpha_1$ , rotation of the bar in zone 1;  $\alpha_2$ , rotation of the bar in zone 3;  $\alpha_3$ , rotation of the bar in zone 4;
- Bar in zone 2 is assumed to remain in horizontal position (assumption of constant deformations in the concrete within the contact plate length ( $l_{\phi}$ ) as observed numerically);
- The origin of the abscissas axis ( $x$ ) is located at the middle of the contact plate length ( $l_{\phi}$ ).

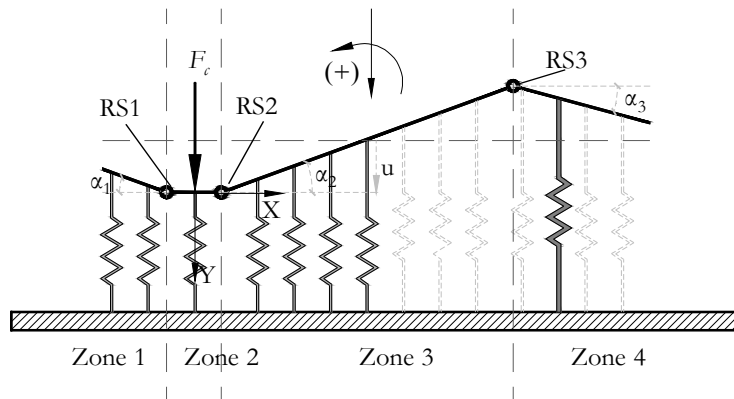


Fig. II.62: Schematic representation of the spring mechanical model for the anchor plate under pure compression

Thus, the displacement field of the model may be expressed as follows.

$$\begin{aligned}
 \text{Zone 1} & \quad u(x) = u + a_1 \left( x + \frac{l_{\phi}}{2} \right) \\
 \text{Zone 2} & \quad u(x) = u \\
 \text{Zone 3} & \quad u(x) = u - a_2 \left( x - \frac{l_{\phi}}{2} \right) \\
 \text{Zone 4} & \quad u(x) = u - a_2 (s_0 + l_{s,b}) - a_3 \left( x - \left( s_0 + l_{s,b} + \frac{l_{\phi}}{2} \right) \right)
 \end{aligned} \tag{II.50}$$

Where:  $x$  is the position of each spring;  $l_{cp}$ ,  $s_0$  and  $l_{sb}$  are geometrical dimensions of the anchor plate connection as defined in Fig. II.56.

In (II.50) is shown that the system is fully defined by the four identified degrees of freedom. Thus, the determination of the plate deformation subject to a load  $F_c$  requires four linearly independent equations. These are obtained expressing the vertical and rotational equilibrium of the different zones of the model. In order to consider the bar in zone 1 in horizontal position, a zero rotation is “enforced” between this bar and the adjacent rotational springs.

Hence, for the vertical and rotational equilibrium the following expressions are written.

$$\Sigma F_v = 0: \quad F_c - \left[ \sum k_{z1} \left( u + \alpha_1 \left( x + \frac{l_{cp}}{2} \right) \right) + \sum k_{z2} (u) + \sum k_{z3} \left( u - \alpha_2 \left( x - \frac{l_{cp}}{2} \right) \right) + \sum k_{z4} \left( u - \alpha_2 (s_0 + l_{sb}) - \alpha_3 \left( x - \left( s_0 + l_{sb} + \frac{l_{cp}}{2} \right) \right) \right) \right] = 0 \quad (II.51)$$

$$\Sigma M_{RS1} = 0: \quad M_1 - \left[ \sum k_{z1} \left( u + \alpha_1 \left( x + \frac{l_{cp}}{2} \right) \right) \left( x + \frac{l_{cp}}{2} \right) + k_{RS1} \alpha_1 \right] = 0 \quad (II.52)$$

$$\Sigma M_{RS2} = 0: \quad M_2 + \left[ \sum k_{z3} \left( u - \alpha_2 \left( x - \frac{l_{cp}}{2} \right) \right) \left( x - \frac{l_{cp}}{2} \right) - k_{RS2} \alpha_2 + \sum k_{z4} \left( u - \alpha_2 (s_0 + l_{sb}) - \alpha_3 \left( x - \left( s_0 + l_{sb} + \frac{l_{cp}}{2} \right) \right) \right) (s_0 + l_{sb}) + k_{RS3} (\alpha_3 - \alpha_2) \right] = 0 \quad (II.53)$$

$$\Sigma M_{RS3} = 0: \quad M_3 + \left[ \sum k_{z4} \left( u - \alpha_2 (s_0 + l_{sb}) - \alpha_3 \left( x - \left( s_0 + l_{sb} + \frac{l_{cp}}{2} \right) \right) \right) \left( x - \left( s_0 + l_{sb} + \frac{l_{cp}}{2} \right) \right) - k_{RS3} (\alpha_3 - \alpha_2) \right] = 0 \quad (II.54)$$

Where:  $F_c$  and  $M_i$  represent the external loading (note that  $M_i$  is zero in the present case);  $k_{z_i}$  represents the stiffness of the extensional springs;  $k_{RSi}$  represents the stiffness of the rotational springs.

The problem can then be expressed in matrix form as in (II.55). Note that the stiffness of each spring ( $k_{z_i}$  and  $k_{RSi}$ ) is the tangential stiffness obtained from the component behaviour according to the respective load-deformation behaviour. Due to the non-linearity of several components, as concrete in compression, pull-out failure and plate in bending, the problem has to be solved by means of iterative process in order to find balance between external loading and internal forces. The numerical method use to solve the non-linear problem is the Newton-Rapshon.

$$\begin{bmatrix} k_{11} & k_{12} & k_{13} & k_{14} \\ k_{21} & k_{22} & 0 & 0 \\ k_{31} & 0 & k_{33} & k_{34} \\ k_{41} & 0 & k_{43} & k_{44} \end{bmatrix} \begin{bmatrix} \Delta u \\ \Delta a_1 \\ \Delta a_2 \\ \Delta a_3 \end{bmatrix} = \begin{bmatrix} \Delta F_c \\ \Delta M_1 \\ \Delta M_2 \\ \Delta M_3 \end{bmatrix} \quad (\text{II.55})$$

With

$$k_{11} = \sum k_{\tilde{x}1} + \sum k_{\tilde{x}2} + \sum k_{\tilde{x}3} + \sum k_{\tilde{x}4}$$

$$k_{12} = k_{21} = \sum k_{\tilde{x}1} \left( x_{\tilde{x}1} + \frac{l_{\varphi}}{2} \right)$$

$$k_{13} = k_{31} = - \sum k_{\tilde{x}3} \left( x_{\tilde{x}3} - \frac{l_{\varphi}}{2} \right) - \sum k_{\tilde{x}4} (s_0 + l_{sB})$$

$$k_{14} = k_{41} = - \sum k_{\tilde{x}4} \left[ x_{\tilde{x}4} - \left( s_0 + l_{sB} + \frac{l_{\varphi}}{2} \right) \right]$$

$$k_{22} = \sum k_{\tilde{x}1} \left( x_{\tilde{x}1} + \frac{l_{\varphi}}{2} \right)^2 + k_{RS1} \alpha_1$$

$$k_{23} = k_{32} = 0$$

$$k_{24} = k_{42} = 0$$

$$k_{33} = \sum k_{\tilde{x}3} \left( x_{\tilde{x}3} - \frac{l_{\varphi}}{2} \right)^2 + k_{RS2} \alpha_2 + \sum k_{\tilde{x}4} (s_0 + l_{sB})^2 + k_{RS3} \alpha_3$$

$$k_{34} = k_{43} = \sum k_{\tilde{x}4} \left[ x_{\tilde{x}4} - \left( s_0 + l_{sB} + \frac{l_{\varphi}}{2} \right) \right] (s_0 + l_{sB}) - k_{RS3} \alpha_3$$

$$k_{44} = \sum k_{\tilde{x}4} \left[ x_{\tilde{x}4} - \left( s_0 + l_{sB} + \frac{l_{\varphi}}{2} \right) \right]^2 + k_{RS3} \alpha_3$$

Where:  $\sum k_{\tilde{x}i}$  is the sum of the stiffness of the springs representing the concrete in compression component, only activated when in compression, and in the particular case of zone 4, one of these springs represents the anchorage and is only activated in tension;  $x_{\tilde{x}i}$  is the position in relation to the referential defined above;  $k_{RSi}$  is the stiffness of the rotational springs.

### II.3.1.3.2 Simplified modelling: Adaptation of the T-stub in compression

For design purposes the application of the above model is inappropriate, as the iterative process, to solve the non-linear problem, requires some computational effort. Thus, the proposal of a simplified model of the anchor plate connection subject to pure compression was envisaged. Taking into account the referred similarities of the problem with column bases, specifically with compression zone, an adaption of the T-stub in compression (EN 1993-1-8, 2005) was sought.

#### a) Direct modifications

The T-stub in compression resistance model was developed regarding its application to column bases where the installation conditions may differ from the anchor plate under study, namely the use of grout which is not expected in the latter. Consequently, the foundation joint material coefficient ( $\beta_j$ ), used to determine the concrete bearing strength,

was set equal to 1. This coefficient should be smaller when the use of grout is considered. Thus, an increase of the concrete bearing strength is obtained and consequently of the resistance of the component. This is consistent assumption that approximates the calculation of the bearing strength to its real value which according to (Weynand, 1999) is underestimated. The author refers to ratios, between the experiments and calculations, ranging from 1,4 to 2,5.

In the same way, for the initial stiffness, the influence of the grout is corrected. As described in (Steenhuis *et al.*, 2008) and (Weynand, 1999), the stiffness coefficient currently in (EN 1993-1-8, 2005) implicitly includes a reduction factor (1,5) for the quality of the concrete surface and the grout layer influence. Neglecting this reduction factor, the stiffness coefficient is rewritten as follows.

$$k'_{T-stub} = \frac{E_c \sqrt{b_{eff} l_{eff}}}{0,85E} \quad (II.56)$$

Where:  $b_{eff}$  and  $l_{eff}$  are the dimensions of the effective T-stub in compression contributing to the initial stiffness;  $E_c$  and  $E$  are the Young's Modulus of concrete and steel, respectively.

b) New proposal for the equivalent rigid plate to determine component resistance

In the current resistance model for the T-stub in compression an equivalent rigid plate dimension under uniform concrete bearing stresses ( $f_c$ ) is assumed. The key parameter of the model is the bearing width of the plate  $c$  (Fig. II.63-a). The latter is obtained calculating a cantilever beam (Fig. II.63-b) with cross-section properties equivalent to the anchor plate ( $b = t_{ap}$ ;  $b = 1$ ). The value of  $c$  is then obtained limiting the bending moment capacity of this cantilever beam to the yielding of the edge fibers ( $f_c t_{ap}^2 / 6$ ) at the support cross-section. However, the process has to be iterative, as the bearing strength of the concrete ( $f_c$ ) is dependent of the bearing width  $c$ . Though, in a few number of iterations convergence is achieved. In the anchor plate under study, this model is valid in all directions except on the non-loaded side (side where anchors are activated in tension). Thus, it is proposed that a new bearing width  $c'$  (Fig. II.63-c) is calculated. The determination of this new bearing width is based on the same principles as in the actual model however, the complexity of the structural problem is increased as: i) the structure becomes hyperstatic due to the presence of the spring on the free edge of the cantilever beam representing the anchors; ii) the stiffness of the beam varies because of the steel bracket welded to the anchor plate; iii) the loading affects only a part of the beam and over a length with variation of inertia. Fig. II.63-d illustrates the structural system to determine the new bearing width ( $c'$ ). Note that the iterative process of determination of  $c'$  is avoided assuming the same bearing strength ( $f_c$ ) as obtained in the former model.

The solution of the hyperstatic structure can be performed using any of the structural analysis method, e.g. the displacement or the force method. The axial deformation was neglected. Though, the structural system represented (Fig. II.63-d) is only one time hyperstatic, the inertia variation and the uncertainty of the load application length, as it corresponds to the sought variable, lead to an unreasonable expression to determine this

variable, especially regarding its practical application. For this reason, it was decided to perform a parametric variation with the analytical formulation and derive an expression which could provide an acceptable approximation of the new bearing width ( $c'$ ).

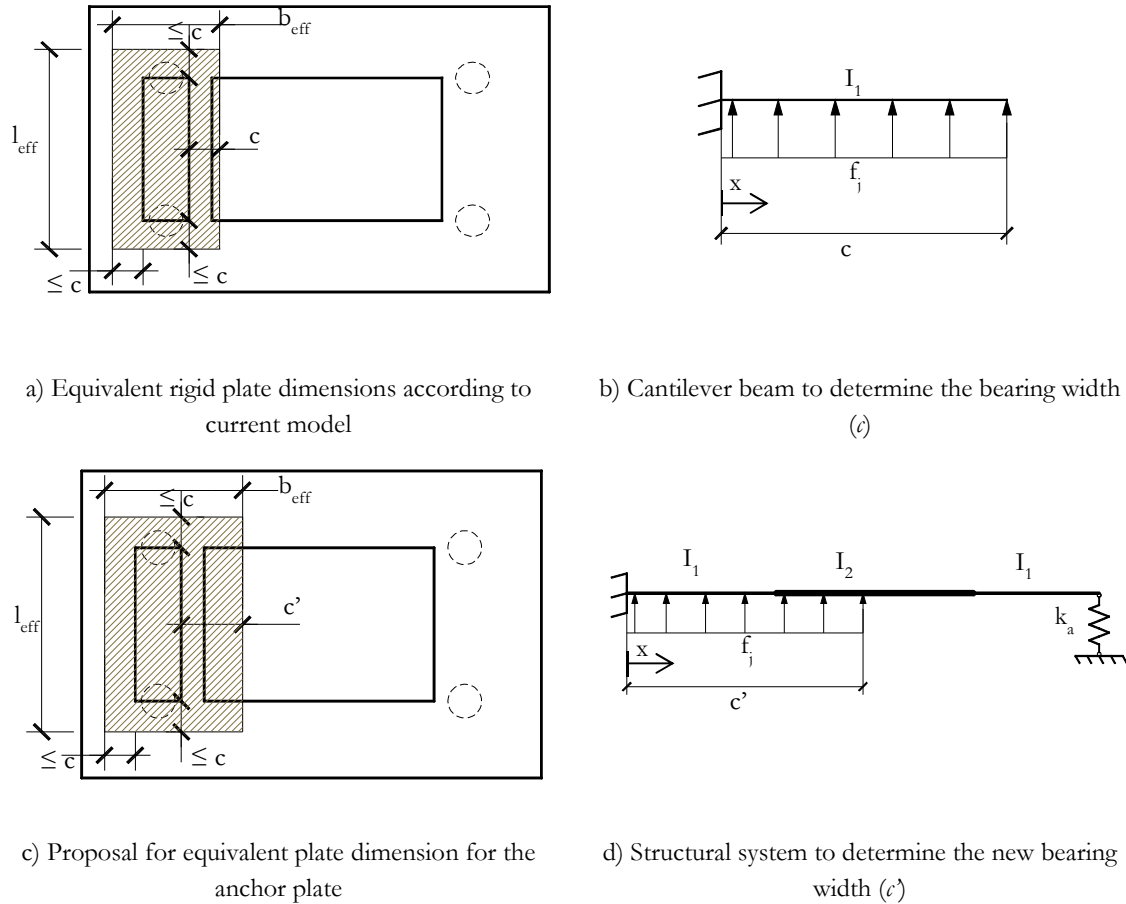


Fig. II.63: Model to determine the concrete in compression resistance using the T-stub model

Thus, first the analytical formulation was validated comparing the results with numerical model of the problem. In the latter, beam elements were used to simulate the plate. In Fig. II.63-d) has been illustrated the structural system under analysis where the problem variables are: anchor plate thickness ( $t_{ap}$ ); steel bracket thickness ( $t_{sb}$ ); length of the steel bracket ( $l_{sb}$ ); distance of the anchors to the contact plate edge ( $p_1 - l_{ap}$ ); steel grade ( $f_y$ ); concrete bearing strength ( $f_j$ ); and anchorage stiffness ( $k_a$ ). Several cases were considered in the validation process. In Table II.16 are given the geometric and mechanical properties used. Note that for all the cases analysed, the distance between the contact plate and steel bracket is assumed sufficiently small so that the new bearing width ( $c'$ ) is greater than this distance. This can be easily assured using the bearing  $c$ , determined with cantilever model, as a limit to this distance. The stiffness of the spring at the right hand side of the beam is determined considering the elastic stiffness of the steel anchors with embedded depth ( $h_{ef}$ ), as a simplification the pull-out failure component is disregarded. Thus, the anchorage stiffness is determined as expressed in (II.57). In order to compare the models, the vertical displacement ( $u$ ) and the rotation ( $\Phi$ ) at the end of the loading length and at the position of

the spring, were used. The observed values are presented in Table II.17. These show a good agreement between numerical calculations and analytical formulation.

Table II.16: Geometric and mechanical properties used in the examples to validate the analytical formulation

	Case 1	Case 2	Case 3	Case 4	Case 5	Case 6
$c'$ [mm]	15	100	15	100	15	100
$t_{ap}$ [mm]	10	10	10	10	10	10
$t_{sb}$ [mm]	20	20	20	20	20	20
$l_{sb}$ [mm]	135	135	135	135	135	135
$p_r \cdot l_{cp}$ [mm]	185	185	185	185	185	185
$f_y^*$ [N/mm <sup>2</sup> ]	355	355	355	355	355	355
$f_j$ [N/mm <sup>2</sup> ]	56	56	56	56	56	56
$k_a^{**}$ [N/mm]	0	0	1E+16	1E+16	1,064E+6	1,064E+6

\* This variable is not relevant for the validation process, only the Young's Modulus is used ( $E_y = 210\,000\text{N/mm}^2$ ).

\*\* The three values of the anchorage stiffness consider three situations: no stiffness (=cantilever beam); fully rigid; and anchorage stiffness considering the use of 2 headed anchors of 22mm diameter and with  $h_{ef} = 150$ .

$$k_a = \frac{E_y A_s}{h_{ef}} \quad (\text{II.57})$$

Table II.17: Comparison between analytical and numerical model for validation of the analytical formulation

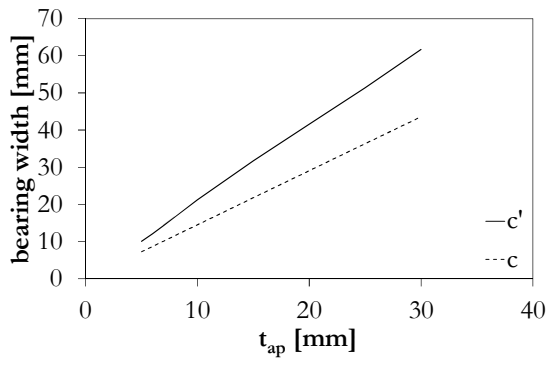
		Case 1	Case 2	Case 3	Case 4	Case 5	Case 6	
$x = c'$	$u$ [mm]	Numerical	2,8E-2	14,92	1,40E-2	1,58	1,40E-2	1,58
		Analytical	0,02	14,73	6,08E-3	1,47	6,08E-3	1,47
	$\Phi$ [mrad]	Numerical	1,74	158,94	0,30	5,30	0,30	5,31
		Analytical	1,74	158,93	0,33	5,42	0,33	5,42
$x = p_r \cdot l_{cp}$	$u$ [mm]	Numerical	0,324	28,43	0	0	1,3E-5	1,13E-3
		Analytical	0,315	28,24	0	0	2,26E-5	1,13E-3
	$\Phi$ [mrad]	Numerical	1,74	158,94	-0,72	-56,90	-0,72	-56,89
		Analytical	1,74	158,93	-0,67	-56,73	-0,67	-56,73

The several variables influencing the mechanics of this structural system and therefore, the new bearing width ( $c'$ ) have been identified above. In order to evaluate their influence, a

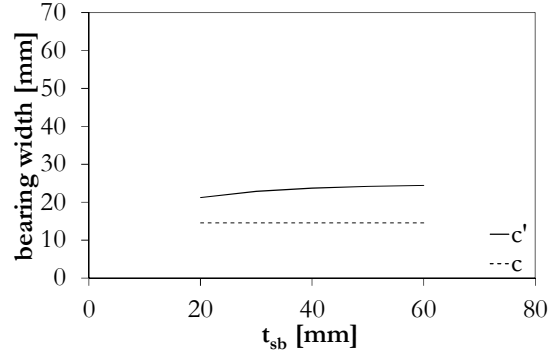
sensitivity analysis was performed before the parametric study. In this way, using a reference example, each parameter is assessed separately. The results of this study are shown in Fig. II.64. The new bearing width ( $c'$ ) is plotted against each one of the above variables. In the same chart are included the results of the former model (without anchors). It can be observe that the anchor plate thickness, the steel grade and the bearing strength of the concrete are the most influencing parameters. These are expected results, as these parameters have direct influence on the bending moment resistance and loading of the plate. The other geometric parameters have a much smaller influence. In what concerns to the stiffness of the spring representing the anchorage on the non-load side, the analysed cases considered the following variations:  $d_a \rightarrow 16$  to  $22\text{mm}$ ;  $h_{ef} \rightarrow 150\text{mm}$  to  $200\text{mm}$ . These variations cover a range of practical cases. The results show that for these range of stiffness's, the variation is of such order that no influence on the new bearing width ( $c'$ ) is observed. Consequently, this parameter may be kept constant in the parametric analysis. Still regarding this parameter, it should be noted that this stiffness is located punctually at the position of the anchors. On the other hand, the problem is analysed per unit of width. Considering the total value of the stiffness is excessive. Therefore, it was performed some simulations considering the distribution of this stiffness through the width. This can be seen as a lower bond of the stiffness. However, the variations observed on the bearing width were below  $0,5\text{mm}$  consequently, this parameter was neglected.

The parametric variation provided an insight on the influence of each parameter; however, the derivation of semi-empirical expression to determine the new bearing width ( $c'$ ) had to be grounded in a much more extensive parametric study, as the performed variations did not cover the possible correlation between variables. In this way, a second parametric study was executed considering the combination of all variables. In Table II.18 are listed the cases considered for each variable. As the variation of each variable is combined with the variation other variables, the total number of cases performed is 972. In order to obtain the new bearing width ( $c'$ ), an expression was constructed introducing the influence of each variable. For each variable a parameter was defined through regression analysis of the bearing width ( $c'$ ) in function of the considered parameter. The final expression is given in (II.58). Note, that the obtained expression has no physical meaning though it is a function of the former bearing width ( $c$ ).

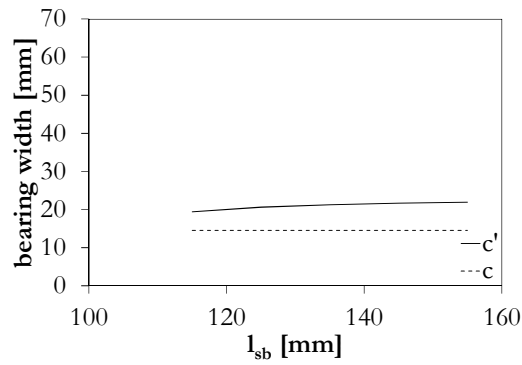




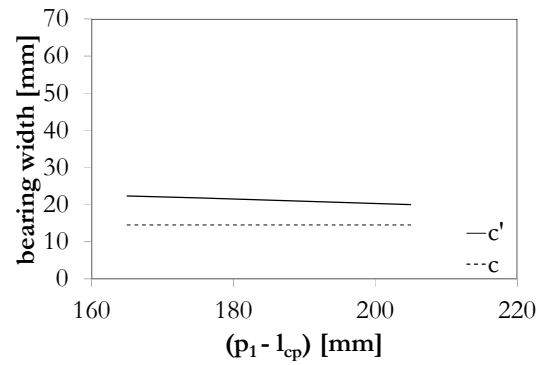
a) Anchor plate thickness ( $t_{ap}$ )



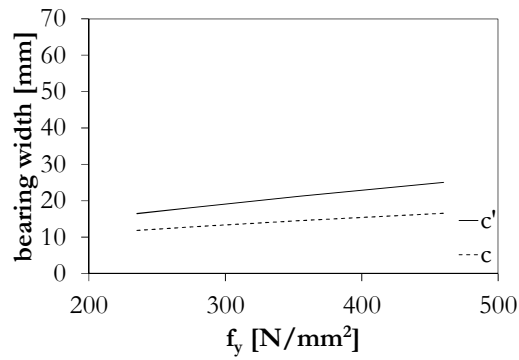
b) Steel bracket thickness ( $t_{sb}$ )



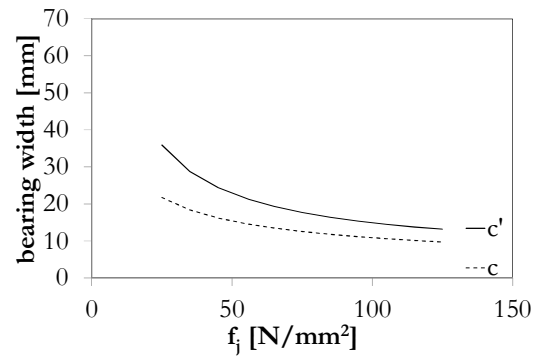
c) Length of the steel bracket ( $l_{sb}$ )



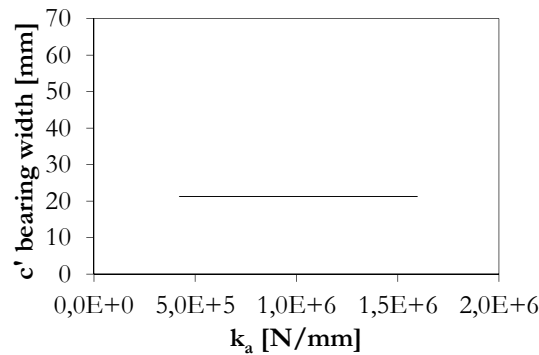
d) Position of the anchors ( $p_1 - l_{cp}$ )



e) Steel grade ( $f_y$ )



f) Concrete bearing width ( $f_c$ )



g) Stiffness of the headed anchors at the edge of the beam ( $k_a$ )

Fig. II.64: Analysis of the influence of the different variables affecting the dimension of the new bearing width ( $c'$ )

Table II.18: Variation of each variable considered in the parametric study

$t_{ap}$ [mm]	$t_{sb}$ [mm]	$l_{sb}$ [mm]	$(p_1-l_{cp})$ [mm]	$f_y$ [N/mm <sup>2</sup> ]	$f_j$ [N/mm <sup>2</sup> ]
10	20	100	180	235	30
20	30	135	200	355	60
30	40	165	220	460	90
					120
Total number of cases for combination of variables					972

$$c' = \chi c^a \quad (II.58)$$

With

$$a = -0,0003f_j + 1,0257$$

$$\chi = \beta \gamma \delta \varepsilon \zeta \eta$$

$$\beta = 1,775f_j^{0,053}$$

$$\gamma = 0,460f_y^{0,135}$$

$$\delta = 572,12 \left( p_1 - \frac{l_{cp}}{2} \right)^{-1,203}$$

$$\varepsilon = 0,102l_{sb}^{0,470}$$

$$\zeta = 0,377t_{sb}^{0,2893}$$

$$\eta = -0,0002t_{ap}^2 + 0,0093t_{ap} + 0,937$$

In Fig. II.65 the exact solution of the new bearing width ( $c'$ ) is plotted against the proposed model. The quality of the approximation is satisfactory, especially given the practical interest of the proposed expression in comparison to the resolution of the hyperstatic structural system to obtain the bearing width. The average ratio between exact and proposal is 1,04 with a standard deviation of 8,74%.

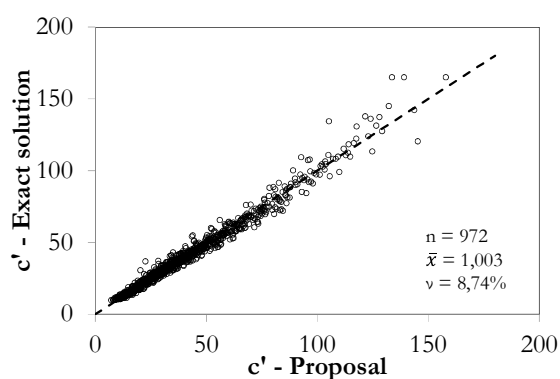


Fig. II.65: Comparison between proposal and exact solution for determination of the new bearing width ( $c'$ )

For practical situations, assuming the variations given in Table II.18, the coefficients involved in expression (II.58) are within the ranges given in Table II.19.

Table II.19: Range of variation of the coefficients to determine the new bearing width ( $c$ )

$1,357 \leq \beta (f_f) \leq 1,461$
$0,962 \leq \gamma (f_f) \leq 1,054$
$0,870 \leq \delta (p_f - l_{fp}) \leq 1,108$
$0,887 \leq \epsilon (l_{sb}) \leq 1,138$
$0,896 \leq \zeta (t_{sb}) \leq 1,095$
$1,010 \leq \eta (t_{ap}) \leq 1,043$
$0,990 \leq \alpha (f_f) \leq 1,017$
$0,912 \leq \chi \leq 2,814$

c) Correction of the bearing width for the stiffness of the component

The stiffness model of T-stub in compression is also based on similar interaction between the concrete and the base plate, as assumed for the resistance. With this model the initial stiffness of the component is estimated. The numerical models used to validate the modifications on the resistance model showed that the initial stiffness of the component was insignificantly affected by the presence of the anchors on the non-loaded side of the plate. Therefore, no specific modification for the stiffness model was sought. Though, using the theoretical stiffness model described in (Steenhuis *et al.*, 2008) and ranging the loading dimensions,  $l_p$  and  $b_{ps}$ , from 20 to 40 and 100 to 200, respectively, a new approximation for the bearing width ( $c$ ), to consider in the stiffness model of the T-stub in compression, was obtained. In (II.59) is expressed the proposed modification.

$$c = 1,4t_{ap} \quad (II.59)$$

d) Summary of the proposal

In Table II.20 is summarized the proposal for adaptation of the T-stub in compression to the anchor plate under pure compression. The base model is also included. The different steps are identified. In the next section, the described model is compared with 3D numerical model of the anchor plate.

Table II.20: Summary of the proposal for the adaptation of the T-stub in compression to anchor plate in compression

T-stub in compression according to (EN 1993-1-8, 2005)	Proposal for adaptation to anchor plate connection
<i>Resistance</i>	
<ul style="list-style-type: none"> <li>▪ Calculation of bearing width (<math>c</math>) using cantilever beam for all directions. Iterative process as the bearing width and the concrete bearing strength are dependent of each other.</li> </ul> $c = t_{ap} \left[ \frac{f_c}{3f_j} \right]^{0,5}$ <ul style="list-style-type: none"> <li>▪ Equivalent rigid plate dimensions are defined according to the bearing width and limited by the plate dimensions</li> </ul> $A_{eff} = \text{Min}(2c + b_{cp}; b_{ap}) \cdot (c + l_{cp} + \text{Min}(c, e_{1,cp}))$ <ul style="list-style-type: none"> <li>▪ Resistance of the component is obtained assuming an uniform distribution of stresses under the equivalent rigid plate and equal to bearing strength of the concrete previously determined in the bearing width calculation</li> </ul> $F_{ap,c} = A_{eff} f_j$	<ul style="list-style-type: none"> <li>▪ Calculation of two bearing widths, <math>c</math> and <math>c'</math>. The first is calculated as in the current model. However, use the foundation joint material coefficient <math>\beta_j</math>, equal to 1.</li> <li>▪ After the new bearing width (<math>c'</math>) on the anchors side is determined as expressed in (II.58).</li> <li>▪ Equivalent rigid plate dimensions are now determined as follows.</li> </ul> $A'_{eff} = \text{Min}(2c + b_{cp}; b_{ap}) \cdot (c' + l_{cp} + \text{Min}(c, e_{1,cp}))$ <ul style="list-style-type: none"> <li>▪ The resistance of the component is then obtained as below.</li> </ul> $F'_{ap,c} = A'_{eff} f_j$
<i>Initial Stiffness</i>	
<ul style="list-style-type: none"> <li>▪ The bearing width (<math>c</math>) is <math>1,25t_{ap}</math>.</li> <li>▪ The equivalent rigid plate dimensions are determined as in the resistance model but using the previous bearing width.</li> </ul> $A_{eff,S} = \text{Min}(2,5t_{ap} + b_{cp}; b_{ap}) \cdot (1,25t_{ap} + l_{cp} + \text{Min}(1,25t_{ap}; e_{1,cp}))$ <ul style="list-style-type: none"> <li>▪ The initial stiffness of the component is then obtained as follows.</li> </ul> $S_{ap,c,ini} = \frac{E_c \sqrt{A_{eff,S}}}{1,275}$	<ul style="list-style-type: none"> <li>▪ The bearing width (<math>c</math>) is <math>1,40t_{ap}</math>.</li> <li>▪ The equivalent rigid plate dimensions are determined as in the resistance model but using the previous proposed bearing width (<math>c</math>).</li> </ul> $A'_{eff,S} = \text{Min}(2,8t_{ap} + b_{cp}; b_{ap}) \cdot (1,4t_{ap} + l_{cp} + \text{Min}(1,4t_{ap}; e_{1,cp}))$ <ul style="list-style-type: none"> <li>▪ The reduction factor because of the use of grout is neglected giving the stiffness coefficient as expressed in (II.56).</li> <li>▪ The initial stiffness of the component is then obtained as follows.</li> </ul> $S'_{ap,c,ini} = \frac{E_c \sqrt{A'_{eff,S}}}{0,85}$

### II.3.1.4 Validation and calibration of the analytical models

#### II.3.1.4.1 Reference case

The performance of the above described models was first analysed in detail for the reference case described in §II.3.1.2.3. The main conclusions of this analysis are given below for each type of analytical model separately.

##### a) Sophisticated model

The main output to extract from this model is force-deformation curve. Fig. II.66 presents the force-deformation curve obtained with the sophisticated model for the reference case. It can be observed that the analytical model provided a stiffer response than the numerical calculation. Though, the approximation of the shape of the curve is excellent. Exploiting the output of the analytical model was observed that all the rotational springs achieved their maximum bending capacity, meaning that the cross-section of the plate at the location of these springs were completely yielded. However, this observation was not confirmed in the numerical model, as plastic deformations were only observed in RS1 and RS2. These deviations are not surprising as the problem in hands is 3D by nature while the analytical model is basically unidirectional. These 3D phenomena of the problem have to be “transferred” into the simplified models through the components constitutive behaviour. Except for the plate in bending component, all other components behaviour were calibrated, as described in §II.3.1.3.1.

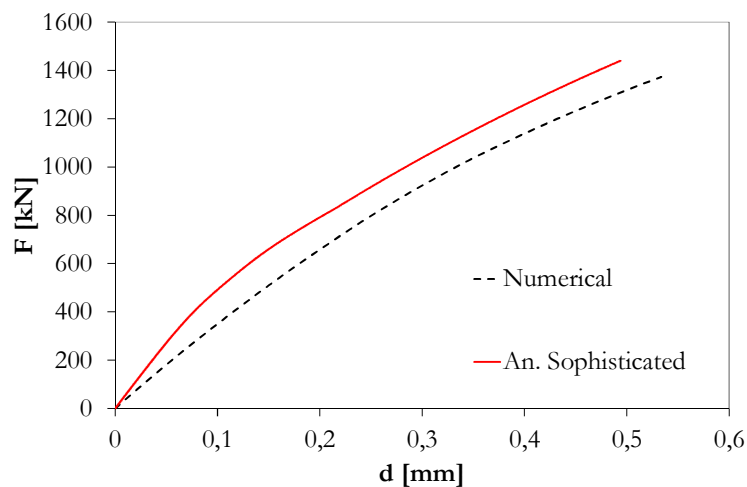


Fig. II.66: Force-deformation curve for the reference case comparing analytical sophisticated model with numerical model

Thus, it was decided to calibrate the complete model affecting the rotational springs behaviour by a factor  $\alpha_{RS}$ . This factor influences the rotational spring deformability so that the agreement with the numerical observations was accomplished. This means that RS1 and RS2 could yield but not completely, while RS3 could not exceed its yield capacity. For these reason, two factors were calibrated, one for the two first and one for the latter. At the same time, an approximation between analytical and numerical global response was envisaged. Therefore, the calibration was performed comparing the global force-deformation curves and checking the loads on the rotational springs. Fig. II.67 shows the

force-deformation curve of the final result. As the model was calibrated, a perfect agreement is now obtained. The values found for the factor  $\alpha_{RS1-2}$  and  $\alpha_{RS3}$  were 0,05 and 0,01, respectively. In this model, rotational springs RS1 and RS2 yield but do not achieve the maximum corresponding to the complete yield of the plate. In what concerns to RS3, the bending moment developed in this spring remained below the value corresponding to the first yielding appearing in the plate. These observations are in line with the numerical calculations.

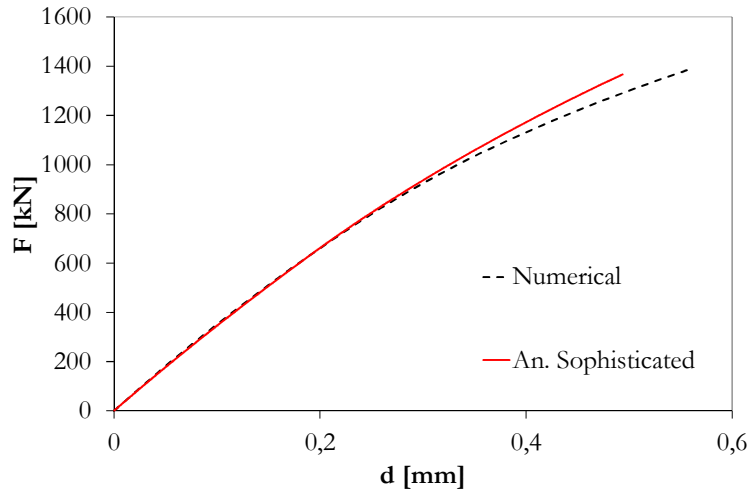


Fig. II.67: Force-deformation curve for the reference case comparing analytical sophisticated model with numerical model after calibration of the rotational springs' behaviour

A physical explanation of the values found for above factors is difficult, as these are result of a calibration process to approximate a 3D problem by an one-dimensional model. Though, it may be understood that the obtained values increase the flexibility of these springs and therefore, higher rotations are observed. As consequence, the number of “concrete” springs activated was reduced and therefore the total load was also reduced.

Finally, in what respects to this analytical model, it must be referred that the tension components, representing the anchorage, were activated by an higher load than in the numerical model. Though, this value is distant of the resistance of these components (below 50%.) These values assure that failure is not governed by this group of components and therefore, an additional calibration was avoided. Furthermore, the deviation is on the safe side.

#### b) Simplified model

The application of the simplified T-stub model, proposed and actual (EN 1993-1-8, 2005), is shown in Fig. II.68 comparing the force-deformation curves obtained with the analytical and numerical approaches. The results show that both analytical models underestimate the resistance of the anchor plate. This justified by the conservative approach of limiting the stresses in the plate to the first fibers to achieve the yield strength. Though, it is clear that the proposed modifications to the actual T-stub model improve its quality. An increase of resistance is approximately of 34%. In terms of initial stiffness, the approximation of the new proposal is excellent and therefore, preferable in relation to the actual model. Finally,

note that in the analytical model a plateau was assumed at maximum resistance however, this plateau is not defined in the code or in the approach described above. In a plastic analysis it may be assumed though, no indication exists for the ultimate deformation. In this particular case the ultimate deformation obtained in the 3D numerical model was assumed.

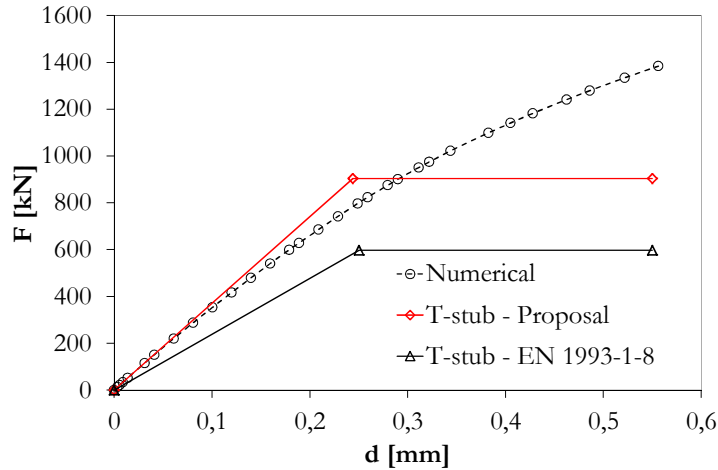


Fig. II.68: Force-deformation curve for the reference case comparing analytical sophisticated model with numerical model

#### II.3.1.4.2 Parametric variation

In order to better evaluate the quality of the analytical models, the influence of several parameters was studied. In this parametric study, the following variables were analysed: thickness of the anchor plate ( $t_{ap}$ ), length of the contact plate ( $l_{cp}$ ), width of the contact plate ( $b_{cp}$ ), length of the steel console ( $l_{sb}$ ), steel grade of the anchor plate ( $f_y$ ) and concrete class ( $f_{cm}$ ). The geometric variables may be recalled in Fig. II.46. In Table II.21 are listed the range of values covered in this study. These values were assumed to be within the practical dimensions and common material properties. For the width of the contact plate ( $b_{cp}$ ) and for the length of the steel console ( $l_{sb}$ ), note the following: i) the variation of the width of the contact plate ( $b_{cp}$ ) was complemented with the variation of the width of the anchor plate, in this way the edge distance was constant; ii) with the variation of the length of the steel console length ( $l_{sb}$ ) the length of the anchor plate ( $l_{ap}$ ) was varied so that the distance between the edge of the both plates was constant.

Table II.21: Range of values considered in the parametric study

$t_{ap}$ [mm]	$l_{cp}$ [mm]	$b_{cp}$ [mm]	$l_{sb}$ [mm]	$f_y$ [N/mm <sup>2</sup> ]	$f_{cm}$ [N/mm <sup>2</sup> ]
10	20	100	105	235	24
15	30	150	140	355	45
20	40	200	175	460	68

The influence of each parameter is analysed through comparison of the force-deformation curves. Both sophisticated and simplified model are assessed. Except for the concrete grade ( $f_{cm}$ ), Fig. II.69 to Fig. II.74 show a good approximation in terms of stiffness, resistance and deformation capacity, between the sophisticated analytical model and the numerical model. The analytical model shows similar sensibility to the geometric variations as the numerical model. Only for the concrete grade, a considerable deviation is obtained when a concrete with high strength is considered. In what respects to the simplified modelling using as basis the T-stub model in (EN 1993-1-8, 2005), the improvements proposed to adapt this model to the anchor plate are visible. A better approximation of the resistance and of the component initial stiffness is clearly obtained. Still, this model is conservative in terms of resistance. However, it has to be taken into account the limitations of the base model which limit the resistance to the first fibers to yield in the anchor plate. Thus, the proposed modifications improved the suitability of this model and are recommended. Apart from the referred deviation, the simplified model sensibility to the parametric variations is also satisfactory as shown from Fig. II.69 to Fig. II.74. As in the sophisticated model, the resistance of the model is overestimated when considering a concrete with high strength. Though, the resistance calculated with simplified model is below the numerical resistance, as shown in Fig. II.74-b), it is observed that the ratio between the analytical and numerical model increased above the average increase obtained for the other parameters. Given the deviations observed in both analytical models for this parameter, a deeper analysis is performed after.

- Thickness of the anchor plate ( $t_{ap}$ )

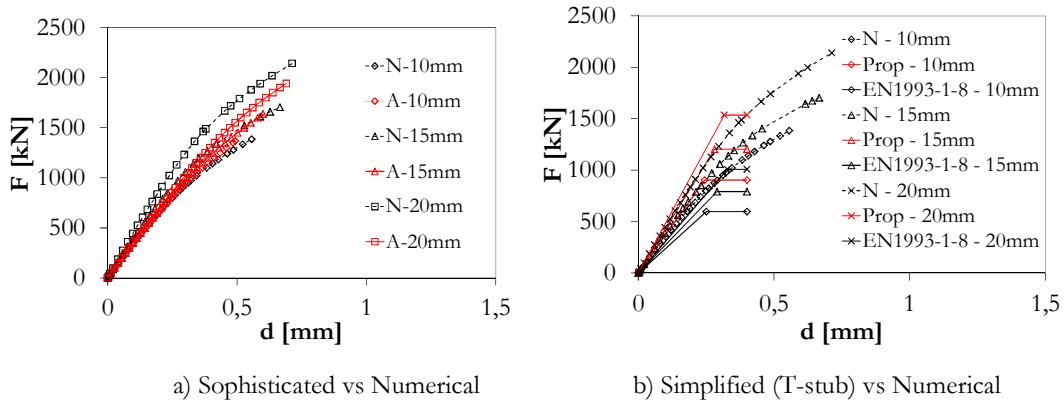


Fig. II.69: Force-deformation curve assessing the sensibility of the analytical models to the anchor plate thickness ( $t_{ap}$ )



▪ Length of the contact plate ( $l_{cp}$ )

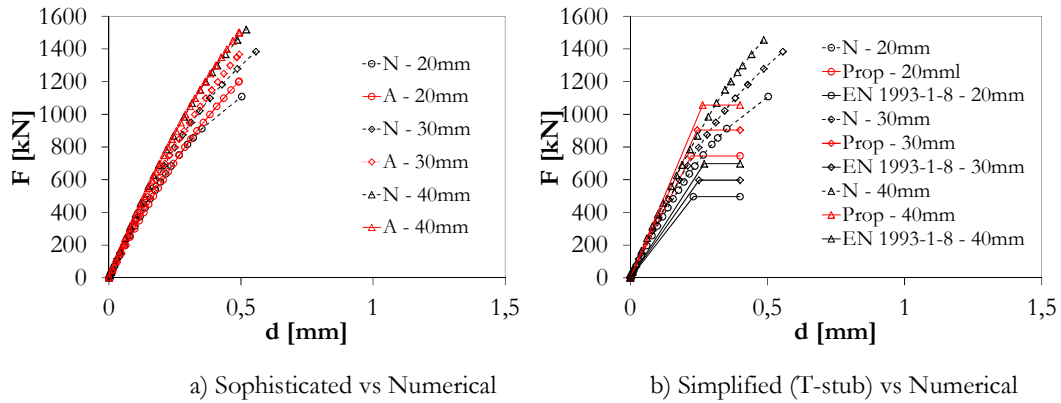


Fig. II.70: Force-deformation curve assessing the sensibility of the analytical models to the length of the contact plate ( $l_{cp}$ )

▪ Width of the contact plate ( $b_{cp}$ )

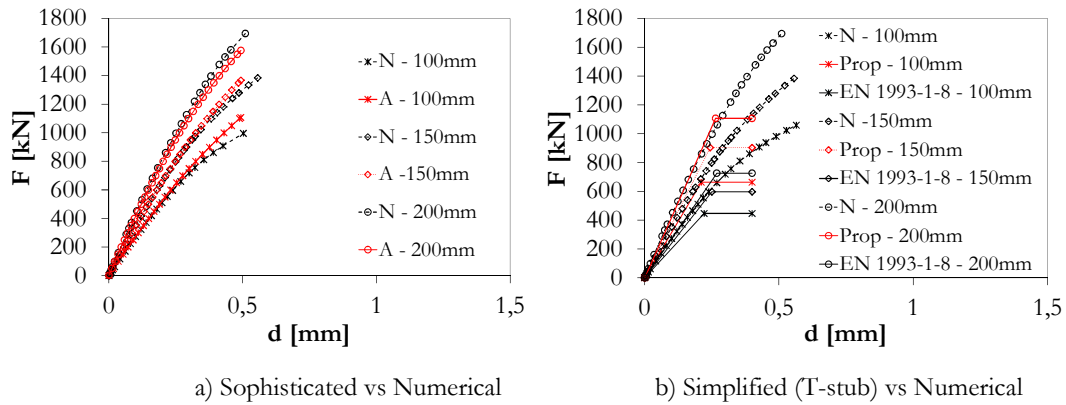


Fig. II.71: Force-deformation curve assessing the sensibility of the analytical models to the width of the contact plate ( $b_{cp}$ )

▪ Length of the steel console ( $l_{sb}$ )

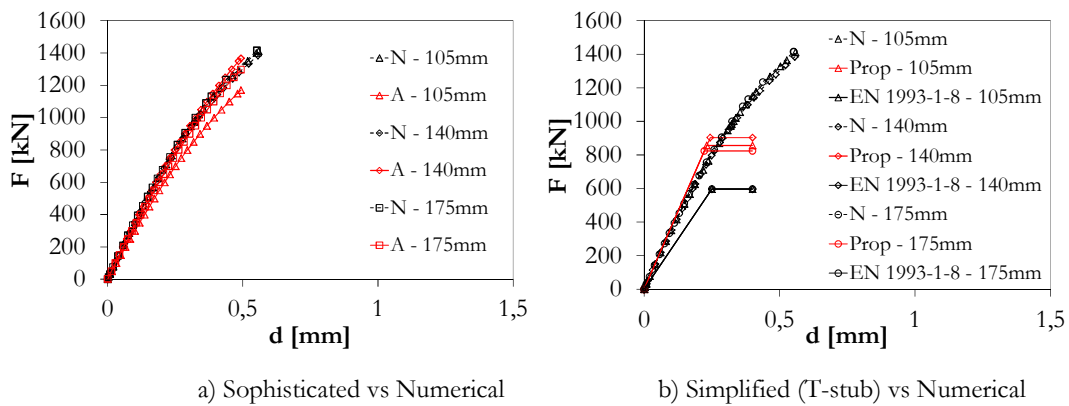


Fig. II.72: Force-deformation curve assessing the sensibility of the analytical models to the length of the steel bracket ( $l_{sb}$ )

▪ Yield strength of the anchor plate ( $f_y$ )

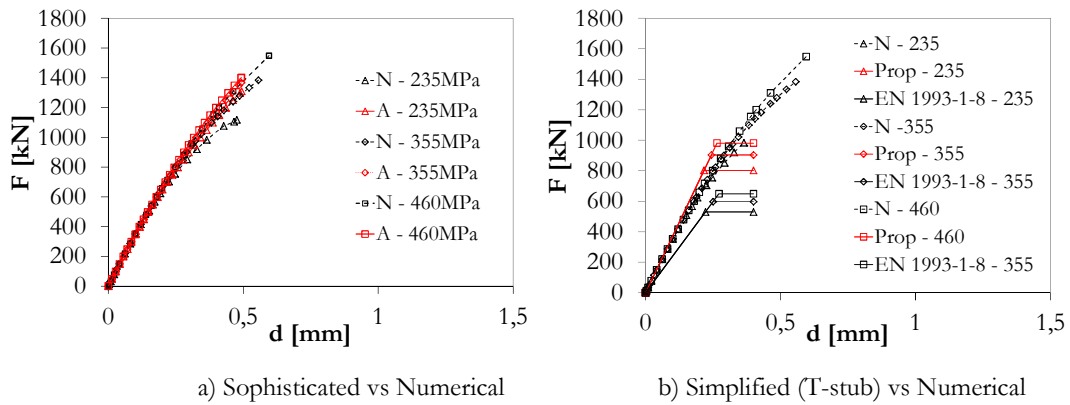


Fig. II.73: Force-deformation curve assessing the sensibility of the analytical models to the steel grade ( $f_y$ )

▪ Concrete class ( $f_{cm}$ )

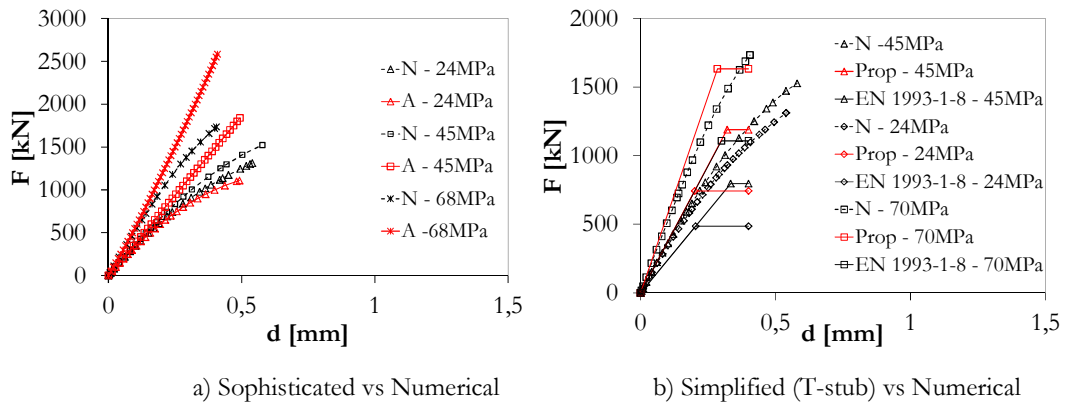


Fig. II.74: Force-deformation curve assessing the sensibility of the analytical models to the concrete grade ( $f_{cm}$ )

A detailed analysis of both models, analytical and numerical, showed that the evolution of the concrete strength under confined conditions ( $f_c$ ) with concrete grade presented a different trend. Fig. II.75-a) shows the evolution of the concrete strength under confined conditions with concrete grade. As for the lower concrete grade a good agreement between numerical and analytical models was observed, the ratio between the concrete strength and the strength of the lowest concrete grade was used in the analysis. For the numerical model, an average value of the minimum principal stresses under the contact plate dimensions was used. The results of this analysis demonstrated that the referred ratio increases considerably for the analytical model in comparison to the numerical model. For example, for a concrete strength of  $68N/mm^2$  the analytical ratio is approximately 3,3 while for the numerical model is approximately 1,6. Given this results, it was decided to calibrate the analytical model for the concrete strength under confined conditions ( $f_c$ ). The strategy consisted in determining a factor ( $\alpha_{f_{cm}}$ ) function of the mean concrete strength. This factor was obtained using a regression analysis of the ratio between numerical and analytical calculations expressed in function of mean concrete strength, as shown in Fig. II.75-b). The factor was then introduced in the analytical models, sophisticated and simplified, affecting the concrete bearing strength ( $f_c$ ) by this factor. In Fig. II.76 is shown the

application of this factor. A good agreement is now obtained between sophisticated and numerical models when the concrete strength is varied. The simplified model is also affected in a consistent way given the limitation referred above. Thus, the analytical models are now suitable to be used in the determination of the properties of the composite beam to reinforced concrete wall joint.

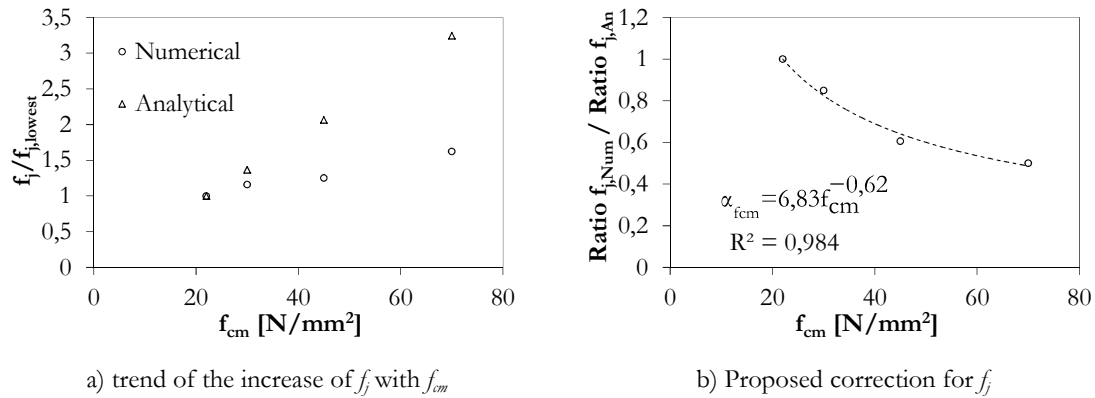


Fig. II.75: Influence of the mean concrete strength on the concrete strength under confined conditions ( $f_j$ )

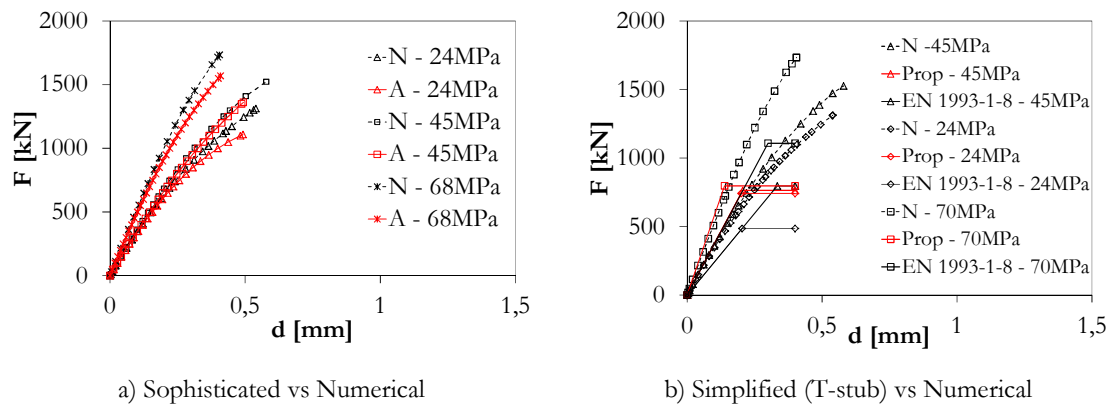


Fig. II.76: Force-deformation curve assessing the sensibility of the analytical models to the length of the steel bracket ( $f_{cm}$ )

## II.3.2 Anchor plate subject to shear

### II.3.2.1 Introduction

In the “Pinned” solution of the joint configuration described in §II.1, and illustrated in Fig. II.2, the anchor plate is externally subjected to shear. Axial load may also be applied though, this combined loading is neglect in the present section. In such conditions, the behaviour of the anchor plate changes in comparison to the case analysed in the previous section. The response of the anchor plate is dependent on the eccentricity of the shear load: for low eccentricities, shear governs the resistance of the joint and high shear resistance is expected; for high eccentricities, secondary bending moment governs behaviour of the connection and lower shear resistance should be obtained.

The analysis of the anchor plate subject to shear requires an extensive work which is outside of the thesis scope, as the main focus is on the semi-continuous joint solution. This

subject was the main research interest of one of the partners of the RFCS research project *InFaSo* (Kuhlmann *et al.*, 2012) at the University of Stuttgart. Within the project an experimental programme (Ozbolt *et al.*, 2011) was accomplished and part of these developments have been described in §II.2.3.2. However, in order to cover all the options for the joint configuration described in §II.1, a brief approach to the behaviour of the anchor plate subject to shear is performed in the present section. This reflects the involvement of the author on the study of the simple joint configuration within referred research project. Thus, numerical models to reproduce two test specimens are presented: one with high and another with low eccentricity. The results of these numerical calculations are analysed identifying the flow of loads through the connection. Then, an analytical component based model to predict the load-deformation behaviour, of this type of joint, is discussed.

### II.3.2.2 Numerical analysis

#### II.3.2.2.1 Numerical tools

The numerical models for the anchor plate subject to shear were developed in the finite element software (Abaqus, 2011) which has been described in §II.3.1.2. Here, the same modelling tools were used as: type of elements, constitutive models, interaction models and numerical strategy for resolution of the non-linear problem. In addition, because in this case the reinforcement in the concrete member has a non-negligible contribution, one of the available techniques to model reinforced concrete was also used.

In Abaqus, the modelling of reinforced concrete in 3D models may be performed using the following options: rebar layer embedded in the concrete; truss element (2 node elements) embedded in concrete; and solid (continuum) elements, embedded or not in the concrete. To model the ordinary reinforcement of the concrete member, the truss elements (T3D2) were preferred to reduce the size of the model. The T3D2 is a 2-node linear 3D truss element which can only transfer axial forces. More information about this element may be found in (Abaqus, 2011).

When using the solid elements, two strategies are available to model the interaction with the concrete:

- 1) Embedded, which corresponds to perfect bond behaviour (rigid link between reinforcement and concrete nodes);
- 2) Bond behaviour, whereby the bond between concrete and reinforcement is modelled by an approximation of the bond-slip response.

The first technique consists of physically superposing the two parts. It is based on master and slave regions, where the nodes of the embedded region (slave, the reinforcement) displace by the same amount as the closest node of the host region (master, the concrete). Such type of modelling enforces a perfect bond between master and slave. However, it is only valid when stress transfer is medium-low. For highly stressed regions, e. g. near cracks, there are different strains in the concrete and in the reinforcement, as slip occurs due to the loss of bond. Therefore, modelling the interaction with perfect bond leads to excessive

stresses in the concrete. In the present case, as only specimens with ordinary reinforcement were modelled, the embedded technique was chosen. The technique to model the reinforcement-concrete bond-slip behaviour is presented later in §II.4.2.1.2.

In order to evaluate the reinforcement-concrete interaction using the selected technique, a benchmark example consisting of a simply supported reinforced concrete beam, loaded at the mid-span with a concentrated load, was used. The description of the experimental test used as benchmark example is out of the scope of this thesis and detailed information may be found in (Matos *et al.*, 2009). The evaluation was mainly focused on the effect of the longitudinal reinforcement on the beam response, verifying its activation. In this way, two models were performed: one with and one without reinforcement. The obtained force-deformation curves are compared in Fig. II.77, where the force is the total load applied to the beam and the deformation corresponds to the mid span deflection. The experimental curve is included. The presence of reinforcement is clearly noticed, as the simulation with reinforcement almost achieves the experimental resistance. The model without reinforcement presents difficulty to converge already at a low load level, as the concrete quickly achieves its tension capacity and there is no reinforcement to transfer the stresses at the bottom part of the beam. Fig. II.78 shows the von Mises stresses developed in the reinforcement for an applied load of approximately 22kN. For this load level and at the mid-span of the beam, the longitudinal reinforcement has already achieved its yield strength.

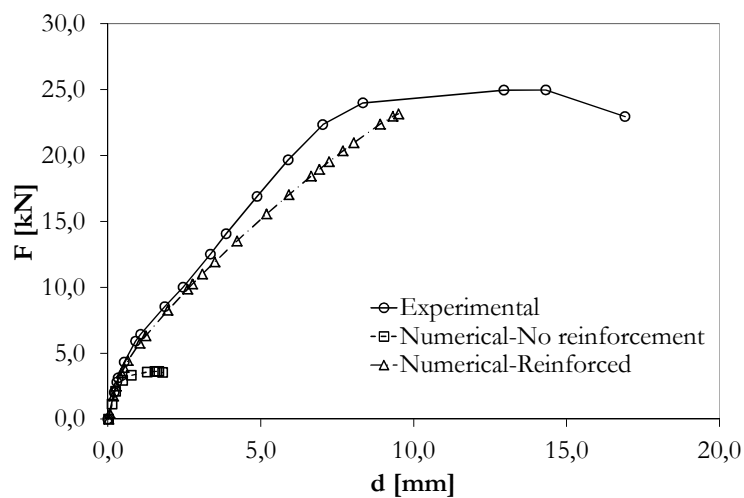


Fig. II.77: Benchmark example to evaluate the reinforcement-concrete interaction in a reinforced concrete beam using the embedded technique: force-deformation curves

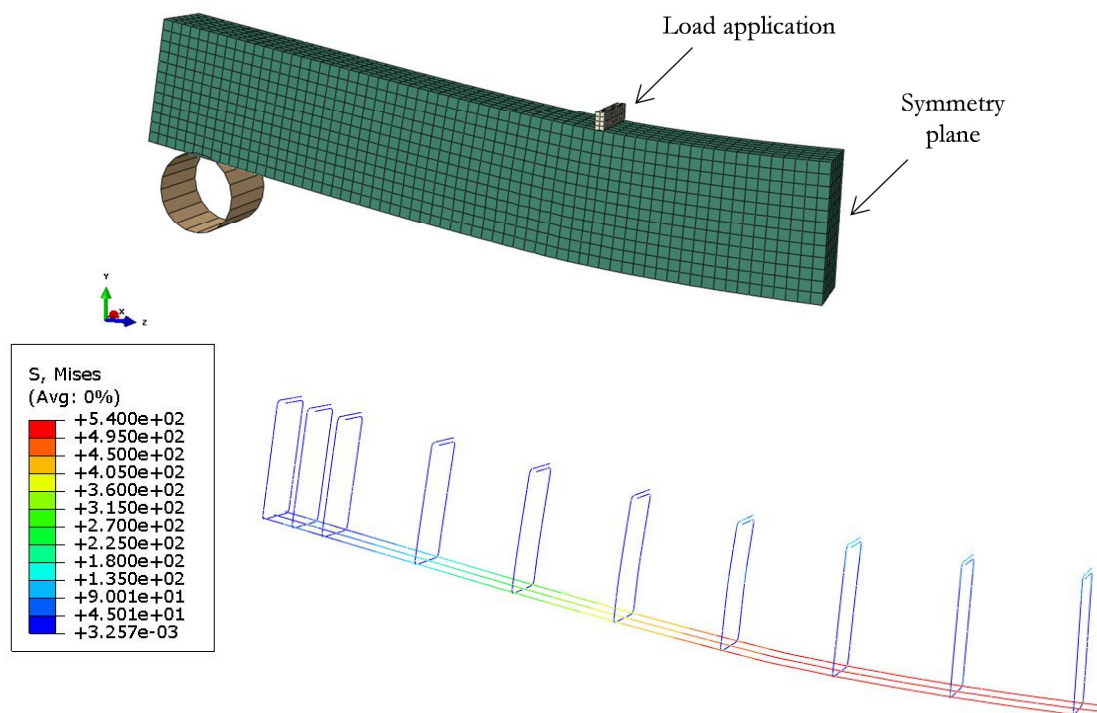
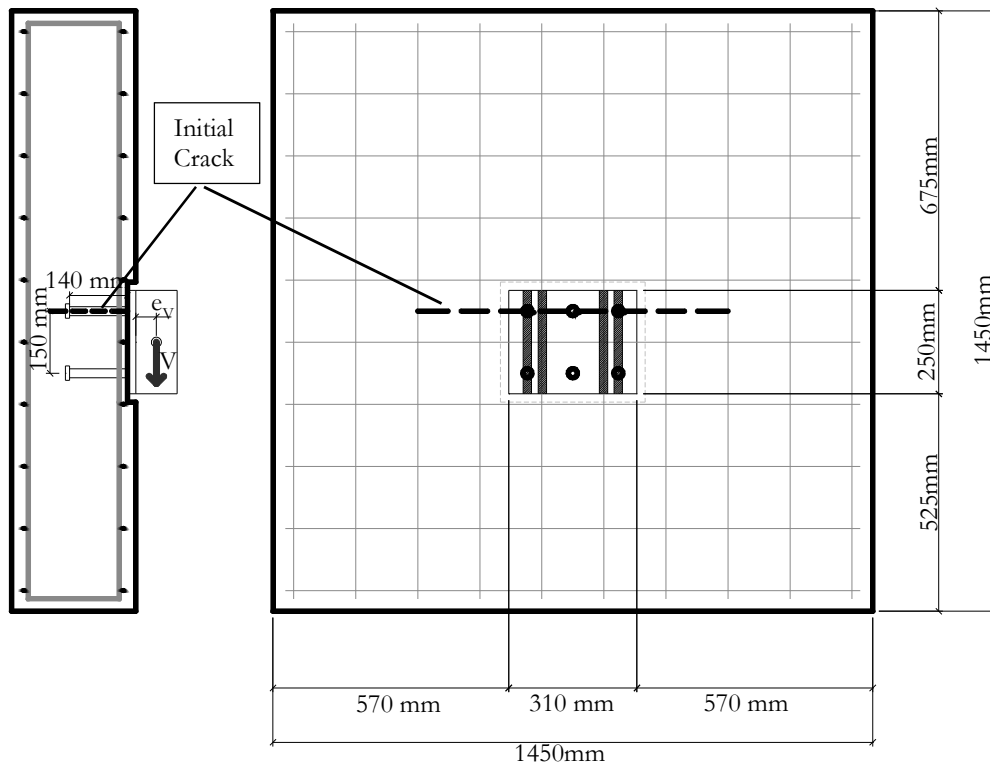


Fig. II.78: Benchmark example to evaluate the reinforcement-concrete interaction in a reinforced concrete beam using the embedded technique: distribution of Von Mises stresses in the reinforcement bars ( $F \approx 22 \text{ kN}$ )

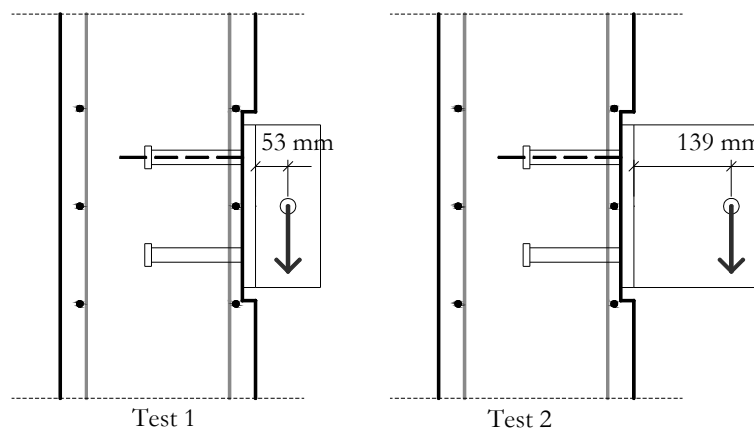
#### II.3.2.2.2 Validation of the numerical model for anchor plate subject to shear

##### a) Summary description of the test specimens, test procedure and test results

The two test specimens selected for numerical simulation present similar geometry in what regards the wall, plate and anchors, as illustrated in Fig. II.79-a). The test procedure consisted in applying the shear load with eccentricity. The difference between the two specimens consists in the eccentricity of the shear load ( $e_V$ ) applied to the connection (Fig. II.79-b). In Table II.22 are summarized the main geometric and material properties of the test specimens. The two tests used in the numerical simulations are here denominated as Test 1 and Test 2. The eccentricity used in each test specimen was  $53 \text{ mm}$  and  $139 \text{ mm}$ , respectively. In order to avoid plastic deformations on the load application system and on the anchor plate, the load is applied to the anchor plate through two double “Fin” plate connections (4 plates were used). These plates and the anchor plate are considerable thick plates ( $20 \text{ mm}$  thick). The loading was monotonic. One of the goals of this test programme was to analyse the behaviour of the anchor plate under cracked concrete conditions therefore, an initial crack was installed at the level of the tension anchor row, perpendicular to the shear load direction, as represented in Fig. II.79-a). The crack width was about  $0,3 \text{ mm}$ . In what respects the concrete member reinforcement detailing reference is given to (Kuhlmann *et al.*, 2012).



a) Test specimen geometry



b) Eccentricities of the shear load in Test 1 and Test 2

Fig. II.79: Tests specimens on anchor plate subject to shear load with low and high eccentricity (Kuhlmann *et al.*, 2012)

The load-deformation curve is presented in Fig. II.80 compares the response of the two test specimens. The load represents the shear load applied to the connection and the deformation is the horizontal displacement of the anchor plate measured at the top anchor row (Fig. II.79). The curves show a clear difference between the test specimens. The load capacity of Test 1, where the shear load had lower eccentricity, is approximately 62% higher than Test 2. In what concerns the initial stiffness the difference is imperceptible. In the post-peak load range, the decrease of load is higher in Test 2 and abrupt. This is justified by the fact the upper anchor row, activated in tension, was the main responsible for the load capacity of the anchor plate. Thus, the mode of failure may be identified as

concrete cone failure. At the maximum load capacity of the connection, the cracks achieve the concrete surface completing the formation of the concrete cone. As consequence, load drops considerably up to a plateau where, within the crack interface, the friction between concrete parts, the mechanical interlock between the aggregates and the ordinary reinforcement of concrete member guarantee a reserve of resistance. In Test 1, shear governs the resistance of the connection and the mode of failure is identified as a pry-out failure (see definition in §II.2.2.2). Though, given some similarities between concrete cone and concrete pry-out failure, the identification of the mode of failure through visualization of the test specimens after the experiments was not immediate.

Table II.22: Summary of the geometric and material properties of the anchor plate subject to shear load (Kuhlmann *et al.*, 2012)

Test Sp.	Fastener	Ecc., $e_v$ [mm]	Anchorage length, $h_{eff}$ [mm]	Concrete condition	Disposition of studs	Concrete, $f_{cm}$ [MPa]	Anchor Plate, $f_y$ [MPa]
Test 1	SD22/150	53	160	Cracked	2x3	25,04	S235JS+ C450
Test 2	SD22/150	139	160	Cracked	2x3	26,22	S235JS+ C450

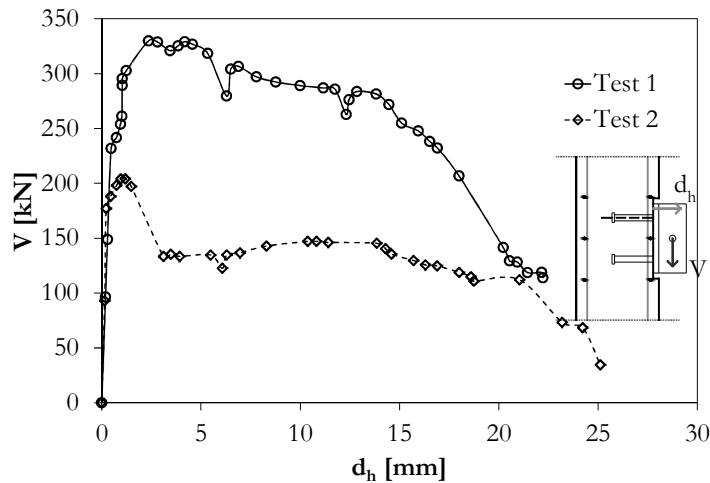


Fig. II.80: Force-deformation comparing the anchor plate subject to shear load with different eccentricities

- b) Numerical models developed to simulate the anchor plate subject to shear load and comparison with experimental results

The numerical model developed to reproduce the test specimens described above are illustrated in Fig. II.81. The numerical techniques referred in §II.3.2.2.1 were implemented. In order to simulate the initial crack, as a simplification, a gap in the concrete member was considered in the region around the tension anchor row (see Fig. II.81). The magnitude of this gap was approximately 0,3mm, as in the experimental tests. Profiting from the



symmetry of the test specimens, only half was modelled. The loading of the anchor plate follow the same configuration of experimental tests; two thick “Fin” plates were rigidly link to the anchor plate (see Fig. II.81). The boundary conditions considered in the model were simplified and considered the restraint of the nodes in the top and bottom surface of the wall, in the three degrees of freedom. Additional boundary conditions were considered because of the symmetry of the specimens.

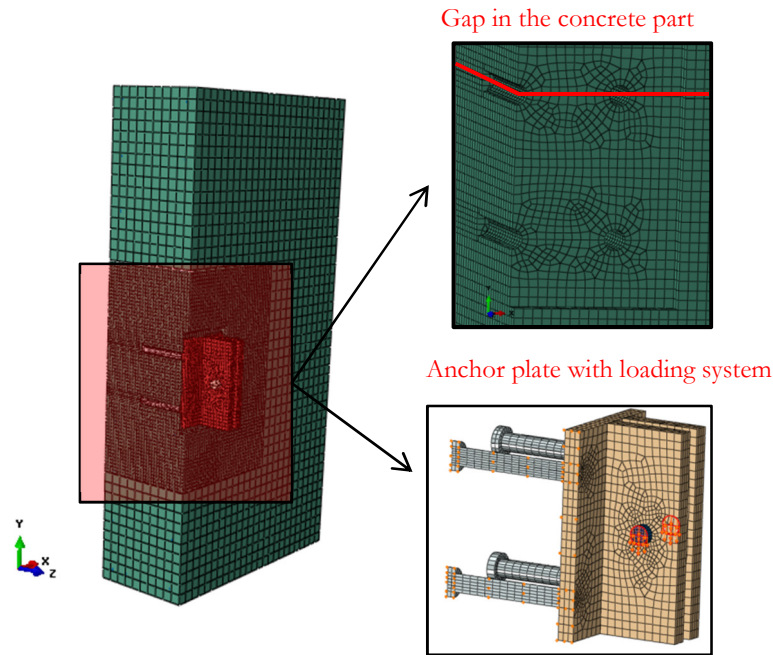


Fig. II.81: Numerical model to simulate the anchor plate subject to shear load with eccentricity

The force-deformation curves comparing experimental and numerical results are shown in Fig. II.82. These show that the numerical model can only reproduce the ascending branch, after the maximum load was achieved, numerical difficulties appeared and the numerical simulations were interrupted due to the lack of convergence. These result from the incapacity of the numerical model to reproduce the complete development of cracks in the concrete. When an element extinguishes its fracture energy, parameter used to define the complete formation of a crack in an element (see definition given in §II.3.1.2.1), the numerical model has difficulty to satisfy the convergence criterion. In (Abaqus, 2011) an explicit numerical solver is available which may overcome these numerical difficulties (Yu *et al.*, 2008). Though, the exploitation of this numerical tool is out of the scope of the present thesis. Furthermore, for the desired approach the numerical results are satisfactory. The ratio of maximum resistance between the numerical simulations and experimental tests, for Test 1 and Test 2, respectively, are 0,86 and 1,09. As the concrete governs the behaviour of these connections, the variability of the material properties and the exact location and extent of the initial crack, have significant influence in the quality of these results. In Fig. II.83 are shown the development of cracks in both numerical models. In both is clear the formation of the concrete cone in the upper row where tension loads are developed due to the secondary bending moment generated with the eccentricity of the shear load. Though, the ultimate load of Test 2 is considerably smaller than in Test 1, the development of

cracks is higher in the first because of the higher eccentricity. This confirms that the numerical simulations can approximately reasonably the experimental tests.

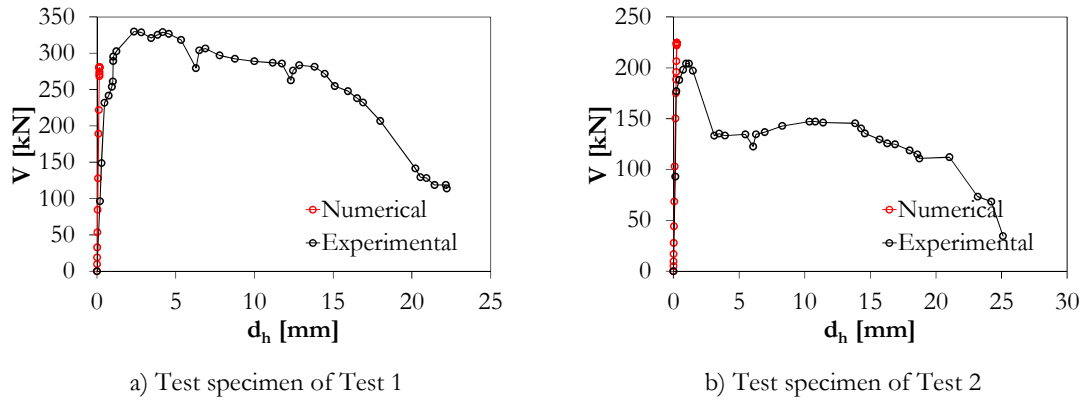


Fig. II.82: Force-deformation curve comparing numerical simulations and experimental tests on the anchor plate subject to shear load with eccentricity

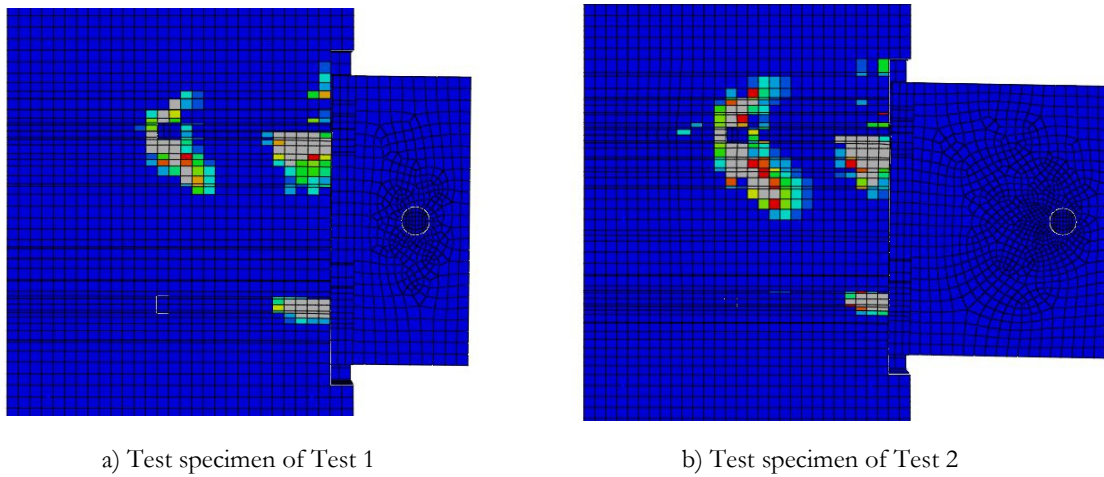


Fig. II.83: Crack pattern at ultimate load in the numerical models simulating the anchor plate subject to shear load with eccentricity

### II.3.2.2.3 Discussion on the numerical simulations of the anchor plate subject to shear

In order to identify the flow of loads through the connection, the numerical simulation of Test 2 is hereafter further analysed.

The shear load applied with eccentricity leads to the development of a secondary bending moment on the anchor plate. As result, besides the reaction to the shear load, tension and compression reactions are developed internally to equilibrate the generated bending moment. An approximation of the compression reaction was obtained through integration of the pressure developed in the plate-concrete contact interface (Fig. II.84), using expression (II.60). Fig. II.84 shows that the compression is limited to the region between the bottom edge of the plate and the bottom anchor row. It is noticed that the pressure (therefore compression) decreases from the plate edge to the referred anchor row showing an concentration of stresses near the plate edge. From this distribution of pressures, it may be assumed that only the upper anchor row is activated in tension and equilibrates the

compression developed at the bottom. The referred integration of pressure stresses resulted in binary force of approximately  $195kN$ .

$$F_c = \int_{A_{pl-con}} CPRESS \quad (II.60)$$

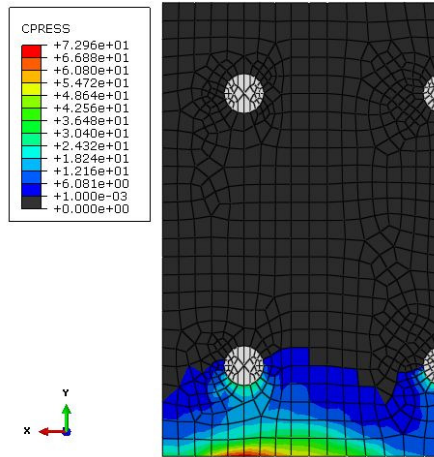
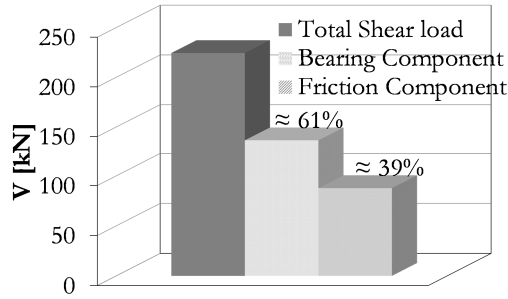


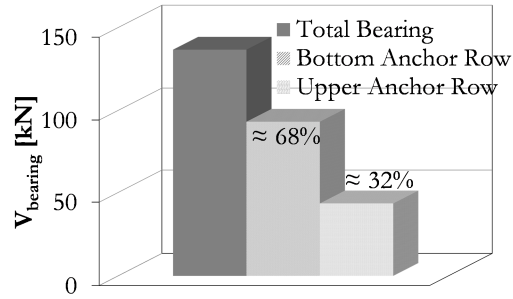
Fig. II.84: Pressure ( $N/mm^2$ ) in the plate-concrete contact interface

In the compressed part of the connection, friction develops contributing to the shear resistance of the connection. Knowing that the friction coefficient assumed in the model, for the plate-concrete interface, was 0,45 (Cook and Klinger, 1992), the total friction reaction was determined. Consequently, the remaining reaction is due to the bearing between anchor shanks and concrete. In Fig. II.85-a) is shown the distribution of the shear load through these two components, friction and bearing, showing that 61% of the shear load is transferred through bearing and 39% through friction. A distribution of the bearing reaction between the anchor rows was approximated integrating the shear stresses on the bottom anchor row, as expressed in (II.61). The quantity  $S_{23}$  represents the shear stresses in the direction of the shear load. Fig. II.85-b) shows the results of this calculation. It can be observed that the bottom anchor row transfers approximately 2 times the load transferred by the upper anchor row. This can be justified by the fact the upper anchor row is also activated in tension and therefore, their stiffness to the shear load is reduced.

$$V_{bear,Bt} = \int_{A_s} S_{23} \quad (II.61)$$



a) Distribution of between shear components



b) Distribution of bearing between bottom and upper row

Fig. II.85: Distribution of shear load in the anchor plate connection simulation of Test 2

As described above, the anchor plate connection is subjected to a combined loading (shear + bending moment). For such conditions, the equilibrium in the plate may be written as expressed in (II.62). The external bending moment ( $M_{ext}$ ), due to shear load ( $V$ ) with eccentricity ( $e_v$ ), is in balance with the internal bending moment ( $M_{int}$ ). The equilibrium equation is written at the centroid of the bearing reaction of the anchors ( $V_{bear,Bt}$  and  $V_{bear,Tp}$ ), as illustrated in Fig. II.86. Thus, the friction component of the shear reaction ( $V_f$ ) has to be taken into consideration. In order to solve the equation and determine the lever arm ( $z_{C-T}$ ) between the internal compression ( $F_c$ ) and tension ( $F_t$ ) forces, the position ( $z_{V,bear}$ ) of the bearing reaction had to be approximated. This approximation was obtained from the numerical model, using the bearing pressure along the anchors shank. The bearing pressure along the bottom anchor shank is plotted in Fig. II.87. It can be perceived the decrease of pressure with the increase of the depth. The evolution is almost linear. From these results, the centroid of the bearing reaction is approximately at  $16mm$  of the depth of the anchor shank. Solving the equation (II.62), in order to the lever arm of the internal binary ( $z_{C-T}$ ), it was obtained an internal lever arm of approximately  $194mm$ . This result gives a compression reaction close to the edge of the plate which demonstrates that the plate behaves as rigid. Though, it should be taken into account that the compression load obtained above may be slightly underestimated, because a percentage of the compression load is also transferred through the bottom anchor row.

$$M_{ext} = M_{int} \rightarrow V \left( e + t_{ap} + z_{V,bear} \right) = F_c z_{C-T} + V_f z_{V,bear} \quad (II.62)$$

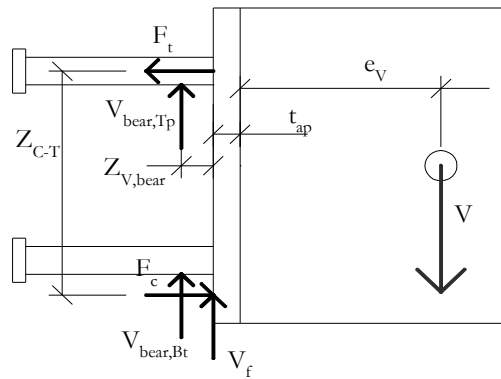


Fig. II.86: Equilibrium of loads in the anchor plate

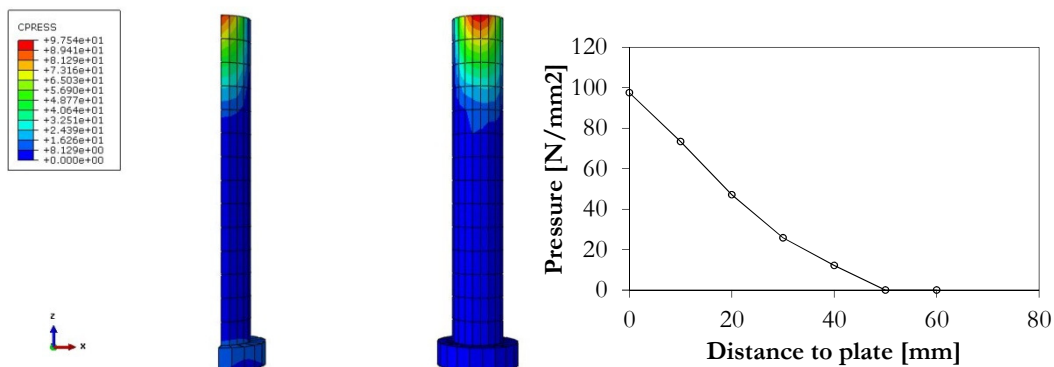


Fig. II.87: Distribution of the bearing pressure along the anchor shanks

### II.3.2.3 Analytical model to characterize the connection behaviour

#### II.3.2.3.1 Components activated in the connection

The simple joint using an anchor plate is a solution composed of two connections: one steel-to-steel and one steel-to-concrete. In the first case, a common “steel” solution, as a “Fin” plate connection, may be used. This type of connection is common in steel structures and consistent guidance for its analysis following the component method principles is available in (Jaspart *et al.*, 2009). In the experimental tests in (Kuhlmann *et al.*, 2012), the failure on this part of the joint was excluded. Consequently, this type of connection is not subject of study on the present thesis. Thus, the focus is on the second connection of the joint, the connection between the anchor plate and the reinforced concrete member. In this connection, “new” joint components are identified that are not covered in (EN 1993-1-8, 2005) or in (EN 1994-1-1, 2004), and regard the failure modes associated to the anchorage in concrete. These components are identified in Fig. II.88 and Fig. II.89, and may be distinguished in two groups of components: i) one representing those related to the anchorage in tension (Fig. II.88); ii) another representing those related to the anchorage in shear (Fig. II.89). As discussed in §II.2.2.2, additional reinforcement (Fig. II.21) may be included in the anchorage to improve behaviour of the anchorage to concrete cone failure or to concrete edge failure. This reinforcement should be considered as an additional component. Note that, as in the tests the edge distances are significant.

Therefore, their effect on the response of the connection maybe disregarded and, the following components are not considered in the analytical model presented here below: splitting failure (Fig. II.88-d); blow-out failure (Fig. II.88-e); concrete edge failure (Fig. II.89-b).

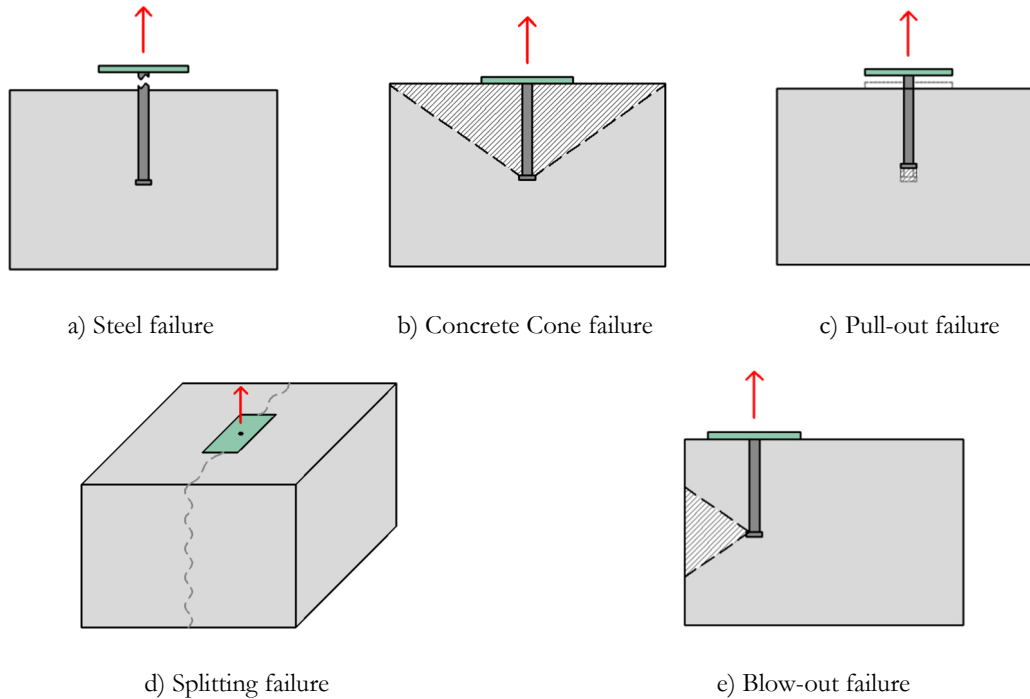


Fig. II.88: Failure modes of anchorage in tension identified as joint components

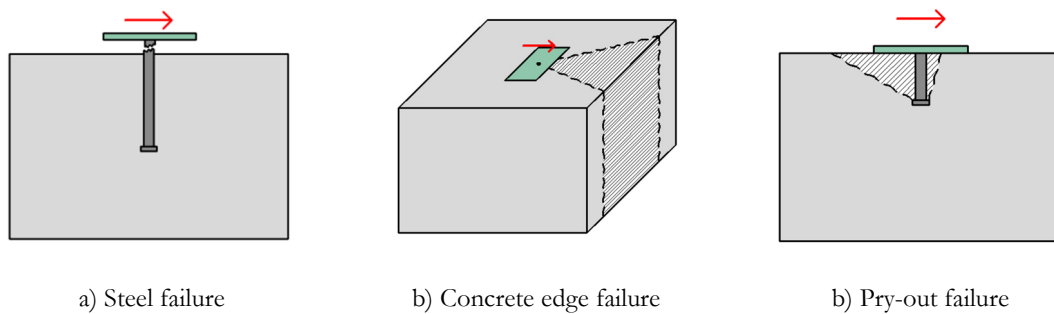


Fig. II.89: Failure modes of anchorage in shear identified as joint components

As required by the component method, these components have to be characterized by means of force-deformation curves. In terms of resistance, the characterization of the different failure models is well documented, as discussed in §II.1. However, the design philosophy is based on capacity (resistance) and disregards the deformation of the connection. Important contribution to the deformation characterization has been obtained in RFCS research project *InFaSo* (Kuhlmann *et al.*, 2012), as described in II.2.3. In Table II.23 are listed these components and reference to the corresponding models given. Note that the components numbering follows that given in Table II.1.

Table II.23: List of components for anchor plate connection (simple joint)

N°	Component	Type	Characterization
6	Concrete in compression	Compression	Resistance: Concrete block $F_c = 3f_{cm} \times b_{ap}$ Deformation (stiffness): $k_c = E_c \times b_{ap} / h_c$ (Ozbolt <i>et al.</i> , 2011)
7	Headed anchor in tension	Tension	Resistance: (II.18) Deformation: (II.19)
8	Concrete cone	Tension	Resistance: (II.26) Deformation: Table II.8 Model proposed in (Berger <i>et al.</i> , 2011)
9	Pull-out of anchor	Tension	Resistance: (II.27) Deformation: (II.28)
10	Anchor plate in bending under tension	Tension	T-stub in tension (EN 1993-1-8, 2005)
12	Hanger reinforcement	Tension	Resistance: (II.32) Deformation: Table II.8 Model improved in (Berger <i>et al.</i> , 2011)
13	Plate-concrete friction	Shear	Conventional Resistance: $V_f = \mu_f F_c$ Deformation: rigid
14	Headed anchor in shear	Shear	Resistance: (II.36) Deformation: -
15	Concrete Pry-out	Shear	Resistance: (II.37) Deformation: -

The evaluation of the concrete in compression component (6) is dependent of the plate stiffness and on the system used to perform the steel-to-steel connection, “Fin plate” or “Steel console”. In the particular case of the tests performed in (Kuhlmann *et al.*, 2012), the plate thickness is considerably thick and may be assumed as rigid. In (Ozbolt *et al.*, 2011), a simplified approach considering a uniform compression block (Fig. II.90) is used and is here applied. Within this compressed region, the concrete is assumed to present an increased strength ( $3f_{cm}$ ). This assumption is based on the confinement effect provided to the concrete by the surrounding concrete and the anchor plate.

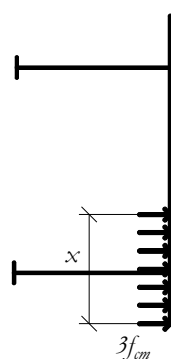


Fig. II.90: Concrete in compression component (6) assuming an uniform compression block (Ozbolt *et al.*, 2011)

### II.3.2.3.2 Component based analytical model

In Fig. II.91-a) is schematically represented the loaded regions in the anchor plate connection of the simple joint. Accordingly, and based on the components identified in the previous sub-section, the component based spring mechanical models represented in Fig. II.91-b) and c), respectively, for bending moment and shear load, were idealized. In what concerns the model for bending moment, note that component 8 (concrete cone) and 12 (hanger reinforcement) are added. According to the experimental observations (Kuhlmann *et al.*, 2012) and the analytical model proposed in (Berger *et al.*, 2011), these components act in parallel, having an added contribution for resistance and stiffness.

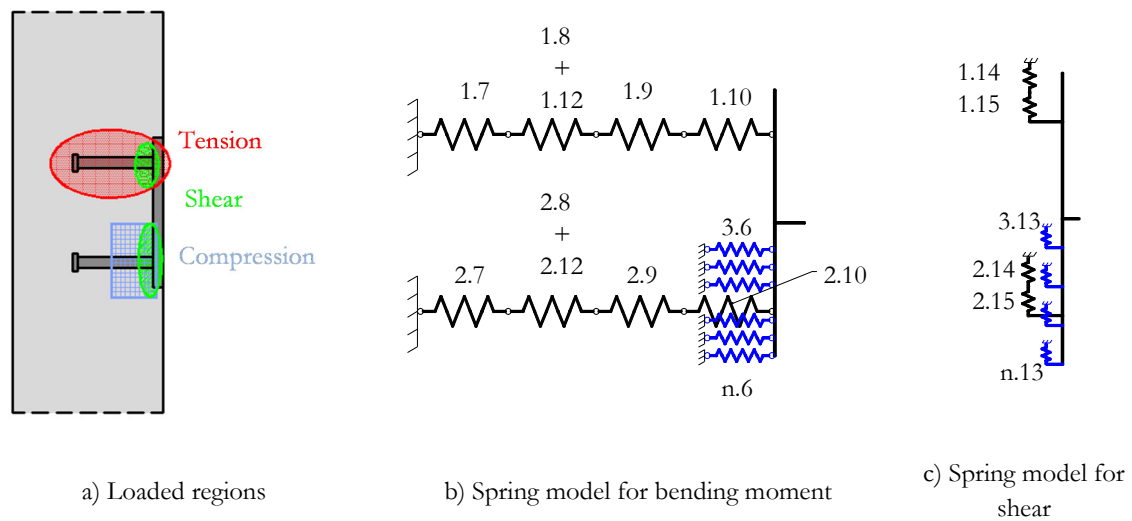


Fig. II.91: Anchor plate connection (simple joint) component models

The assembly of the model represented in Fig. II.91-b) may be separated in two steps: assembly of components per row; and assembly of the joint model. In the first case, each row is represented by a single equivalent spring, which requires the assembly of the components properties, strength and stiffness. In order to calculate the strength, a distribution of resistance per anchor row taking into account the group effects has to be performed. A distribution of loads can be based on a similar procedure applied to steel joints according to (EN 1993-1-8, 2005). However, experimental evidence and numerical results have to be performed to sustain the application of these principles. Such research work is out of the scope of the present thesis. Furthermore, according to the numerical analysis in §II.3.2.2, for the tested joints, assuming only the upper row is activated in tension appears to be sufficiently accurate. Thus, the tension resistance of the upper anchor row is given as follows.

$$F_t = \text{Min}\{F_{t,i}\} \text{ with } i=7, 8 \text{ (or } 8+12), 9, 10 \quad (\text{II.63})$$

The tension force should be in equilibrium with the compression force. Thus, the dimension of the compression region ( $A_{comp}$ ) may be determined as follows.



$$F_c = F_t \rightarrow A_{comp} = \frac{F_t}{3f_{ck}} \quad (\text{II.64})$$

It should be remarked that the determination of the forces ( $F_t$  and  $F_c$ ) requires an iterative procedure, as the resistance of the anchorage is dependent on the distance from the anchorage to the centre of compression ( $\Psi_m$ ), as described in §II.2.2.2.2. Though, a small number of iterations are usually required.

In order to determine the connection bending moment resistance, the lever arm ( $z_{C-T}$ ) of the internal binary force ( $F_{C-T}$ ) is obtained from the distance between the tension anchor row axis and the mid height of the compression region ( $A_{comp}$ ). Thus, the connection bending moment resistance is obtained as follows.

$$M_{ap,R} = F_{C-T} z_{C-T} \quad (\text{II.65})$$

In what respects to the deformation, the plate rotation is determined. Considering only one row in tension, the determination of the plate rotation requires the calculation of the horizontal deformation component of the plate deformation, between the tension and compression components. At each load step, the horizontal component of the connection deformation ( $d_{h,C-T}$ ) can be obtained from the connection components deformation as follows.

$$d_{h,C-T} = \sum d_i \text{ with } i=6, 7, 8 \text{ (or } 8+12), 9, 10 \quad (\text{II.66})$$

Subsequently, the connection rotation is determined.

$$\Phi_{ap} = \frac{d_{h,C-T}}{z_{C-T}} \quad (\text{II.67})$$

For the shear load, the experimental tests (Kuhlmann *et al.*, 2012) showed that the connections was considerably stiff to assume the behaviour as rigid. Thus, from the model in Fig. II.91-c) only the shear resistance of the connection is determined.

$$V_{ap,R} = \sum_{i=1}^2 \text{Min}\{F_{i,14}; F_{i,15}\} + \sum_{i=3}^n F_{i,13} \quad (\text{II.68})$$

The bending moment and shear load resistance determined according to (II.65) and to (II.68), respectively, are obtained as isolated resistance. As equilibrium has to be verified within the connection, expression (II.62) has to be applied and the bending and the shear resistance reduced accordingly. Finally, note that in (II.68) it is assumed that the upper anchor row is capable of reaching its maximum bearing capacity. Though, as this anchor row is also subjected to tension, the interaction between tension and shear on the anchor row has to be verified, as described in §II.2.2.2.4. Conservatively, only the bottom anchor row may be assumed to contribute to the shear resistance through bearing.

### II.3.2.3.3 Assessment of the accuracy of the analytical model

The application of the described analytical model is compared with experimental tests (Kuhlmann *et al.*, 2012). In order to introduce the effect of the hanger reinforcement in this type of connection, two additional tests were used. The test specimens' geometric and mechanical properties are given in Table II.24. The comparison of results presented in Fig. II.92 uses the shear load versus anchor plate rotation. Test 3 (Fig. II.92-a) represents the specimen without reinforcement. The concrete in tension at the upper row is responsible for the failure of the connection. Load capacity is smaller and a brittle behaviour is observed. The analytical curve presents an excellent approximation in the ascending branch. The maximum load is underestimated (11% below) but with a sufficient accuracy. In what regards to the descending branch, the level of the accuracy decreases. Though, given the absence of model to characterise the deformation of the component concrete cone, the obtained approximation has to be considered satisfactory. In Test 4 (Fig. II.92-b), failure also occurs on the concrete in tension at the upper anchor row however, now influenced with the presence of the hanger reinforcement. Consequently, higher load capacity and ductility was obtained. Again, the analytical model underestimates the load capacity (12% below) but with satisfactory accuracy. The analytical model reproduces the ascending branch of the curve very accurately. As for Test 3, accuracy is lost in the descending branch. Though, it can be noticed that the analytical model predicts an increase of deformation capacity due to the hanger reinforcement with satisfactory approximation.

Table II.24: Geometrical and mechanical properties of the test specimens' used for evaluation of the analytical model for anchor plates

Test Sp.	Fastener	Ecc., $e_v$ [mm]	Anchorage length, $h_{eff}$ [mm]	Concrete condition	Disposition of studs	Concrete, $f_{cm}$ [MPa]	Anchor Plate, $f_y$ [MPa]
Test 3	SD22/150	139	160	Cracked	2x2	31,07	S235JS+C450
Test 4	SD22/150	139	160	Cracked	2x2	30,74	S235JS+C450

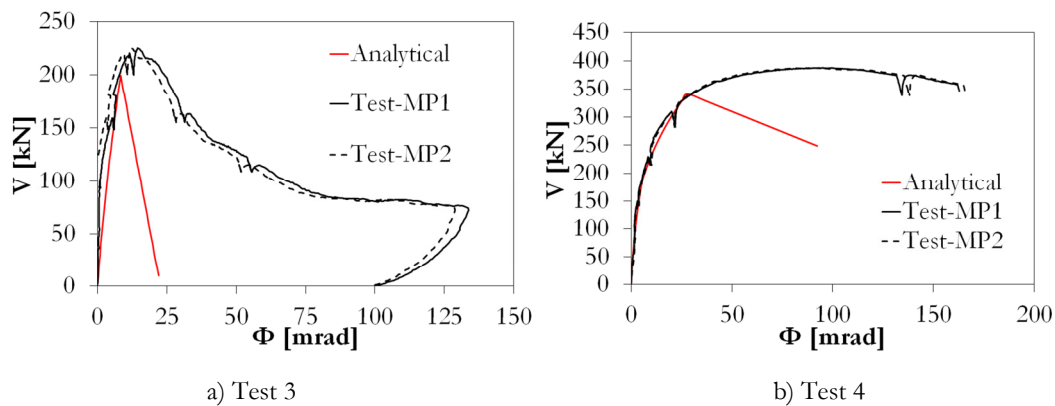


Fig. II.92: Shear load to anchor plate rotation curve comparing experimental and analytical results

## II.3.3 Anchor plate subject to combined shear and compression

### II.3.3.1 Introduction

The real loading conditions of the anchor plate within composite beam to reinforced concrete wall joint are the combination of shear and compression loads. However, as discussed in §II.1, for the tested joint configurations the compression load is clearly dominant and the effect of the shear load may be neglected. The cases where the shear load becomes more relevant are those where the external load is applied to the beam closer to the joint, decreasing the bending moment acting on the joint and consequently increasing the ratio between shear and compression loads (Fig. II.93). Though, this situation is more theoretical than practical, as the joint configuration was conceived to be a bending moment resistant joint solution. For these reasons, a brief approach to the anchor plate subject to combined shear and compression load is performed in the present section. This relies on numerical simulations as no experimental data for such cases is available.

The most efficient way to express the influence of the combined loading is by means of interaction curves. In order to obtain an interaction curve several numerical models, using the dimensions and mechanical properties of the reference case presented in §II.3.1, were performed considering the following:

- One model with anchor plate subject to pure compression
- One model with anchor plate subject to pure shear
- Several models with anchor plate subject to X% maximum compression and shear load increased up to failure, from model to model, X varies from 10 to 90.

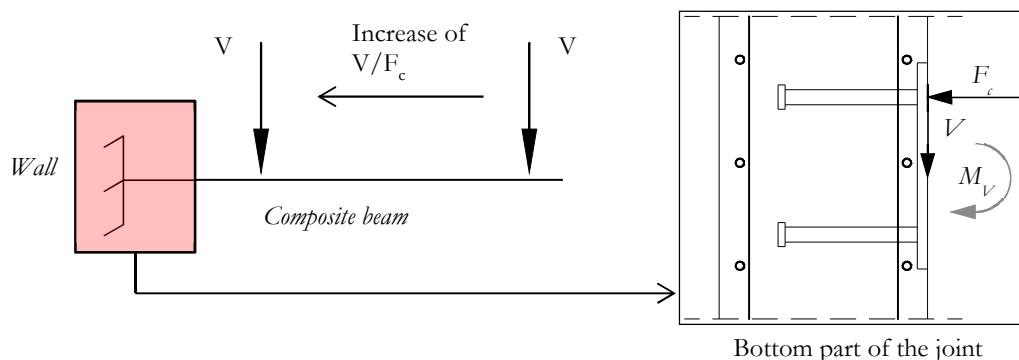


Fig. II.93: Influence of the position of the shear load (V), along the composite beam, on  $V/F_c$  ratio

### II.3.3.2 Numerical analysis of the anchor plate under combined shear and compression

The developed numerical models are summarized in Table II.25. In the present analysis, the presence of shear load requires that the upper anchor row was considered, contrarily to the numerical simulations performed in §II.3.1. For detail description on the numerical models characteristics, please check §II.3.1. The results of these models are summarized in Table II.26. Note that as in §II.3.1, not limit of strain was assumed for the steel therefore, only concrete failure was obtained. The interaction curve obtained with the performed

numerical simulations is depicted in Fig. II.94. It can be observed that the presence of compression load as a favourable influence in the shear resistance of the connection. Higher the compression load acting on the joint, higher the shear resistance. Part of this increase of shear resistance is due to the friction component between the anchor plate and the concrete block which is directly proportional to the compression load. From the interaction curve an expression to determine the shear capacity of the connection was obtained through regression analysis. In (II.69), the shear resistance is calculated in function of three parameters: i) the compression resistance without shear load ( $N_{V=0}$ ); ii) the shear resistance without compression load ( $V_{N=0}$ ); iii) the compression load acting on the joint ( $N$ ). The first two may be calculated using the approaches described in §II.3.1 and §II.3.2, respectively.

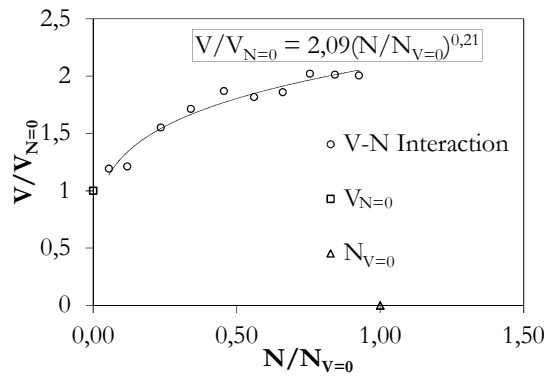


Fig. II.94: Interaction curve resulting of the numerical simulations to analyse the anchor plate under combined shear and compression loading

Table II.25: Numerical models executed for the analysis of the anchor plate under combined shear and compression loading

Model	Description
AP-100N	This model is the reference model described in §II.3.1 Only compression load is applied to the anchor plate The load is increased up to failure
AP-100V	The model considers the same geometrical and mechanical properties of the previous model Only shear load is applied to the anchor plate The shear load is applied in the steel bracket with 25mm of eccentricity to the anchor plate The shear load is applied up to failure
AP-X%N+V	The same geometric and mechanical properties of the previous models Compression and shear load are applied to the anchor plate, as in the previous models First, the compression load is applied up to X% of the resistance obtained in model AP-100N Then, the shear load applied and increased up to failure

Table II.26: Summary of the simulations results to analyse the anchor plate under combined shear and compression loading

Model	Failure Mode	Comment
AP-100N	The model is limited by the concrete elements in compression in the region under the contact plate where the load is applied (remember reference case in §II.3.1)	The maximum concrete compression strain is attained limiting the load capacity
AP-100V	The load capacity is limited by the concrete elements under anchor shanks	<p>The maximum concrete compression strain is attained limiting the load capacity (due to bearing between the anchor shank and concrete)</p> <p>The bearing between anchor shanks and concrete is the main source of resistance</p> <p>The eccentricity of the shear load is relatively small and therefore, the tension stresses due to the secondary bending moment developed did not govern the anchor plate resistance</p>
AP-X%N+V	The same as previous	The same as previous

$$V = \begin{cases} V_{N=0} & \text{if } N=0 \\ V_{N=0} (2,09 (N/N_{V=0})^{0,21}) & \text{if } N>0 \end{cases} \quad (\text{II.69})$$

## II.4 Joint Link

### II.4.1 Introduction

The part of the semi-continuous joint configuration, within the reinforced concrete wall, adjacent to the connection, is analysed in the present chapter. This has been identified in Fig. II.7 and is denominated as “Joint Link”. The main objective is to introduce the behaviour of this component in the global analysis of the joint which is commonly disregarded, as it “concerns” reinforced concrete design. Though, the limitations of the analysis have to be taken into consideration, as no specific tests on this part of the joint are available and the experimental investigations performed within *InFaSo* research project (Kuhlmann *et al.*, 2012) focussed in other components. In this way, the approach is strongly based on numerical calculations. The developed numerical models are used to: i) investigate the behaviour of the joint link in terms of stress flow and critical regions; iii) evaluate the influence of relevant geometric parameters and characterize the response in terms of force-deformation curves; iii) form the basis of an analytical model. The latter is proposed to include the joint link in the complete joint model. Due to the referred limitations, the proposals are conservative approaches which envisage avoiding premature failure of the joint link and include its deformation in the complete model. Given the nature of this part of the joint, the proposed analytical model is STM based. In the following sections the numerical calculations are discussed, and the analytical model presented and validated.

For the present analysis the geometrical and the mechanical properties of the reinforced concrete wall used in the tests performed in the *InFaSo* research project (Kuhlmann *et al.*, 2012) were considered as reference. The study is focussed on the reinforced concrete wall therefore, only the following parts are considered:

- Reinforced Concrete Wall (including its ordinary reinforcement);
- Longitudinal reinforcement of the composite beam (only part extended into the wall);
- Anchor plate (anchors were neglected);
- Contact plate (introduction of load).

Fig. II.95 provides detail of the reinforced concrete wall under consideration. The main mechanical properties of the reference test specimen are given in Table II.27. According to the problem under study the following assumptions were considered in the analysis:

- Loading: Binary action was considered with tension applied at the reinforcement bars and compression at contact plate;
- Supports: the boundary conditions were assumed at top and bottom wall faces;
- Materials: non-linear behaviour was considered only for concrete, all steel parts were assumed linear elastic.

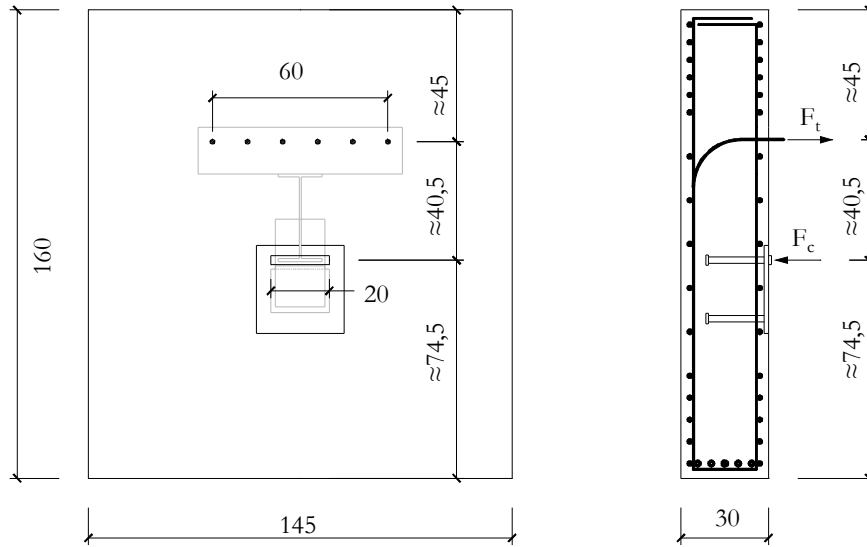


Fig. II.95: Reinforced concrete wall used in the joint tests performed in the *InFaSo* research project (Kuhlmann *et al.*, 2012) and reference for the study of the joint link component (*cm*)

Table II.27: Mechanical properties of the reference case for analysis of the joint link component

Concrete		Longitudinal reinforcement		Wall ordinary reinforcement		Steel plates	
$f_{cm}$ [N/mm <sup>2</sup> ]	$E_c$ [N/mm <sup>2</sup> ]	$f_{sym}$ [N/mm <sup>2</sup> ]	$E_s$ [N/mm <sup>2</sup> ]	$f_{yk}$ [N/mm <sup>2</sup> ]	$E_s$ [N/mm <sup>2</sup> ]	$f_{yk}$ [N/mm <sup>2</sup> ]	$E_s$ [N/mm <sup>2</sup> ]
70,3	39,49E3	520	210E3	500	210E3	355	210E3

## II.4.2 Numerical modelling basis of analytical modelling

### II.4.2.1 Description of the numerical model

#### II.4.2.1.1 General

The numerical tool used is the non-linear finite element package ABAQUS (Abaqus, 2011) that has been previously presented.

The mechanical problem illustrated in Fig. II.95 has relevant discontinuities which influence the type of numerical model developed. First, the loading zones, tension and compression, are asymmetric leading to a non-uniform flow of stresses within the wall. In addition to this asymmetry, the tension load is introduced by the longitudinal reinforcement interaction with the surrounding concrete, either by bond or by mechanical contact. For these reasons, a 3D modelling of the problem instead of a simplified 2D model is required. Thus, the C3D8R finite element and the constitutive models described in §II.3.1.2.1 are used. In what concerns the interactions, three types have to be distinguished: i) contact plate to anchor plate; ii) anchor plate to concrete; iii) reinforcement (both ordinary and longitudinal) to concrete. In what concerns the two first, respectively, the tie constraint and the hard contact without friction models, described in the previous sections, were used. For the third, the interaction model considered a bond model which can rely in an approximation of the bond-slip behaviour or in a perfect bond model. The

choice depends on the type reinforcement in consideration. Given the importance of the reinforcement-concrete interaction, the following section is dedicated to the discussion bond-slip model available in (Abaqus, 2011). The perfect bond model has been described in §II.3.2.2.1. In what concerns the boundary conditions, as stated, these were considered at the top and bottom surfaces of the wall where the displacements of the elements nodes were constrained in all degrees of freedom. The developed model is illustrated in Fig. II.96. No sensitivity study was performed, the conclusions of the analysis presented in §II.3.1.2.3 were taken into account. Thus, using an acceptable element dimension, the main effort in the mesh construction was to obtain low aspect ratios. However, in the regions where concentrations of stresses were expected, as around the longitudinal reinforcement and the steel plate, the finite element mesh was finer.

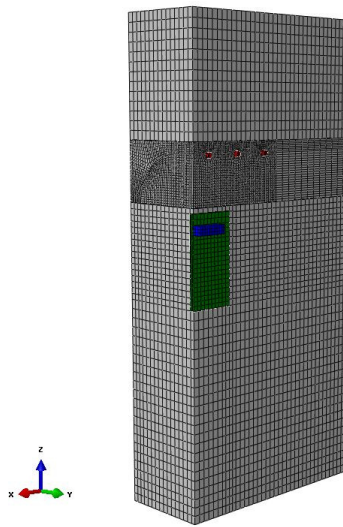


Fig. II.96: Numerical model of reinforced concrete wall for study of the joint link component

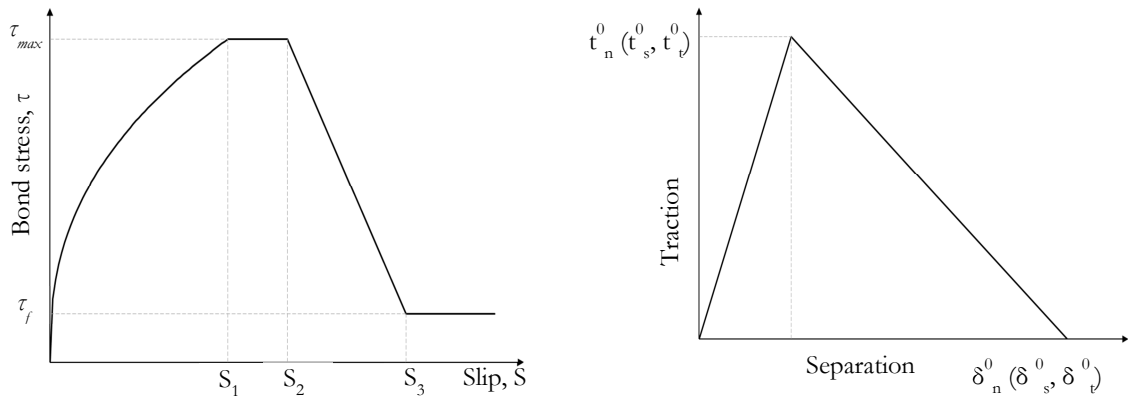
#### II.4.2.1.2 Reinforced concrete numerical modelling

To model the bond behaviour in the reinforcement-concrete interface two strategies are possible: i) using cohesive elements between reinforcement and concrete; ii) modelling the contact interface with cohesive behaviour. Both techniques imply that the reinforcement and the concrete elements are not superposed, contrarily to the embedded technique. Consequently, their implementation is much more time consuming. In the present problem, the contact with cohesive behaviour was chosen to model the bond between concrete and longitudinal reinforcement bar.

The theoretical basis for the modelling of the reinforcement-concrete bond behaviour is the stress-slip relation proposed by (Eligehausen *et al.*, 1983). It constitutes the basis of the model prescribed in (CEB-FIP, 1993) as represented in Fig. II.97-a). It is characterized by an increasing non-linear branch, up to a maximum bond stress ( $\tau_{max}$ ). Then, depending on the concrete confinement, a plateau may be assumed followed by a linearly decreasing branch which achieves a second plateau at the ultimate bond resistance ( $\tau_f$ ). The slip at maximum stress ( $S_1$  and  $S_2$ ) and at ultimate bond resistance ( $S_3$ ) depends on the confinement and bond conditions. Within the present work, no tests were performed to characterize the stress-slip relation. Therefore, the evaluation of the different parameters



required to define this behaviour were taken from (CEB-FIP, 1993) according to the concrete resistance and assuming good bond conditions in unconfined concrete. In ABAQUS, this type of behaviour can be approximated by the traction-separation law Fig. II.97-b). For the increasing branch only a linear response is allowed. Subsequently, the beginning and evolution of damage can be reproduced. This type of behaviour is valid for both, cohesive elements and contact with cohesive behaviour. The elastic definition is written in terms of nominal tensile stresses and nominal strains. According to (Abaqus, 2011), for contact with cohesive behaviour, deformations are considered directly as separations (displacements). The constitutive relation can be uncoupled or coupled, as expressed in (II.70) and (II.71), respectively.



a) Bond-slip model proposed by (Eligehausen *et al.*, 1983) and prescribed by the Model Code (CEB-FIP, 1993)

b) Typical traction-separation response available in (Abaqus, 2011) to simulate the bond behaviour

Fig. II.97: Constitutive models for the bond-slip interaction between reinforcement and concrete

$$\mathbf{t} = \begin{Bmatrix} t_n \\ t_s \\ t_t \end{Bmatrix} = \begin{bmatrix} k_{nn} & 0 & 0 \\ 0 & k_{ss} & 0 \\ 0 & 0 & k_{tt} \end{bmatrix} \begin{Bmatrix} \delta_n \\ \delta_s \\ \delta_t \end{Bmatrix} = k \delta \quad (\text{II.70})$$

$$\mathbf{t} = \begin{Bmatrix} t_n \\ t_s \\ t_t \end{Bmatrix} = \begin{bmatrix} k_{nn} & k_{ns} & k_{nt} \\ k_{ns} & k_{ss} & k_{st} \\ k_{nt} & k_{st} & k_{tt} \end{bmatrix} \begin{Bmatrix} \delta_n \\ \delta_s \\ \delta_t \end{Bmatrix} = k \delta \quad (\text{II.71})$$

In both equations, the quantities  $t_n$ ,  $t_s$  and  $t_t$  represent the nominal tractions in the normal and the two local shear directions, respectively;  $\delta_n$ ,  $\delta_s$  and  $\delta_t$  are the displacements related to corresponding nominal strains ( $\varepsilon_n$ ,  $\varepsilon_s$ ,  $\varepsilon_t$ ); and  $k_{ij}$  are the stiffness coefficients.

There is not much information on how to determine the stiffness coefficients ( $k_{ij}$ ) and consequently it was decided to use the uncoupled behaviour. The coefficients related to the shear deformation,  $k_{ss}$  and  $k_{tt}$ , are obtained by approximation of the model described in Fig. II.97-a), as expressed in (II.72). Regarding  $k_{nn}$ , according to (Gan, 2000), the stiffness of the normal traction is higher than in the shear direction as expressed in (II.73).

$$k_{ss} = k_{tt} = \tau_{max} / S_1 \quad (\text{II.72})$$

$$k_{nn} = 100k_{ss} = 100k_{tt} \quad (\text{II.73})$$

Finally, in what concerns the ordinary reinforcement of the wall, its interaction with concrete is modelled with perfect bond (embedded option), as the stress transfer expected is much lower.

#### II.4.2.1.3 Validation of the reinforcement-concrete bond-slip modelling

The numerical simulation of the reinforcement-concrete interaction was evaluated using experimental tests on reinforcement stirrups performed at the University of Stuttgart within the *InFaSo* research project (Kuhlmann *et al.*, 2012). These tests consisted in pull-out tests (Fig. II.98-a). For detailed information on the tests reference is given to (Berger *et al.*, 2011). Fig. II.98-b) shows the numerical model developed for this benchmark example. Profiting from the symmetry of the problem, only half of the specimen was considered. Solid (continuum) elements type C3D8R are used in both parts; reinforcement and concrete. Only in the straight part of the reinforcement bar embedded in the concrete, the bond-slip behaviour was considered. In this region, the concrete block elements do not superpose with the reinforcement bar elements (hole created in the concrete block). In this way, the contact interface between concrete and reinforcement was handled numerically as contact problem with bond behaviour. This technique was described in the previous section. For the hook, the embedded technique, also described above, is used.

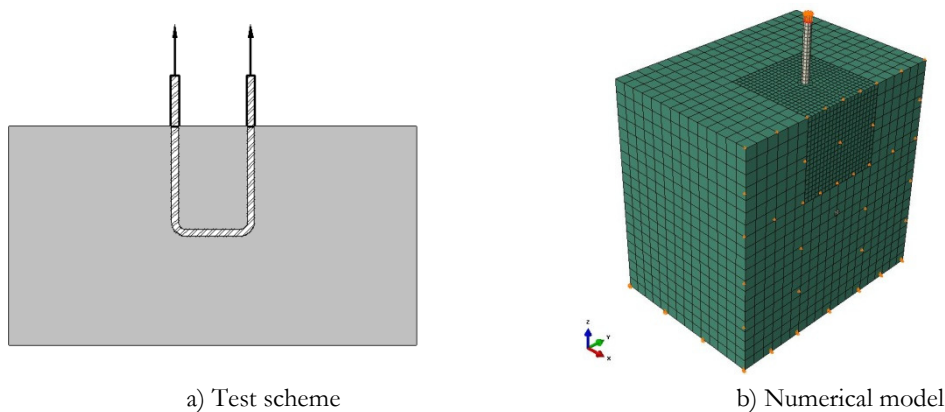


Fig. II.98: Benchmark example to calibrate the numerical modelling of the reinforcement-concrete interaction

The force-deformation curves presented in Fig. II.99 compare numerical and experimental results. The force represents the pull-out load applied to the reinforcement bars and the deformation corresponds to the displacements measured in the reinforcement bar at the concrete surface. The numerical curve is close to a linear relation which may be justified by the traction-separation law approximating a linear stress-slip response, as described in §II.4.2.1.2. Besides this deviation, there is a good approximation of the numerical model. The plateau observed in the numerical result is due to the yielding of the reinforcement. The latter occurs early in the numerical calculations because nominal properties (EC2 values) of the steel were used instead of the real material properties which were not available. Fig. II.100-a) shows the von Mises stresses along the reinforcement bar for an applied load of about 100kN. Note the degradation of stresses in the reinforcement bar

starting at the concrete surface and following within the embedded part. In Fig. II.100-b) is shown the bond stresses in the contact surface. A decrease of these stresses is also observed with the embedment depth.

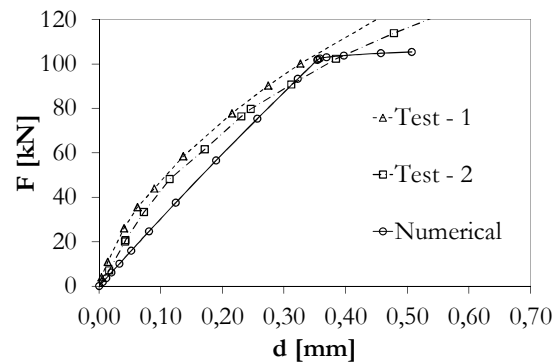


Fig. II.99: Force-deformation curve evaluating the application of a bond model to simulate reinforcement-concrete interaction

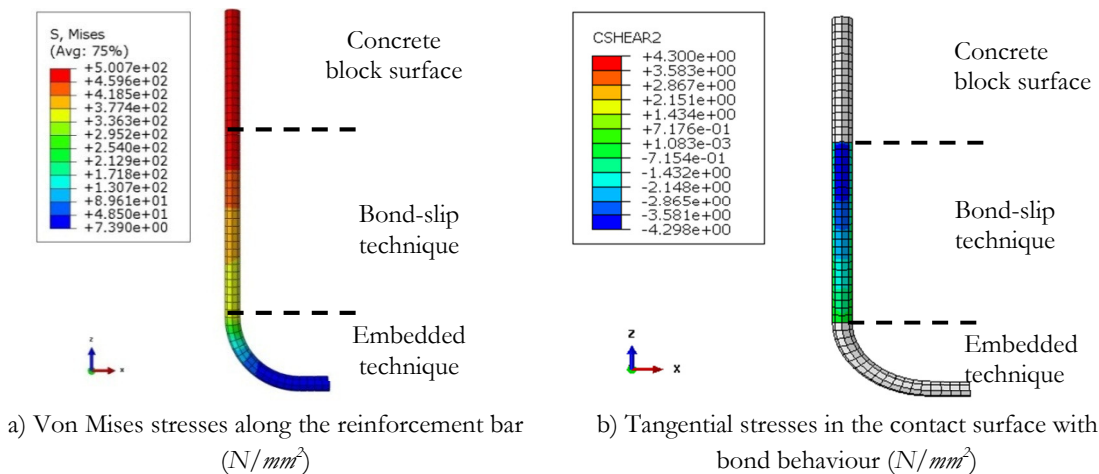


Fig. II.100: Reinforcement and bond stresses in the numerical model implementing the contact with bond behaviour

## II.4.2.2 Elastic analysis of the joint link

### II.4.2.2.1 Wall response to joint loading

In the elastic analysis of the joint link was considered the geometric properties and the loading conditions of the wall are illustrated in Fig. II.95. In this calculation, all materials were considered with a linear elastic behaviour.

The joint configuration implies that the tension load is distributed within a higher length than the compression load. For this reason, high local deformations were observed at the level of the contact plate where the compression load is concentrated (Fig. II.101). These local deformations are accounted for in the anchor plate connection, discussed in §II.3.1, and therefore have to be disregarded in the analysis of joint link component. In Fig. II.101 are presented the amplitude of the displacements ( $U = \sqrt{u_x^2 + u_y^2 + u_z^2}$ ) within the wall which degraded towards the free edge (lateral edge). According to the magnitude of deformations observed near the free edge, it can be concluded that the load transfer zone is

not significantly affected by this edge. Moreover, the wall deformation shows that due to the bending deformation of the wall, the ordinary reinforcement has an important contribution to transfer the tension forces developed mainly at the back of the wall.

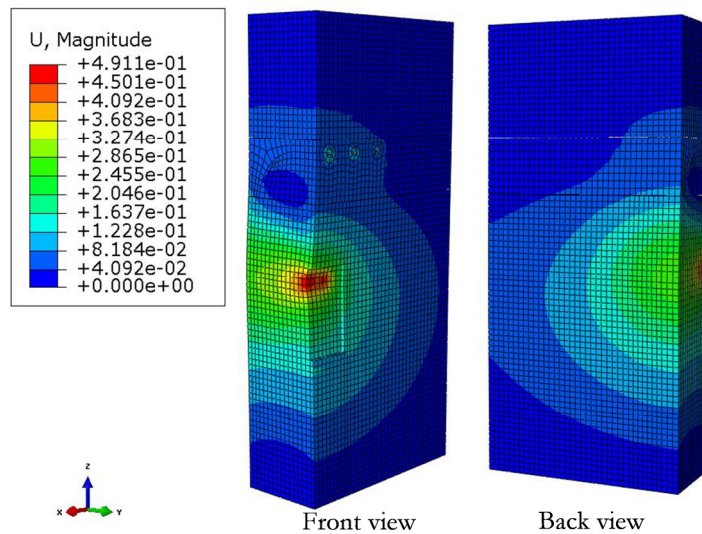
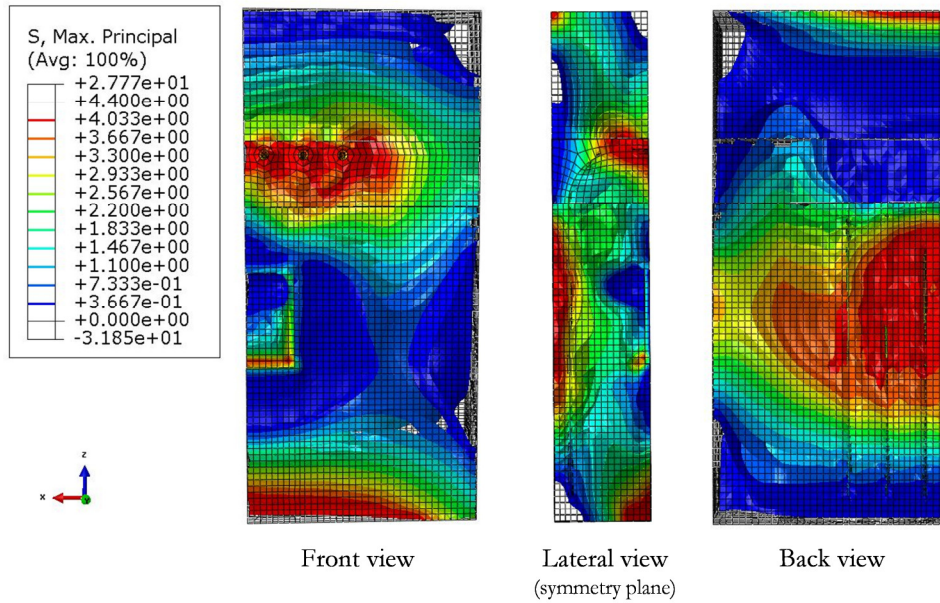


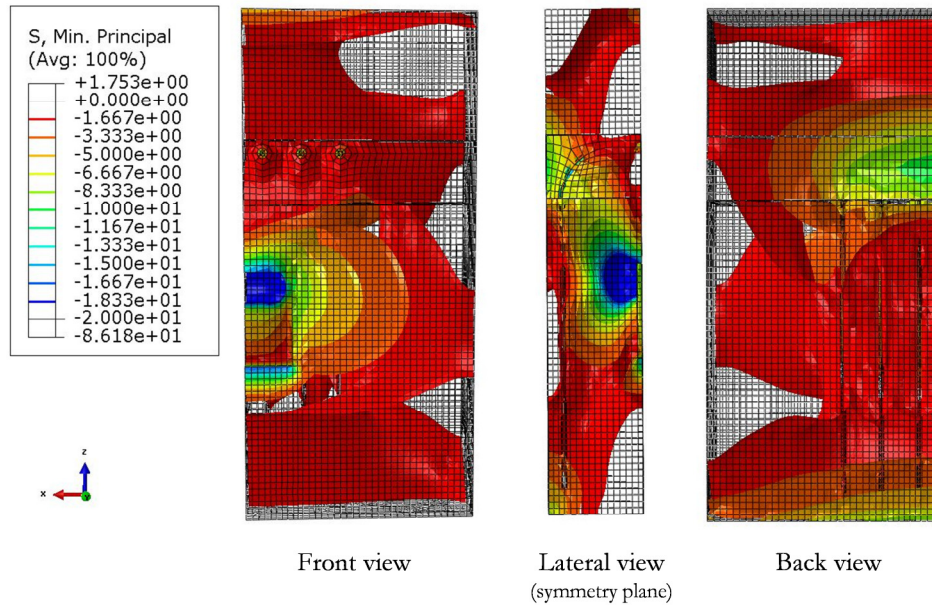
Fig. II.101: Deformation of the reinforced concrete wall resulting from the elastic analysis ( $F_c = F_t = 1000\text{kN}$ )

Fig. II.102 shows the maximum principal and minimum principal stresses for an applied load of  $1000\text{kN}$ . In Fig. II.102-a), the maximum principal stresses represent tension stresses within the wall, as the plotting was limited to positive values. The red zones are those where higher values are observed while blue show the regions of zero or negative values. In Fig. II.102-b), the minimum principal stresses represent compression stresses within the wall, as the plotting was limited to negative values. Here, opposite to Fig. II.102-a), in red are the zones where the values are near zero and blue identifies the regions with higher absolute values (higher compression zones). According to these results, the following was observed:

- Tension is predominant around the longitudinal reinforcement bars and in the back of the wall at the level of the compression loading region;
- Compression is predominant in the zone around the anchor plate and in the back of the wall at the level of the hook of the reinforcement bar;
- The zone around the anchor plate is highly compressed in comparison to the other regions of the wall; the concrete in this region may be considered to be under a triaxial state of compression as it is confined by the external load, the flow of compression stresses, from the hook and from the support, and by the “lateral” concrete, as the distance to the edge is significantly high;
- The load on the reinforcement bars is transferred to the concrete through bond and through mechanical contact of the hook, for this reason the maximum principal stresses are higher around the longitudinal bars, and the minimum principal stresses under the hook.
- The asymmetry of the loading zones dimensions generates a non-uniform flow from reinforcement bars bend to anchor plate, as stresses tend to spread between these two zones.



a) Maximum principal stresses



b) Minimum principal stresses

Fig. II.102: Isosurfaces showing the distribution of stresses ( $N/mm^2$ ) within the reinforced concrete wall resulting from the elastic analysis ( $F_c = F_t \approx 1000kN$ )

The activation of the ordinary reinforcement is illustrated in Fig. II.103 for an applied load of approximately  $1000kN$ . The plotted von Mises stresses confirm the higher participation of the reinforcement located in the back of the wall.

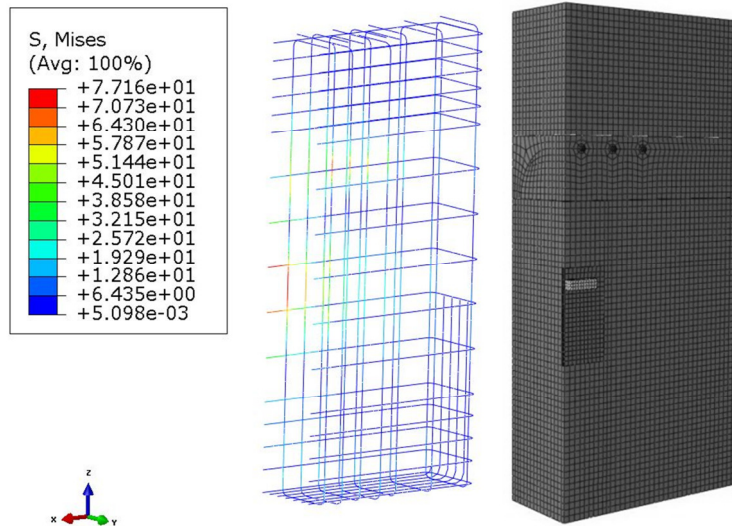


Fig. II.103: von Mises stresses ( $N/mm^2$ ) within the ordinary reinforcement of the wall resulting from the elastic analysis ( $F_c = F_t \approx 1000kN$ )

#### II.4.2.2.2 Identification of load path and critical regions

In order to identify the load path within the wall, a more refined analysis of the flow of stresses flow is presented in this sub-section. For this purpose, the considered system of axes is represented in Fig. II.104. The origin of this system is defined in the symmetry plane, at the bottom and back edge of the wall.

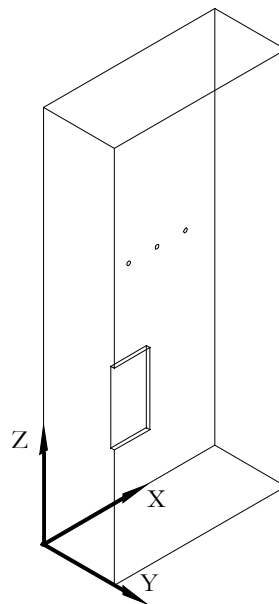
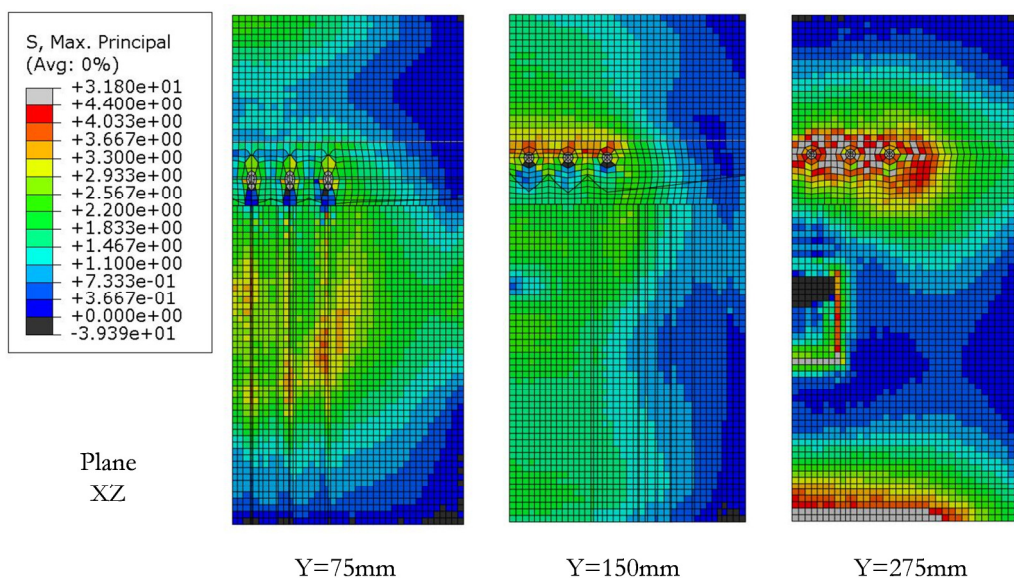


Fig. II.104: System of axes assigned to the model for identification of the planes of analysis

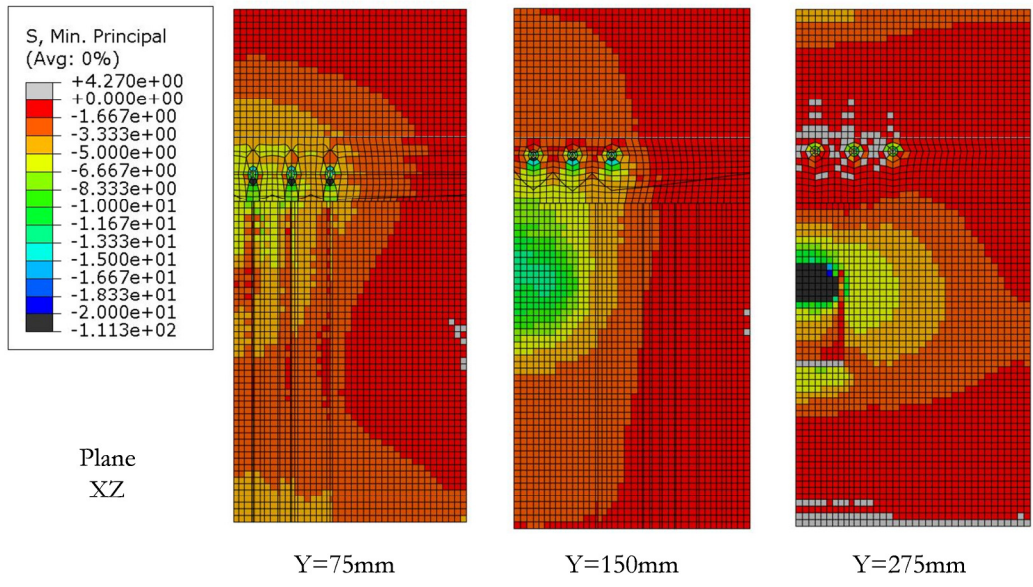
Fig. II.105 shows the plot of maximum and minimum principal stresses within different planes of the reinforced concrete wall for an applied load of approximately  $1000kN$  ( $F_c = F_t$ ). As in the previous sub-section, the maximum principal stresses represent tension stresses, and the minimum principal stresses show compression stresses. For the first, red represent the highest while dark blue the lowest. For the latter, red represent the lowest

(absolute value) and blue the highest (absolute value). Accordingly, the following is observed:

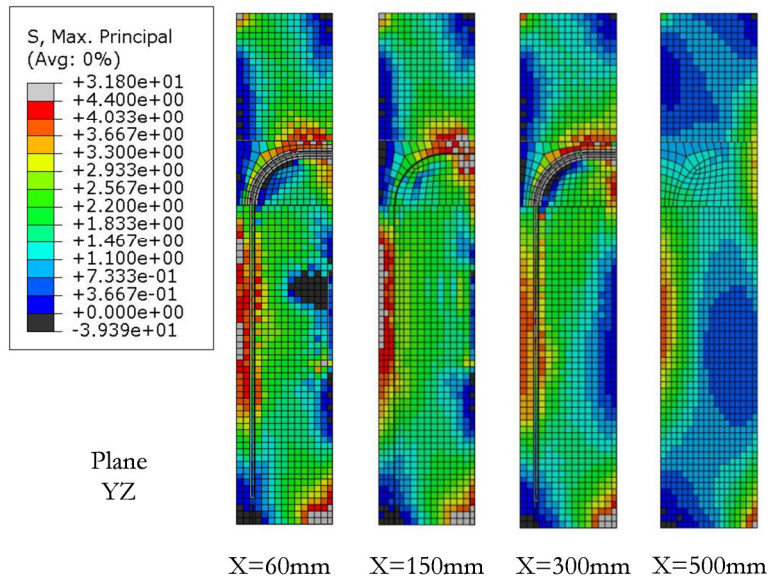
- Maximum principal stresses are higher at the level of anchor plate in the plane closer to the back of the wall ( $Y=75\text{mm}$ ) and at the level of the longitudinal reinforcement in the plane closer to the front of the wall ( $Y=275\text{mm}$ ) (Fig. II.105a);
- Maximum principal stresses under the anchor plate ( $Y=275\text{mm}$ ) are negative indicating that concrete is under multi-axial compression state (Fig. II.105-a);
- Under the hook ( $Y=75\text{mm}$ ), maximum principal stresses are low and minimum principal stresses are high, as part of the load introduced by the longitudinal reinforcement is transferred to the hook through contact pressure (Fig. II.105-a) and b);
- At the level of the longitudinal reinforcement, from the symmetry plane up to the outer bar, the stresses distribution is non-uniform, achieving the peak (maximum values) under the reinforcement bars and the lowest values are observed between bars (Fig. II.105-a) and b);
- With the increase of the plotting plane coordinate ( $Y$ ), the location of the highest minimum principal stresses is obtained at a lower value of coordinate ( $Z$ ), being higher at the level of the longitudinal reinforcement, close to the back, and at the level of the anchor plate close to the front (Fig. II.105-b and d);
- The maximum principal stresses follow an opposite trend (Fig. II.105-c);
- Both type of stresses decrease from the centre of the wall towards the free edge (Fig. II.105-c) and d) showing that the latter has a minor/none influence on the behaviour of the joint;
- The flow of stresses to the supports is responsible for the peak of stresses close to the top and bottom faces of the wall (Fig. II.105);
- Finally, a diagonal concrete strut is idealized to represent the joint link (Fig. II.105-d).



a) Maximum principal stresses in plane XZ

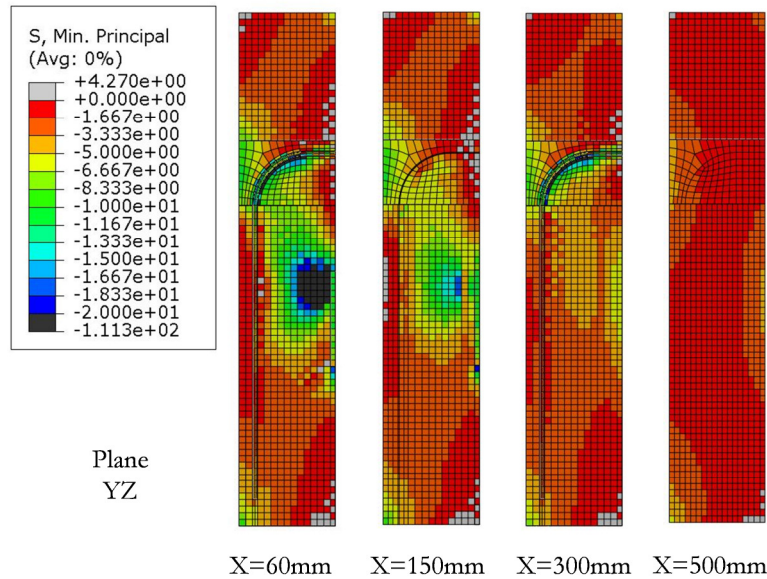


b) Minimum principal stresses in plane XZ



c) Maximum principal stresses in plane YZ





d) Minimum principal stresses in plane YZ

Fig. II.105: Maximum and minimum principal stresses within different planes of the reinforced concrete wall resulting from the elastic analysis ( $F_c = F_t \approx 1000\text{kN}$ )

According to the previous, the following critical regions were identified:

- Under the anchor plate, high compression zone;
- Under the bend of the longitudinal reinforcement, high pressure because of the hook of the bars;
- Around the longitudinal reinforcement, near the joint face, high shear stresses due to the bond between concrete and reinforcement;
- In the back of the wall at the level of the anchor plate, due to the bending deformation of wall.

Thus, the first two are considered within the components of the joint link and will be later included in the proposed analytical model, as the boundary conditions of the referred diagonal strut. Near the joint face, first cracks are expected around the reinforcement bars, as the bond resistance is overcome. However, this should not limit the load to be transferred as further load can be transferred along the reinforcement bars and at the hook. Finally, the tension stresses at the back of the wall are controlled by the wall reinforcement, and according to the reinforcement detail should not limit the wall capacity.

### II.4.2.3 Non-linear analysis of the joint link

#### II.4.2.3.1 Introduction

The non-linear calculations of the reinforced concrete wall are discussed in the present section to characterize the joint link component. In these calculations, only the concrete is modelled with non-linear behaviour. First, the reference case given in §II.4.1 was analysed and then several parametric variations considering the geometry of wall and longitudinal reinforcement were performed to complement the discussion. According to the observations in the previous section, to the joint link concerns essentially the following: the

load capacity of the region within the hook of the longitudinal reinforcement and the anchor plate; the deformation of the concrete within this region. Note that for the latter, high local deformations under anchor were disregarded, as they were considered in the anchor plate connection response.

#### II.4.2.3.2 Reference case

The behaviour of the joint link is analysed in terms of force-deformation curves. The force represents the load applied to the reinforcement bar; it is directly obtained. In what concerns the deformation, the following was considered:

- At each load step considering the relative position of two measuring points (MP) was considered, as represented in Fig. II.106.

$$d_i^{MP1-MP2} = l_i^{MP1-MP2} - l_0^{MP1-MP2} \quad (\text{II.74})$$

Where:

$$l_i^{MP1-MP2} = \sqrt{(y_i^{MP1} - y_i^{MP2})^2 + (z_i^{MP1} - z_i^{MP2})^2} \quad (\text{II.75})$$

- These nodes were located within the diagonal line identified between the hook of the reinforcement bar and the anchor plate at the level of the contact plate.
- To avoid the influence of the local deformations, the bottom reference node was selected outside the zone considered as participating in the anchor plate connection deformation and defined by the equivalent rigid plate dimensions and equivalent concrete height, as discussed in §II.3.1.
- The MP were located within the width of the contact plate, as this is the region with most influence on the joint deformation; within this region the variation of the deformation was small, as is shown in Fig. II.107.
- The final value of deformation was obtained through extrapolation of the measured deformation to the total length of the referred diagonal.

$$d_i^{final} = d_i^{MP1-MP2} \frac{l_i^{final}}{l_i^{MP1-MP2}} \quad (\text{II.76})$$

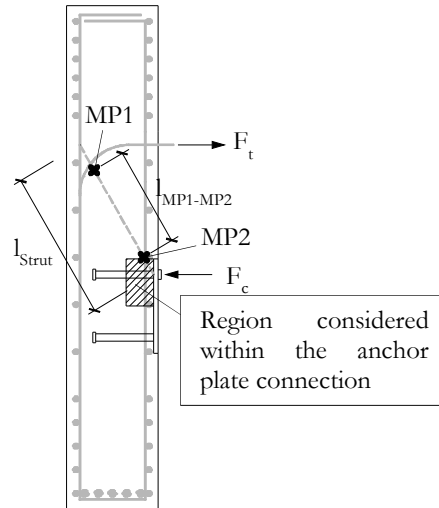


Fig. II.106: Location of the measuring points to obtain the joint link deformation

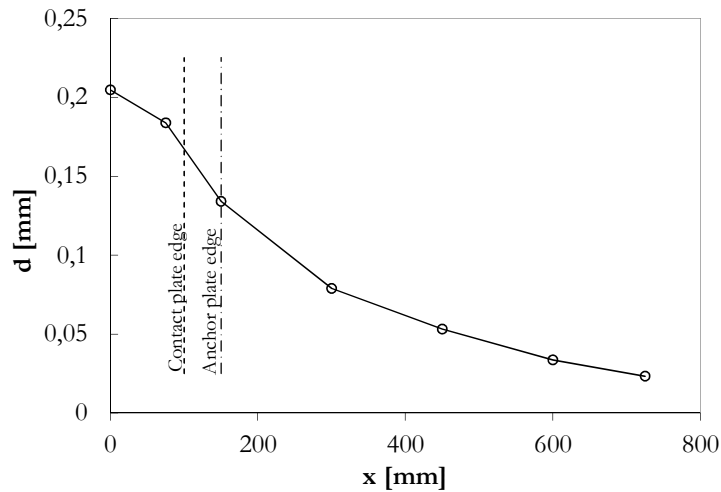


Fig. II.107: Measured displacement of MP2 along the width of the wall ( $F_c = F_t \approx 1000\text{kN}$ )

Thus, the force-deformation curve characterizing the joint link behaviour is shown in Fig. II.108. The force represents the horizontal load directly applied to the reinforcement bars and displacement is the deformation within the diagonal strut calculated as described previously. Two curves are presented which differ in the fracture energy of concrete considered in the model. Remember, that this parameter defines the behaviour of concrete after the maximum tension strength is achieved and cracking begins. One model (JL-Approx  $G_f$ ) considers the value of fracture energy determined with application of expression (II.42). The other model (JL-Higher  $G_f$ ) considers a higher value of the fracture energy. The reason for performing the latter model relies in the fact that in the first problems of convergence were observed leading to the interruption of the calculations. These convergence problems were due to the concrete elements that experience high tensile equivalent plastic strains (PEEQT) around the reinforcement bars, as located in Fig. II.109-a). Fig. II.109-b) shows that the crack in the element with higher PEEQT is almost complete. Consequently, this element has no strength and numerical difficulties appear. Though, notice that the maximum resistance of the longitudinal reinforcement was already exceeded when the convergence problems appear (Fig. II.108). Furthermore, as the

problems with concrete appear locally it may be assumed that if higher number of bars was used, a higher load could be transmitted. Hence, as the capacity of the joint link was not attained, it was decided to increase the fracture energy, without increasing the tension capacity of the concrete, in order to overcome the numerical difficulty. This procedure allowed achieving higher load without failure of the joint link at the reinforcement hook.

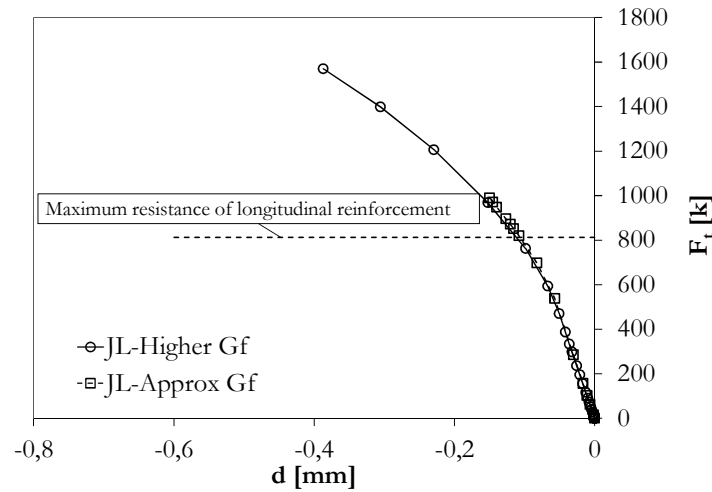


Fig. II.108: Numerical force-deformation curve characterizing the response of the joint link for the reference case

As the previous models did not provide a representative load capacity of the joint link a new model was developed which assumed no bond between longitudinal reinforcement bars and concrete. Thus, the interaction is simulated using the mechanic contact model, transferring forces through pressure without friction. In this way, the numerical simulations could seek the maximum capacity of the joint link without numerical difficulties in the concrete interacting with longitudinal reinforcement bars through bond. This assumption is acceptable as physically the bond between reinforcement bar and concrete is gradually exceeded from the edge of concrete member (on the loaded side) towards the hook of the reinforcement bar. In an extreme case, no bond exists and all restraint is given at the hook of the reinforcement bar through contact pressure. This situation allows exploiting the maximum capacity of the reinforcement bar hook. Finally, in this model fracture energy of the concrete considered the approximation given with expression (II.42). The force-deformation curve obtained in this model is shown in Fig. II.110. The curve shows now that the maximum force is below the latter model with high fracture energy attributed to the concrete. This maximum load is attained because the concrete “under” the hook attains its load capacity. Though, compression stresses are observed in concrete elements under the reinforcement bar hook, it is the tension capacity of the concrete in the vicinity of these elements that limits the resistance of this model, as illustrated in Fig. II.111-a). The Maximum Principal Stresses (Tension Stresses) to Equivalent Plastic Strains (PEEQT) curve in Fig. II.111-b) shows that the latter elements have no further tension capacity.

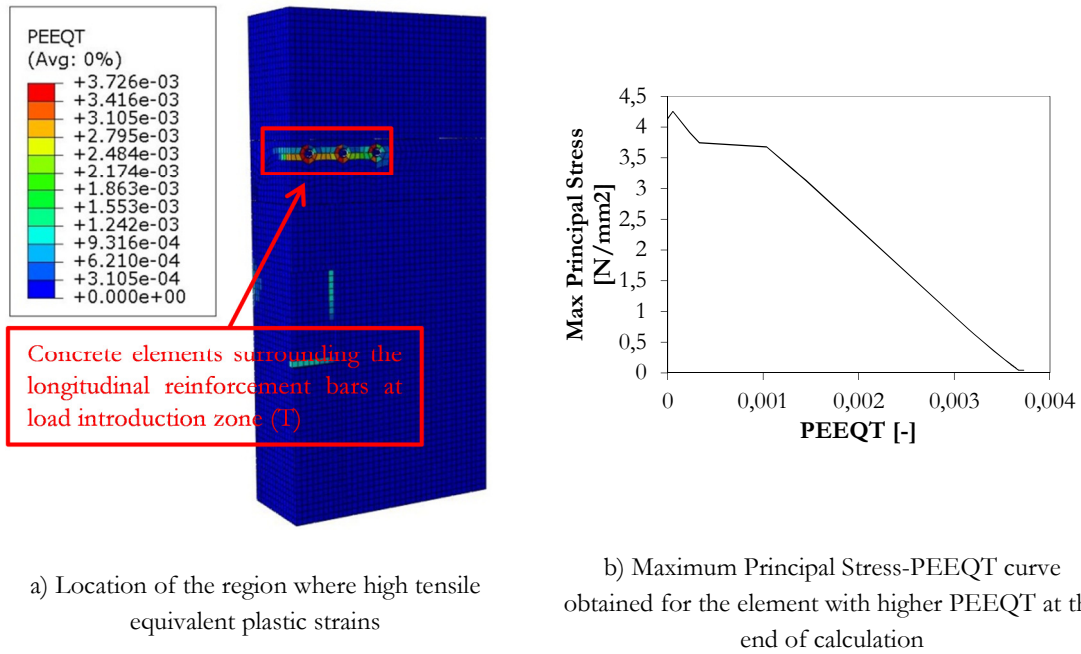


Fig. II.109: Identification of the development of cracks in the concrete leading to numerical difficulties

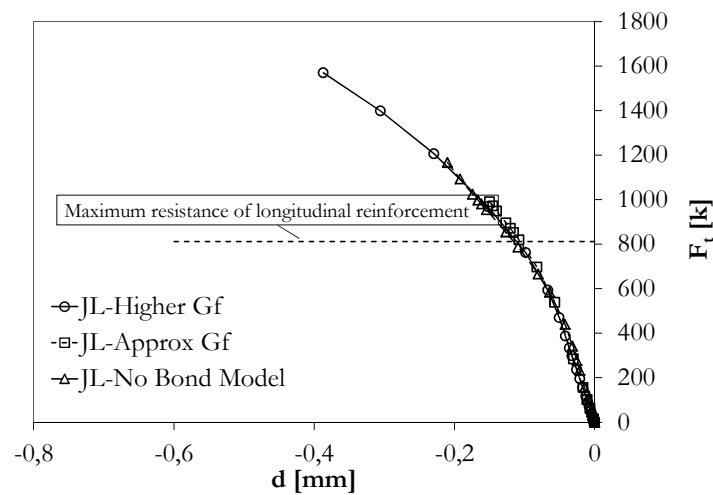
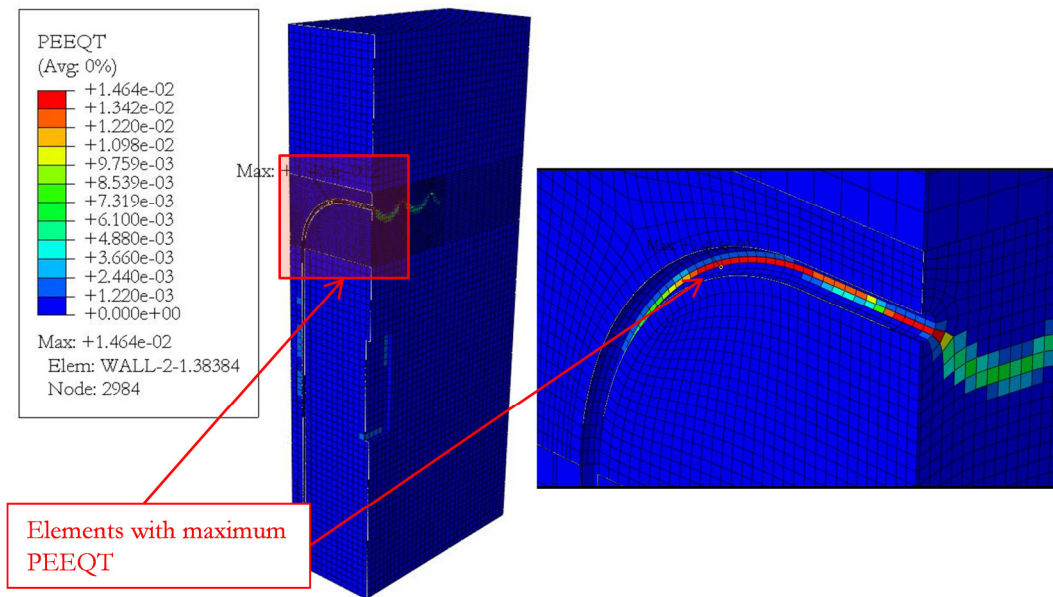
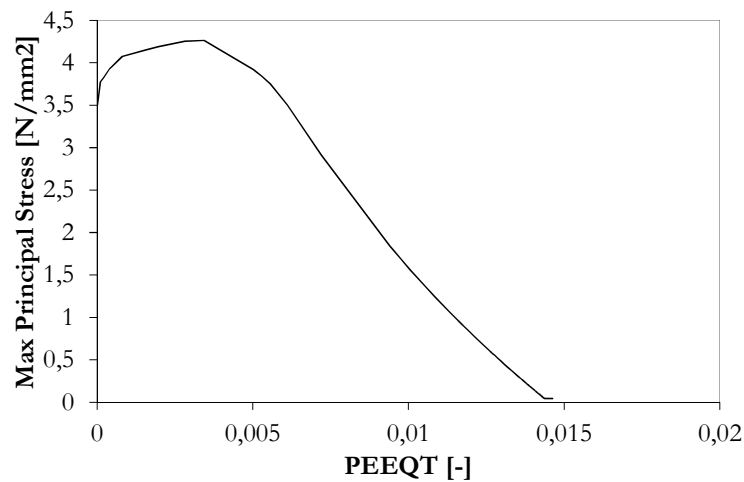


Fig. II.110: Force-deformation curve of the joint link reference numerical model without reinforcement-concrete bond behaviour



a) Location of the critical elements limiting the joint link load capacity



b) Maximum Principal Stress-PEEQT curve obtained in critical element

Fig. II.111: Identification of the limiting elements in the joint link numerical model without reinforcement-concrete bond-slip behaviour

#### II.4.2.3.3 Parametric variations

Up to this section, the joint link has been analysed using the geometric properties of the reference specimen tested within the *InFaSo* research project (Kuhlmann *et al.*, 2012). In order to verify the sensibility of the component to other geometries a parametric variation was accomplished. The number of variables involved in the problem is significant, however, in the present study the analysis was limited to the following: i) thickness of the concrete wall; ii) height of the composite beam; iii) bend radius of the longitudinal reinforcement bar. These were considered the most relevant. The influence of the edges is disregarded, as these were excluded of the scope of the present thesis. Furthermore, no variation on the material properties was performed. In Table II.28 are listed the analysed cases. In the case of the thickness of the wall, has the dimension of the wall is affected; was

decided to consider the same percentage of reinforcement as in the reference case. Thus, the ordinary wall reinforcement and the longitudinal reinforcement introducing the tension to the wall were varied according to each case. The numerical model developed for each of the referred cases is based on the final model of the previous section; therefore, the model neglects the reinforcement-concrete bond-slip behaviour.

Table II.28: List of geometric variations performed for the numerical analysis of the joint link

Model ID	Thickness of the wall [mm]	Model ID	Height of the beam [mm]	Model ID	Bend radius of Long. Rebar [mm]
JL-T150	150	JL-H226	226	JL-R80	80
JL-T200	200	JL-H406	406	JL-R120	120
JL-T250	250	JL-H620	620	JL-R160	160
JL-T300 [Ref]	300				
JL-T350	350				
JL-T400	400				

Fig. II.112 shows the influence of the wall thickness on the joint link response. The following is observed:

- The initial stiffness is similar regardless of the thickness of the wall (Fig. II.112-a).
- The resistance is governed by concrete in the vicinity of the hook of the reinforcement bar, as shown in Fig. II.111; the maximum load increases with the thickness of the wall.
- The pattern of force-deformation curve is similar to all models.
- Except for the model with lowest wall thickness (150mm), the maximum resistance of the longitudinal reinforcement was exceeded (Fig. II.112-b); though the reinforcement bar diameter was varied proportionally between models, the trend is that the ratio between model resistance and reinforcement bars resistance increases with the thickness of the wall; note that for the determination of the presented ratios, the mean ultimate strength of the reinforcement bars, used in the experimental tests of the *InFaSo* research project (Kuhlmann *et al.*, 2012), was considered; accordingly, the joint link is almost never governing component.

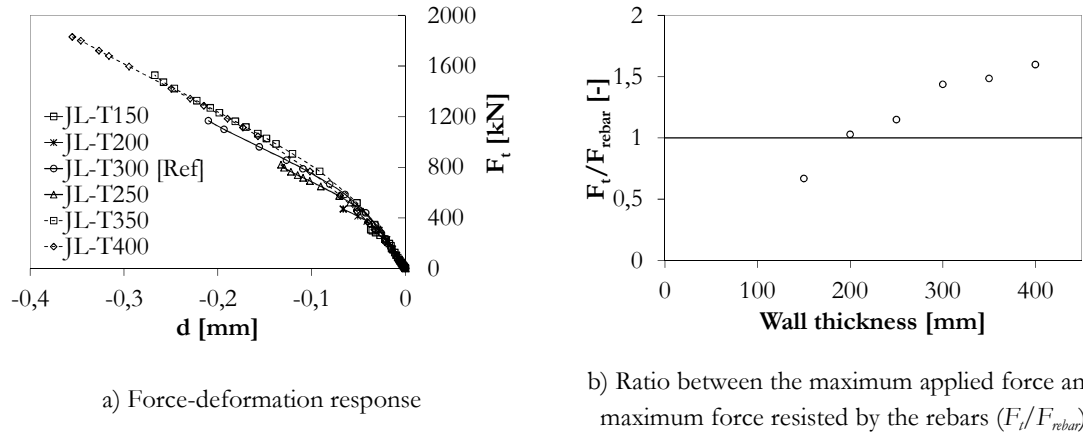


Fig. II.112: Influence of the wall thickness on the joint link response

The influence of the composite beam height on the joint link force-deformation response is shown in Fig. II.113. The following is observed:

- The resistance of the model increases with the decrease of the beams height.
- The force-deformation curve pattern is similar to all cases, as observed in the analysis of the thickness of the wall.
- In all cases the model capacity was governed by the concrete elements in region of the hook of the bar.

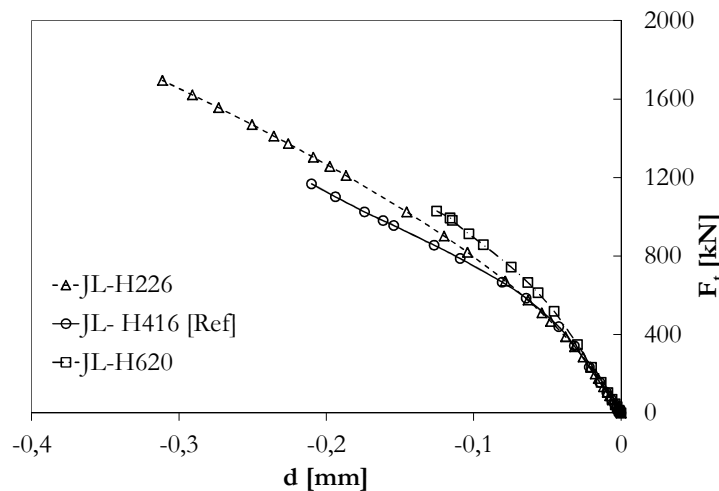


Fig. II.113: Influence of the composite beam height on the joint link response

The radius of the bar bend affects the transmission of stresses from the longitudinal reinforcement bar to the concrete through pressure. As illustrated in Fig. II.26-b), smaller the radius, higher is the concentration of stresses. Fig. II.114 shows the force-deformation curves of the numerical models considering the variation of the bend radius of the longitudinal reinforcement bars. The following is observed:

- In terms of resistance, the model resistance decreases with the decrease of the size of the bend radius, this is in agreement with the model illustrated in Fig. II.26-b).
- The force deformation response of the different models is barely same.



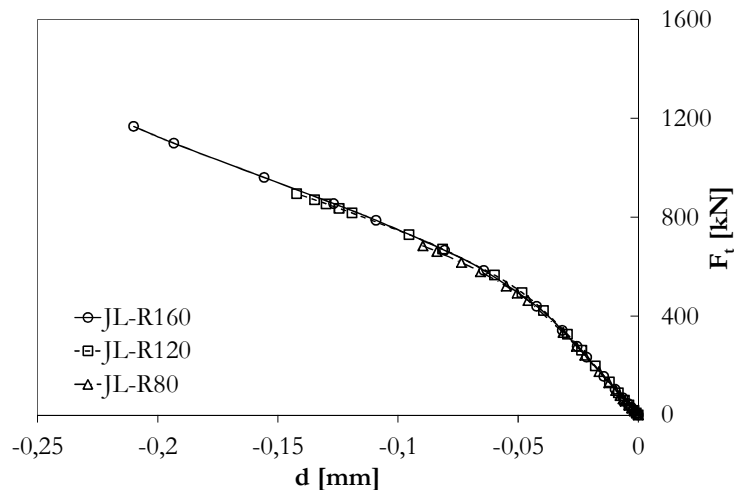


Fig. II.114: Influence of the bend radius of the longitudinal reinforcement on the joint link response

## II.4.3 Analytical modelling of the joint link

### II.4.3.1 Idealized model

#### II.4.3.1.1 Conception and principles

Based on the analysis performed within §II.4.2 and based on the STM principles, a simplified model to reproduce the joint link behaviour is proposed in the present section. In §II.4.2.2 a main flow of compression stresses between the bend of the longitudinal reinforcement bar and the anchor plate connection was identified. Accordingly, the proposed model for the joint link is illustrated in Fig. II.115. As in STM model, this comprises the following components: single diagonal concrete strut and two nodes. The numerical calculations demonstrated that the flow of compression stresses between nodes is similar to a “bottle shape”, as illustrated in Fig. II.25-b). This is justified by the different loading widths (distance between outer longitudinal reinforcement bars and contact plate width). In the numerical calculations, a flow of tension stresses was identified in the perpendicular direction to the compression flow, and this should be taken into account in the failure criterion of the concrete strut. However, as stated by (Schlaich *et al.*, 1987), because nodes are bottlenecks of the stresses, it can be assumed that the concrete strut is safe if the nodes failure criterion is satisfied. In addition, in the present thesis the edge distances are not considered to affect the joint. In this way, the nodes are most relevant components of the proposed model. The nodes identified are of the following type: N1 is CTT; N2 is CCC. In the case of Node N1, the type of node is defined by two ties converging to the node. Node N2 is defined as CCC, as only compression struts converge to the node. Furthermore, the numerical calculations presented in §II.4.2.3 showed that the stresses in this region were high, exceeding considerably the uni-axial compressive strength of the concrete, and triaxial compressive state was proved by the negative values of all principals stresses, as shown in Fig. II.116. Finally, it should be stated that the horizontal reinforcement ties are considered as a component of the complete joint and not as part of the joint link, and are discussed in the next chapter.

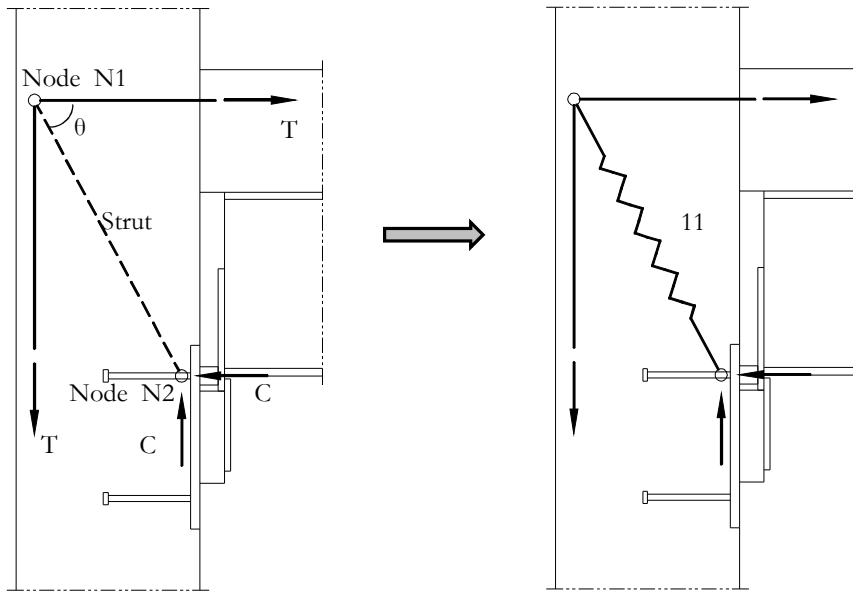


Fig. II.115: Model proposed for the joint link component

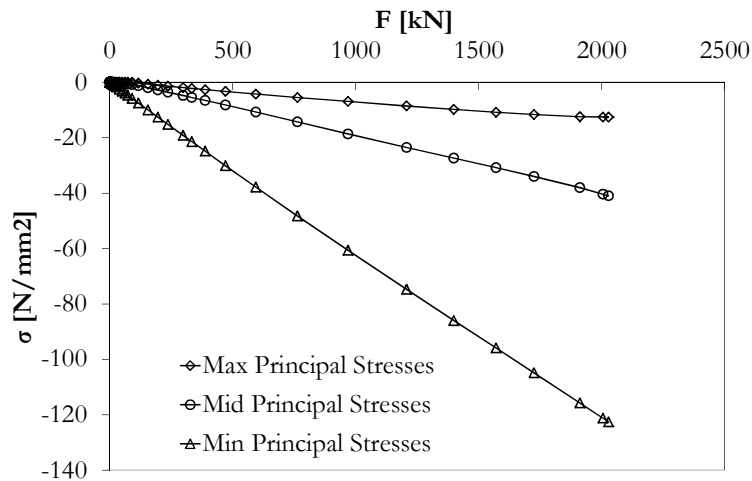


Fig. II.116: Principal stresses in concrete element under the anchor plate

Thus, the following principles were considered in the joint link model:

- Components: Single diagonal concrete strut (bottle shape) and two nodes (1 type CTT and 1 type CCC).
- Failure is governed by the nodal regions, and is disregarded within the strut ;
- The flow of stresses through the wall to supports are not considered as part of the joint link and therefore not analysed.
- Ties (longitudinal reinforcement) are components considered in the analysis of the complete joint and therefore are neglected for the joint link behaviour.
- The deformation of the diagonal concrete strut is assumed to contribute to the global response of the joint and is determined as described in the next section.

#### II.4.3.1.2 Characterization of the components and determination of joint link properties

In terms of resistance, the model is characterized by the resistance of the nodes at the edge of the diagonal strut. Accordingly, the maximum admissible stresses (Table II.7) and the geometry of these nodes define the joint link load capacity. Remember, the resistance of the concrete strut was not considered for the reasons given before. Hence, the resistance of the nodes is obtained as follows.

##### a) Node N1 (type CTT)

The admissible stresses for this type of node were given in Table II.7. The geometry of the node is defined in one direction by the bend radius of the longitudinal reinforcement and by the strut angle, as illustrated in Fig. II.26-b) with the dimension ( $a$ ). In the other direction (along the width of the wall), initially, the distance between the outer longitudinal reinforcement bars ( $b_{rb}$ ), as represented in Fig. II.117, was assumed. Though, the analytical approach assumes that the stresses are constant within the dimension  $b_{rb}$ . As it was observed in the numerical calculations (Fig. II.105-a and b), the stress field “under” the hook and along this dimension is non-uniform. High stresses are develop under the reinforcement and lower between reinforcement bars. Consequently, assuming constant stresses over the total width ( $b_{rb}$ ) overestimates the resistance of this node.

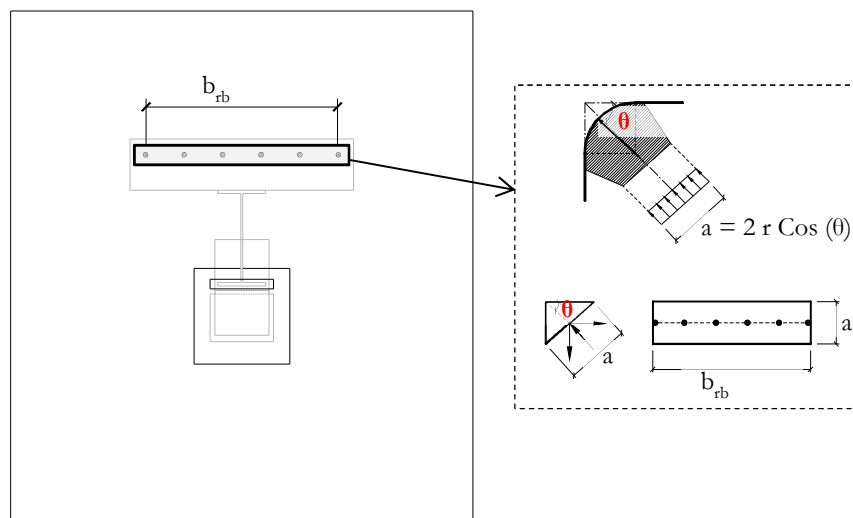
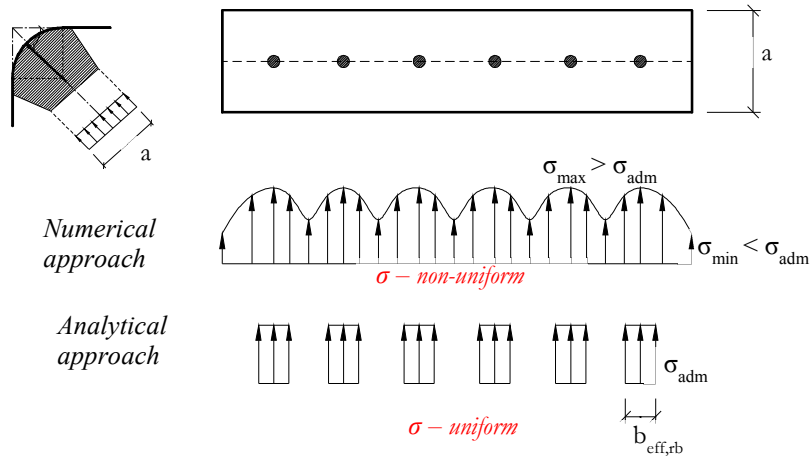
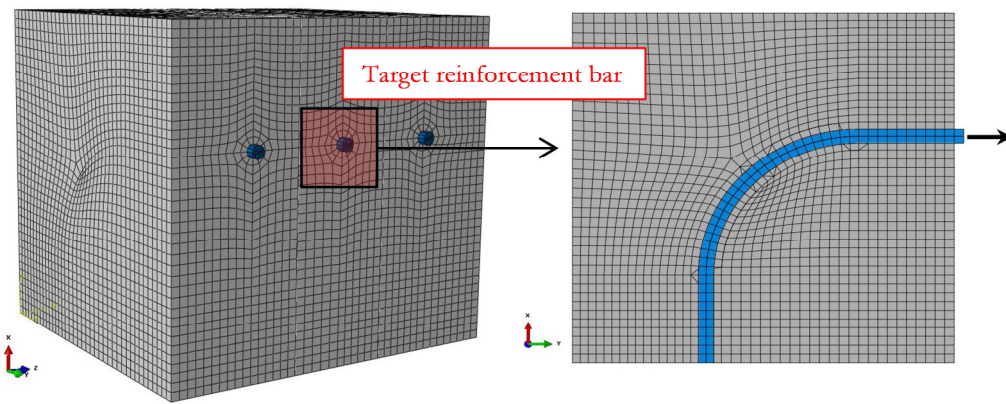


Fig. II.117: Definition of the width of the node N1

In order to obtain a more accurate approach, an analytical expression was derived to estimate an effective width “under” each reinforcement bar where constant stresses can be assumed, as illustrated in Fig. II.118-a). The basis of this analytical expression was a parametrical study performed by means of numerical calculations. A simplified numerical model focussing only the region of the reinforcement bar bend was used. Fig. II.118-b) shows the developed model. The force transferred by central reinforcement bar was the target of the study. The reinforcement bar diameter ( $d_{rb}$ ), the spacing of bars ( $s_{rb}$ ) and strut angle ( $\theta$ ) were identified as the main parameters influencing the effective width ( $b_{eff,rb}$ ). The influence of the wall edges was disregarded.



a) Scheme of stresses “under” the reinforcement bars



b) Numerical model used in the parametrical study

Fig. II.118: Approach to derive the effective width under each reinforcement bar subjected to constant admissible compression stresses in a CTT node with bended reinforcement bars

In the several numerical simulations performed, the load capacity was obtained as in the numerical simulations of the complete wall presented in the previous section. The concrete elements in the vicinity of the reinforcement bar, in the region of the bar bend, attained their tension capacity. In Fig. II.119 are plotted the maximum resistance obtained in the target reinforcement bar (central reinforcement bar) in function of the bars spacing ( $s_{rb}$ ). The results show that above  $80mm$ , the load capacity has small variation. Below this value, the resistance decreases almost linearly. It is also clear that the load capacity increases with the diameter of the bar ( $d_{rb}$ ).

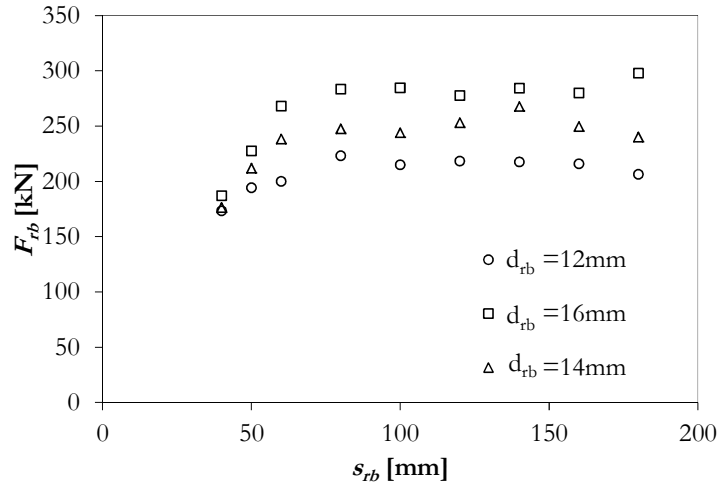


Fig. II.119: Results of parametric study to derive the effective width in nodes with bent bars

According to the above numerical results, the effective width ( $b_{eff,rb}$ ) was determined for each of the simulated cases as expressed in (II.77). In this calculation, an uniform distribution of stresses, as represented in Fig. II.26-b), with amplitude equal to the maximum admissible stresses ( $\sigma_{adm}$ ) in a CTT node (see Table II.7) was assumed. In the perpendicular direction to ( $b_{eff,rb}$ ), the dimension of the node is taken as represented in Fig. II.117.

$$b_{eff,rb} = \frac{(F_{Num,rb} / \cos(\theta))}{a\sigma_{adm}} \quad (II.77)$$

In order to obtain an expression which could approximate the effective width ( $b_{eff,rb}$ ) with sufficient accuracy, a regression analysis, using the data produced in the parametric study, was performed. According to the results shown in Fig. II.119, the analytical proposal (II.78) distinguishes two ranges based on the reinforcement bars spacing ( $s_{rb}$ ): 1) equal or greater than  $80\text{mm}$ , where a constant resistance is assumed; 2) below  $80\text{mm}$ , where a decreasing resistance is considered. The proposal uses the problem variables referred above: the diameter of the reinforcement bar ( $d_{rb}$ ), the spacing between bars ( $s_{rb}$ ) and the strut angle ( $\theta$ ). The application of this proposal is shown in Fig. II.120. The resistance of one reinforcement bar obtained with numerical models is compared with the analytical calculations. The results show a good agreement. Though, further validation of this model is performed later when the complete analytical model of the joint link is compared with the numerical simulations of the complete reinforced concrete wall.

$$\begin{cases} s_{rb} \geq 80\text{mm}: & b_{eff,rb} = 2,62 d_{rb}^{0,96} (\cos \theta)^{-1,05} \\ s_{rb} < 80\text{mm}: & b_{eff,rb} = 2,62 d_{rb}^{0,96} (\cos \theta)^{-1,05} \left(\frac{s_{rb}}{80}\right)^{0,61} \end{cases} \quad (II.78)$$

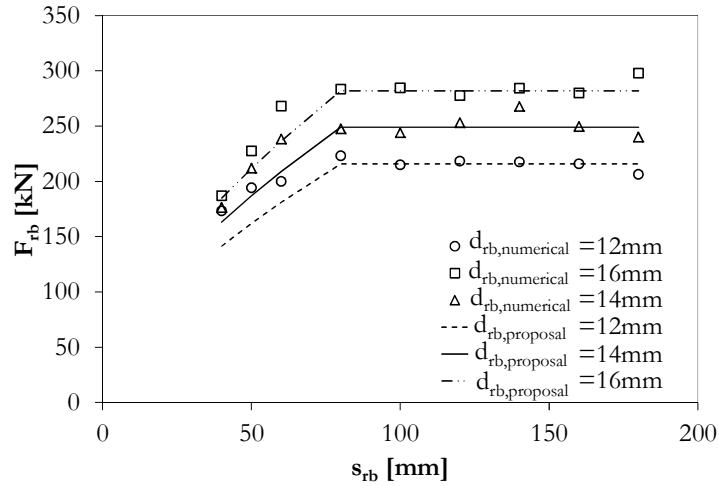


Fig. II.120: Comparison between numerical model and analytical proposal for the effective width ( $b_{eff,rb}$ )

Subsequently, the node dimensions are determined as follows.

$$A_{N1} = b_{eff,rb} 2r \cos(\theta) \quad (II.79)$$

Where:  $A_{N1}$  is the cross-section area of the diagonal concrete strut at node N1 where the admissible stresses have to be verified;  $b_{eff,rb}$  effective width of the concrete contributing to the node resistance;  $r$  is the bend radius of the longitudinal reinforcement bars; and  $\theta$  is the angle of the concrete strut with the horizontal direction.

Finally, the resistance of the node is obtained as below.

$$F_{r,N1} = A_{N1} 0,75 \nu f_{cd} \quad (II.80)$$

#### b) Node N2 (type CCC)

The admissible stresses for this type of node have been given in Table II.7. The geometry of the node, on the concrete strut edge, is defined by the projection of the dimensions of the equivalent rigid plate, representing the anchor plate subjected to compression, to the direction of the concrete strut. Fig. II.121 illustrates the definition of the dimension of this node. Subsequently, the node dimensions are determined as follows.

$$A_{N2} = \frac{l_{eff}}{\cos(\theta)} b_{eff} \quad (II.81)$$

Where:  $A_{N2}$  is the cross-section area of the diagonal concrete strut at node N2 where the admissible stresses have to be verified;  $l_{eff}$  and  $b_{eff}$  are the dimensions of the equivalent rigid plate determined as described in §II.3.1.3.2.

Considering the admissible stresses and the node dimensions, the resistance of the node is obtained.

$$F_{r,N2} = A_{N2} 3 \nu f_{cd} \quad (II.82)$$

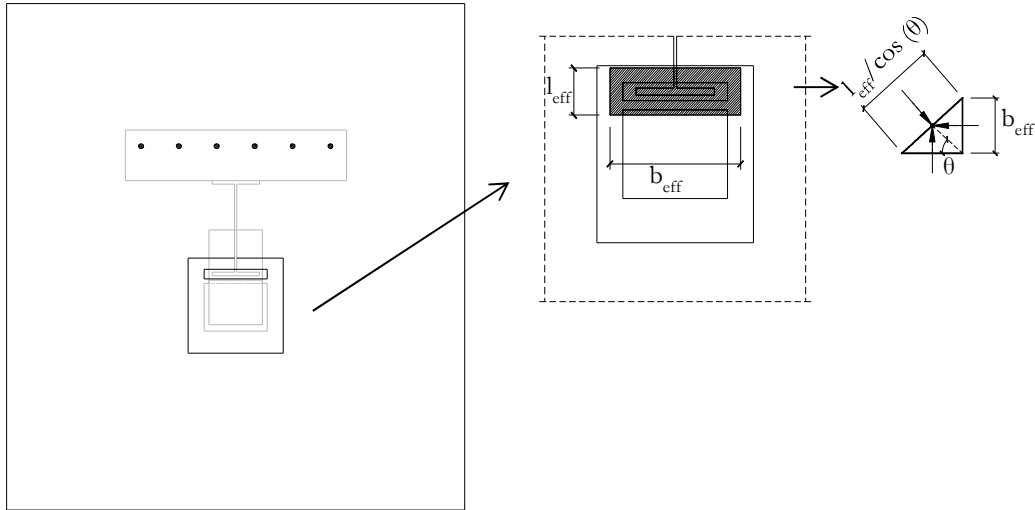


Fig. II.121: Definition of the dimensions of node N2

### c) Joint link properties

Finally, the resistance of the joint link in the direction of the binary force generated by the bending moment applied to the joint is obtained by the minimum resistance of the two nodes, N1 and N2, as expressed in (II.83). Note that the resistance is projected to the horizontal direction, as it will be required later for the complete joint. It should be remarked that in order to have equilibrium in node N1, the vertical component of the load in the diagonal strut has to be equilibrated by the vertical reinforcement in the wall. The design of this reinforcement is not analysed in the present study.

$$F_{C-T,JL} = \text{Min}(F_{r,N1}; F_{r,N2}) \text{Cos}(\theta) \quad (\text{II.83})$$

In terms of deformation, the problem is more complex as the strain field within the diagonal strut is highly variable. Though, as observed in numerical analysis presented in §II.4.2, the deformation pattern of the joint link is very similar independently of the geometric variations performed. Thus, as a simplification, a pure mathematical equation which approximates the deformation of the joint link in function of the loading is proposed. The equation proposed in (II.84) was obtained using the numerical force-deformation curve of the case JL-H226 presented in §II.4.2.3.3, as this was the case achieving higher load capacity. Thus, the horizontal projection of the deformation of the diagonal strut is obtained in function of the horizontal component of the load on the strut. In (II.84), the load ( $F_{C-T,JL}$ ) is introduced in  $kN$  and the deformation is obtained in  $mm$ . The application of both resistance and deformation models is performed in the following subsection.

$$d_{b,JL} = \left( 6,48E^{-8}F_{C-T,JL}^2 + 7,47E^{-5}F_{C-T,JL} \right) \text{Cos} \theta \quad (\text{II.84})$$

### II.4.3.2 Application of the analytical model

In order to assess the quality of the analytical model proposed for the joint link, an application of this model was performed using the same geometrical and material properties of the cases used in the numerical study presented in §II.4.2.3.3. The results of these calculations are here compared with the results of the numerical simulations.

The most important validation is the resistance model, as it can have relevant influence on the predication of the joint failure mode. In addition, the numerical simulations demonstrate that deformation of the joint link is considerably small in comparison to what is expected from other components, e. g. the longitudinal reinforcement component. Furthermore, the deformation model consists in a mathematical equation expressing the deformation in function of the load on the joint link and derived from one of the numerical simulations. Therefore, the suitability of the proposed equation to other geometries is expected. The ratios between the resistance of analytical and numerical models are presented in Table II.29. In both models, numerical and analytical, and for all the cases, the governing component of the joint link was the upper node. A good agreement is observed between models. The exception is the case considering a thin wall (150mm) where the ratio is below 0,6. Plotting the same ratio in function of the angle of the strut ( $\theta$ ), as shown in Fig. II.122, it can be observed that the analytical model loses accuracy. For angles above 70°, the analytical model is too conservative. For these cases, a different model should be assigned for the joint link, e. g. considering two diagonal springs with height equal to half of the lever arm. However, this was excluded from the scope of the present work.

Table II.29: Ratio between  $F_{JL-An}/F_{JL-Num}$

Thickness of wall	Ratio [-]	Height of composite beam	Ratio [-]	Bend radius of longitudinal reinforcement	Ratio [-]
JL-T150	0,588	JL-H226	0,998	JL-R80	0,850
JL-T200	0,855	JL-H416 [Ref]	0,997	JL-R120	0,974
JL-T250	0,965	JL-H620	0,826	JL-R160 [Ref]	0,997
JL-T300 [Ref]	0,997				
JL-T350	0,977				
JL-T400	0,951				



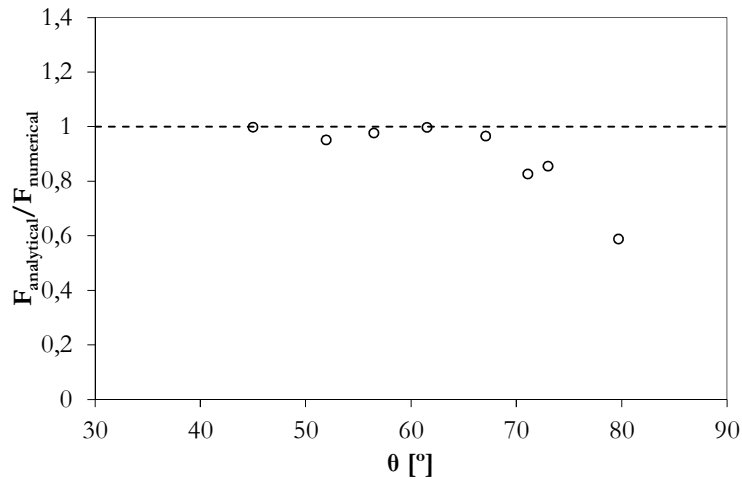


Fig. II.122: Influence of the strut angle ( $\theta$ ) on the analytical prediction

Fig. II.123 compares the force-deformation (horizontal component) curves obtained with analytical and numerical models. The quality of the approximation is good. As the deformation model was derived “directly” from JL-H226 case, the agreement is perfect for this case. For the other cases, depending on the parameter under consideration, small deviations are observed. Given the magnitude of these deviations and of the deformations, the proposed model is suitable for application.

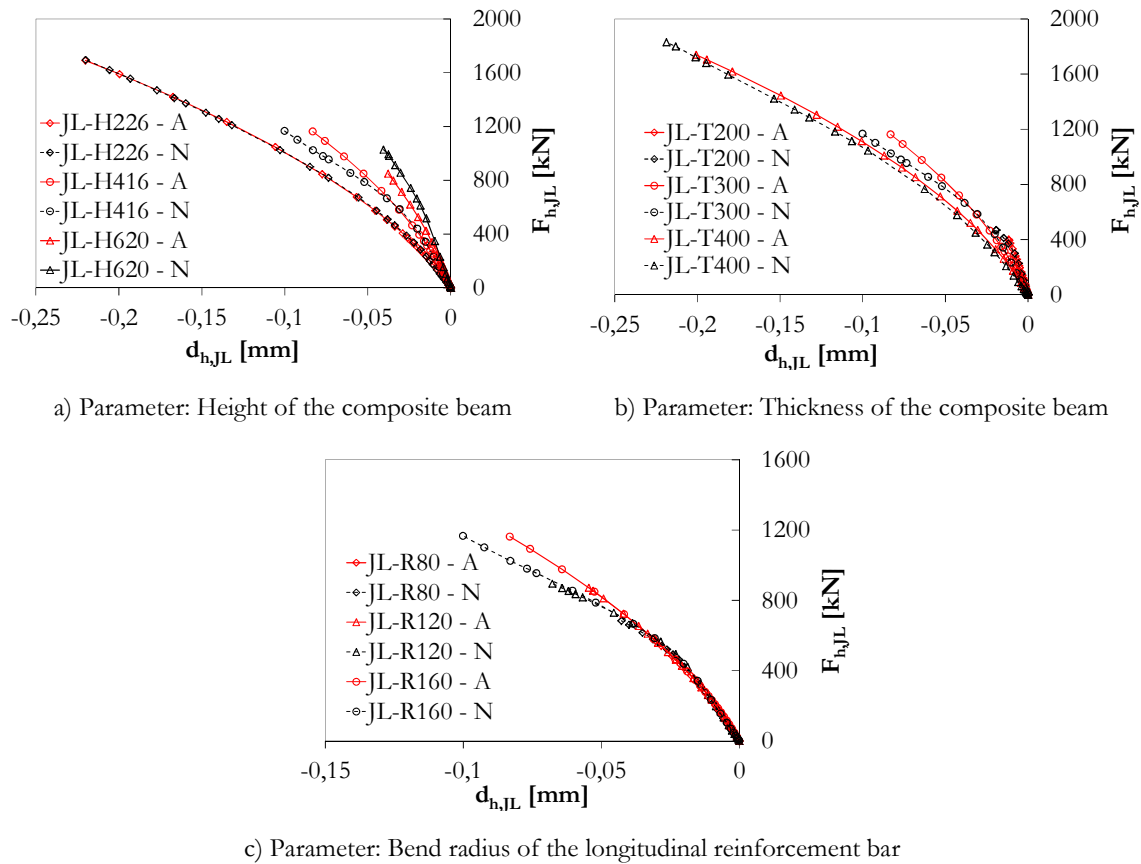


Fig. II.123: Force deformation curves comparing analytical and numerical models (A – Analytical; N – Numerical)

## II.5 Moment-resisting composite beam to reinforced concrete wall joint

### II.5.1 Introduction

In the present chapter is discussed the behaviour of the complete joint configuration for the semi-continuous solution described in §II.1 and illustrated in Fig. II.1. In order to study the joint behaviour, a numerical model was developed and an analytical model proposed. The validation of both models is obtained through comparison against experimental results. For this purposes, the tests on composite beam to reinforced concrete wall joints performed within the RFCS research project *InFaSo* (Kuhlmann *et al.*, 2012), described in §II.2.3.3, were used. Therefore, the experimental tests considered the study of the joint only to hogging bending moment; the analysis in this chapter is mainly focussed on this type of loading. In what concerns the geometrical dimensions and material properties of the test specimens, required for numerical and analytical calculations, these have been summarized in §II.2.3.3. In order to simplify the test nomenclature, in this chapter the referred tests have the following denomination: Test 1 (SP13); Test 2 (SP14); Test 3 (SP15); Test 4 (P15-20); Test 5 (P15-50); Test 6 (P15-10).

### II.5.2 Numerical model

#### II.5.2.1 Description of the finite element model

##### II.5.2.1.1 Identification of the joint components to be simulated

The joint was only tested under hogging bending moment. The main components that influence the joint response are identified in Fig. II.124 and consist in the following:

- i. Longitudinal reinforcement: according to the tests, this is the governing component. Therefore, the accuracy of the model will much depend on this component. The plastic failure mechanism of the steel reinforcement bar is therefore critical.
- ii. Reinforcement-concrete interaction: taking into account the importance of the longitudinal reinforcement, its interaction with concrete also plays an important role, especially in the highest stressed region, located in the slab-wall interface.
- iii. Slab-wall interface: as described above, slab and wall are considered disconnected where only the longitudinal reinforcement performs the connection between these two parts.
- iv. Composite behaviour: the concrete slab to steel beam interaction influences the strength of the composite beam and the slip between these parts contributes to the joint rotation.
- v. Beam bottom flange in compression: under compression load, the yielding of the bottom flange of the steel beam may limit the resistance of the joint.

- vi. Anchor plate in compression: in this part of the joint, concrete crushing or the yielding of the steel components can introduce limitations to the load carrying capacity of the joint.

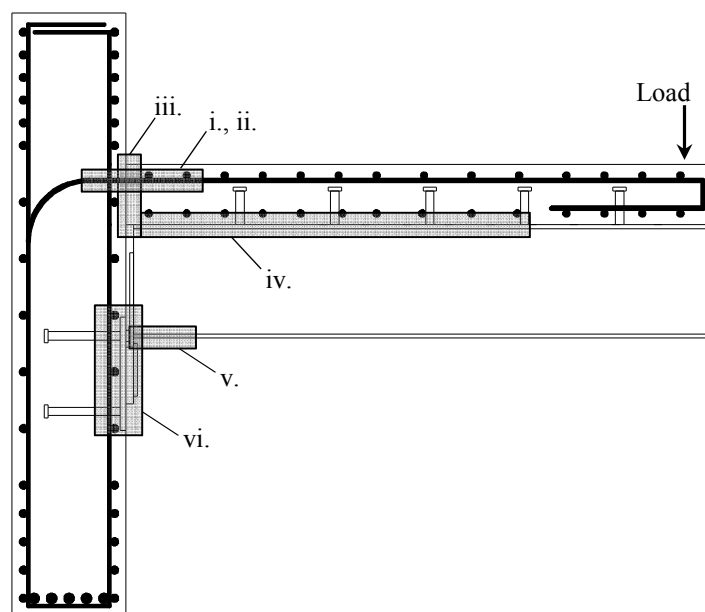


Fig. II.124: Identification of the main joint components to be simulated

#### II.5.2.1.2 Description of the numerical tools

The numerical tool used is the non-linear finite element package ABAQUS (Abaqus, 2011) which has been previously described. In the numerical simulation of the anchor plate connection and the joint link, shown in sub-section II.3.1.2 and II.4.2.1, part of the numerical tools, available in this software, have been already presented and calibrated. These consider the following: 3D solid and truss finite elements; the concrete and steel constitutive model; reinforcement-concrete interaction; mechanical contact model. Though, for the simulation of the complete joint, additional tools were required to deal with the composite behaviour which are described here below.

In a composite beam, the relative slip between the concrete slab and the steel beam is unavoidable, even in the case of full connection, as the shear studs deform when submitted to shear stresses. This slip may have an important contribution to the joint rotation, as verified by (Aribert, 1995). In (Abaqus, 2011), composite behaviour may be modelled using the following options: i) modelling the shear studs physically and establishing contact between concrete and studs; ii) using special elements, either connectors' elements or springs elements. The first option is the most realistic, but it leads to increased calculation time and convergence difficulties due to contact problems. The geometry of the shear studs also adds significant difficulties for the mesh generation. For the second option there are two alternatives, the connector and the spring elements. The main difference between these alternatives is that connectors are much more generic, allowing the combination of different degrees of freedom in a single connector element. In the case of springs, one element has to be defined for each degree of freedom to be connected; however, its

definition is simpler. Thus, the use of springs is preferred because of their satisfactory accuracy, simplicity of definition, less time consumed and fewer convergence problems. This option was also adopted by (Gil and Bayo, 2008) where the composite behaviour was successfully modelled in (Abaqus, 2011) using this type of elements. Thus, to model the shear connection, two springs are used per shear connector, one for longitudinal and one for normal (vertical) interaction. The mechanical behaviour of the springs representing the shear connectors depend on the direction of the spring. For the connection in the normal direction, this spring is assumed to be fully rigid and therefore an infinite stiffness is considered. For the connection in the longitudinal direction, the response of the spring is tested in three different forms: i) elastic; ii) elastic-perfectly plastic and iii) full non-linear. For the two first options, the properties are obtained from (EN 1994-1-1, 2004) and these rely on: initial stiffness ( $k_{sc}$ ); resistance ( $P_{Rk}$ ) and ultimate slip ( $\delta_{u,slip}$ ). The full non-linear response is based on the (Ollgaard *et al.*, 1971) model. The application of these three models is analysed in the next sub-section.

Finally, geometric non-linearities are also taken into account in the calculations. At each load increment, the previous deformed configuration is the reference configuration. In this way, the analyses can be performed with large displacements, large rotations and large strains. To solve the non-linear problem, the modified Riks method (Static Riks) is chosen amongst the techniques available in (Abaqus, 2011). This method allows solving geometrically nonlinear static problems showing negative stiffness in the load displacement response.

#### II.5.2.1.3 Benchmark example for calibration of the joint components modelling

The calibration of part of the numerical tools, referred above, has been accomplished in chapter II.3 and II.4. In the present sub-section, the calibration process of these tools, used in the numerical simulation of the composite beam to reinforced concrete wall joint, is completed. Thus, several benchmark examples dealing with different components of the joint are presented. Moreover, these simulations consider the analysis of: i) type of finite element, 3D solid first and second order elements, and type of stress-strain curve for steel reinforcement bars; ii) interactions, slab-wall interface and iii) composite behaviour and; iv) steel beam bottom flange discretization. The validation of the simulated benchmark examples is accomplished by means of convergence studies and comparison with experimental tests. The accuracy obtained within these benchmark examples puts in evidence the appropriate simulation of the different phenomena to be dealt with in the analysis of composite beam to reinforced concrete wall joints.

- a) Longitudinal steel reinforcement bar: type of element, discretization and stress-strain curve

The experimental tests of the joint configuration (Fig. II.124) (Kuhlmann *et al.*, 2012) reveal that the longitudinal steel reinforcement bar is the governing component. Consequently, this component plays a key role in the joint response, controlling resistance and deformation capacity. Thus, two benchmark examples were carried out to accurately model this component.

In the first case, as solid finite elements of hexahedral shape were used, the bar cross-section had to be discretized so that the resulting polygon circumscribed by the circular cross-section (Fig. II.124-a) minimizes the error of a non-circular shape. In addition, the required discretization to use C3D8R type of elements is calibrated performing a convergence analysis using the second order elements with reduced integration (C3D20R).

The example illustrated in (Fig. II.124-b), is very simple and considers the simulation of a steel bar with 16mm diameter (size of longitudinal reinforcement bar in the reference specimen of the joint configuration under study) subject to a tensile load. The load is applied at one edge of the bar, imposing displacements, and at the opposite edge of the bar all nodes are fully fixed in all degrees of freedom. The material properties assigned to the steel bar were the values obtained in the material tests of the longitudinal steel reinforcement bars of the joint configuration tested in (Kuhlmann *et al.*, 2012). The yield and the ultimate strength of the steel are  $450\text{N}/\text{mm}^2$  and  $745\text{N}/\text{mm}^2$ , respectively.

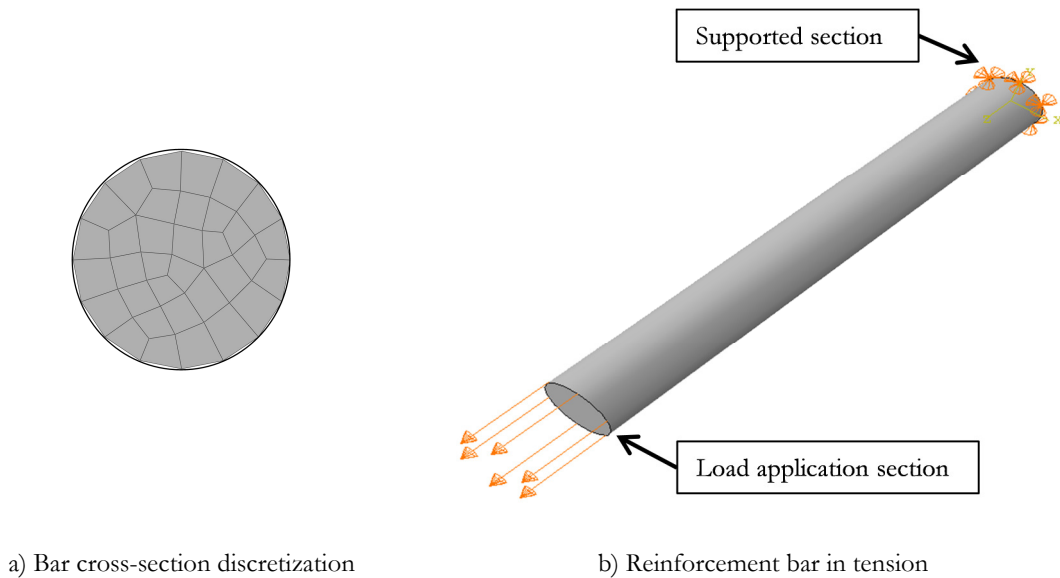


Fig. II.125: Benchmark example to calibrate the reinforcement bar discretization

Several numerical simulations were carried out. Two consider the use of second order elements (C3D20R) to obtain convergence of results and to be used as the correct solution. Then, the implementation of C3D8R elements was performed. The required discretization of the cross-section was obtained through convergence of results. Table II.30 summarizes the performed simulations. The comparison of results was performed by means of force-deformation. The force represents the applied load while deformation regards to the displacement at the edge of the applied load, in the load direction. Fig. II.126 shows the performance of the different models. The curves of the models using the second order elements are barely undistinguishable, indicating that these may be assumed as the correct solution (convergence obtained). The application of the first order elements demonstrate that the edge of the cross-section should be discretized in at least 20 nodes to obtain a good approximation. The main deviations are observed in the plastic range where the maximum load capacity is underestimated in the models with less nodes to define the edge

of the cross-section. For example, in case of using only 8 nodes, the maximum load is 11% lower.

Table II.30: Performed models to calibrate reinforcement bar modelling

Model ID	Description
R-C3D20R-8	Element type: C3D20R Cross-section edge nodes: 8
R-C3D20R-16	Element type: C3D20R Cross-section edge nodes: 16
R-C3D8R-8	Element type: C3D8R Cross-section edge nodes: 8
R-C3D8R-16	Element type: C3D8R Cross-section edge nodes: 16
R-C3D8R-20	Element type: C3D8R Cross-section edge nodes: 20
R-C3D8R-32	Element type: C3D8R Cross-section edge nodes: 32

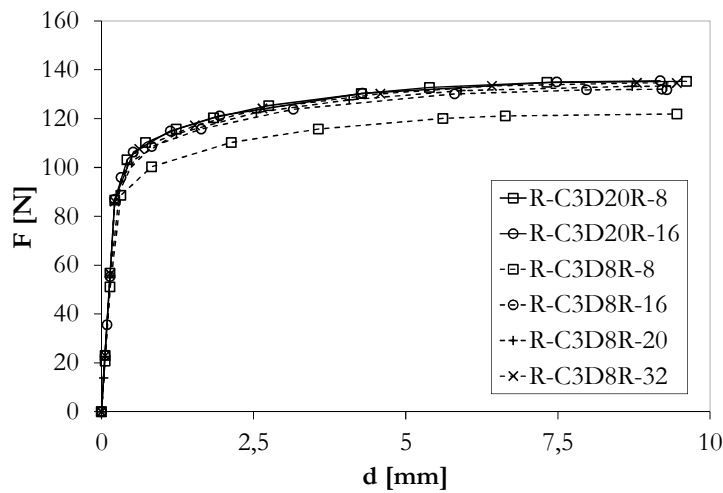


Fig. II.126: Force-deformation curves of the convergence study for reinforcement bar discretization using first order elements (C3D8R)

The second benchmark example for the reinforcement bar analysis regarded the two following aspects: i) the type of stress-strain curve for the material behaviour, nominal or true; ii) a failure criterion. The true properties were calculated using equations (II.85) and (II.86) (Girão Coelho *et al.*, 2006), and the nominal properties ( $\epsilon$ ,  $\sigma$ ) were obtained from material testing. A common uniaxial tension tests (Coupon Test) of a steel reinforcement bar was used as benchmark. This test was part of the experimental programme presented in

(Henriques *et al.*, 2013). The numerical simulation considered same loading strategy as illustrated in Fig. II.125 however, now the diameter of the bar was 12mm. The nominal yield and ultimate strength are  $494\text{N}/\text{mm}^2$  and  $705\text{N}/\text{mm}^2$ , respectively.

$$\sigma_{true} = \sigma (1 + \varepsilon) \quad (\text{II.85})$$

$$\varepsilon_{true} = \ln (1 + \varepsilon) \quad (\text{II.86})$$

As the reinforcement bar in the joint (Fig. II.124) was taken up to failure, the stress-strain curve should consider the real properties. Two numerical simulations were performed to compare the obtained response when considering the following material properties: i) nominal stress-strain curve; ii) true stress – logarithmic strain curve. The results of the numerical simulation are presented in Fig. II.127. The force-elongation ( $\Delta l$ ) curve measured in the tested bar is used for comparison. If the nominal stress-strain curve is used instead of the true stress-logarithmic strain curve, a worse approximation is obtained when plastic deformation appears. This result is expected and demonstrates that (Abaqus, 2011) requires the true stress-logarithmic strain if the problem enters in the large deformation range.

Common to both numerical simulations is a descending branch appearing earlier than in the experimental test. This deviation is justified by the fact that the correction of the nominal curve to real properties using expressions (II.85) and (II.86) is only valid up to the phenomenon of necking occurs in the bar. After this stage, the data obtained in a common Coupon Test cannot reproduce with sufficient approximation the properties of the material. The considerable reduction of the bar cross-section, in the necking region, leads to a decrease of the external applied load however, the material strength is still increasing (hardening). The decrease of strength is only observed when damage of the material takes place. Though, the nominal properties are computed in function of the initial cross-section and therefore, a reduction of the material strength is reported before it really occurs. Therefore, the true properties determined with (II.85) and (II.86) are affected by this phenomenon. Without sufficient information to correct the material curve, subsequently to necking (identified by the maximum strength of the material obtained from the Coupon Test) a plateau was considered (Fig. II.128-a). As result, in the numerical simulations when the reduction of the cross-section begins to be significant and the stress on the material has achieved its maximum, a decrease on the applied load is observed.

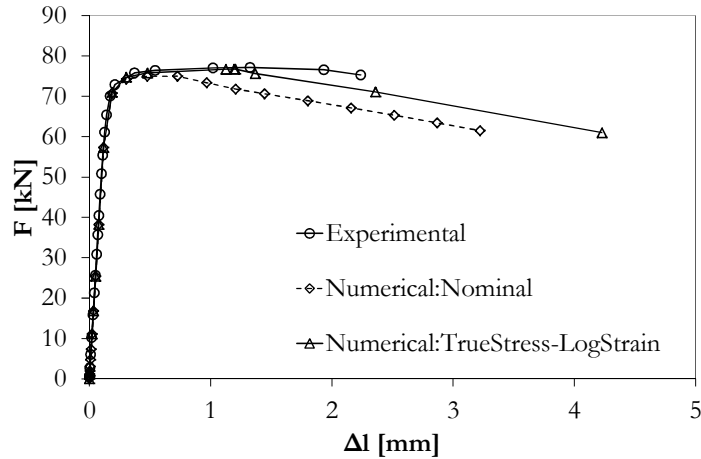
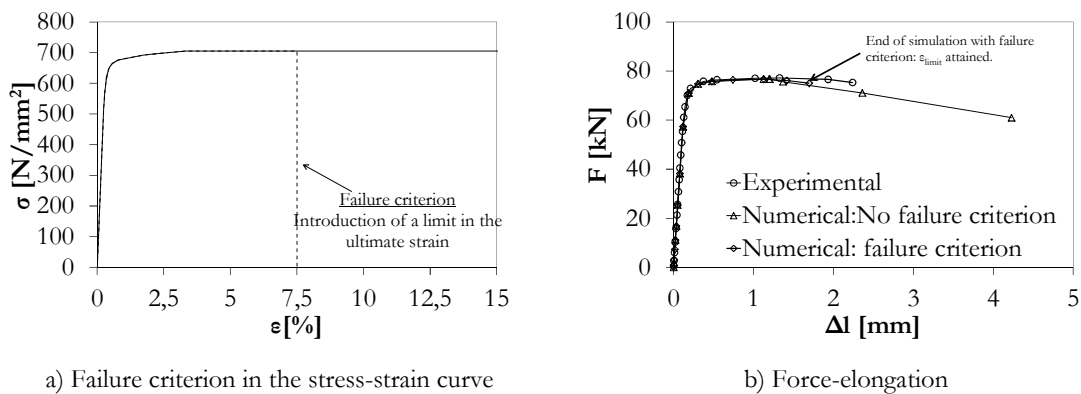


Fig. II.127: Force-elongation curves comparing the type of nominal and true stress-strain material properties

In what regards to a failure criterion, it was decided to introduce a limitation on the material strain to the maximum obtained in the tensile test (Coupon Test). Thus, in the material properties curve, when the maximum strain is achieved, the stress of the material is decreased to zero, as illustrated in Fig. II.128-a). Fig. II.128-b) shows the force-deformation curve comparing the experimental results with the numerical simulations. The model without failure criterion is also included. As expected, the simulation with failure criterion limits the response before the test results. However, taking into account the simplicity of the implementation of the considered failure criterion, the approximation is acceptable. Furthermore, the ultimate strain assumed is also affected by the local phenomenon described above, as the value considered was obtained from the nominal results.



a) Failure criterion in the stress-strain curve

b) Force-elongation

Fig. II.128: Application of a failure criterion to the numerical simulations

b) Slab-wall interface

To perform the benchmark of two concrete members only connected by steel reinforcement bars no specific test was available besides the complete joint between the composite beam and the reinforced concrete wall. So, an academic example was idealized using the tested joint configuration. The example considered the connection between composite beam and a reinforced concrete wall, as illustrated in Fig. II.129. The main scope of this study was to verify the capability of the model to consider only the



connection at the tension zone through the longitudinal reinforcement and to verify the influence of the bond model applied to this particular case. Thus, only a portion of the composite beam and wall is modelled, as the focus is on the connection with the longitudinal reinforcement. The concrete slab, wall and the steel beam were considered elastic ( $E_c=32000N/mm^2$  and  $E_s=210000N/mm^2$ ) and full interaction was assumed in the composite beam. For the steel reinforcement bars elastic-plastic behaviour was considered with a yield and ultimate strengths of  $450N/mm^2$  and  $600N/mm^2$ , respectively. The simulated portion of the wall, at the edge opposite to the wall-slab interface, and the steel beam bottom flange, are fully fixed. Two simulations were performed in order to evaluate the approximation to “real” bond-slip model (Traction-Separation) and the perfect bond model (Embedded technique). These techniques have been described before in §II.3 and §II.4. In the wall-slab interface the “hard” contact model, allowing normal pressure when in contact and free separation was used.

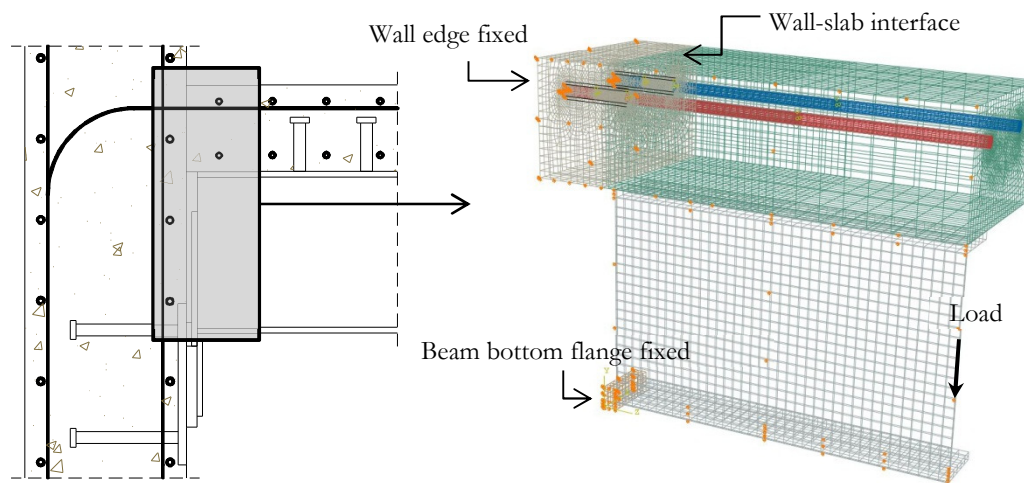


Fig. II.129: Benchmark example for connection of concrete parts using only longitudinal reinforcement

Fig. II.130 shows the results of the numerical simulations in terms of applied load at the free edge of the composite beam versus beam deflection. It is clear that the embedded option provides a stiffer response than the previous. Furthermore, because of the perfect bond assumption, in this model the response is linear, as the yield of the longitudinal reinforcement is achieved for much higher loads. Fig. II.131 shows the separation between wall and slab for both models. There is no separation in the case of the model with perfect bond because of the rigid connection between reinforcement and concrete nodes conditioning the deformation in the interface. Furthermore, in the case of the perfect bond the reinforcement remains in the elastic domain for much higher loads than in the case of the model with approximation to “real” bond behaviour. In the latter, the maximum is limited by the steel strength of the reinforcement which is attained for a load of approximately  $160kN$ . These results reinforce the need to consider the bond model in order to approximate the real interaction between the concrete and the reinforcement bars in this critical zone of the joint.

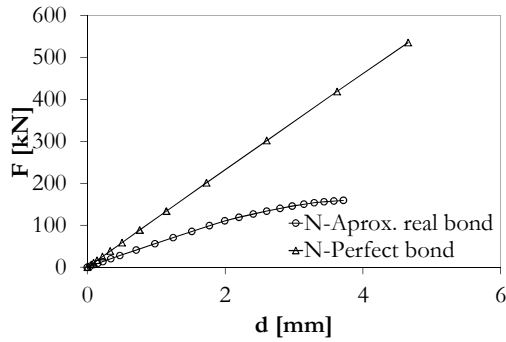


Fig. II.130: Load-deformation curve comparing the models of connection between concrete parts using only reinforcement bars

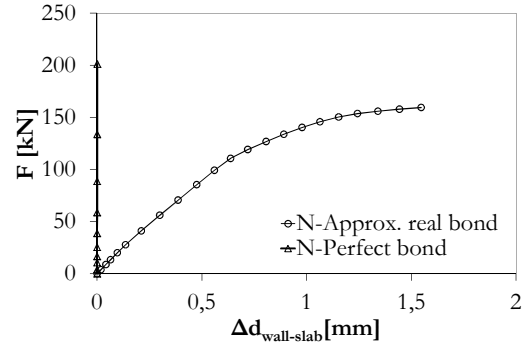


Fig. II.131: Load-separation curves comparing the models with approximation to “real” bond behaviour and with perfect bond

### c) Composite behaviour

The composite behaviour of steel-concrete composite beam was validated using as benchmark example the test of a simply supported composite beam reported in (Chapman and Balakrishnan, 1964). This example was also used for validation of the software VULCAN presented in (Huang *et al.*, 1999). The latter numerical results are included here for general comparison. The geometric dimensions and the material properties considered for this benchmark example are given in Fig. II.132 and in Table II.31. The beam was loaded with a concentrated load at the mid-span. More detailed information is available in the given references.

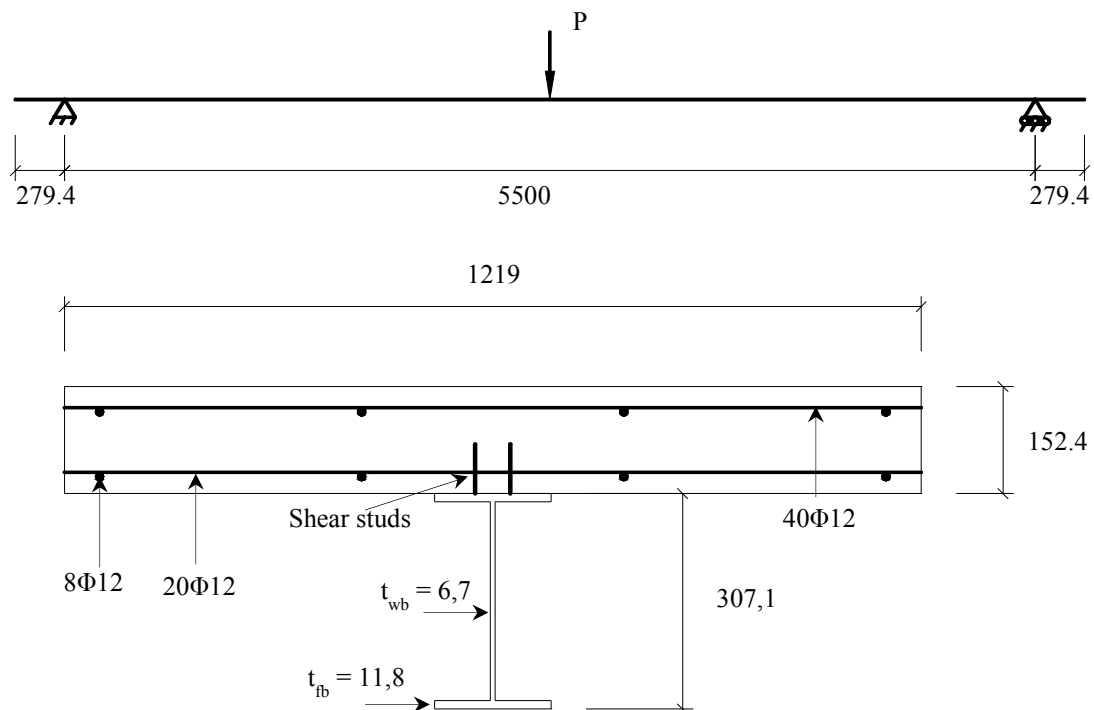


Fig. II.132: Geometry of the benchmark example for the composite behaviour (dimensions in mm) (Chapman and Balakrishnan, 1964)

Table II.31: Material properties, stud number and dimension of the benchmark example for the composite behaviour (Chapman and Balakrishnan, 1964)

$f_y$ [N/mm <sup>2</sup> ]	$f_c$ [N/mm <sup>2</sup> ]	$f_{sry}$ [N/mm <sup>2</sup> ]	N <sup>o</sup> studs	$d_a$ [mm]	$f_u$ [N/mm <sup>2</sup> ]
302	27	600	68	19	600

In the numerical model, the connection between the concrete slab and the steel beam was performed by means of spring elements, as described previously. For each shear connector, two springs were used. One performs the vertical connection and other the longitudinal connection (along the length of the beam). For the first it was assumed that there is full connection and therefore an infinite stiffness was attributed to this spring. For the direction of slip, the mechanical response incorporates both the steel connector and the surrounding concrete behavior. These were calculated according to (EN 1994-1-1, 2004). The quality of the developed model is shown in Fig. II.133-a) comparing the obtained load-beam mid-span deflection curve with experimental result (Chapman and Balakrishnan, 1964) and the numerical calculation performed in VULCAN (Huang *et al.*, 1999). In the case of the latter, the result of a model with zero interaction is included to verify the effect of the concrete slab-steel beam interaction. A good agreement was observed between the numerical model developed and the experimental tests and numerical simulations performed in VULCAN. The simulation performed in VULCAN (Huang *et al.*, 1999) with zero interaction (only contact between slab and steel beam) demonstrates that the degree of composite action is relevant because it influences the maximum load to be attained. The end-slip measured experimentally and predicted in the numerical models are compared in Fig. II.133-b). Here, a good agreement is also observed, confirming the accuracy of the model developed in ABAQUS.

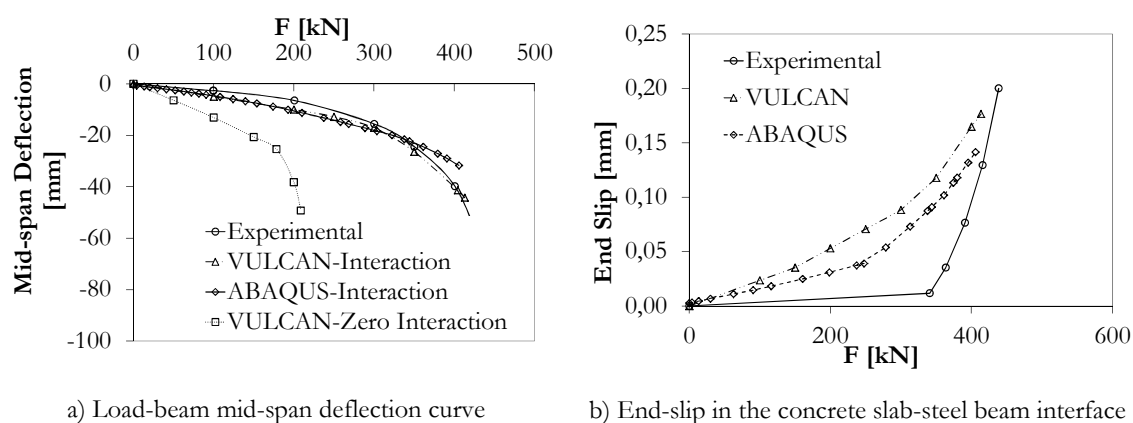


Fig. II.133: Composite beam benchmark example comparison of results for evaluation of the model developed in ABAQUS

In the previous model, the behaviour of the shear connection in the composite beam considers a non-linear shear-slip relation as defined by (Ollgaard *et al.*, 1971). As the shear connection was not taken to its ultimate deformation, like in the tests of the composite beam to reinforced concrete wall joint, two additional simulations were executed to assess the influence of considering a linear relation between shear-slip instead of the non-linear

model. These two models considered the following: linear elastic relation (CB-LIN); elastic-plastic relation (CB-EP). The three constitutive models assigned to the springs modelling the shear connection are shown in Fig. II.134-a). Note that the maximum load observed in the most loaded spring is represented by the horizontal line. The maximum force on the shear connectors is 48% of their capacity. Fig. II.134-b) shows the global force-deflection curves for the composite beam. It can be observed that the behaviour of the shear connection has negligible influence on the global behaviour. The response of all models is very similar as the load in each shear stud is small, remaining in the range where the difference between the models is minor.

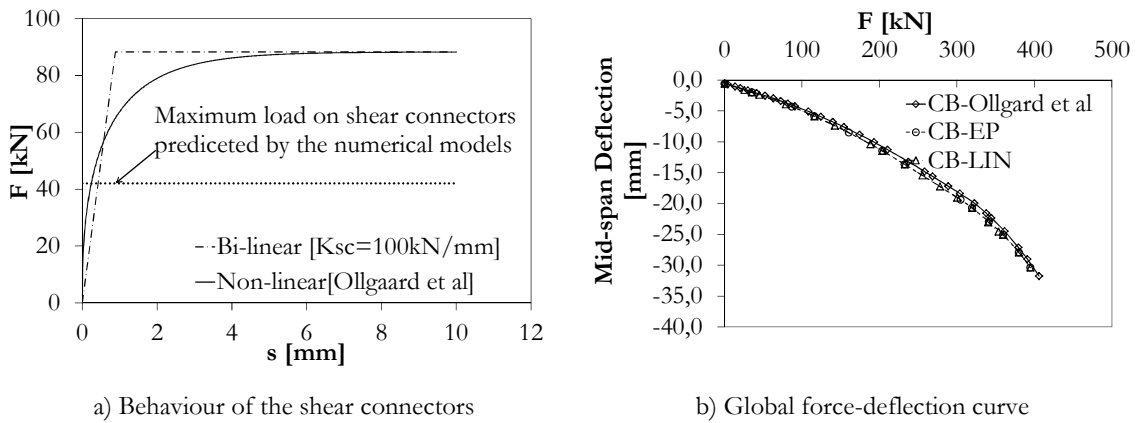


Fig. II.134: Evaluation of the influence of the shear connection behaviour

d) Steel beam bottom flange in compression

To analyse the steel beam bottom flange in compression, a pure academic example was conceived to calibrate the mesh refinement required to use C3D8R type of elements. This consists in a simple case of a cantilever beam loaded by a concentrated load at the free edge, as illustrated in Fig. II.135. The values considered for the length of the beam, the cross-section and the material properties are similar to the ones used in the composite beam to reinforced concrete wall joint tested in (Kuhlmann *et al.*, 2012). For the material model of the steel, an elastic-perfectly-plastic behaviour was assumed and the yield strength considered the nominal value of a S355 steel ( $f_y = 355 \text{ N/mm}^2$ ).

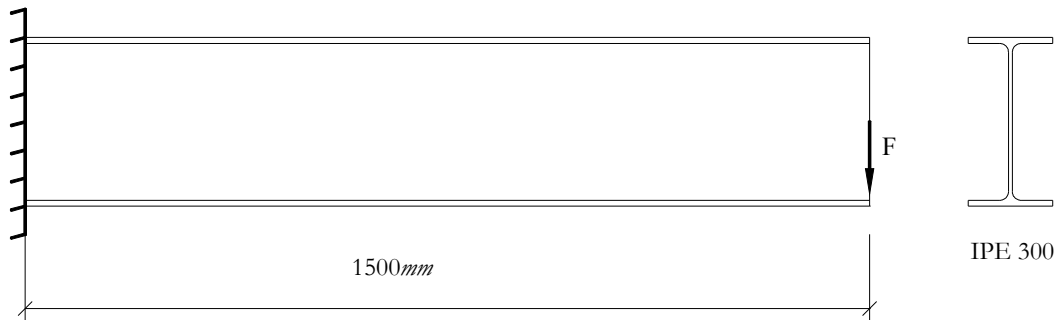


Fig. II.135: Cantilever beam example for calibration of the mesh required to use first order elements (C3D8R) in the steel beam

As for the longitudinal reinforcement bar, several models were executed which are summarized in Table II.32. First, the correct solution was obtained through convergence of the models using the second order elements (C3D20R). Then, the first order elements (C3D8R) were implemented and the mesh validated through comparison with results of the previous models. This analysis was mainly focused on the number of elements to use through the web thickness, and specially, through the compression flange thickness. After, an optimization of the mesh regarding the size of the model was performed. Finally, the consideration of the fillet radius in the cross-section was evaluated. In the latter models, first tetrahedral elements were used in order to model the fillet radius with acceptable element aspect ratios. According to the ABAQUS manual (Abaqus, 2011), the first order elements of this type should be avoided so, the second order elements (C3D10) were used. Finally, a model was calibrated for the use of type elements C3D8R in the fillet radius. In all the previous models, the fillet radius was neglected.

Table II.32: Summary of the models performed to calibrate discretization of the steel beam

Model ID	Description	Model ID	Description
CB-C3D20R-T1	Element type: C3D20R Number of elements through thickness: 1 Fillet radius not modelled	CB-C3D8R-T2LE	Element type: C3D8R Number of elements through thickness: 2 Longer elements Fillet radius not modelled
CB-C3D20R-T2	Element type: C3D20R Number of elements through thickness: 2 Fillet radius not modelled	CB-C3D10-T2FR	Element type: C3D10 Number of elements through thickness: 2 Fillet radius modelled
CB-C3D8R-T1	Element type: C3D8R Number of elements through thickness: 1 Fillet radius not modelled	CB-C3D8R-T2FR	Element type: C3D8R Number of elements through thickness: 2 Fillet radius modelled
CB-C3D8R-T2	Element type: C3D8R Number of elements through thickness: 2 Fillet radius not modelled		

The evaluation of the mesh quality was made by means of moment-rotation curves calculated at the support section, as shown in Fig. II.136. The bending moment ( $M$ ) and rotation ( $\Phi$ ) using the applied load ( $F$ ) and the deflection of the beam at the free edge, respectively. In terms of initial stiffness, all models provide the same results, showing convergence. However, when the plastic deformation appears, the use of C3D8R, with

only one element through the flange thickness, diverged from the other models. For the model CB-C3D8R-T1, the load decreases approximately 14%. With two elements through the thickness (CB-C3D8R-T2) a good approximation is already obtained (Fig. II.136-a). In the first models, the length of the elements is approximately 10mm. Initially, higher lengths were not considered as this would result in elements with high aspect ratios. Then, in order to reduce the model size, the length of the elements was increased from 10mm to 20mm (closer to the supported section) and 30mm (near the free edge). This fact only affects the results for high plastic deformations, above 30mrad, however, the deviations observed are acceptable.

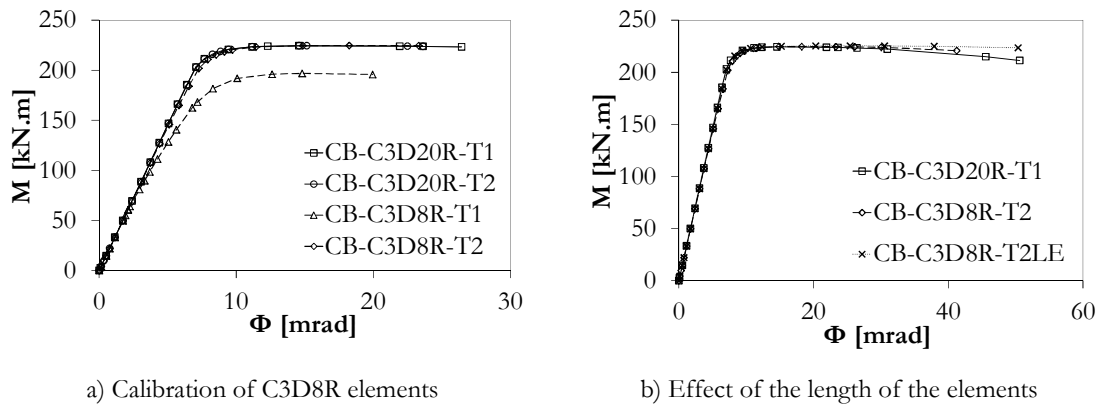


Fig. II.136: Moment-rotation curves comparing the models for calibration of the mesh discretization of the steel cantilever beam

In what concerns the fillet radius of the steel profile, Fig. II.137-a) shows the effect of neglecting this part of the beam by comparing the previous models with model CB-C3D10-T2FR. The increase on the load capacity is approximately 4,5%. No variation is noticed in the initial stiffness. Experimentally, in (Kuhlmann *et al.*, 2012), the load on the beam bottom flange was estimated to be approximately 780kN. According to (EN 1993-1-1, 2005), the yielding of the first fibers on IPE 300 subjected to pure bending occurs for a load on the beam bottom flange of approximately 684kN. Although, the real properties of the material are expected higher than the nominal ones, these values indicate that yielding on the beam bottom flange may occur. Consequently, modelling the fillet radius should be considered. Thus, an additional numerical simulation (CB-C3D8R-T2RF) was performed to attest the use of C3D8R in the fillet radius. In order to implement this type of elements, the fillet radius was considered with a triangular shape being inscribed in the real shape. In this conservative way, less material is considered than in reality. This option was taken in order to have a good aspect ratio of the elements so that convergence problems were avoided due to bad element shape. In Fig. II.137-b), it is verified that the two models considering the fillet radius converge.

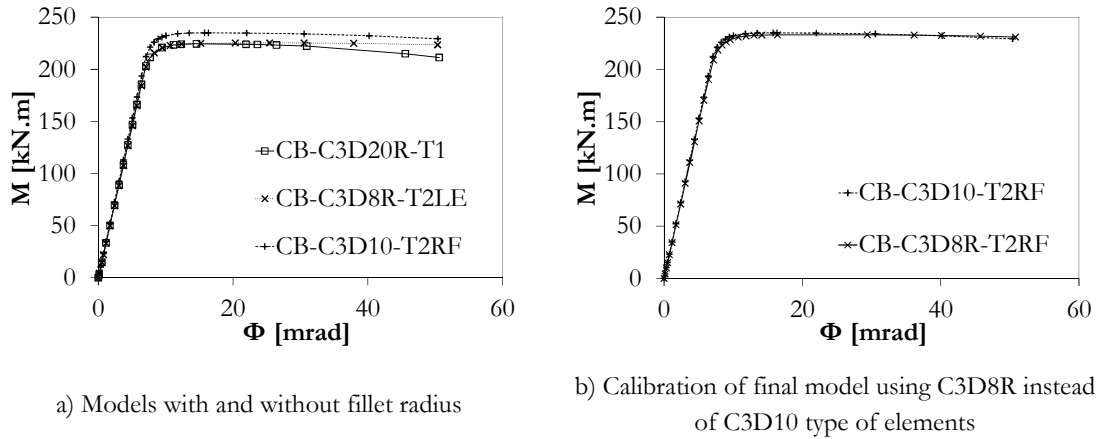


Fig. II.137: Moment-rotation curves evaluating the effect of modelling the fillet radius

II.5.2.1.4 Description of the numerical model developed to simulate the composite beam to reinforced concrete wall joint

The finite element models for calibration of the key components of the composite beam to reinforced concrete wall joint have been presented in previous sub-sections II.3.1.2, II.4.2.1.2 and II.5.2.1.3. Table II.33 summarizes the main characteristics of the numerical model developed for the complete joint illustrated in Fig. II.138. Profiting from the symmetry of the problem, only half of the specimen was modelled. In colour are highlighted the elements where the boundary conditions were assigned: i) red – symmetry boundary conditions, nodes in external surface (in YZ plane) constrained in X direction; ii) dark green – top boundary conditions, nodes in the external surfaces (in XZ planes) constrained in Y direction; iii) light green – bottom boundary conditions 1, similar to previous; iv) dark blue – bottom boundary conditions 2, nodes in the external surface (in XY plane) constrained in Z direction.

Table II.33: Summary of the numerical model characteristics

<p><b>Type of finite elements</b></p>	<ul style="list-style-type: none"> <li>▪ Majority of the parts were modelled using the 3D solid element of first order with reduced integration (C3D8R)</li> <li>▪ Ordinary reinforcement bars were modelled with 3D truss linear elements (T3D2)</li> <li>▪ Shear connectors in the composite beam were modelled with spring elements (axial springs)</li> </ul>
<p><b>3D Interactions</b></p>	<ul style="list-style-type: none"> <li>▪ Reinforcement-concrete: two types were used, for the longitudinal reinforcement bars, in the region adjacent to the joint face (see below the detailing of this region), an approximation to the bond-slip behaviour is considered using contact with cohesive behaviour model; in remaining parts of this reinforcement bars and in for all ordinary reinforcement, within slab and wall, a perfect bond model was used</li> <li>▪ Steel beam-concrete slab, steel anchors and anchor plate to concrete wall: “hard” contact with friction (<math>\mu=0,45</math>)</li> <li>▪ Contact between steel pieces: “hard” contact with friction (<math>\mu=0,3</math>)</li> <li>▪ Concrete slab to concrete wall: “hard” contact without friction</li> <li>▪ Welded steel pieces: welds not modelled, rigid link is considered between welded steel pieces</li> </ul>

<p><b>Constitutive models for materials and interactions</b></p>	<ul style="list-style-type: none"> <li>▪ Concrete: Concrete Damage Plasticity model (according to (Abaqus, 2011)); uni-axial response non-linear in compression according to (EN 1992-1-1, 2004) and linear in tension up to failure, post-cracked response defined by the fracture energy, calculated according (fib, 2010)</li> <li>▪ Steel for reinforcement: von Mises Plasticity model (isotropic yielding); plastic range defined according to experimental curve (see detail below)</li> <li>▪ All other steel pieces: von Mises Plasticity model (isotropic yielding); material properties according to the mean values obtained in the material tests (Kuhlmann <i>et al.</i>, 2012)</li> <li>▪ Bond behaviour: traction-separation model according to (Abaqus, 2011) (detailed description after this table)</li> <li>▪ Shear connection: linear elastic behaviour assumed; properties calculated according to (EN 1994-1-1, 2004)</li> <li>▪ “Hard” contact with friction: unlimited pressure transmitted when in parts are in contact; no penetration allowed; classical isotropic Coulomb friction model considered for frictional behaviour</li> </ul>
<p><b>Other modelling issues</b></p>	<ul style="list-style-type: none"> <li>▪ Geometric non-linearities included</li> <li>▪ No initial imperfections and residual stresses</li> <li>▪ Loading strategy considered the imposition of displacement</li> <li>▪ Modified Riks method to solve the non-linear problem</li> </ul>

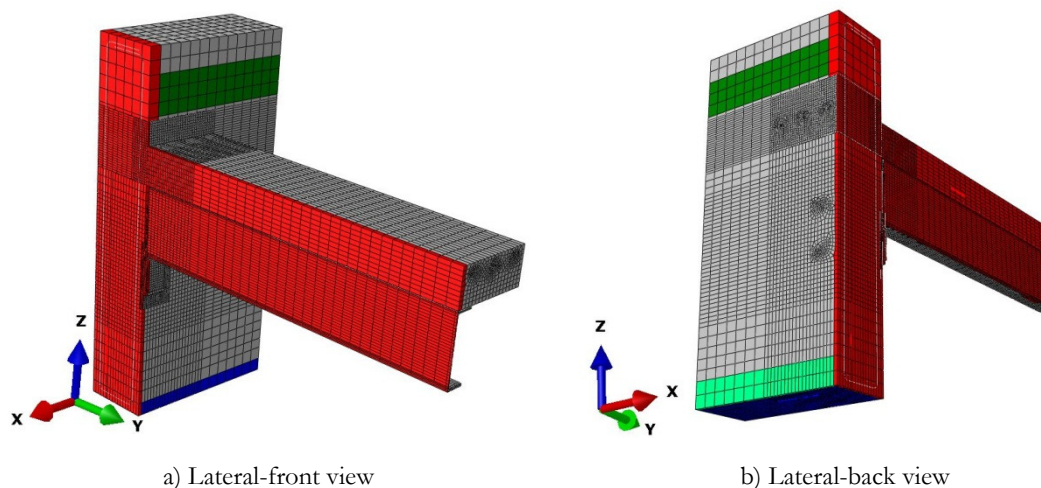


Fig. II.138: Finite element idealization of the composite beam to reinforced concrete wall joint tested within (Kuhlmann *et al.*, 2012)

Because of the importance of some parts of the model, the following are further detailed:

a) Additional 3D interactions

Besides the interactions described above, reinforcement-concrete and concrete slab-steel beam, the following interactions were considered in the analysis (Fig. II.139):

- i. Concrete slab to concrete wall
- ii. Top flange of the steel beam to concrete slab
- iii. Steel beam to beam end-plate
- iv. Beam end-plate to steel contact plate
- v. Beam end-plate to steel bracket



- vi. Steel contact plate to anchor plate
- vii. Anchor plate to steel bracket
- viii. Anchor plate to concrete wall
- ix. Headed anchors on anchor plate to concrete wall

These interactions were included in the analysis as contact problems. Accordingly, two types of contacts were considered: 1) “hard” contact with and/or without friction, where contact is modelled based on contact-pairs, master-slave surface interaction; 2) rigid link (tie option), which is also based on master and slave interaction, but no sliding is allowed and the parts are rigidly connected. The types of contact used for the above list of interactions are identified in Table II.34 and also illustrated in Fig. II.139. Note that welds were not modelled and therefore the tie option was used to connect welded steel parts.

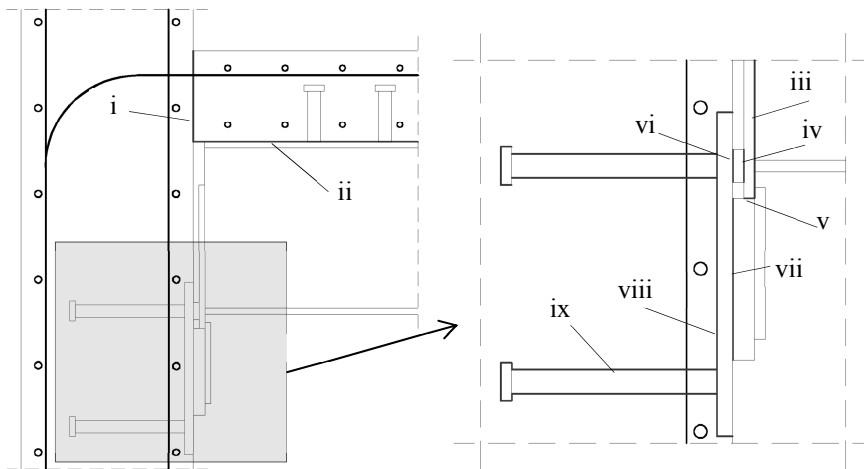


Fig. II.139: Localization of the different parts in contact

Table II.34: Identification of the type of contacts considered in the model

Interaction	Type of contact
i	1) without friction
ii	1) without and with friction (both options were tested)
iii	2)
iv	2)
v	1) without friction
vi	1) without friction
vii	2)
viii	1) with friction
ix	1) without friction

- b) Length of the longitudinal reinforcement bars where interaction with concrete is modelled using contact with cohesive behaviour (approximation of the “real” bond-slip behaviour)

The implementation of the contact with cohesive behaviour to model the reinforcement-concrete interaction is much more time consuming than the perfect bond interaction. In addition, this technique implies that from the concrete parts is removed the material in the position of the reinforcement bars introducing geometrical discontinuities which affect the mesh shape and therefore, require more refinement. Furthermore, the numerical difficulties are increased as the model has to deal with additional contact problems. For all these reasons, the length of the reinforcement bar, where this type of modelling is considered was minimized. In this way, this type of behaviour was considered only in the region located around the wall-slab interface (reinforcement highly stressed region). The length of this region was assumed as the sum of the following dimensions: i) inside the wall, from the joint face up to the beginning of the bar bend (hook); ii) inside the slab, from the joint face up to a distance  $L_t$ , which according to (ECCS, 1999) is defined as the elongation length ( $L_t$ ) and is determined as in (II.13). The total length to consider is illustrated in Fig. II.140 and the calculated values are given in Table II.35, for each of the test specimens numerically simulated.

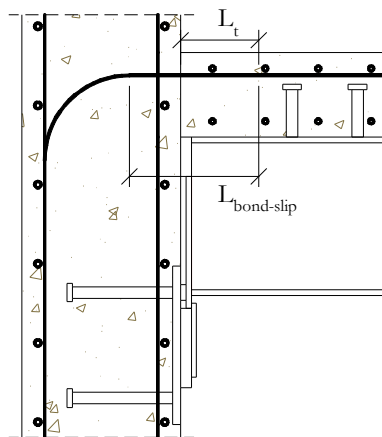


Fig. II.140: Illustration of the length of the longitudinal reinforcement bar considering the contact with cohesive behaviour

Table II.35: Length of the reinforcement bar considering contact with cohesive behaviour

	Test 1	Test 2	Test 3
$L_t$ [mm]	76,41 ( $\approx 80$ )	95,65 ( $\approx 100$ )	76,64 ( $\approx 80$ )
$L_{bond-slip}$ [mm]	170	190	170

- c) Stress-strain curve of the steel longitudinal reinforcement bars

The longitudinal reinforcement bars are the key component of the present joint as failure was experimentally attained with rupture on these bars (Kuhlmann *et al.*, 2012). In §II.5.2.1.3, it was demonstrated that the software (Abaqus, 2011) expects the true stress-log

strain curve if the simulation enters in the field of the large deformations. Accordingly, for this component, the material true stress – log strain curve was determined based on the material test results. Fig. II.141 presents the curves considered in the model for the longitudinal reinforcement bars of 12mm and 16mm. The failure criterion introduced consists in limiting the steel strain to the maximum reported value. This was done by considering a vertical branch when this strain is attained.

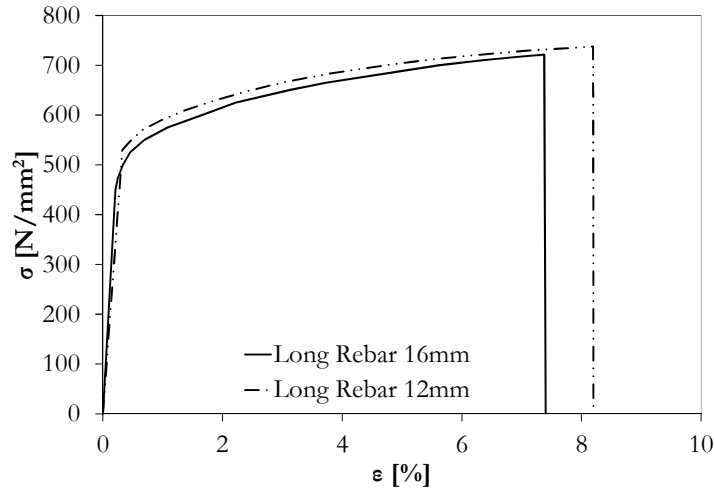


Fig. II.141: True stress-Log strain curve for the steel longitudinal reinforcement bars

d) Approximation of the real bond behaviour modelled with traction-separation law

In (Abaqus, 2011), the bond-slip behaviour of the steel reinforcement bars-concrete interaction can be approximated using one of the following techniques: i) cohesive elements with traction-separation behaviour; and ii) contact with cohesive behaviour (traction-separation law). Here, the latter is used to model the steel reinforcement-concrete interface within  $L_{bond-slip}$  length (Fig. II.140). This modelling technique has been described in §II.4.2.1. Accordingly, the main parameters required were calculated and are given in Table II.36. Based in (fib, 2010) the bond conditions were considered good in both members, slab and wall, while for the confinement, based on the concrete cover, for the first, unconfined concrete was assumed, and for the latter, confined concrete was considered. In (Abaqus, 2011), the ascending branch of the traction-separation law has to be linear therefore only the stiffness coefficients  $k_{nn}$  (normal direction),  $k_{ss}$  and  $k_{tt}$  (tangential directions) were required. Then, the damage range, for sake of simplicity, considers a linear relation. For the normal direction no damage is assumed. In Table II.36 the parameters  $\tau_{max}$ ,  $\delta_{\tau,max}^{ss,tt}$  and  $\delta_u^{ss,tt}$  represent the maximum bond strength, the slip at maximum bond strength and the slip at ultimate bond strength. Fig. II.142 compares the traction-separation curve with the bond-slip model for reinforcement-concrete (wall) interaction of Test 1 according to (fib, 2010). Similar curves were defined for all other cases.

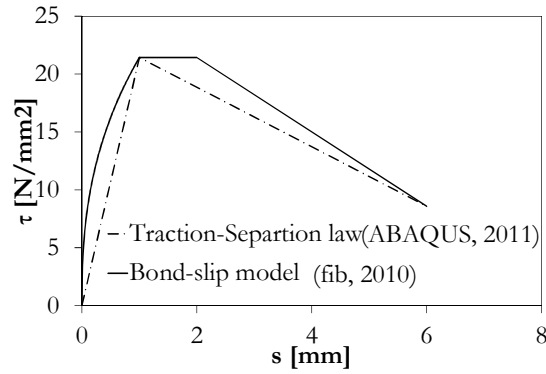


Fig. II.142: Comparison between the traction-separation law (Abaqus, 2011) and the bond model in (fib, 2010)

Table II.36: Parameters required for the traction-separation law to approximate the bond-slip behaviour of reinforcement-concrete interaction

	Test 1		Test 2		Test 3	
	Slab	Wall	Slab	Wall	Slab	Wall
$K_m$ [N/mm <sup>3</sup> ]	2815,00	2143,00	2710,00	2115,00	2787,00	2096,00
$K_{st}=K_{tt}$ [N/mm <sup>3</sup> ]	28,15	21,43	27,10	21,25	27,87	20,96
$\tau_{max}$ [N/mm <sup>2</sup> ]	16,89	21,43	16,26	21,15	16,72	20,96
$\delta_{\tau,max}^{st,tt}$ [mm]	0,60	1,00	0,60	1,00	0,60	1,00
$\delta_u^{st,tt}$ [mm]	1,00	6,00	1,00	6,00	1,00	6,00

### II.5.2.2 Validation and calibration of the finite element model for the composite beam to reinforced concrete wall joint

#### II.5.2.2.1 Validation through comparison of results in terms of moment-rotation curves ( $M-\Phi$ )

The accuracy of the finite element model developed for the composite beam to reinforced concrete wall joint was first performed for the global response of the joint. To this purpose, the computed joint bending moment to joint rotation curves ( $M_j-\Phi_j$ ) are compared with experimental results for Test 1, 2 and 3. For both, numerical and experimental approach, the joint rotation was determined using the beam deflection at the free edge and neglecting the wall rotation. Experimentally, the maximum wall rotation was approximately 1mrad. As Test 4 was a repetition of Test 3, and as the experimental results showed no significant variation between Tests 4, 5 and 6, for sake of brevity, these are not included. Furthermore, the results of the latter tests lead to the conclusion that the bottom part of the joint does not influence the joint response within the range of the geometric variations performed. After validated, the numerical model was used to extend these geometric variations and to further comment the influence of the bottom part of the joint.

In Fig. II.143 joint bending moment to joint rotation ( $M_j-\Phi_j$ ) relationship determined by the finite element model is superimposed upon the corresponding experimental result. It is

evident that the model approximates with good accuracy the measured results. Like in experimental tests, the numerical simulations were governed by the longitudinal reinforcement bars in the slab, limiting load and rotation capacity, and the effect of the geometric variations, percentage of reinforcement and position of the first shear connector, simulated accurately. Table II.37 presents ratios between numerical and experimental results for the joint maximum bending moment ( $M_{j,max}$ ), the joint initial rotational stiffness ( $S_{j,ini}$ ), and joint ultimate rotation ( $\Phi_{j,u}$ ), quantifying the quality of the approximation obtained. The initial joint rotational stiffness was calculated using the joint bending moment and joint rotation corresponding to 1/2 of the maximum joint bending moment capacity. The ultimate joint rotation was assumed in the experimental tests when the first bar fails, which is identified by the abrupt loss of resistance. In terms of maximum bending moment and initial rotational stiffness, the achieved approximation is excellent. In terms of joint ultimate rotation, the approximation is less accurate but good. However, it must be taken into account that this property is much sensible to different parameters as: i) material properties deviations; ii) initial imperfections. Remember that the latter were not introduced in the numerical simulations as they were unknown. In this particular case of the joint ultimate rotation, the unequal loading of the reinforcement bars leads to early failure of some bars before others. This is the most reliable explanation for the deviation obtained in Test 2. The geometric and the loading conditions were assumed perfect in the numerical models, and therefore, as the slab width was relatively small, all reinforcement bars were loaded equally up to failure. However, the observed deviations are acceptable and attest the failure criterion considered for the steel reinforcement bars.

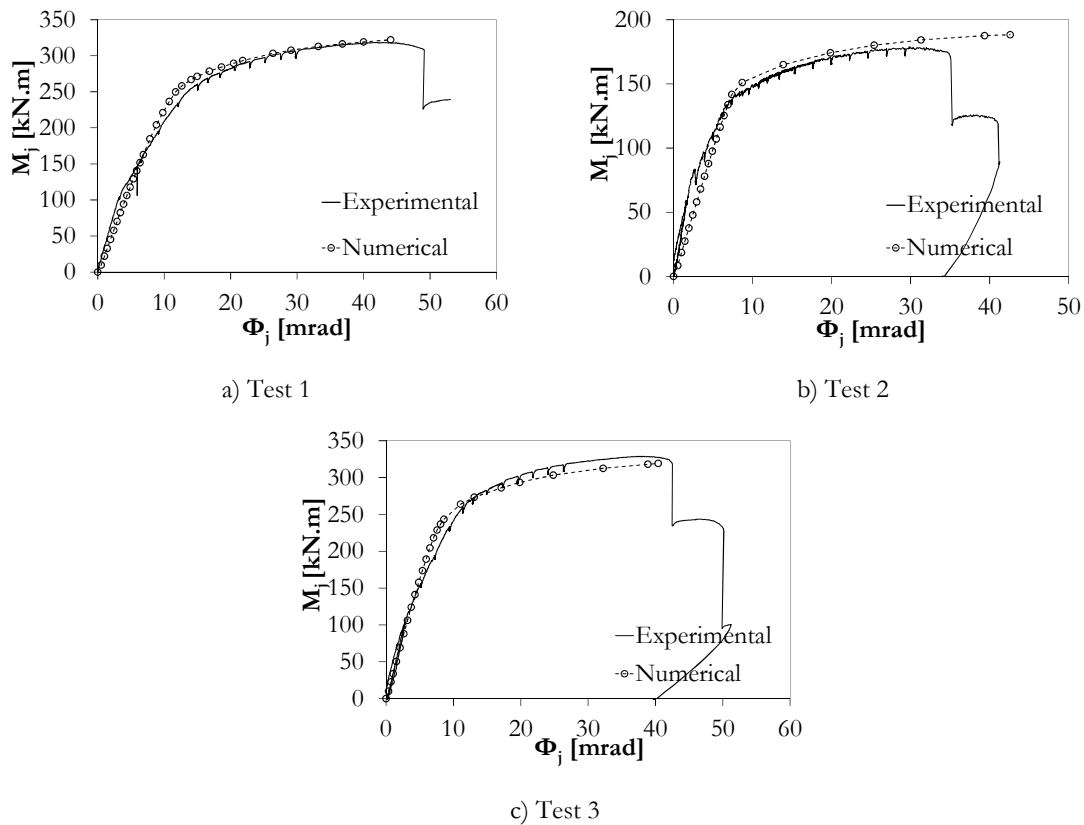


Fig. II.143: Computed and experimental joint bending moment to joint rotation curve

Table II.37: Summary of the approximation by means of ratio (numerical/experimental)

	$M_{j,max,Num} / M_{j,max,Test}$	$S_{j,ini,Num} / S_{j,ini,Test}$	$\Phi_{j,u,Num} / \Phi_{j,u,Test}$
Test 1	1,01	1,05	0,90
Test 2	1,05	0,80	1,21
Test 3	0,97	1,02	0,95

II.5.2.2.2 *Assessment of the quality of the numerical model for experimental parameters other than the  $M-\Phi$  curve*

The primary objective of the numerical model was to simulate the global response of the joint. However, the 3D finite element model developed should also be capable to reproduce local phenomena. Accordingly, the numerical model accuracy was further assessed by comparing the results with local measurements.

a) Separation between concrete wall and concrete slab

Displacement transducers were installed in the concrete slab top surface to measure experimentally the separation between the concrete slab and the concrete wall, at the joint interface. The same parameter was evaluated numerically. Fig. II.144 compares numerical predictions with experimental observations by means of joint bending moment ( $M_j$ ) to slab-wall separation ( $\Delta d_{wall-slab}$ ) curve. An excellent agreement is observed. The separation between concrete wall and concrete slab was governed by the longitudinal reinforcement deformation, and is the region with higher contribution for the joint rotation. The good approximation obtained strengthens the quality of the finite element model developed.

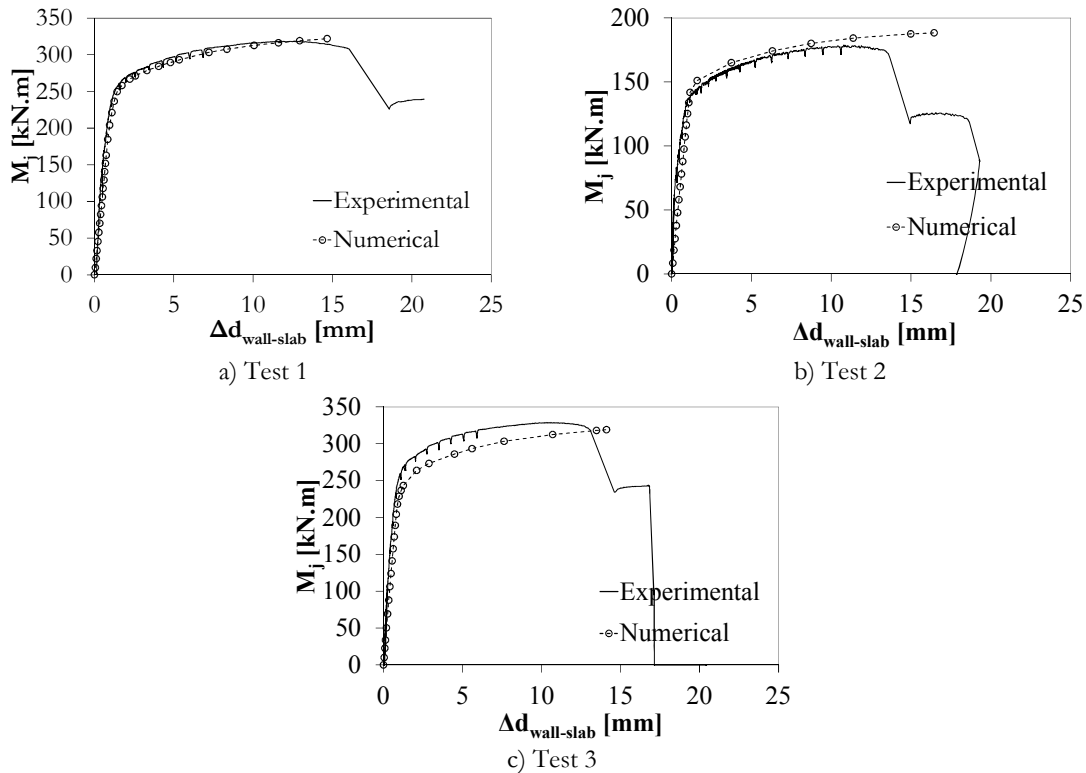


Fig. II.144: Comparison between predictions and experiments: wall-slab separation at joint interface

### b) Longitudinal reinforcement strains

In the experimental tests, strains were measured in the longitudinal steel reinforcement bars, at different sections along the reinforcement bars near the joint face and within the slab. The location of the installed strain gauges was similar in all test specimens and is identified in Fig. II.145. A comparison with the strains predicted by the numerical model is presented in Fig. II.146. Logarithmic strains in longitudinal direction (local direction), extracted from the numerical model, are used. The results compare strains close to the joint face and before the 1<sup>st</sup> shear connector of the composite beam. A good approximation is obtained. These results show that near the joint face, plastic deformation is observed, while in a distance farthest from the joint face, the reinforcement bars are in their elastic range.

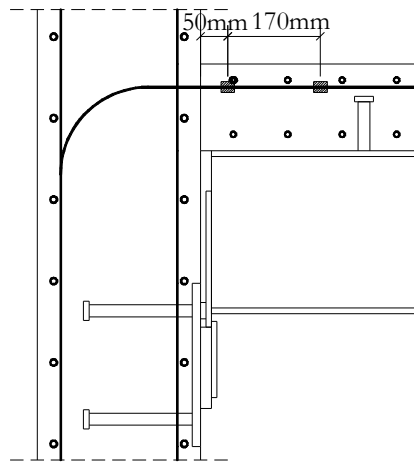


Fig. II.145: Location of the strain gauges in the longitudinal reinforcement bars

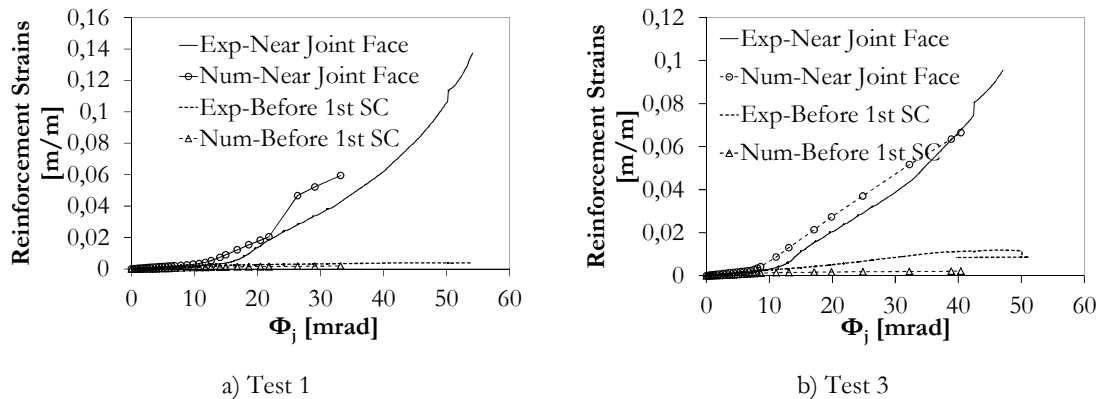


Fig. II.146: Comparison between predicted and experimental: strains measured in the longitudinal reinforcement bars

### c) Steel beam strains

In the steel beam, strains were measured in two transversal cross-sections, in the flanges and in the web, close the joint face, as illustrated in Fig. II.147. These measurements are compared with the numerical predictions, for the bottom flange (most stressed part of the beam) and for the web. Fig. II.148 shows a good approximation, in both cross-sections. The results in steel beam bottom flange close to the joint face, Test 3 (one of tests with higher percentage of longitudinal reinforcement), show that this part of the beam is close

to the nominal yield strength ( $427\text{N}/\text{mm}^2 \rightarrow \varepsilon_y \approx 0,002033$ ). This indicates that for higher percentage of reinforcement this part of the joint may limit the joint resistance.

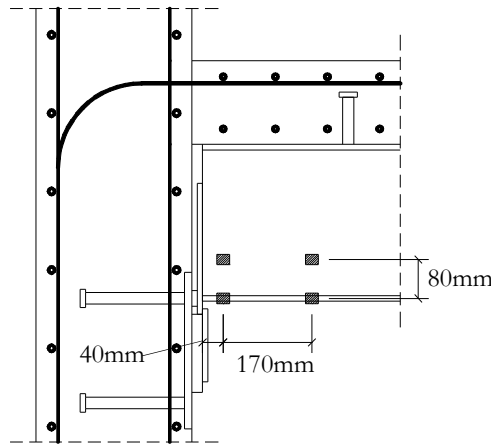


Fig. II.147: Location of the strain gauges in the steel beam

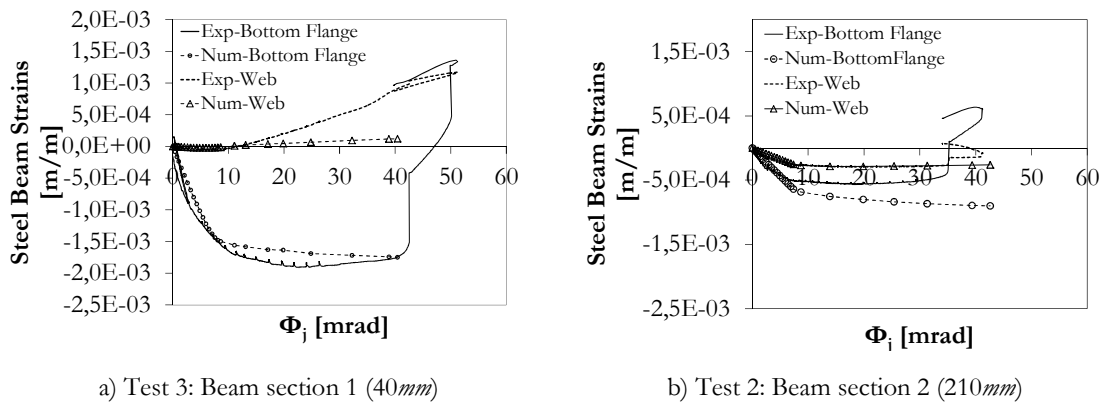


Fig. II.148: Comparison between predictions and experiments: Strains in the steel beam

d) Headed anchors strains

The experimental monitorization of the headed anchors, only considered the upper anchors. In one of these anchors, strain gauges were installed in the anchor shanks. Fig. II.149 compares the numerical predictions with experimental measurements. The result for specimen with higher percentage of longitudinal reinforcement, Test 3, is shown. The agreement is satisfactory. It can be observed that the top anchors are distant from their yield strength, as only 8,7% of their capacity is mobilized. The majority of the compression stresses are transferred to the concrete wall through the plate-concrete interface.

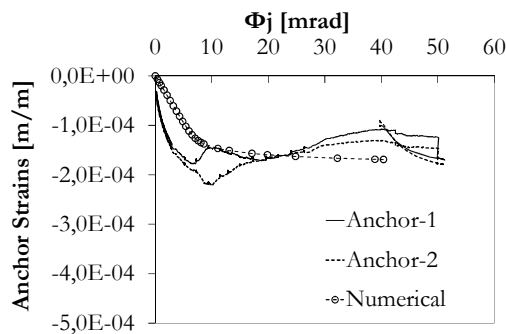


Fig. II.149: Comparison between predictions and experiments: Strains in the top headed anchors shank



e) Concrete cracks “opening” in the slab

The concrete cracks “opening” in the slab were estimated in the experimental tests by installing LVDT’s in the top surface of the slab, measuring the distance between two fixed points. Analogously, in the numerical model the relative position between these points was extracted and was compared with experimental observations. In Fig. II.150 is located the position of the crack measuring device used for comparison. Fig. II.151 shows the comparison of results for Test 1 and Test 3. The numerical predictions underestimate the experimental measurements however; the shape of the numerical and test curves results is similar. The deviations increase with the increase of the applied load. Despite these differences, the global response is not significantly affected because the separation between wall and slab which is “responsible” for the majority of the joint rotation capacity. For example, in Test 1, the ratio between crack opening and wall-slab separation, at ultimate load, is approximately 0,06. Consequently, the accuracy of the numerical model is not significantly affected, as it can reproduce accurately the wall-slab separation. Although the referred deviations, the numerical model crack pattern in the slab is consistent with the experimental observations, as illustrated in Fig. II.152 for Test 3.

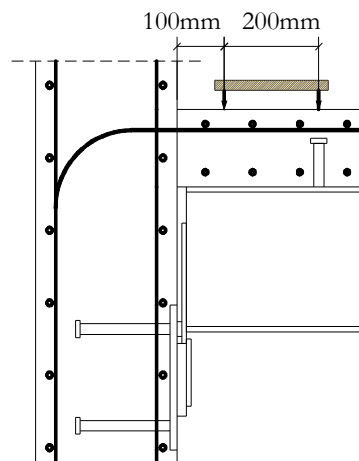


Fig. II.150: Location of the crack measuring device used for comparison between numerical simulations and experimental tests

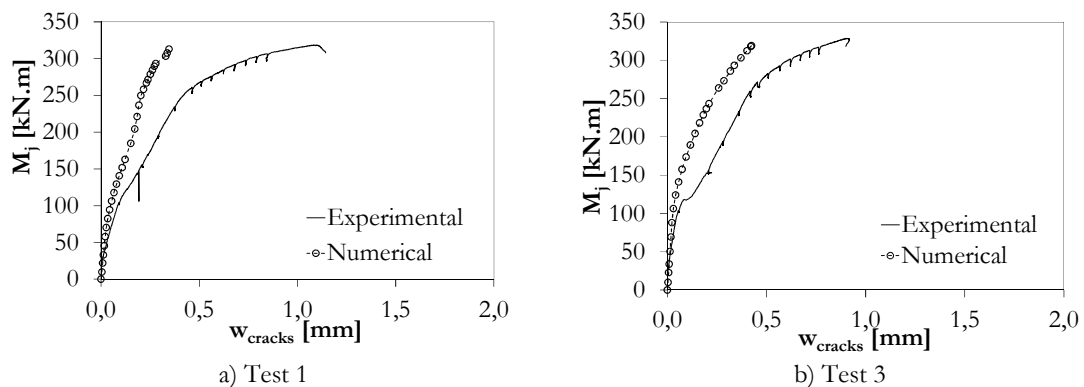
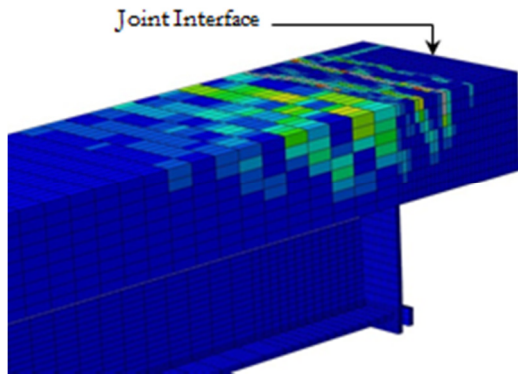
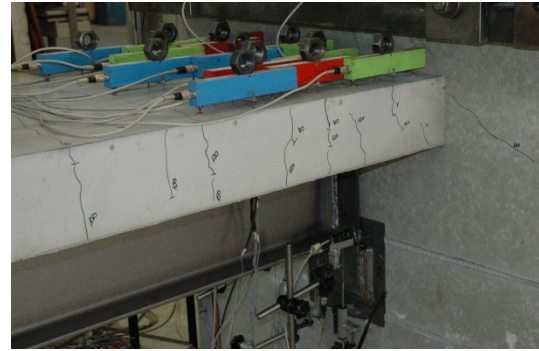


Fig. II.151: Comparison between predictions and experiments: Concrete cracks “opening” in the slab



a) Numerical

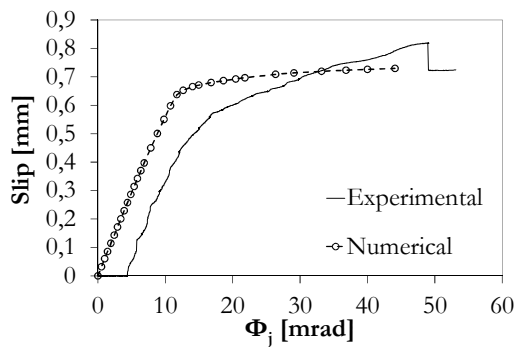


b) Experimental (Kuhlmann *et al.*, 2012)

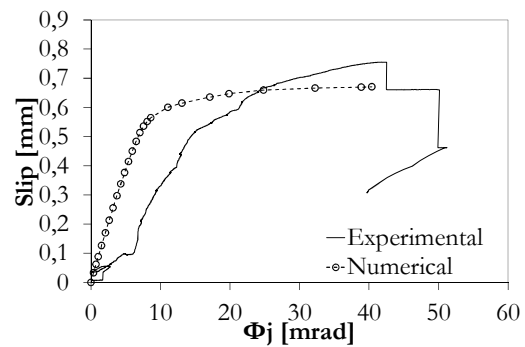
Fig. II.152: Comparison between predictions and experiments: crack pattern in the concrete slab

f) Slip between steel beam and concrete slab

The slip of the steel beam and the concrete slab was measured experimentally along the composite beam. Fig. II.153 compares predictions with measured values for the monitoring device closer to the first shear connector, where the values of slip were higher. Two specimens with different position of the first shear connector (Test 1 and Test 3) are used. In the beginning, it can be observed that on the experimental tests the slip is smaller than in the numerical simulations. Initially, there is some bond between the steel beam and the concrete slab which restricts the slip between these members. After this bond is overcome, slip occurs. Numerically, the bond was not considered therefore the initially deviations. Similar effect was observed in the calibration example using ABAQUS (Abaqus, 2011) or using VULCAN (Huang *et al.*, 1999). After this initial stage, there is a satisfactory approximation, where the final slip presented an average deviation of approximately 10%.



a) Test 1



b) Test 3

Fig. II.153: Comparison between predictions and experiments: slip between steel beam and concrete slab

### II.5.2.3 Further analysis of the joint through exploitation of the finite element model

#### II.5.2.3.1 Participation of joint components

The joint components have been identified in Table II.1 and Fig. II.7. Accordingly, Table II.38 presents the list of the considered components and quantifies the percentage of resistance mobilized at the ultimate load capacity of the tested joints. The resistance of the components was obtained according to the existing approaches, numerical and/or analytical. The evaluation of the load acting on the compression components (bottom part of the joint), was approximated by integration of the normal stresses in the contact plate ( $\sigma_{\phi,n}$  - stresses in the contact plate in direction of the thickness), as expressed in (II.87).

Table II.38: List of components participating in the joint resistance and percentage of resistance mobilized at ultimate load capacity of the joint

Joint component	Component resistance mobilized			Comment
	Test 1	Test 2	Test 3	
Longitudinal reinforcement in tension	100%	100%	100%	This is the governing component; its capacity was therefore fully used up to the ultimate strength ( $f_u$ ) in all specimens.
Slip of composite beam	53%	54%	53%	The resistance is proportional to the number of shear connectors (Aribert, 1995) and calculated according to (EN 1994-1-1, 2004).
Beam web and flange in compression	98%	56%	98%	Component resistance was obtained with the benchmark example presented in §II.5.2.1.3, limiting the stresses to the yield strength and assuming a lever arm equal to beam height subtracted of the flange thickness.
Steel contact plate in compression	32%	18%	32%	Component resistance was determined limiting the steel strength to its yield capacity, as in (EN 1994-1-1, 2004).
Anchor plate in compression	39%	22%	39%	Simplified approach: the component resistance is determined using the T-stub in compression approach (EN 1993-1-8, 2005).
Joint link	68%	50%	68%	Analytical approach proposed in §II.4.3.

$$F_c = \int_{A_{\phi}} \sigma_{\phi,n} \quad (\text{II.87})$$

Where:  $F_c$  is the compression load applied to the anchor plate through the contact plate;  $A_{\phi}$  is the cross-section area of the contact plate in the interface plane with the beam end-

plate;  $\sigma_{cp,n}$  are the normal stresses in contact plate in the direction of plate thickness (direction of the compression force).

As the governing component, the resistance of the longitudinal reinforcement bars is fully used. Nevertheless, it can be observed that the steel beam bottom flange, for the tests with higher percentage of reinforcement, is close to its limit yield capacity, approximately 95%. This is in line with strains measured experimentally (Fig. II.148-a), where the registered strain was approximately 0,002 ( $\epsilon_y \approx 0,002033$ ). Consequently, for higher percentages of reinforcement, the plastic deformations may play an important role in the joint behaviour. Concerning the other joint components, the applied load is significantly lower than the corresponding calculated capacity.

#### II.5.2.3.2 Load on shear connectors of the composite beam and position of the 1st shear connector

Based on the numerical calibrations presented in §II.5.2.1.3, the behaviour of the shear connectors was considered linear elastic. The shear connection resistance and stiffness were determined as prescribed in (EN 1994-1-1, 2004). For the three test specimens, the steel connector governed the resistance of the shear connection. The adopted properties in the numerical model were the following;  $P_{Rk} = 174\text{kN}$ ;  $k_{sc} = 100\text{kN/mm}$ . The load on the shear anchors predicted by the numerical simulations, for three load levels, is shown in Fig. II.154 using Test 1. Except for the outer shear connectors, the shear load is distributed uniformly amongst the shear connectors. At ultimate joint load capacity, the shear connector closest to the joint carries approximately 32% more load than the others. However, it is clear that all shear connectors participate on the composite action from the beginning contrarily to the assumption in (Anderson and Najafi, 1994) where, under increasing load, the first shear connector takes the entire load until it becomes plastic; additional load is then resisted by the next shear connector deforming elastically, and so forth. This is also justified by the fact that in the tests the shear load is constant along the beam.

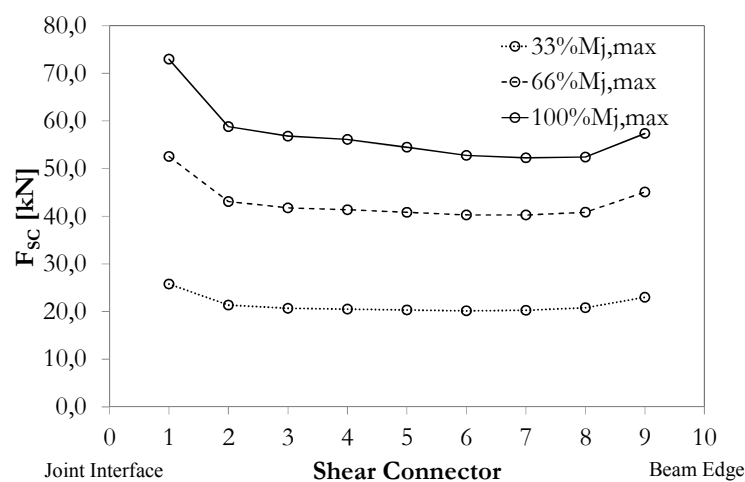


Fig. II.154: Distribution of steel beam-concrete slab interaction load amongst shear connectors (Test 1)

According to (Schäffer, 2005), the position of shear connector adjacent to the joint, affects the crack pattern, increasing the number of cracks with the distance of this first shear

connector. Consequently, the reinforcement reaches higher stresses over a higher length and as result higher deformation is obtained. Thus, higher rotation capacity is obtained with higher distances between first shear connector and the joint. In the joint under study, a “preliminary” crack exists in the slab-wall interface. As observed in Fig. II.144, the majority of the deformation occurs in this region of the joint; therefore, less significance is attained/observed for the cracks. Though, the effect of the position of the first shear connector is still noticeable, from Test 3 to Test 1 there is i) a decrease of  $\approx 27\%$  in initial stiffness; ii) a increase of  $\approx 10\%$  in deformation capacity.

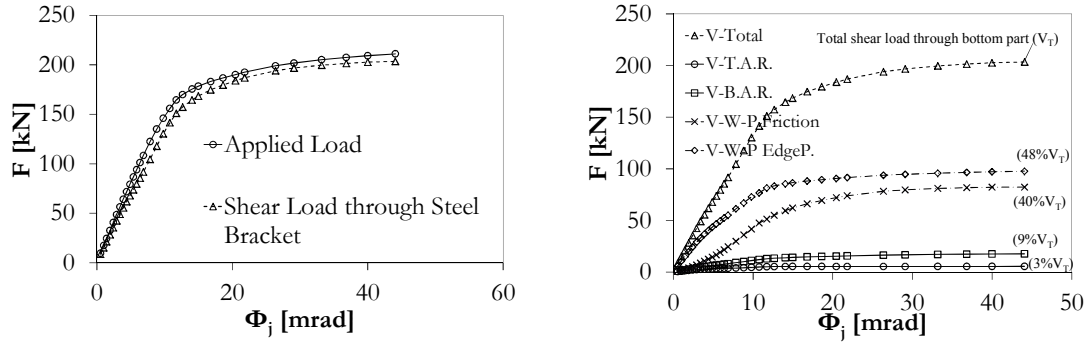
### II.5.2.3.3 Shear load path

According to the joint erection process, as the slab and wall are concreted in separate stages, the shear load is assumed to be completely transferred through the bottom part of the joint. The bond developed between the concrete members is rapidly exceeded, and is neglected. In addition, the shear stiffness of the longitudinal reinforcement bars, which are highly activated by the tension component of the load, is insignificant in comparison to the shear stiffness of the bottom zone of the joint. Thus, the shear load transfer is assumed to be fully accomplished in the latter zone. In order to verify this assumption, the shear load transferred by the anchor plate was evaluated through integration of the tangential stresses on the steel bracket in elements in contact with the anchor plate, as expressed in (II.88).

$$V_{bottom} = \int_{A_{sb-ap}} \tau_{sb} \quad (II.88)$$

Where:  $\tau_{sb}$  is the tangential stresses in the steel-bracket;  $A_{sb-ap}$  is the cross-section area of the steel bracket in the interface with anchor plate.

Fig. II.155-a) compares the calculated load with the total shear load applied to the joint. The results fully attest the described assumption. Also interesting is to know how this shear load is then transferred to the wall through the shear components. The following components are identified: i) bearing of the anchors shanks with concrete, top (V-T.A.R.) and bottom (V-B.A.R.) anchor row; ii) bearing of the anchor plate with concrete at the bottom edge of the plate (V-W-P. Edge P.); iii) friction between anchor plate and concrete (V-W-P. Friction). Fig. II.155-b) depicts how the shear load is distributed amongst these components. The bearing between anchor plate and concrete at the bottom is the main loaded component, 48%, followed by the friction component, 40%. In what regards to the top and bottom anchor rows, it can be observed that the carried load is very low, only 3% and 9%, respectively. From these results it can be concluded that there is still a considerable reserve of shear resistance in this joint.



a) Shear load on the anchor plate connection      b) Shear load distribution amongst components

Fig. II.155: Evaluation of the shear load transferred by the anchor plate in comparison (Test 1)

## II.5.2.4 Sensitivity of the joint behaviour to some parametric variations

### II.5.2.4.1 Parametric study

The parametric variations were focused on the following three issues: i) the steel class of the longitudinal reinforcement bars (influencing ductility); ii) the anchor plate and steel bracket issues (influencing the flexibility of the anchor plate and the eccentricity of the shear load acting on the anchor plate); iii) a variant of the joint configuration considering two rows of longitudinal reinforcement bars to connect slab to wall (improvement of joint and distribution of tension load). Table II.39 lists the parameters subject of study and their range of variation. Test 3 specimen was used as reference. When studying the influence of the reinforcement class, the stress-strain curve represented in Fig. II.156 was used for the parametric study, instead of the material curve presented in Fig. II.141. Also, several  $f_u/f_y$  ratios were considered. The complete material stress-strain curve requires the definition of the ultimate strain, a key parameter to be analysed. In this way, for each ratio  $f_u/f_y$ , the ultimate strain is obtained using a linear interpolation of the limits of ultimate strain provided in (EN 1992-1-1, 2004) for the classification of the steel reinforcement ductility class. Only steel grade S500 was used in the study. The considered values are given in Table II.40. In what concerns the geometric variations, some local modifications were introduced in the model geometry, in order to maintain the original proportions. In the particular case of the joint with two rows of longitudinal reinforcement bars, 10mm diameter steel bars were considered (Fig. II.157).

Table II.39: List of parameters object of study and corresponding range of variation

Parameter	Range of variation	Model ID	Number of models
Steel class of the longitudinal reinforcement bar	The reinforcement class was varied from A to C, where $f_u/f_y$ and $\varepsilon_u$ are defined according to (EN 1992-1-1, 2004)	Reinf_XY where X is A, B or C and Y is “1, ... n (starting for each class)	10
Steel bracket thickness	The thickness of the steel bracket varied from 20mm to 50mm with increments of 5mm	StB_X where X is the thickness of the steel console	7
Anchor plate thickness	The thickness of the anchor plate varies from 5mm to 15mm with increments of 2.5mm and from 15mm to 40mm with increments of 5mm	AP_X where X is the thickness of the anchor plate	10
Joint configuration variant	Two rows of longitudinal reinforcement were used to connect the concrete slab to the concrete wall	Joint-2Reb	1
Total			28

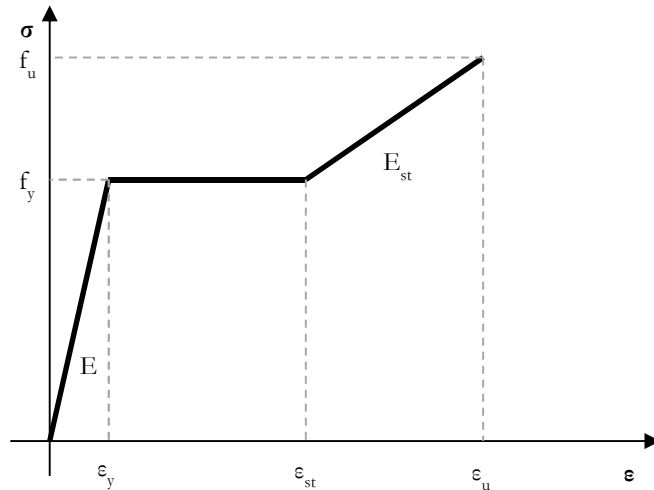


Fig. II.156: Parametric stress-strain curve to model the steel constitutive behaviour

Table II.40: Range of variation of steel class for longitudinal reinforcement bars ( $f_u/f_y$ ) and  $\epsilon_u$

Model ID	$f_u/f_y$	$\epsilon_u$ [%]	Model ID	$f_u/f_y$	$\epsilon_u$ [%]
<b>Reinf_A</b>	<b>1.05</b>	<b>2.5</b>	<b>Reinf_C</b>	<b>1.15</b>	<b>7.5</b>
Reinf_A1	1.06	3.33	Reinf_C1	1.20	9.28
<b>Reinf_B</b>	<b>1.08</b>	<b>5.0</b>	Reinf_C2	1.25	11.07
Reinf_B1	1.10	5.71	Reinf_C3	1.30	12.85
Reinf_B2	1.12	6.42	Reinf_C4	1.35	14.64

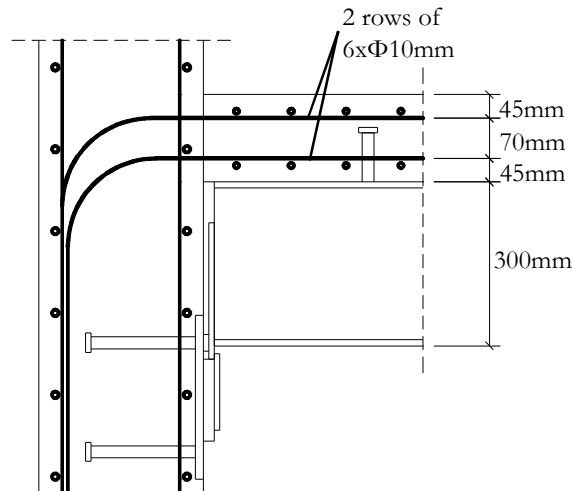


Fig. II.157: Joint configuration with two rows of longitudinal reinforcement bars



#### II.5.2.4.2 Discussion and analysis on the results

##### II.5.2.4.2.1 Steel class of the longitudinal reinforcement bars

The longitudinal steel reinforcement bars, as the governing component of the studied joint configuration, strongly influences the joint behaviour. Consequently, the variation of the steel class directly influences the joint response. The performed variation allows detecting the gains on the joint rotation capacity with the increase of the ultimate strain of steel bars. The evolution of the ultimate joint rotation ( $\Phi_{j,u}$ ) with the variation of the ultimate strain ( $\epsilon_u$ ) is shown in Fig. II.158. The linear relation obtained shows a direct and strong correlation between these two variables. The boundaries for the steel class, according to the ultimate strain, are included in the same figure. It can be observed that depending on the required joint rotation, the steel reinforcement class can be selected. Thus:

- Up to 25 mrad – class A
- Up to 40 mrad – class B
- Above 40 mrad – class C

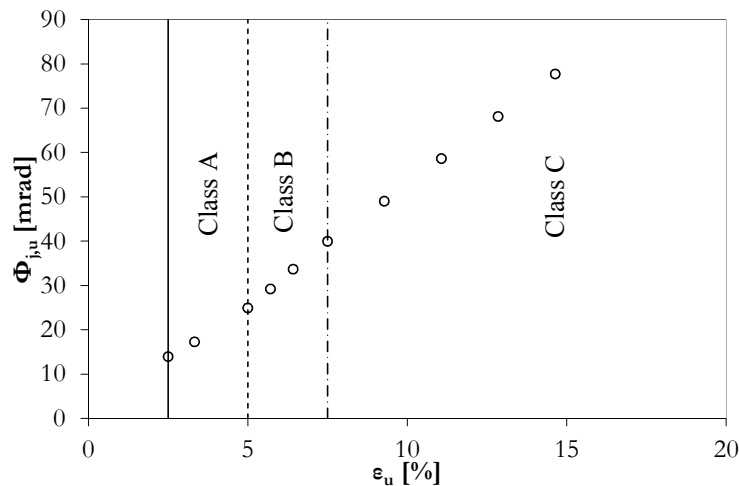


Fig. II.158: Influence of the steel ductility properties on ultimate joint rotation

##### II.5.2.4.2.2 Thickness of the steel bracket

The thickness of the steel bracket defines the eccentricity at which the shear load is transferred to the anchor plate. In all simulations, the steel longitudinal reinforcement remained the governing component of the joint. With the increase of the steel bracket thickness is observed: i) an increase of the bending moment capacity of the joint; ii) an increase of the initial joint rotational stiffness; iii) a decrease of the joint rotation at maximum bending moment. Though, as shown in Fig. II.159, the variations are negligible below 5%.

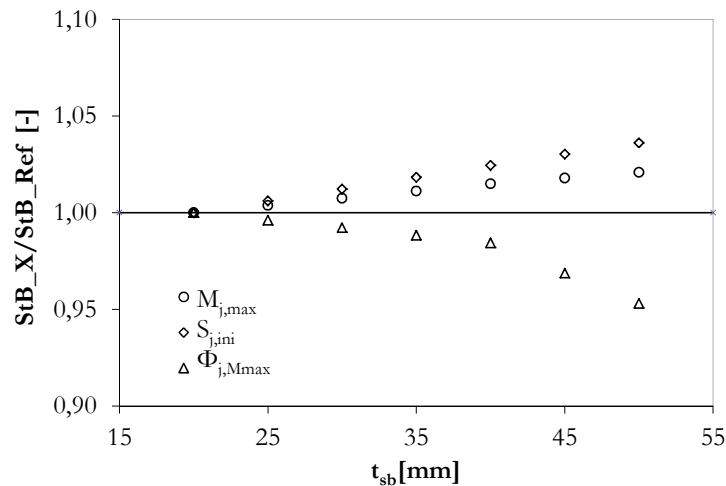
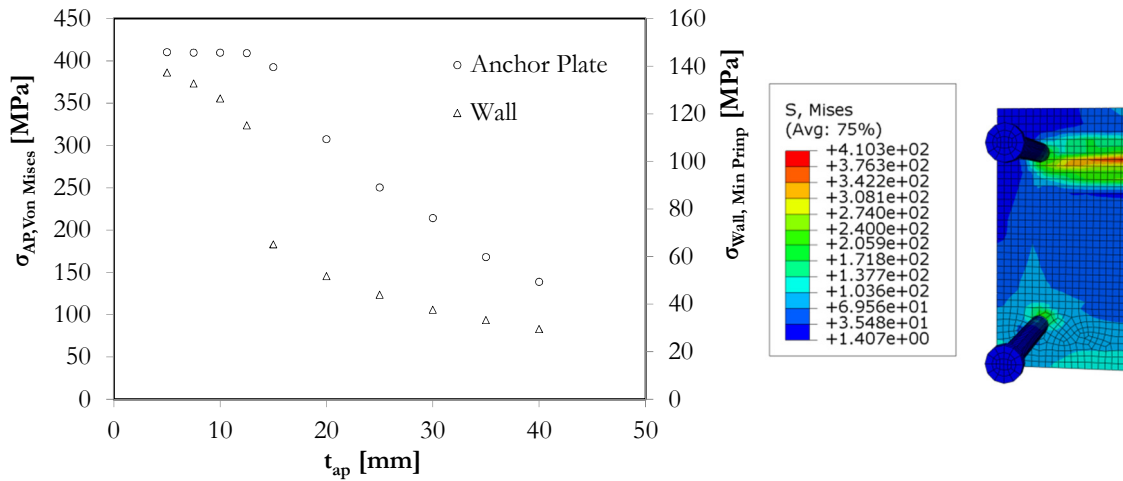


Fig. II.159: Evaluation of the influence of the steel bracket thickness on the joint response: Maximum joint bending moment; joint initial rotational stiffness; and joint rotation at maximum joint bending moment

#### II.5.2.4.2.3 Thickness of the anchor plate

For the range of values considered, it was observed that the resistance of the joint was not affected by the anchor plate thickness. The local effect of the variation of the anchor plate thickness is shown in Fig. II.160-a), where the maximum stresses on the most stressed elements of the anchor plate are presented. The principal compression stresses on the concrete wall in contact with the anchor plate are also included in Fig. II.160-a). The location of these elements is at the middle-line of the anchor plate width and at the level of the upper anchor, as illustrated in Fig. II.160-b). It can be noticed that for thicknesses below  $12,5\text{mm}$ , the anchor plate starts to yield. However, the ultimate strength of the plate is not reached and the longitudinal reinforcement still governs the joint resistance. The maximum stress is similar for all models considering a thickness equal or smaller than  $12,5\text{mm}$ , and any differences consist only in the spread of plasticity. This is higher in the model with  $5\text{mm}$  anchor plate thickness and decreases with the increase of the plate thickness. The maximum stresses in concrete increase exponentially with the decrease of the anchor plate thickness. For the lowest thickness ( $5\text{mm}$ ) the stresses exceeded the uniaxial compressive strength ( $70,3\text{MPa}$ ) of the concrete used in the wall. These values are attained because of the triaxial state of the concrete. Because this most stressed region has large edge distances, the confinement effect allows achieving such strength.



a) von Mises stresses on anchor plate most stressed element and Principal Stresses (Compression) on concrete wall in contact with plate      b) location of the most stressed zone

Fig. II.160: Local effect of the anchor plate thickness

#### II.5.2.4.2.4 Joint configuration variant: two rows of longitudinal reinforcement bars

In this variant of the joint configuration, the material properties of the Test 2 were used. Fig. II.161 compares the joint response of this new configuration with numerical simulations of Test 2 and 3 using the relative joint bending moment to joint rotation curves. The joint bending moment of each model was normalized with the maximum joint bending moment of the three models (Test 3). In terms of load capacity, this variant of the joint configuration provides an increase of resistance of 25% in comparison to configuration of Test 2. However, the increase of the percentage of longitudinal reinforcement is of approximately 39%. This is justified by the fact that the bottom row is not fully used when the failure on the upper anchors occurs and because of the lower lever arm. In comparison to the configuration of Test 3, the resistance was lower as the percentage of reinforcement was also lower. For the joint initial rotational stiffness, it can be observed that this new configuration approximates the joint rotational stiffness of Test 2. As lower diameter of reinforcement bars were used in the new configuration, this indicates that the use of two rows increases the joint initial rotational stiffness. In what regards to joint ultimate rotation, an increase was observed in comparison to the previous models of approximately 15%.

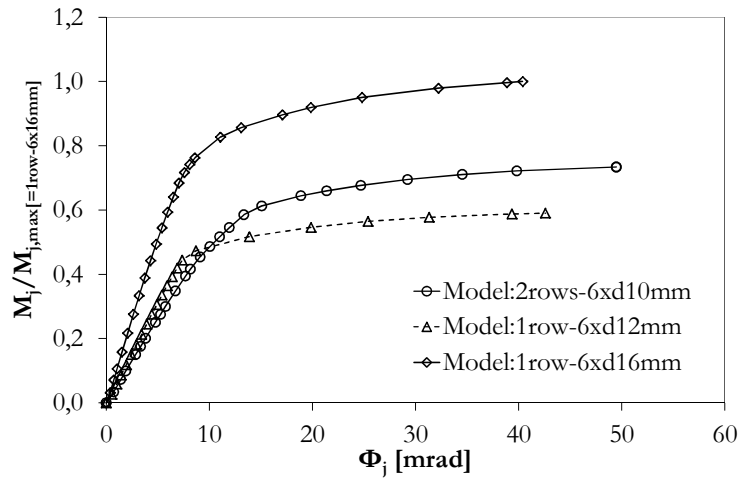
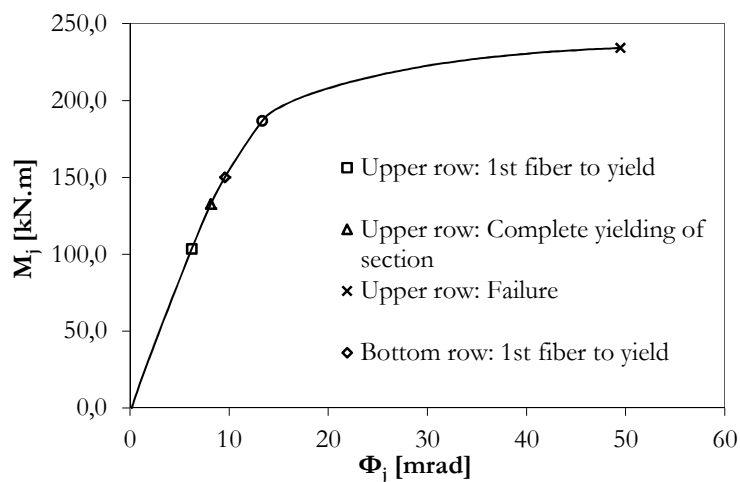
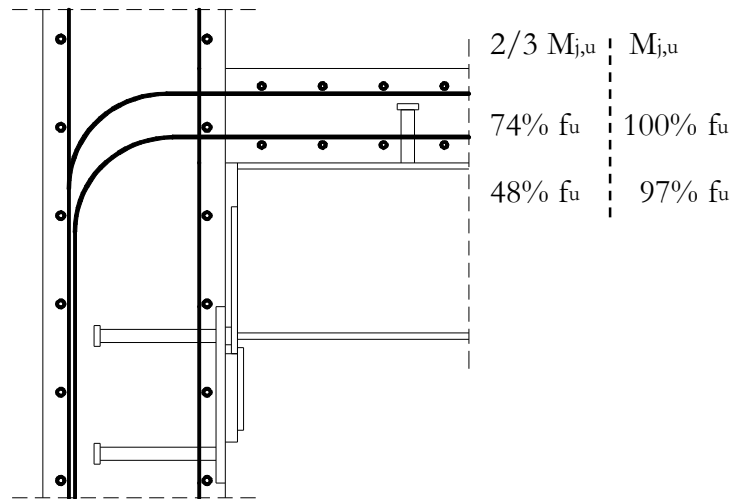


Fig. II.161: Relative joint bending moment to joint rotation curve comparing models with 1 and 2 row of longitudinal reinforcement bars

In order to understand the behaviour of this new configuration in what concerns the load on the two rows of reinforcement bars, Fig. II.162-a) presents the joint bending moment to joint rotation curve identifying the following load steps: i) 1<sup>st</sup> fibers to yield in the upper and lower rows; ii) complete yielding of the reinforcement bars section (upper and lower); and iii) failure (only attained in the upper rebars). It can be observed that the bottom reinforcement bars achieve the complete yielding of the cross-section. After this stage, the increase of resistance is highly reduced in comparison to the increase of rotation. Fig. II.162-b) shows the percentage of ultimate strength activated in each row for two load steps: i)  $2/3$  of  $M_{j,u}$ ; ii)  $M_{j,u}$ . The first load step approximates the limit of the elastic range and shows that the lower row participates with less 35% of strength than the upper row. At ultimate load capacity, the difference was reduced, as the bottom row can achieve 97% of its ultimate strength. This demonstrates that using the considered steel class (Class C), a plastic distribution of load can be accomplished in such joint configuration.



a) Joint bending moment to joint rotation curve



b) Percentage of ultimate strength activated in the two rows of reinforcement bars

Fig. II.162: Analysis of the activation of the longitudinal reinforcement bars

## II.5.3 Analytical component base model

### II.5.3.1 Joint model

In chapter II.1, the joint components activated in the composite beam to reinforced concrete wall joint, subjected to hogging bending moment, have been identified (see Table II.1 and Fig. II.7-a). Accordingly, a representative spring and rigid link model was idealized and illustrated in Fig. II.163-a). Three groups of springs are separated by two vertical rigid bars. The rigid bars avoid the interplay between tension and compression components, simplifying the joint assembly. Another simplification was introduced by considering a single horizontal spring to represent the joint link. In what concerns the tension springs, it was assumed that slip and the longitudinal reinforcement are at the same level although slip is observed at the steel beam – concrete slab interface. In Table II.41 are listed the joint components considered in this model. As deeply discussed in II.3.1, components 7, 8, 9 and 10 should not control the behaviour of the joint as their activation only results from the out-of-plane deformation of the bottom and top edges of the anchor plate in compression. Though, these joint components affect the response of component 6 and are therefore considered in the response of the latter, as proposed in II.3.1.3.2. This simplified model of the anchor plate in compression at the bottom part of the joint incorporates also component 5. Thus, a simpler joint model was obtained as illustrated in Fig. II.163-b). This considers an equivalent translational spring representing the contribution of the anchor plate to the joint response. The joint components characterization is discussed in the next section. After, the accuracy of the proposed joint model is evaluated against the experimental and numerical results.

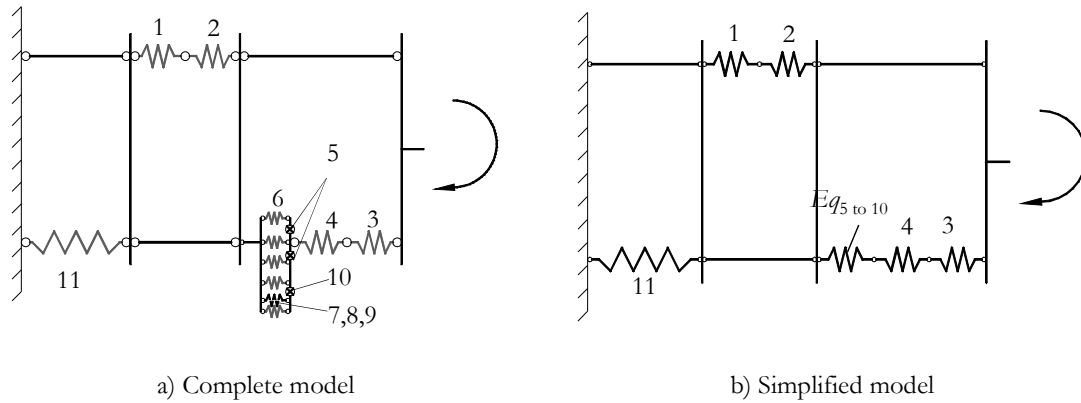


Fig. II.163: Joint component model for the composite beam to reinforced concrete wall joint

Table II.41: List of active components in the composite beam to reinforced concrete wall joint subject to hogging bending moment

Component ID	Basic joint component	Type/Zone
1	Longitudinal reinforcement bar in the slab	Tension
2	Slip of composite beam	Tension
3	Beam web and flange	Compression
4	Steel contact plate	Compression
5	Anchor plate in bending under compression	Bending/Compression
6	Concrete in compression	Compression
7	Headed anchor in tension	Tension
8	Concrete cone	Tension
9	Pull-out of anchor	Tension
10	Anchor plate in bending under tension	Bending/Tension
11	Joint link	Tension and Compression

### II.5.3.2 Characterization of the activated components

#### II.5.3.2.1 Longitudinal steel reinforcement in the slab

In the joint configuration under analysis, the longitudinal reinforcement in tension is the single component able to transfer tension forces to the supporting member. The experimental tests performed within the *InFaSo* research project (Kuhlmann *et al.*, 2012) demonstrated that this component governed the behaviour of the joint. Thus, the accuracy of analytical joint model to predict the joint response will much depend on the level of accuracy on the model of this component.

The application of the component method to composite joints assumes each layer of longitudinal reinforcement bars as additional bolt rows. According to (EN 1994-1-1, 2004), the longitudinal steel reinforcement bar may be stressed to its design yield strength. It is assumed that all the reinforcement within the effective width of the concrete flange is used to transfer forces. The models to characterize this component have been presented in §II.2.2.1 and are in the present chapter used. Table II.42 summarizes the analytical equations required to determine the force-deformation response of the component. The code approach is a conservative approach, as it limits the resistance to the yield strength of the steel reinforcement bars. In addition, it is absent in what concerns the evaluation of the ultimate deformation capacity. Though, if reinforcement bars class C are used, it may be assumed sufficient deformation capacity to redistribute the load in the case of more than one layer (Demonceau, 2008). Still regarding the deformation, both models require the definition of the elongation length. In the case of the code approach, this value is constant as it only considers the elastic range. Thus, analogously to the code provisions for single-sided composite joints, the dimension  $b$  involved in determination of the components stiffness coefficient ( $k_{sp}$ ) was assumed, as represented in Fig. II.164. Without sufficient experimental data to derive another value, the coefficient 3,6 is kept. In what regards to the model given in (ECCS, 1999), the elongation length to consider depends on the range of the deformation and on the percentage of reinforcement, as given in the Table II.42.

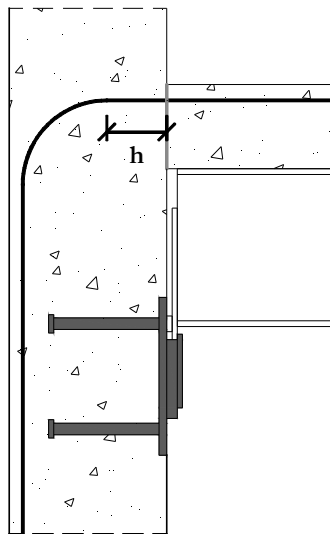


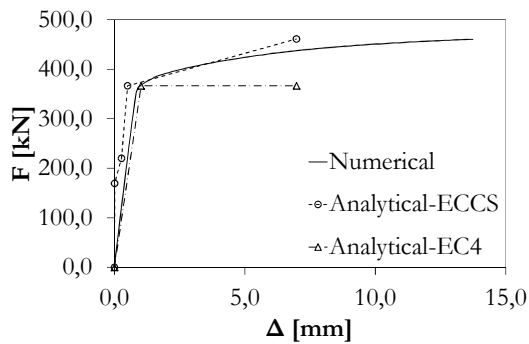
Fig. II.164: Definition of dimension  $b$  for the elongation length of the joint component longitudinal steel reinforcement bar in the slab

In order to evaluate the performance of the described models, the response of the longitudinal steel reinforcement bar in the slab determined with the referred models was compared with the numerical calculations described in §II.5.2. Fig. II.165 compares the force-deformation curves. Below the load corresponding to the yield strength of the reinforcement, the model according to (ECCS, 1999) is stiffer than the numerical model. This may be justified by the fact that in this model was ignored the initial “crack” assumed in the numerical model between slab and wall. In this range, a good approximation is obtained with the code model. Above this load, the approximation between the (ECCS,

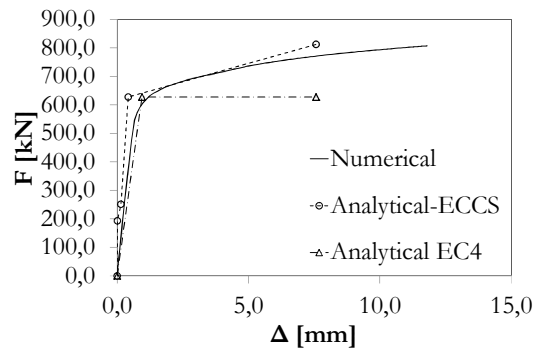
1999) model and the numerical model is satisfactory however, the first underestimates the ultimate deformation. The (EN 1994-1-1, 2004) model does not consider resistance of the reinforcement bars above its yield strength therefore the plateau represented.

Table II.42: Summary of the approach to characterize the longitudinal steel reinforcement bar in the slab component

Reference	Property	Expressions
(EN 1994-1-1, 2004)	Resistance	$F_{sry} = f_y A_{sr}$
	Stiffness coefficient	$k_{sr} = \frac{A_{sr}}{3,6b}$
	Deformation capacity	Not given
(ECCS, 1999)	Resistance	$F_{sr} = \sigma_{sr} A_{sr}$ With $\sigma_{sr1} = \frac{f_{ctm} k_{sc}}{\rho} \left[ 1 + \rho \frac{E_s}{E_c} \right]$ $\sigma_{srn} = 1,3 \sigma_{sr1}$
	Deformation	$\Delta \leq \Delta_{sry}: \quad \Delta = \varepsilon (b + L_t)$ $\varepsilon_{sr1} = \frac{\sigma_{sr1}}{E_s} \cdot \Delta \varepsilon_{sr}$ $\Delta \varepsilon_{sr} = \frac{f_{ctm} k_{sc}}{E_s \rho}$ $\rho < 0,8\%: \quad \Delta_{srn} = 2L_t \varepsilon_{srnu}$ $\rho \geq 0,8\% \text{ and } a < L_t: \quad \Delta_{srn} = (b + L_t) \varepsilon_{srnu}$ $\rho \geq 0,8\% \text{ and } a > L_t: \quad \Delta_{srn} = (b + L_t) \varepsilon_{srnu} + (a - L_t) \varepsilon_{srny}$



a) Test 2



b) Test 3

Fig. II.165: Comparison of force-deformation curves between numerical and analytical models to reproduce the longitudinal steel reinforcement bar component behaviour



### II.5.3.2.2 Slip of the composite beam

The slip of composite beam is not directly related to the resistance of the joint though; the level of interaction between concrete slab and steel beam defines the maximum load acting on the longitudinal reinforcement bar. In (EN 1994-1-1, 2004), the slip of composite beam component is not evaluated in terms of resistance. The level of interaction is considered on resistance of the composite beam. In what concerns to the deformation of the joint, (Anderson and Najafi, 1994) demonstrated that the shear connection flexibility could not be excluded from the connection stiffness derivation. Non-negligible influence of the slip between concrete slab and the steel beam on the joint rotation was also observed numerically in (Aribert, 1995). In the (EN 1994-1-1, 2004), the influence of the slip of composite beam is taken into account. The stiffness coefficient of the longitudinal reinforcement ( $k_{sr}$ ) in Table II.42 should be affected by a reduction factor ( $k_{slip}$ ) determined as follows.

$$k_{slip} = \frac{1}{1 + \frac{E_s k_{sr}}{K_{SC}}} \quad (\text{II.89})$$

With

$$K_{SC} = \frac{N k_{sc}}{v \cdot \left( \frac{v-1}{1+\xi} \right) \frac{b_s}{d_s}} \quad (\text{II.90})$$

$$v = \sqrt{\frac{(1+\xi) N k_{sc} l d_s^2}{E_a I_a}} \quad (\text{II.91})$$

$$\xi = \frac{E_a I_a}{d_s^2 E_{sr} A_{sr}} \quad (\text{II.92})$$

Where:  $b_s$  is the distance between the longitudinal reinforcing bars and the centre of compression of the joint, that may be assumed as the midpoint of the compression flange of the steel beam;  $d_s$  is the distance between the longitudinal reinforcing bars and the centroid of the steel beam section;  $I_a$  is the second moment area of the steel beam section;  $l$  is the length of the beam under hogging bending moment adjacent to the joint, in the case of the tested specimens is equal to the beam's length;  $N$  is the number of shear connectors distributed over the length  $l$ ;  $k_{sc}$  is the stiffness of one shear connector.

In a joint model, as depicted in Fig. II.163, where the slip is considered as a component, the force-deformation behaviour of the slip component is required. According to (Aribert, 1995), the slip resistance may be obtained from the level of interaction as expressed in (II.93). Note that the shear connectors were assumed to be ductile allowing redistribution of the slab-beam interaction load.

$$\begin{cases} N/N_f \geq 1: F_{slip} = F_{sr} \\ N/N_f < 1: F_{slip} = NP_{RK} \end{cases} \quad (II.93)$$

Where:  $N_f$  represents the number of shear connectors required to have full interaction;  $N$  is the real number of shear connectors; and  $P_{RK}$  is characteristic resistance of the shear connectors that can be determined according to (EN 1994-1-1, 2004) as follows. Note that the safety factors are not included.

$$P_{RK} = \text{Min} \left( 0,8f_u \pi d^2 / 4; 0,29ad^2 \sqrt{f_{ck} E_{cm}} \right) \quad (II.94)$$

With

$$\begin{cases} 3 \leq \frac{h_{SC}}{d} \leq 4: & a = 0,2 \left( \frac{h_{SC}}{d} + 1 \right) \\ \frac{h_{SC}}{d} > 4: & a = 1 \end{cases} \quad (II.95)$$

Where:  $f_u$  is the ultimate strength of the steel shear stud;  $d$  is the diameter of the shear stud;  $f_{ck}$  is the characteristic concrete cylinder resistance;  $E_{cm}$  is the secant modulus of elasticity of the concrete;  $h_{sc}$  is the height of the shear connector including the head.

In what concerns the deformation of the component one of the following cases are proposed:

- i) Shear load distribution is uniform along the beam: in this case, an equal distribution of the load amongst the shear studs is expected. This is the case observed in the numerical models presented in §II.5.2.3. Accordingly, as suggested by (Ahmed and Nethercot, 1997) the stiffness of the component is obtained in function of the number of shear studs and of the stiffness of single row of shear studs, and may be obtained as follows. The deformation capacity is then limited by the shear stud with lowest deformation capacity.

$$k_{slip} = Nk_{sc} \quad (II.96)$$

- ii) Shear load distribution is non-uniform along the beam: in this case, an unequal distribution of load of the load amongst the shear studs is expected. For this case, it is considered the proposal in (Anderson and Najafi, 1994) which considers that the slip at the connection depends on the nearest stud to the wall face. Under increasing load this stud provides resistance to slip until it becomes plastic. Additional load is then assumed to be resisted by the next stud deforming elastically until its plastic resistance is reached. Further load is then carried by the next stud and so forth. Thus, the deformation due to the slip of the composite slab may be determined, at each load step, as expressed in (II.97). The deformation capacity of

the component is then limited by the deformation capacity of the first loaded shear connector.

$$\Delta_{slip} = \left( \frac{F_{slip}}{P_{RK}} \right) \left( \frac{P_{RK}}{k_{sc}} \right) = \frac{F_{slip}}{k_{sc}} \leq \delta_{u,ISC} \quad (II.97)$$

It is clear that the model expressed in (II.96) is stiffer, as all the shear studs are assumed contributing to the stiffness of the shear connection, while the latter assumes the stiffness is provided only by one shear stud at the time. In the latter model, a plastic distribution of the interaction load can only be obtained if ductile studs are used. In Fig. II.166 are illustrated both models. As expressed in (II.96) and (II.97), these are dependent of the stiffness of one shear connector ( $k_{sc}$ ). The range of variation of this parameter is considerable. According to (Ahmed & Nethercot) it range between  $110 \text{ kN/mm}$  and  $350 \text{ kN/mm}$ . In the code (EN 1994-1-1, 2004) the value of  $100 \text{ kN/mm}$  is suggested for  $19 \text{ mm}$  diameter headed stud.

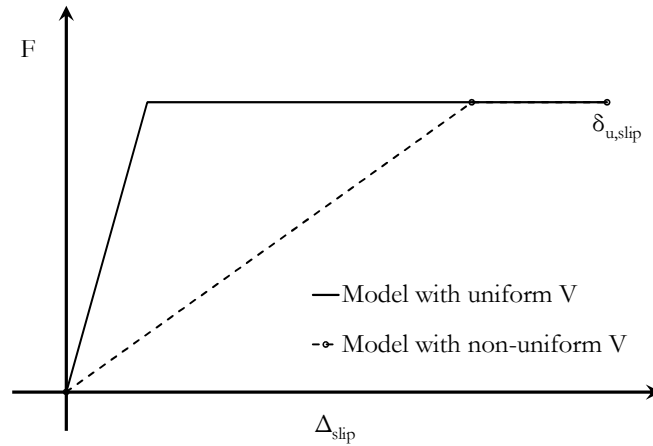


Fig. II.166: Force-deformation model for the slip of the composite beam component

In the case of the composite beam to reinforced concrete wall joint tested in the *InFaSo* research project (Kuhlmann *et al.*, 2012), the appropriate deformation model is the one expressed in (II.96). The model was applied to the test specimens considered in Fig. II.153. Initially, as no specific tests on the shear connection were performed, the shear stiffness of one stud was assumed equal to  $100 \text{ kN/mm}$ . Then, a shear stiffness was determined using the slip observed in the tests. In Table II.43 are presented results of these calculations. The stiffness of one shear connector calculated with the slip measured in the tests, shows that the value of  $100 \text{ kN/mm}$  is acceptable for this joint.

Table II.43: Results of the application of the deformation model for slip of the composite beam component

	Test 1	Test 3
$k_{sc} = 100 \text{ kN/mm}$	$\Delta_{slip} = 0,870 \text{ mm}$	$\Delta_{slip} = 0,898 \text{ mm}$
	$k_{sc}^{calc} = 106,36 \text{ kN/mm}$	$k_{sc}^{calc} = 118,97 \text{ kN/mm}$

### II.5.3.2.3 Other joint components

The other joint components are: i) those activated in anchor plate connection; ii) the joint link; iii) beam web and flange; iv) steel contact plate. These have been subject of discussion in §II.3.1 and §II.4 and therefore their behavioural characterization was performed accordingly. Table II.44 summarizes the analytical models used to determine the response of these components. The obtained force-deformation curves are later assigned to the respective springs of the joint model depicted in Fig. II.163-b).

Table II.44: Summary of the other joint components models

Joint Component	Model	Reference
Anchor Plate in compression	Optimized: §II.3.1.3.1	§II.3.1
	Simplified: Table II.20	
Joint link	Resistance: expression (II.77) to (II.83)	§II.4.3
	Deformation: expression (II.84)	
Beam web and flange in compression	Resistance: $F_{c,fb,Rd} = \frac{M_{c,Rd}}{(h_b - t_{fb})}$	(EN 1993-1-8, 2005)
	Stiffness: infinite rigid	
Steel contact plate	Resistance: $F_{cp} = f_{y,cp} A_{eff,cp}$	(EN 1994-1-1, 2004)
	Stiffness: infinite rigid	

In the above table for the anchor plate, the sophisticated model is denominated as optimized model as with this model a better approximation to the resistance of this connection is obtained than with the simplified code model. The model is of complex application in comparison to the latter. Though, it can better predict the resistance of this component and therefore the joint can be optimized.

For the beam web and flange in compression, and for the steel contact plate components, the involved parameters represent the following:  $M_{c,Rd}$  is the design moment resistance of the steel beam cross-section determined according to (EN 1993-1-8, 2005);  $h_b$  is the height of the steel beam cross-section;  $t_{fb}$  is the flange thickness of the steel beam;  $f_y$  is the yield strength of the steel contact plate; and  $A_{eff,cp}$  is the effective area of the steel contact plate. In cases where the contact plate dimensions (height and width) exceeds the steel beam flange dimensions, the effective area of a contact plate ( $A_{eff,cp}$ ) should be determined assuming dispersion at 45° through the contact plate. Otherwise, the real plate dimension may be considered.

### II.5.3.3 Joint assembly and determination of the joint properties

In order to obtain the joint properties, the assembly of the components and of the joint models is described in the present section. For the joint under hogging bending moment, the assembly procedure was based on the mechanical model depicted in Fig. II.163-b). The determination of the joint properties to bending moment was performed using two different approaches: “sophisticated” and code based. In the first case, the longitudinal steel reinforcement bar in slab, the slip of the composite beam and the anchor plate components consider the “sophisticated” models described before. As referred in the previous sub-section, these models allow obtaining a closer approximation to the real behaviour of the components and therefore heron denominated “Optimized”. In the latter case, the components models consider the codes recommendations.

#### a) “Optimized” model

The mechanical model represented in Fig. II.163-b) presents only one row of components in tension and another in compression. This implies that the assembly procedure is much simpler, as no distribution of load is required amongst rows, as in steel/composite joint with two or more tension rows. Thus, the first step is the assembly of the components per row. Equivalent springs are defined per row, as represented in Fig. II.167. The equivalent component/spring should perform as the group of components/springs it represents. The determination of its properties takes into consideration the relative position of the components: acting in series or in parallel. In the present case, either for the compression row either for the tension row, all joint components are acting in series. Thus, the determination of the properties of equivalent components/springs was performed as expressed in (II.98) and (II.99), for resistance ( $F_{eq,t}$  and  $F_{eq,c}$ ) and deformation ( $\Delta_{eq,t}$  and  $\Delta_{eq,c}$ ), respectively.

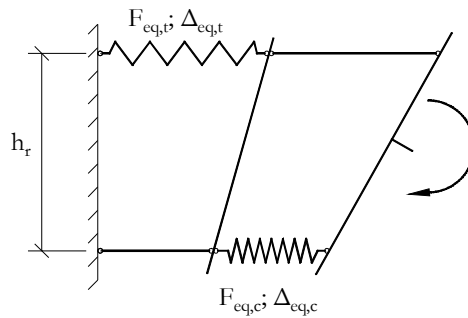


Fig. II.167: Simplified joint model with assembly of components per row

$$F_{eq} = \text{Min}\{F_i \text{ to } F_n\} \quad (\text{II.98})$$

$$\Delta_{eq} = \sum_{i=1}^n \Delta_i \quad (\text{II.99})$$

Where: the index  $i$  to  $n$  represent all components to consider either in tension either in compression, depending on the row under consideration.

Then, because only one tension row and one compression row was considered, the determination of the joint properties ( $M_j$ ,  $\Phi_j$ ) becomes relatively easy. In order to determine the joint rotation, it is important to define the lever arm  $h_r$ . According to the joint configuration, it was assumed that the lever arm is the distance between the centroid of the longitudinal steel reinforcement bar and the mid thickness of bottom flange of the steel beam. The centroid of steel contact plate is assumed to be aligned with this reference point of the steel beam. Accordingly, the joint properties are obtained as follows:

$$M_j = \text{Min}\{F_{eq,t}, F_{eq,c}, F_{JL}\} h_r \quad (\text{II.100})$$

$$\Phi_j = \frac{\Delta_{eq,t} + \Delta_{eq,c} + \Delta_{JL}}{h_r} \quad (\text{II.101})$$

Where:  $F_{eq,t}$  and  $F_{eq,c}$  are the equivalent resistance of the tension and compression rows, respectively, determined using (II.98);  $\Delta_{eq,t}$  and  $\Delta_{eq,c}$  are the equivalent deformation of the tension and compression rows, respectively, determined using (II.99).

#### b) Code based model

In terms of resistance, the model of the joint components differs; e. g. the longitudinal steel reinforcement in the slab limits the stresses in the bars to the yield strength. Though, the maximum bending moment resistance was determined as in (II.98) and (II.100). The main difference is in the deformation model which consists in the calculation of the joint initial rotational stiffness. Using the stiffness coefficients of the joint components, the joint rotational stiffness may be determined as expressed in (II.102). Note that the slip of the composite beam was considered multiplying the coefficient  $k_{slip}$  by the stiffness coefficient of the longitudinal steel reinforcement bar. For the joint link, no stiffness coefficient was derived though, as demonstrated in §II.4, the contribution of this component is considerably small. Thus, as for two of the compression components presented in Table II.44, this component may be assumed as infinite rigid.

$$S_{j,ini} = \frac{Eb_r^2}{\left(\frac{1}{k_{eq,t}} + \frac{1}{k_{eq,c}}\right)} \quad (\text{II.102})$$

Where:  $k_{eq,t}$  and  $k_{eq,c}$  are the equivalent stiffness coefficient of the tension and compression components, respectively.

In the case of structural non-linear analysis, the joint characterization requires the determination of its ultimate rotation capacity. This property is strongly dependent on the limiting component. As observed in the joint tests, this component is the longitudinal steel reinforcement bar. In the code, no estimation of the ultimate deformation capacity of this component is provided. As seen in §II.5.3.2.1, the ECCS publication (ECCS, 1999) proposes a model to evaluate this parameter. This model is suggested for evaluation of the joint rotation capacity. As conservative approach, the joint ultimate rotation capacity may be determined using only the ultimate deformation capacity of the longitudinal steel

reinforcement bar in the slab, and neglecting the contribution of the other joint components. Thus, in (II.103), the component ultimate deformation ( $\Delta_{sm}$ ) should be obtained using the appropriate equation given in §II.5.3.2.1.

$$\Phi_{j,u} = \frac{\Delta_{sm}}{h_r} \quad (\text{II.103})$$

The complete moment-rotation curve was obtained using the same principles as in (EN 1993-1-8, 2005) for steel joints. According to the code, the joint behaviour may be reproduced by means of: bi-linear; tri-linear or non-linear law (Fig. II.168). In the first case, the joint behaviour is represented by an elastic-plastic behaviour where the modified rotational stiffness ( $S_j$ ) are used to determine the joint rotation at maximum bending moment. The modified ( $S_j$ ) stiffness was determined using the appropriate joint stiffness modification coefficient  $\eta$ , as expressed in (II.104). The tri-linear moment-rotation curve was obtained using the initial rotational stiffness ( $S_{j,ini}$ ) up to  $2/3$  of  $M_{j,Rd}$ . After, hardening is simulated changing the rotational stiffness of the joint. This may be performed using the limit of elastic rotation obtained in the first case (bi-linear). Finally, the non-linear moment-rotation curve was defined using the joint stiffness expression prescribed by (EN 1993-1-8, 2005), as reproduced in (II.105). In this expression, the stiffness ratio ( $\mu$ ) is constant and equal to 1 up to  $2/3$  of  $M_{j,Rd}$  after a non-linear range is defined up to  $M_{j,Rd}$ , as expressed in (II.106).

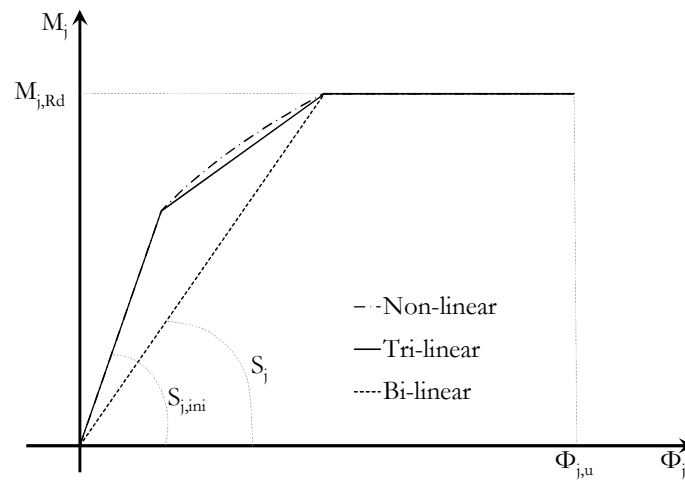


Fig. II.168: Moment-rotation curve to represent the joint behaviour

$$S_j = \frac{S_{j,ini}}{\eta} \quad (\text{II.104})$$

$$S_j = \frac{Eb_r^2}{\mu \sum_i \frac{1}{\kappa_i}} \quad (\text{II.105})$$

With

$$\begin{cases} \text{if } M_{j,Ed} \leq \frac{2}{3} M_{j,Rd}: & \mu=1 \\ \text{if } \frac{2}{3} M_{j,Rd} < M_{j,Ed} \leq M_{j,Rd}: & \mu = \left( \frac{1,5 M_{j,Ed}}{M_{j,Rd}} \right)^\Psi \end{cases} \quad (\text{II.106})$$

Where: the coefficient  $\Psi$  is taken equal 1,7 as recommend in (EN 1994-1-1, 2004) for a contact plate joint. This consideration is an assumption as no proposal for this factor for the joint configuration under study exists.

Values for the rotational stiffness modification coefficient ( $\eta$ ) are provided in (EN 1993-1-8, 2005). These vary according to the joint configuration. In the case of beam-to-column joints the value of 2 is proposed. In the case of composite beam to reinforced concrete walls, no information is available and therefore the use of the value for steel and composite joints is suggested.

The application and validation of the described models is performed in the next section.

#### II.5.3.4 Validation of the analytical model

The application of the described model to determine the joint properties is shown in Fig. II.169. The joint bending moment to joint rotation curves compare analytical models and experimental tests. The quality of the model varies with parameter under analysis and with the type of model, “optimized” or code based. For the resistance, the approximation of the “optimized model” is excellent. The code model limits the governing component, the longitudinal steel reinforcement bar, to its yield capacity therefore, the lower resistance obtained with this model was expected. In terms of initial stiffness, the quality of the models is reversed. For this parameter, the code model provides a better approximation, being very close to the experimental results. The “optimized” model presents a stiffer response than the experimental results. Again this result is due to the model of the govern component. In Fig. II.165 has been shown that the analytical “optimized” model for the longitudinal steel reinforcement bar was stiffer than the numerical model. This stiffer response was then reproduced in the global joint behaviour. The reason for this stiffer response may be attributed to the fact that the “optimized” model neglects discontinuity in the wall-slab interface. Because these members are concreted in different stages, the small bond developed between these members is rapidly exceeded. Consequently, an initial “crack” between wall and slab may be assumed from the beginning of loading and therefore the joint is a more flexible than if full continuity existed between these members. In what respects to the ultimate rotation, the “optimized” model is conservative though, also the analytical model to determine the ultimate deformation of the longitudinal steel reinforcement bar should be affected by the wall-slab interface behaviour. The code based model is absent in what concerns this parameter. The limit of the represented plateau was assumed equal to the ultimate joint rotation determined with the “optimized” model.



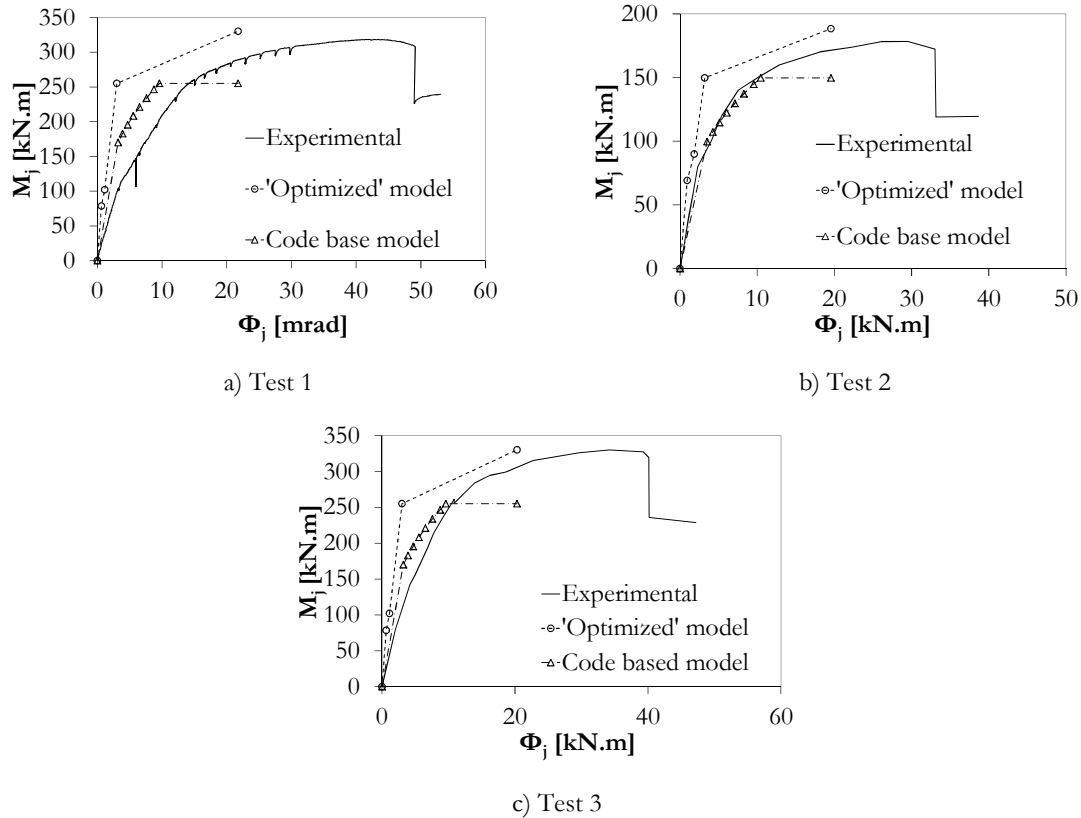


Fig. II.169: Joint bending moment to joint rotation curve ( $M_j-\Phi_j$ ) comparing analytical models with experimental results

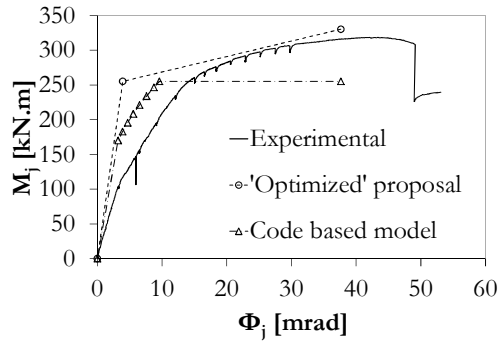
Given the base principles of the code base model, and according to the results presented Fig. II.169, the model is suitable for application and no improvement is required. In what concerns the “optimized” model, it was seen that the initial stiffness requires improvement. As the code base model provided a good approximation for this parameter, it was decided to propose a modification to the joint component model described in §II.5.3.2.1. In this way, the initial stiffness is determined using same elongation length as used in the code based model:  $3,6b$ . See Fig. II.164 for definition of the dimension  $b$ . Subsequently, the model to determine the ultimate deformation was also modified introducing the previous consideration. In Table II.45 is summarized the modifications proposed for the “optimized” model of the longitudinal steel reinforcement bar in the slab component. In Fig. II.170 is shown the application of this described modifications. It is now observed a better approximation. Though, it should be noted that if wall and slab are concreted at the same time, the initial proposal for the “optimized” model should be more accurate and therefore used instead of the proposed modification. Finally, in Table II.46 are quantified the approximation of the analytical models in terms of ratio between model and test.

Table II.45: Proposed modifications for the “optimized” model of the longitudinal steel reinforcement in slab component

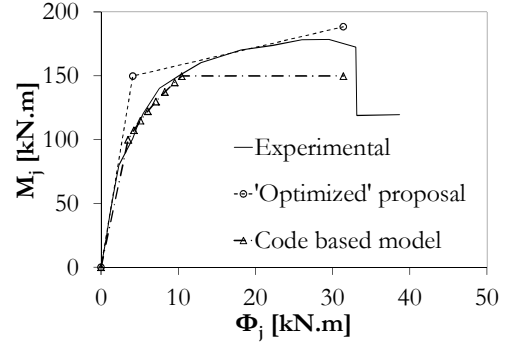
<b>Elongation length</b>	$3,6b$
<b>Ultimate deformation</b>	$\rho < 0,8\%: \Delta_{sru} = 3,6h\varepsilon_{srmu}$ $\rho \geq 0,8\% \text{ and } a < L_t: \Delta_{sru} = 3,6h\varepsilon_{srmu}$ $\rho \geq 0,8\% \text{ and } a > L_t: \Delta_{sru} = 3,6h\varepsilon_{srmu} + (a - 3,6h)\varepsilon_{srmu}$

Table II.46: Summary of the approximation of the analytical models to the experimental results by means of ratio Model/Test

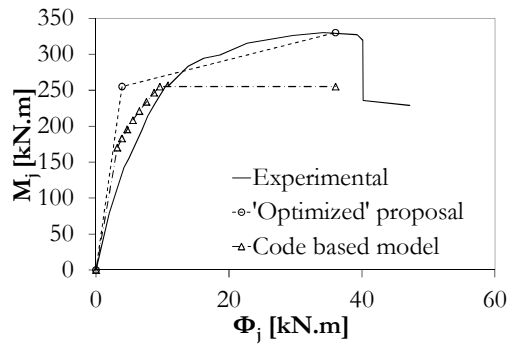
		“Optimized” model	Code base model	“Optimized” model (modified)
$S_{j,ini}$	Test 1	3,96	1,70	2,08
	Test 2	2,26	0,86	1,10
	Test 3	3,64	1,56	1,91
$M_{j,max}$	Test 1	1,04	0,80	1,04
	Test 2	1,06	0,84	1,06
	Test 3	1,00	0,77	1,00
$\delta_u$	Test 1	0,44	-	0,77
	Test 2	0,59	-	0,95
	Test 3	0,51	-	0,90



a) Test 1



b) Test 2



c) Test 3

Fig. II.170: Joint bending moment to joint rotation curve ( $M_j-\Phi_j$ ) comparing modification on the “Optimized” model with experimental tests and code based model results

## II.6 Concluding remarks

In the present part, the behaviour of steel-to-concrete joints has been discussed in detail. The basis of the presented study has been the joint configurations developed, within the RFCS research project *InFaSo* (Kuhlmann *et al.*, 2012), for beam to wall joints. These configurations covered two main typologies regarding the structural demands: simple joint, no capacity to transfer bending moment between members, and semi-continuous/continuous joint, with capacity to transfer bending moment. The main focus of this thesis and of the present section has been the second option. Therefore, the presented study aimed the different parts of this joint typology. Though, as the simple joint may be identified as a variant of the complete joint, a brief approach to this type of joint has been included. The main objective of this part, was to characterize the behaviour of steel-to-concrete joints providing analytical tools for a simple design. In order to accomplish this goal, and giving the limited number of experimental results available, the use of numerical models, developed in finite element software (Abaqus, 2011), was the main support of the presented analysis and of the validation process of the proposed analytical models.

The background of the presented approach has been summarized in chapter II.2. In this state-of-the art chapter, the extent of the subject was evident. In such joints, to the designer/engineer is required the knowledge on steel, composite and reinforced concrete design. From the two first, the component method is essential, as the proposed analytical methodologies represent an extension of this approach to steel to concrete joints. For the latter, the strut-and-tie model was identified as the key tool to perform the bridge between the steel/composite part and the reinforced concrete part. Subsequently, the experimental and analytical developments of the RFCS research project *InFaSo* (Kuhlmann *et al.*, 2012), were summarized given their essential contribution to accomplish the tasks proposed in this thesis.

In chapter II.3 the behaviour of anchor plate connection has been analysed. As referred in §II.1, this part of the complete joint can be joint by itself therefore, an entire chapter was dedicated to its study. Though, as the main focus of the thesis was the composite beam to reinforced concrete wall joint, more detail was given to the analysis of the anchor plate under the same conditions as in the semi-continuous/continuous joint solution. Thus, it was identified that the compression load was dominant and that the shear load could be disregarded. For this reason, the analysis of the anchor plate subjected only to compression was performed. In the analysis of the behaviour of the connection under such conditions was developed a numerical model. The validation of the numerical tool was accomplished using experimental results available in the literature and performing a sensitivity study. Similarities between the anchor plate under compression and the T-stub in compression used in the characterization of column bases, were found. Consequently, the analytical models developed were grounded in the models to characterize the referred type of joints. Two analytical models were proposed in thesis for the anchor plate, one more sophisticated and one simplified. The first is an adaptation of the model proposed in (Guisse *et al.*, 1996).

This complex model includes all the components participating on the anchor plate response and discretizes the plate-concrete contact. Though, given the complexity of this model, an adaptation of the simplified T-stub in compression model used in column bases, was also proposed. The modifications consisted in including the effect of the row of anchors on the non-load side of the connection. The comparison between analytical models and numerical simulations demonstrated that the sophisticated model allowed a better approximation of the ultimate resistance and deformation. However, this model required a previous calibration. This is understandable because, though its sophistication, the model is uni-dimensional while the anchor plate behaviour is clearly three-dimensional. In this way, the calibration was performed at the level of the components behaviour. Subsequently, in order to assess the sensibility of the proposed analytical models to geometrical and materials variations, a parametric study was performed which considered the variation of the referred parameters within a practical range of values. The comparison between numerical and analytical models showed the suitability of the proposed models. In terms of resistance, the comparison of results indicated that the simplified model is conservative while the sophisticated presented an interesting accuracy. Given the different level of complexity of application the first is recommend for a daily practice while the second should be used in a more advanced analysis where an optimization of the joint components is foreseen.

In order to complete the analysis of the anchor plate connection, section II.3.2 and II.3.3 were dedicated to the analysis of the anchor plate subject to shear loading and combined shear and compression loading, respectively. The analyses were not the main focus of the presented research work. Though, it was important that this was performed so that a complete approach of the joint configuration, and its variants, was accomplished. Thus, for the anchor plate subject to shear load with eccentricity two numerical models were developed considering the variation of the eccentricity of the shear load. The complete validation of these models was not accomplished, as the post peak behaviour was not predicted by these simulations. This range of the anchor plate behaviour is characterized by the crack state of the concrete on the tension side of the connection. The numerical simulation of the concrete in such cracked state is quite complex and of difficult realization, as the few numerical works existing on this subject demonstrates. For the above reasons, the numerical work performed on this connection was limited to the determination of the load capacity. This was achieved with satisfactory accuracy, as demonstrated by the presented comparison curves. After, an analytical model was presented extending the component method to this type of connection. The model developed within RFCS research project (Kuhlmann *et al.*, 2012), and presented in (Ozbolt *et al.*, 2011), introduces in the component method new components related to the anchorage in concrete. The application of the model to two experimental tests shows a satisfactory approximation of the load deformation curve of the connection. Finally, the chapter II.3 was concluded with a section dedicated to the analysis of the anchor plate subjected to combined loading (shear + compression). The approach was pure numerical providing an approximation for an interaction curve. Obviously, this proposal requires an experimental verification which was not performed within this work. Though, this

numerical analysis gave an insight to the behaviour of the anchor plate in such conditions. From these results, it is clear that the presence of compression at the level of the upper anchor row increases the shear capacity of the connection.

In the steel to concrete joints under analysis, an important bridge between the steel/composite part and the reinforced concrete wall is performed with the component identified as the joint link and analysed in chapter II.4. The complexity of this part of the joint is evident. In addition, no experimental evidence was available neither from the referred research project neither in the literature. Thus, the study of this part of the joint was purely based on the numerical analysis. The numerical study was reduced to a limited range of geometrical dimensions considered within the practical applications. This numerical study allowed characterizing the joint link component in terms of force-deformation curve. Subsequently, in order to include the response of this component in the model of the complete joint, a simplified strut-and-tie model was proposed. The developed model is based on same principles of the approach commonly used in design of reinforced concrete and relied in a single strut model connecting the tension and the compression zones. The application of this model to the cases numerically analysed demonstrated that the resistance of the component can be assessed with accuracy. In terms of deformation, the development of a model with physical meaning is very complex given the highly non-uniform distribution of strains within this component. Though, as the deformation pattern found in the numerical analysis was similar for all the considered geometries, it was decided to approximate an mathematical equation which provided the deformation of the component in function of the loading. In this way, the accuracy of the model was guaranteed.

Finally, in chapter II.5 the complete joint was approached. First a numerical model capable of reproducing the behaviour of the composite beam to reinforced concrete wall joint was developed. The experimental results obtained in the RFCS research project *InFaSo* (Kuhlmann *et al.*, 2012) validated this model. The comparison of results between tests and numerical simulations showed the accuracy to reproduce the global response of the joint and approximate reasonably local phenomena. The numerical model provided a rational basis for the estimation of the ultimate resistance and ductility of joint between composite beam and reinforced concrete wall. It allowed the identification of the key phenomena that control the nonlinear moment-rotation response of the joint and provided guidance for the modelling of those phenomena:

- Concrete constitutive model: Concrete Damage Plasticity model, tension stiffening (behaviour after crack initiation), concrete plasticity
- Steel constitutive model: von Mises plasticity model (isotropic Yielding)
- 3D interaction between concrete, reinforcement bars and steel parts: reinforcement-concrete bond behaviour, “hard” contact with frictional behaviour
- Composite behaviour of the steel-concrete composite beam: shear connectors, contact and interface stresses

The moment-resisting joint between composite beam and reinforced concrete wall was developed to transfer shear and hogging moment. Furthermore, for the typical range of geometries, it behaves as a partial-strength joint, so that the requirement of sufficient ductility is crucial. To ensure that these goals are achieved, a small parametric study was carried out with respect to the steel class of the longitudinal reinforcement bar, the thickness of the steel bracket and the thickness of the anchor plate. In the experimental tests, the two parameters related to the bottom part of the joint have been also subject of variation. The main numerical conclusions are in line with the experimental observations. For the studied joint configuration, submitted to a hogging moment, and for the range of geometrical properties considered, the longitudinal steel reinforcement bar controls the joint stiffness, resistance and ductility. The bottom part of the joint has minor influence and does not affect these mechanical properties of the joint. It was concluded that whenever the joint is detailed such that the resistance is controlled by the (upper) tension zone, the ductility of the joint is directly dependent on the ductility class of the steel longitudinal reinforcement in the slab. In practical terms, the percentage of reinforcement in the slab is 1,08%, corresponding to a common value for composite beams. Consequently, taking into account the good performance of the studied joint, keeping the longitudinal reinforcement bars as the governing component, may be a practical option. The resistance can be easily and accurately evaluated, and, with an appropriate specification of the steel rebars, the required ductility can be obtained. The bottom zone of the joint did not influence the moment resistance significantly. However, it was observed that parts of some components reached the yield stress. This hints at the possibility of design load combinations with different bending to shear ratios acting at the joint leading to a shift of the critical components towards the bottom zone of the joint.

For the geometric variations, a variant of the joint configuration was numerically simulated considering the use of two rows of longitudinal reinforcement bars connecting slab and wall. In order to be closer to a standard solution, this reinforcement bar was of 10mm diameter. The results confirmed the increase of resistance and demonstrated that using reinforcement bars of Class C, a plastic distribution of load may be achieved, as both levels of reinforcement bars overcome the yield capacity at ultimate state.

To conclude this chapter, a design model based on the component method for composite beam to reinforced concrete wall was proposed to determine the joint properties in terms of moment-rotation ( $M_j-\Phi_j$ ) curve. According to the models of the joint components, namely the longitudinal steel reinforcement bar in the slab and anchor plate in compression, two options were distinguished: one providing a more optimized design and one resulting in a conservative/simplified design. The application this model to the test specimens of the experimental programme of the RFCS research project *InFaSo* (Kuhlmann *et al.*, 2012) showed that the proposed models can provide an accurate characterization of the joint properties. As the governing component, the longitudinal steel reinforcement bar in the slab plays an important role on the joint properties as initial stiffness, bending moment resistance and rotation capacity. Consequently, the quality of the proposed model is strongly dependent on the model of this component.

## References

- (Abaqus, 2011) Abaqus 6.11, Theory Manual and Users Manuals, Dassault Systèmes Simulia Corp., 2011.
- (ACI, 1998) American Concrete Institute – ACI. Design Guide to ACI 349-85. ACI Committee 349, Detroit, 1988.
- (ACI, ACI 318: ACI Standard 318. Building code requirements for structural concrete, 2001) American Concrete Institute – ACI. ACI 318: ACI Standard 318. Building Code Requirements for Structural Concrete. Detroit, 2001.
- (Ahmed and Nethercot, 1997) Ahmed, B, Nethercot, D A. Prediction of Initial Stiffness and Available Rotation Capacity of Major Axis Composite Flush Endplate Connections. *Journal of Constructional Steel Research*, vol. 41, N° 1, pp. 31-60, 1997.
- (Anderson and Najafi, 1994) Anderson, D, Najafi, A A. Performance of Composite Connections: Major Axis End Plate Joints. *Journal of Constructional Steel Research*, vol. 31, pp. 31-57, 1994.
- (Aribert, 1995) Aribert, J M. Influence of Slip on Joint Behaviour. in: *Connections in Steel Structures III: Behaviour, Strength and Design*, Third International Workshop, Trento, pp. 29-31, 1995.
- (Berger *et al.*, 2011) Berger, W, Hofmann, J, Kuhlmann, U. Connections between steel and concrete: Joints with supplementary reinforcement. *Proceedings of the 6th European Conference on Steel and Composite Structures* (Eds.: L. Dunai, M. Iványi, K. Jármai, N. Kovács, L. Gergely Vigh), Volume A, pp. 585-590, Budapest, 2011.
- (Bjordhove *et al.*, 1990) Bjordhove, R., Colson, A., Brozetti, J. Classification system for beam-to-column connections. *Journal of Structural Engineering*, ASCE, 116(11), pp. 3059-3076, 1990.
- (Bode and Hanenkamp, 1985) Bode, H, Hanenkamp, W. Zur Tragfähigkeit von Kopfbolzen bei Zugbeanspruchung (Load-bearing capacity of headed anchors under tension loads). *Bauingenieur* (in German), pp. 361-367, 1985.
- (Bursi and Jaspert, 1997) Bursi, O, Jaspert, J-P. Benchmarks for Finite Element Modelling of Bolted Steel Connections. *Journal of Constructional Steel Research*, 43(1-3), pp.17-42, 1997.
- (CEB-FIP, 1993) Comité Euro-International du Béton - CEB. CEB-FIP Model Code 1990 : Design Code. Lausanne, 1993.
- (CEB, 1997) Comité Euro-International du Béton -CEB. CEB Design Guide: Design of Fastenings in Concrete. Lausanne, 1997.
- (CEN/TS 1992-4, 2009) European Committee for Standardization – CEN. CEN/TS 1992-4: Design of fastenings for use in concrete, Final Draft, Brussels, 2009.



- (Chapman and Balakrishnan, 1964) Chapman, J C, Balakrishnan S. Experiments on composite beams. *The Structural Engineer*, 42(11): 369-83, 1964.
- (Cook and Klingner, 1992) Cook, A, Klingner, R. Ductile Multiple-Anchor Steel-to-Concrete Connections. *Journal of Structural Engineering*, 118, 1992.
- (Demonceau, 2008) Demonceau, J. Steel and composite building frames: sway-response under conventional loading and development of membrane effects in beam further to an exceptional actions. PhD Thesis, University of Liège, Liège, 2008.
- (Eligehausen and Balogh, 1995) Eligehausen, R, Balogh, T. Behaviour of Fasteners Loaded in Tension in Cracked Concrete“, *ACI-Structural Journal*, 92(3), pp. 365-379, 1995.
- (Eligehausen and Fichtner, 2003) Eligehausen, R, Fichtner, S. Einfluss des Achsabstandes auf die Betonausbruchlast von biegebeanspruchten Gruppenbefestigungen (Influence of axial spacing on the concrete failure of groups under bending). Report (not published and in German), Institut für Werkstoffe im Bauwesen, University of Stuttgart, 2003.
- (Eligehausen and Lehr, 1993) Eligehausen, R, Lehr, B. Quersugtragfähigkeit von Dübeln mit grossem Randabstand (Shear capacity of anchors with large edge distance). Report No. 10/20-93/11 not published (in German), Institut für Werkstoffe im Bauwesen, University of Stuttgart, Stuttgart, 1993.
- (Eligehausen and Ozbolt, 1992) Eligehausen, R, Ozbolt, J. Influence of Crack Width on the Concrete Cone Failure Load. In: Bazant, Z. P. (Editor): *Fracture Mechanics of Concrete Structures*. Elsevier Applied Sciences, pp. 876-884, London, 1992.
- (Eligehausen *et al.*, 1983) Eligehausen, R, Popov, E, Bertero, V. Local bond stress-slip relationship of deformed bars under generalized excitations. Report No. UCB/EERC-83/23, Earthquake Engineering Centre, University of California, Berkeley, 1983.
- (Eligehausen *et al.*, 1989) Eligehausen, R, Fuchs, W, Lotze, D, Reuter, M. Befestigungen in der Betonzugzone (Fixings in the concrete tensile zone). *Beton und Stahlbetonbau* (in German), 84(2) and (3), (2) pp. 27-32, (3) pp. 71-74, 1989.
- (Eligehausen *et al.*, 2006) Eligehausen, R, Mallée, R, Silva, J F. *Anchorage in Concrete Construction*. Ernst & Sohn, Berlin, 2006.
- (ECCS, 1999) European Convention for Constructional Steelwork – ECCS. *Design of Composite Joints for Buildings*. ECCS Publication n°109, Technical Committee 11, Composite Structures, First Edition, Belgium, 1999.
- (EN 1992-1-1, 2004) European Committee for Standardization – CEN. EN 1992-1-1. *Eurocode 2: Design of concrete structures. Part 1-1: General rules and rules for buildings*, Brussels, 2004.
- (EN 1993-1-1, 2005) European Committee for Standardization – CEN. EN 1993-1-1. *Eurocode 3: Design of steel structures – Part 1-1: General rules and rules for buildings*. Brussels, 2005.

(EN 1993-1-8, 2005) European Committee for Standardization – CEN. EN 1993-1-8. Eurocode 3: Design of steel structures. Part 1-8: Design of joints, Brussels, 2005.

(EN 1994-1-1, 2004) European Committee for Standardization – CEN. EN 1994-1-1. Eurocode 4: Design of composite steel and concrete structures. Part 1-1: General rules and rules for buildings, Brussels, 2004.

(EOTA, 1997) European Organization for Technical Approval – EOTA. ETAG 001: Guideline for European Technical Approval of Anchors (metal anchors) for use in concrete. Part 1, 2 and 3 and annexes A, B, and C. Brussels, 1997.

(Farrow and Klingner, 1995) Farrow, C B, Klingner, R E. Tensile Capacity of Anchors with partial overlapping failure surfaces: Evaluation of existing formulae on an LRFD Basis. ACI Structural Journal, 92 (6), pp. 698-710, 1995.

(Farrow *et al.*, 1996) Farrow, C B, Frigui, I, Klingner, R E. Tensile capacity of single anchors in concrete: Evaluation of existing formulae on an LRFD Basis, ACI Structural Journal, 93(1), pp. 128-137, 1996.

(fib, 2007) Federation International du Béton – fib. Guide for the Design of fastenings in Concrete: Part 1: General, Part 2: Post-installed Anchors – Mechanical, Part 3: Post-installed Anchors – Bonded Anchors and Rebar Systems, Part 4: Headed Anchors, Part 5: Anchor Channels. Lausanne, 2007.

(fib, 2008) Federation International du Béton – fib. Practitioners' guide to finite element modelling of reinforced concrete structures. fib – Bulletin 45, Lausanne, 2008.

(fib, 2010) fib: CEB-FIP, fib Bulletin 55: Model Code 2010. Final draft – Volume 1, Lausanne, 2012.

(Feldmann + Weynand GmbH, 2011) Feldmann + Weynand GmbH. CoP 2 – The connection program. Version 1.3.6, 2011.

(Furche, 1994) Furche, J. Zum Trag- und Verschiebungsverhalten von Kopfbolzen bei zentrischem Zug. PhD Thesis (in German), University of Stuttgart, Stuttgart, 1994.

(Gan, 2000) Gan, Y. Bond stress and slip modeling in non-linear finite element analysis of reinforced concrete structures. Master Thesis, Department of Civil Engineering, University of Toronto, 2000.

(Gil and Bayo, 2008) Gil, B, Bayo, E. An alternative design for internal and external semi-rigid composite joints. Part II: Finite element modelling and analytical study. Engineering Structures, 30(1), pp. 232-246, 2008.

(Girão Coelho *et al.*, 2006) Girão Coelho, A, Simões da Silva, L, and Bijlaard, F. Numerical evaluation of the behaviour of the T-Stub. Journal of Structural Engineering, 132(6), 918-928 (2006).

(Guisse *et al.*, 1996) Guisse, S, Vandegans, D, Jaspard, J-P. Application of the component method to column bases: Experimentation and development of a mechanical model for

characterization. Research Centre of the Belgian Metalworking Industry, MT195, Liège, 1996.

(Henriques *et al.*, 2011) Henriques, J, Ozbolt, A, Zizka, J, Kuhlmann, U, Simões da Silva, L, Wald, F. Behaviour of steel-to-concrete joints: moment resisting joint of a composite beam to reinforced concrete wall. *Steel construction: Design and Research* (Ed. Ernst & Sohn), 4(3), pp. 161-165, 2011.

(Henriques *et al.*, 2013) Henriques, J, Raposo, J M, Simões da Silva, L, Costa Neves, L. Tensile resistance of steel reinforced anchorages: experimental evaluation. *ACI Structural Journal*, 110(2) March-April, pp. 329-250, 2013.

(Heron, 2008) Heron. Special issue: Steel Column Bases, 53 (1/2), 2008.

(Huang *et al.*, 1999) Huang, Z, Burgess, I W, Plank. R J. The influence of shear connectors on the behavior of composite steel-framed buildings in fire. *Journal of Constructional Steel Research*, 51, pp. 219-237, 1999.

(Huber, 1999) Huber, G. Nicht-Linear Berechnungen von verbundquerschnitten und biegeweichen knoten. PhD Thesis (in German), Innsbruck, 1999.

(Jankowiak and Lodygwski, 2005) Jankowiak, T, Lodygwski, T. Identification of parameters of concrete damage plasticity constitutive model. *Foundations of civil and environmental engineering*, 6, pp.53-62, 2005.

(Jaspart, 1991) Jaspart, J.-P. Étude de la semi-rigidité des nœuds poutre-colonne et son influence sur la résistance des ossatures en acier. PhD Thesis (in French), University Liège, Liège, 1991.

(Jaspart and Maquoi, 1992) Jaspart, J-P, Maquoi, R. Survey of existing types of joint modelling. COST C1 – Semi-Rigid Behaviour of Civil Engineering Structural Connections, ed. André Colson. Proceedings of the First State of the Art Workshop, Strasbourg, pp. 370-381, 1992.

(Jaspart and Vandegans, 1998) Jaspart, J-P, Vandegans, D. Application of the component method to column bases. *Journal of Constructional Steel Research*, 48(89-106), 1998.

(Jaspart *et al.*, 2009) Jaspart, J-P, Demonceau, J F, Rekin, S, Guillaume, M L. European Recommendations for the Design of Simple Joint in Steel Structures. ECCS Publication N° 126, Technical Committee 10, Structural Connections, First Edition, Belgium, 2009.

(Klingner *et al.*, 1998) Klingner, R E, Muratli, H, Shirvane, M. A technical basis for revision to anchorage criteria. Report No. NUREC/CR-5563, University of Texas, Austin, 1998.

(Kuhlmann and Immiger, 2003) Kuhlmann, U, Immiger T. Ankerplatten und Einbaudetails zur Kraftüberleitung im Stahlbau. Final report (in German), Forschungsvorhaben im Auftrag des Deutschen Ausschusses für Stahlbau (DASt), Institut für Konstruktion und Entwurf – Stahl, Holz und Verbundbau – Universität Stuttgart, Stuttgart, 2003.

- (Kuhlmann and Rybinski, 2005) Kuhlmann, U, Rybinski, M. Load-carrying capacity of anchor plates with welded studs. COST C12 Final Conference Proceedings *Improvement of buildings' Structural Quality by New Technologies*, Ed. Schaur *et al.* pp. 463-471, London, 2005.
- (Kuhlmann and Rybinski, 2007) Kuhlmann, U, Rybinski, M. Component Method for Anchor Plates. Eligehausen, R. (Ed.), Proc. 2nd International Symposium Connections between Steel and Concrete, 2, pp. 1049-1058, Stuttgart, 2007.
- (Kuhlmann *et al.*, 1998) Kuhlmann, U, Davison, J B, Kattner, M. Structural systems and rotation capacity. Proceedings of COST Conference on Control of the Semi-rigid Behaviour of Civil Engineering Structural Connections, pp. 167-76, Liège, 1998.
- (Kuhlmann *et al.*, 2012) Kuhlmann K, Hofman J, Wald F, da Silva L, Krimpmann M, Sauerborn N *et al.*, New market chances for steel structures by innovative fastening solutions BETWEEN STEEL AND CONCRETE (INFASO). Final report, Report EUR 25100 EN, European Commission, 2012.
- (Kunz, 2009) Kunz, J. Missing links: solutions to add reinforcement in existing concrete. SIRR09-Seminário internacional de Reforço e Reabilitação-Ligações Estruturais, FEUP, pp. 1-18, Porto, 2009.
- (Liang, 2006) Liang, Q.Q. Performance-based optimization of strut-and-tie models in reinforced concrete beam-column connections. Real Structures: Bridges and Tall Buildings, Proceedings of the Tenth East Asia-Pacific Conference on Structural Engineering and Construction, Bangkok, pp. 347-352, 2006.
- (Matos *et al.*, 2009) Matos, J A C, Valente, I B, Cruz, P J S. Avaliação de Incertezas no Comportamento até à rotura de Vigas de Betão Armado. 1º Congresso Nacional para a Segurança e Conservação de Pontes, pp. II-5 a II-12, Lisboa, 2009.
- (Narayanan and Beeby, 2005) Narayanan, R S, Beeby, A. Designers' Guide to EN1992-1-1 and EN 1992-1-2. Eurocode 2: Design of concrete structures. General rules and rules for buildings and structural fire design. Series editor Haig Gulvanessian, Thomas Telford, London, 2005.
- (Ollgaard *et al.*, 1971) Ollgaard, J, Slutter, R, Fisher, J. Shear Strength of Stud Connectors in Lightweight and Normal-Weight Concrete. AISC Engineering Journal, 8, pp.55-64, 1971.
- (Ozbolt *et al.*, 2011) Ozbolt, A, Berger, W, Henriques, J, Kuhlmann, U, Eligehausen, R, Simões da Silva, L. Behaviour of steel-to-concrete joints I: Pinned joint of a steel beam to a reinforced concrete wall. Proceedings of the 6th European Conference on Steel and Composite Structures (Eds.: L. Dunai, M. Iványi, K. Jármai, N. Kovács, L. Gergely Vigh), Volume A, pp. 471-476, Budapest, 2011.
- (Raposo, 2006) Raposo, J M. Reforço com armaduras em ligações com chumbadouros de cabeça à tracção. PhD Thesis (in Portuguese), University of Coimbra, Coimbra, 2006.
- (Rehm *et al.*, 1988) Rehm, G, Eligehausen, R, Mällée, R. Befestigungstechnik (Fixing Technology). Betonkalender 1988 (in German), Part II, Ernst & Sohn, pp. 569-663, Berlin, 1988.

- (Schlaich *et al.*, 1987) Schlaich, J., Schäfer, K., Jennewein, M. Toward a Consistent Design of Structural Concrete, *PCI Journal*, 32(3), pp. 74-150, 1987.
- (Schlaich and Schäfer, 1991) Schlaich, J., Schäfer, K. Design and detailing of structural concrete using strut-and-tie models. *The Structural Engineer*, 69(6), 1991.
- (Schäffer, 2005) Schäffer, M. Zum Rotationsnachweis teiltragfähiger Verbundknoten in verschieblichen Verbundrahmen. PhD Thesis (in German), University of Stuttgart, Stuttgart 2005.
- (Simões da Silva *et al.*, 2001) Simões da Silva, L., Simões, R.D., Cruz, P.J.S. Experimental behaviour of end-plate beam-to-column composite joints under monotonical loading. *Engineering Structures*, 23, pp. 1383-1409, 2001.
- (Simões da Silva *et al.*, 2002) Simões da Silva, L., Santiago, A, Vila Real, P. Post-limit stiffness and ductility of end-plate beam-to-column steel joints. *Computers and Structures* 80, pp. 515-531, 2002.
- (Simões da Silva, 2008) Simões da Silva, L. Towards a consistent design approach for steel joints under generalized loading. *Journal of Constructional Steel Research*, 64, pp. 1059-1075, 2008.
- (Sokol and Wald, 1997) Sokol Z, Wald F. Experiments with T-stubs in tension and compression. Research report, Czech Technical University in Prague, Prague, 1997.
- (Steenhuis *et al.*, 2008) Steenhuis M, Wald F, Sokol Z, Stark J. Concrete in compression and base plate in bending. *Heron*, 53(1/2), pp. 51-68, Delft, 2008.
- (Tschemmerneegg *et al.*, 1998) Tschemmerneegg, F., Rubin, D., Pavlov, A. Application of the component method to composite joints. *COST C1 – Control of the semi-rigid behaviour of civil engineering structural connections*, Proceedings of the international conference, pp. 145-154, Liège, 1998.
- (Vandegans, 1997) Vandegans, D. Column Bases: Experimentation and Application of Analytical Models. Research Centre of the Belgian Metalworking Industry, MT 196, pp. 80, Brusselss, 1997.
- (Wald *et al.*, 1996) Wald, F, Sokol, Z, Steenhuis, M. Proposal of the Stiffness Design Model of the Column Bases. in *Connections in Steel Structures III: Behaviour, Strength and Design*, Proceedings of the Third International Workshop, pp. 237-249, Trento, 1996.
- (Wald *et al.*, 1998) Wald, F., Gresnigt, A. M., Weynand, K., Jaspart, J.-P. Application of the Component Method to Column Bases. *COST C1 – Control of the semi-rigid behaviour of civil engineering structural connections*, Proceedings of the international conference, pp. 155-166, Liège, 1998.
- (Wald *et al.*, 2008) Wald, F, Sokol, Z, Steenhuis, M, Jaspart, J-P. Component method for steel column bases. Special Issue: Steel Column Bases, *Heron*, 53(1/2), pp. 3-20, 2008.

(Weynand *et al.*, 1996) Weynand, K., Jaspart, J.-P., Steenhuis, M. The Stiffness Model of Revised Annex J of Eurocode 3. in Bjorhovde R. Colson A. Zandonini R. (eds.) *Connections in Steel Structures III*, Pergamon, Oxford and New York, pp. 441-452, 1996.

(Weynand, 1999) Weynand, K. Column bases in steel building frames. COST C1 - Semi-rigid behaviour of civil engineering structural connections, Luxembourg, 1999.

(Yu *et al.*, 2008) Yu, H, Burgess, I W, Davison, J B, Plank, R J. Numerical simulation of bolted steel connections in fire using explicit dynamic analysis. *Journal of Constructional Steel Research*, 64, pp. 515-525, 2008.

(Zhao and Eligehausen, 1992) Zhao, G, Eligehausen, R. Tragfähigkeit von Befestigungen unter kombinierter Zug und Querlast (Load-bearing capacity of fastenings under combined tension and shear loading). Report No. 10/17-92/2 not published (in German), Institut für Werkstoffe im Bauwesen, University of Stuttgart, Stuttgart, 1992.

(Zhang, 1997) Zhang, Y G. Dynamic Behaviour of Multiple-Anchor Connections in Cracked Concrete. PhD Thesis, The University of Texas, Austin, 1997.

(Zoetemeijer, 1974) Zoetemeijer, P. A design method for tension side of statically«-loaded bolted beam-to-column joints. *Heron*, 20(1), pp. 1-59, 1974.

*III. Behaviour of mixed steel-concrete structures: influence of the joint modelling and requirements to steel-to-concrete joints*





## III.1 Introduction

In steel and composite structures the behaviour of the joints may be relevant for the structural analysis, as prescribed in (EN 1993-1-8, 2005) and (EN 1992-1-1, 2004). Depending on the joint properties, in comparison to the members they connect, the structural response, distribution of internal forces and deformations, is significantly or slightly affected. Likewise, in mixed steel-concrete structures, besides the steel and/or the composite joints, the steel-to-concrete joints may influence the structural response. In this way, in order to complement the study of the steel-to-concrete joints presented in Part II, the approach is here extended beyond the joint level to the structural analysis incorporating the joint behaviour. Though, this is not a primary objective of the present thesis. Consequently, a general evaluation of the effect of the joint properties on the structural response was performed. In addition, the demands to the joints properties, to accomplish the structural functionality, were characterized within the range of the structural typologies analysed. With the aim of covering several typologies (load conditions and members dimensions), two types of building structures were subject of the present study: offices and car parks. In order to reduce the time of modelling and calculation, the performed analysis is limited to plane sub-structures extracted from the reference building structures. More precisely, three sub-structures were the target of study: two representing the office building type and one representing the car park building type. Several calculations including service limit state, ultimate limit state and accidental action were performed varying the joint properties. For the structural calculations the numerical tool (Abaqus, 2011) was used. From these analyses, requirements for the steel-to-concrete joints were obtained regarding the resistance, stiffness and rotation capacity. To conclude, a comparative analysis with the joint properties of the joint configuration studied in part II is performed.

## III.2 Background

### III.2.1 Structural analysis including the joint behaviour

The analysis of structures regarding the steel and composite joints modelling has been conventionally based on the concept of rigid (infinite rotational stiffness) or pinned (no rotational stiffness). However, it is well recognized that the real behaviour is often intermediate between these extreme situations (Jaspart, 2002). In these cases, the joints are designated as semi-rigid. In such joints, partial relative rotation between connected members is assumed, contrarily to the traditional concept of no or free rotation. Consequently, the behaviour of the joint has a non-negligible influence on the structural analysis [ (Jaspart, 1998); (Maquoi and Chabrolin, 1998)] affecting: distribution of internal forces and deformations. In terms of resistance, the influence of the joint properties is obvious, as the structural capacity can be limited if the joint is not fully capable of transmitting the internal forces, namely the bending moments. In such cases, the joint rotation capacity also becomes critical, defining the type of failure and the possibility to redistribute the internal forces. Thus, joints are keys parts of the structure, playing an important role in the behaviour of the structure. In what regards to the reinforced concrete joints, the structural analysis remains in the classical concept of rigid or pinned joints (EN 1992-1-1, 2004). This is understandable due to the nature of the joints. In what concerns the steel-to-concrete joints, from Part II it is clear that the joint behaviour is similar to steel or composite joints. In this way, the effect of the steel-to-concrete joint on the structural behaviour should be considered as in steel or composite structures.

With the component method (Weynand *et al.*, 1996), the real behaviour of the steel/composite joints may be efficiently evaluated and characterized in terms of rotational stiffness, bending moment resistance and rotation capacity. Subsequently, their behaviour can be introduced in the structural analysis. This allows integrating the joint design with the structural design. Such type of analysis is recommended by the codes, (EN 1993-1-8, 2005) and (EN 1994-1-1, 2004) , and should follow the subsequent steps:

- 1) Characterization of the joint properties in terms of rotational stiffness, bending moment resistance and rotation capacity;
- 2) Classification of the joint;
- 3) Joint modelling on the structural model;
- 4) Joint idealization.

The first step has been the main subject of the thesis and deeply discussed in Part II. In what regards to steps 2 to 4, the approach used for steel and composite joints is hereafter used for the steel-to-concrete joints.

The joint classification consists in determining the boundaries for the conventional type of joint modelling regarding the stiffness (rigid or pinned), Fig. III.1-a), and the resistance (full-strength or pinned), Fig. III.1-b). The classification of the joint determines the type of joint modelling that should be adopted for the structural analysis. In Table III.1 are reproduced the expressions given in (EN 1993-1-8, 2005) to define these boundaries for

frames with effective bracing systems (reduction of 80% of the horizontal displacement). For stiffness classification, the stiffness of the connected beam is used to define the boundaries. In terms of resistance, the classification is set according to the minimum capacity of the connected members. In terms of rotation capacity, the information available is quite limited. In the code (EN 1993-1-8, 2005) only a qualitative classification is given which consists in the following: i) ductile joints (suitable for plastic analysis) - ductile components govern the behaviour of the joint; ii) semi-ductile joints - components with limited deformation capacity govern the joint response; iii) and brittle joints (do not allow redistribution of internal forces) - brittle components control the joint response. In the present case of the steel-to-concrete joints, it is assumed that the reinforced concrete (RC) wall is fully rigid and its resistance is higher than the connected beam.

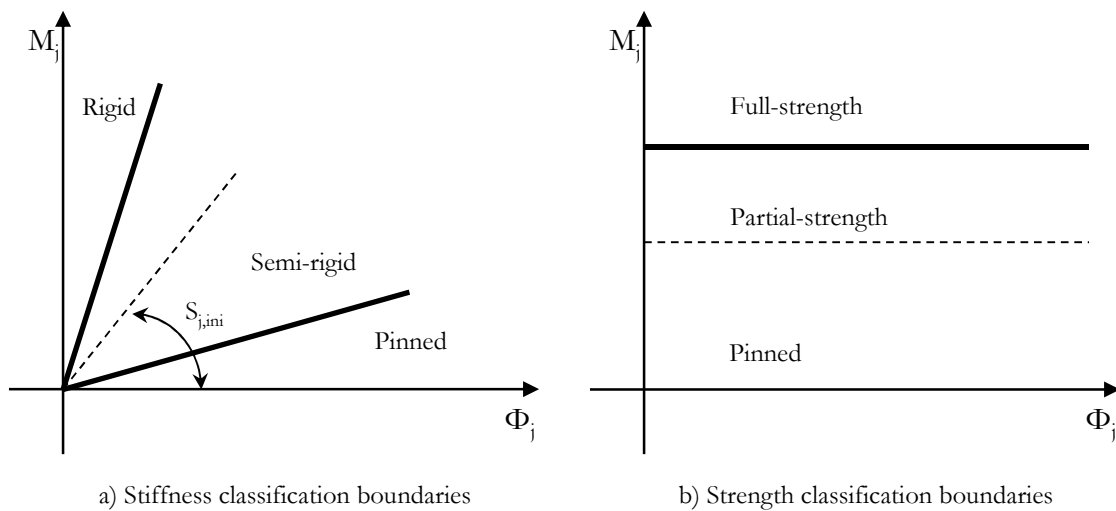


Fig. III.1: Boundaries for classification of the steel and composite joints

Table III.1: Criteria to define the boundaries for classification of beam-to-column steel and composite joints (EN 1993-1-8, 2005)

<b>Stiffness</b>	
Rigid/Semi-rigid	$8EI_b/L_b$
Semi-rigid/Pinned	$0,5EI_b/L_b$
<b>Resistance</b>	
Full-strength/Partial-strength	Top of column: $\text{Min}\{M_{c,pl,Rd}; M_{b,pl,Rd}\}$ Within column height: $\text{Min}\{2M_{c,pl,Rd}; M_{b,pl,Rd}\}$
Partial-strength/Pinned	25% of Full-strength/Partial-strength

In the structural analysis, according to the stiffness and strength classification, three types of joint modelling are possible, as listed in Table III.2. In the case of continuous joint, the full rotation continuity is guaranteed between the connected members. In the case of simple joint, all rotational continuity is prevented between the connected members. Otherwise, the joint is semi-continuous. In what concerns the physical representation of

the joint in the structural model, different approaches may be used, as illustrated in Fig. III.2. In Fig. III.2-a) the actual behaviour of the joint is modelled; L-springs ( $S_{r,l}$ ) represent the connecting zone, and the panel zone is represented by the S-springs ( $S_{r,s}$ ). The infinite rigid stubs assure that the flexibility of the joint will not be taken into consideration more than once. In Fig. III.2-b) is presented a model to be used in the software which does not support flexural springs. Stubs with adequate bending stiffness ( $EI$ ) and resistance ( $M$ ), maintaining the clear separation between bending and shear influences are used to replace rotational springs. Finally, in Fig. III.2-c) is represented the concentrated model. In this model, L-springs and S-springs are assembled into one single spring and displaced to the column axis ( $S_c$ ). The overall joint behaviour is then represented by a single rotational spring (two in the case of double sided joints). This simplified modelling solution is prescribed by (EN 1993-1-8, 2005). The simplifications adopted are compensated in the so-called joint transformation. The joint transformation takes into account the shear force acting in the column, and the combination of the shear panel and connections in the joint spring at the beam-to-column axis intersection point (Huber and Tschemmernegg, 1998).

Table III.2: Types of joint modelling

<b>Joint modelling</b>	<b>Joint Classification</b>
Continuous	Full-strength and Rigid
Semi-continuous	Full-strength and Semi-rigid Partial-strength and Rigid Partial-strength and Semi-rigid
Simple	Pinned and Pinned

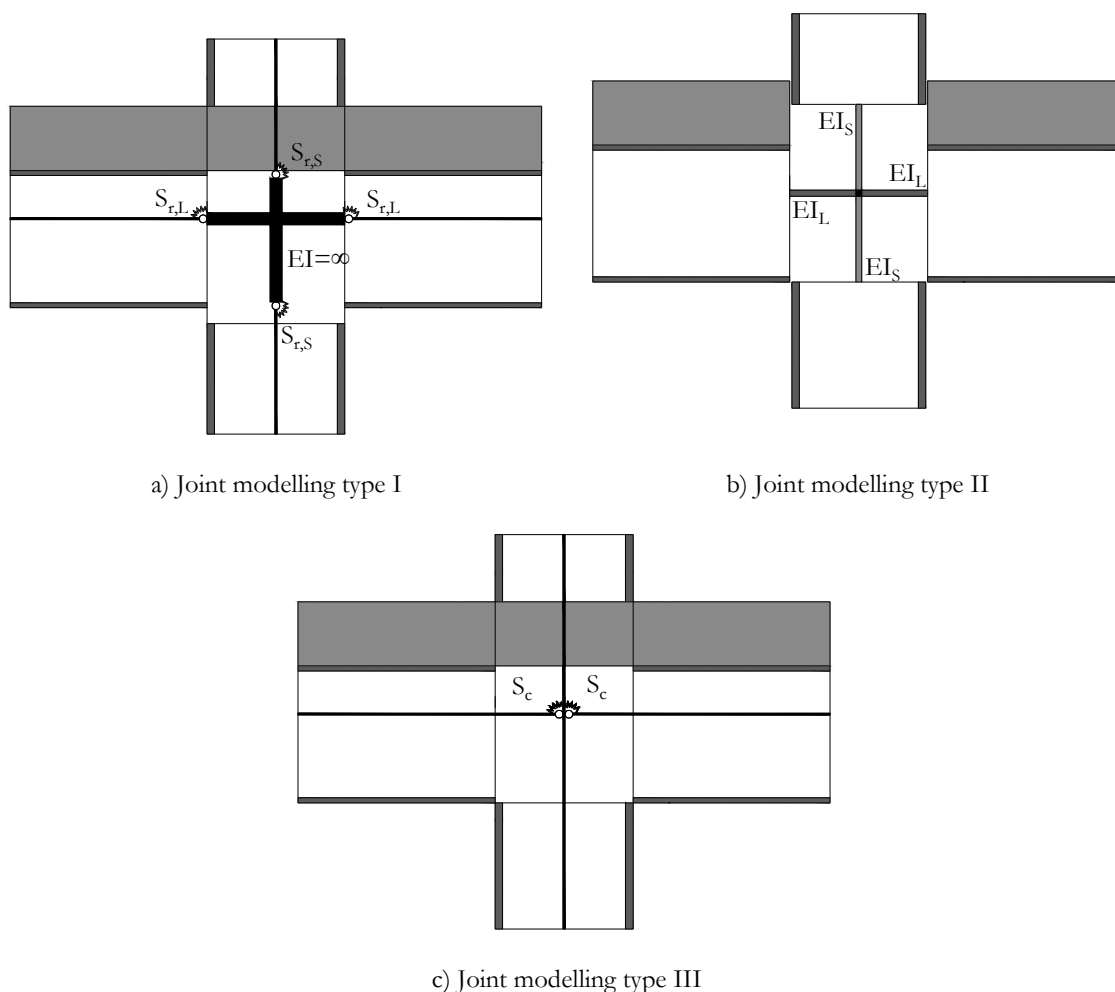


Fig. III.2: Physical representation of the joint in the structural model

The joint idealization consists in defining the type of flexural curve which will be attributed to the flexural spring representing the joint. The behaviour of the joints is typically nonlinear; however, its implementation in the flexural spring is not practical for everyday design. In this way, the behaviour of the joint may be simplified as schemed in Fig. III.3. The selection of the appropriate curve depends on the type of analysis to perform: elastic, elastic-plastic, rigid-plastic. Accordingly the following behaviours may be assumed: i) linear elastic (Fig. III.3-a) - only requires rotational stiffness; ii) bi-linear or tri-linear elastic-plastic (Fig. III.3-b) - requires rotational stiffness, resistance and deformation capacity; iii) rigid plastic (Fig. III.3-c) - requires resistance and rotation capacity. In the case of semi-rigid joint, the joint rotational stiffness to be consider depends on the expected load on the joint, thus the following is considered: i) the acting bending moment is smaller than  $2/3$  of the joint bending moment resistance ( $M_{j,Rd}$ ) and the joint initial rotational stiffness ( $S_{j,ini}$ ) may be used; ii) in the other cases, the joint secant rotational stiffness ( $S_j$ ) should be used. The latter is obtained dividing the joint initial stiffness ( $S_{j,ini}$ ) by the stiffness modification coefficient ( $\eta$ ). The codes (EN 1993-1-8, 2005) and (EN 1994-1-1, 2004) provide the stiffness modification coefficient to consider according to the type of connection.

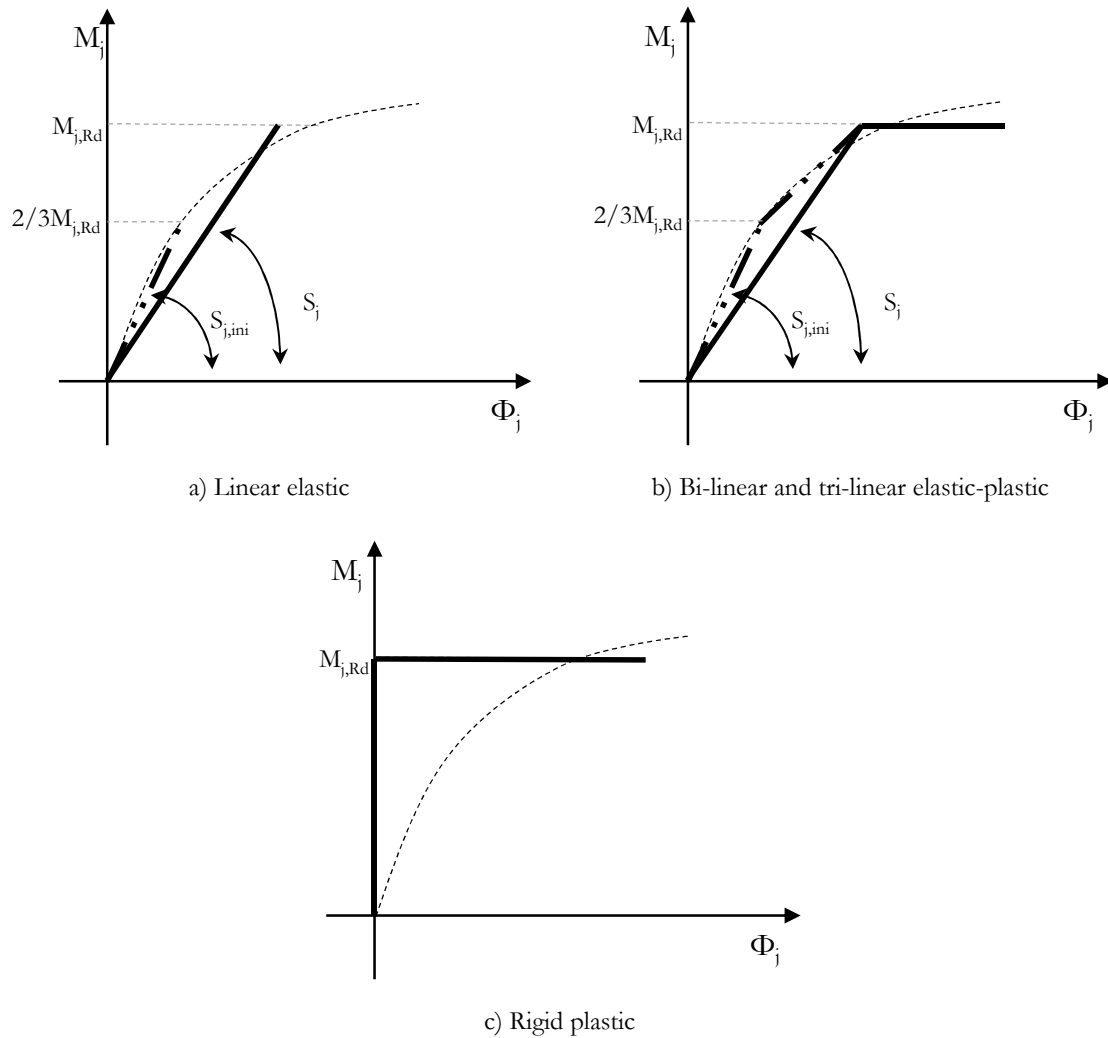


Fig. III.3: Different  $M-\Phi$  curves idealized for the joint behaviour

## III.2.2 Definition of case studies

### III.2.2.1 Description of the reference building structures

The building structures selected for the present study considered two types of occupancy: office and car park. For the first type, the building structure erected in Cardington and subject to fire tests (British Steel plc, 1999) was chosen. The building was designed to represent a typical multi-storey building for offices. For the car park building type, the structure used in a recent RFCS project regarding Robustness in car park structures subject to a localized fire (Demonceau *et al.*, 2012) was elected. The reason for the use of these two building structures consisted in the fact that the information on the characteristics was available to the author without requiring a design to be performed. Though the main characteristics of the reference building structures are used, modifications were performed whenever required to adapt the structures. Furthermore, as referred in §III.1, the performed calculations will only consider the analysis of plane sub-structures which were extracted from the complete building structures. As higher variation of the structural system may be found in the conception of office type, two sub-structures were selected to

represent this type of building occupancy while for the car park only one sub-structure was used.

The main characteristics and the adopted modifications of the referred building structures are summarized here below [(Kuhlmann *et al.*, 2012) and (Fang *et al.*, 2011)]. Detailed information on the sub-structures is given in a later section.

- The office building structure

In Table III.3 are summarized the main geometrical and mechanical properties of this type of building. In the same table are given the adopted modifications. In Fig. III.4 is illustrated the floor layout.

Table III.3: Summary of the main properties and performed modifications of the reference structure representing the office building type

Reference Structure	Modifications
<p>N° of floors and height: <math>1 \times 4,34m + 7 \times 4,14m</math></p> <p>N° of spans and length in longitudinal direction: <math>5 \times 9m</math></p> <p>N° of spans in transversal direction: <math>2 \times 6m + 1 \times 9m</math></p>	<p>No modifications</p>
<p>Columns: British steel profiles, grade S355, cross-section variation along height</p> <p>Beams: composite (British steel profiles + composite slab); grade S355 and grade S275; Lightweight concrete</p> <p>Bracing system: cross bracing flat steel</p>	<p>All British steel profiles were replaced by common European steel profiles with equivalent mechanical properties.</p> <p>Bracing systems were replaced by shear walls in order to introduce in the structural system, steel-to-concrete joints.</p>
<p>Beam-to-column joints: simple joints</p> <p>Column bases: continuous</p>	<p>The type of joint between horizontal members and vertical members was one of the key parameters of the study. The joint modelling was varied from continuous to simple.</p> <p>Column bases were assumed as simple joints.</p>

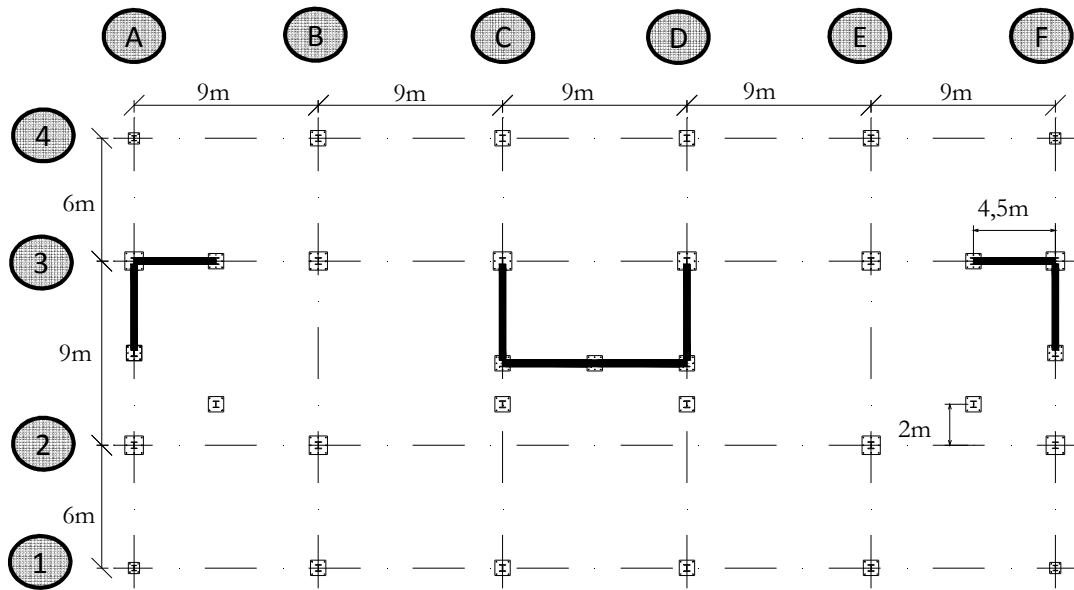


Fig. III.4: Floor layout of the reference structure representing the office building type

- The car park building structure

For this type of building, the complete information was not available, as this structure was idealized for the research project and not really constructed. It represents the standard configuration of a car park structure in Europe. In Table III.4 are summarized the main geometrical and mechanical properties of this type of building; only a few modifications were required. Fig. III.5 depicts the floor layout.

Table III.4: Summary of the main properties and performed modifications for the car park building type

Reference Structure	Modifications
<p>N° of floors and height: 8x3m</p> <p>N° of spans and length in longitudinal direction: 6x10m</p> <p>N° of spans in transversal direction: 2x16m</p>	No modifications
<p>Columns: steel profiles, grade grade S460, cross-section variation along height</p> <p>Beams: composite (steel profiles + composite slab); grade S355; normal weight concrete</p> <p>Bracing system: concrete core (assumed but not defined)</p>	Dimensions given to the concrete core
<p>Beam-to-column joints: semi-continuous joints</p> <p>Column bases: simple joints</p>	No modifications



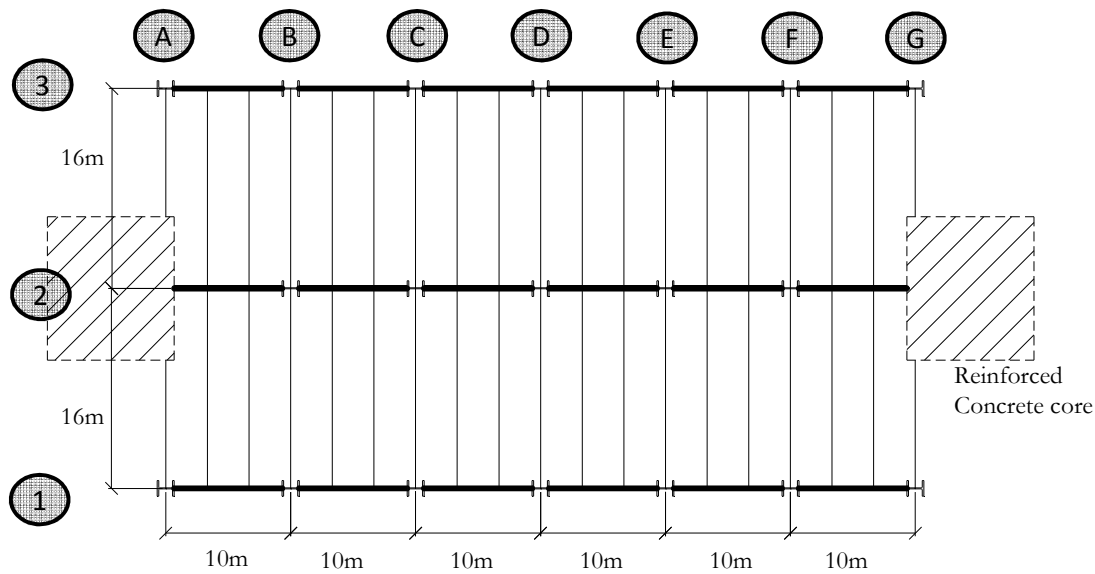


Fig. III.5: Structural layout of the car park building type

### III.2.2.2 Performed calculations

The structural calculations performed considered an elastic-plastic analysis. In all members and joints, except RC walls, plastic deformations were admissible. For sake of simplicity, the wall behaviour was always assumed elastic without limitation of capacity. However, it should be noted that the steel-to-concrete joint includes the part of the wall surrounding the joint, as discussed in Part II. In this way, partially, hypothetic localized failure of the wall was accounted. In terms of loading, three types of combinations were considered: i) Service Limit State; ii) Ultimate Limit State; iii) Accidental Combination considering the exceptional event of loss of a column. The accidental action was chosen, as it is becoming a subject of growing interest in research [(Stuttgart University, 2008), (Demonceau, 2008) and (Demonceau *et al.*, 2012)], and therefore a small extension to the steel-to-concrete joints was here accomplished.

In what concerns the calculations, the strategy consisted in performing several numerical simulations where the beam-to-column and beam-to-wall joint properties were varied within the boundaries for joint classification. In addition, two cases considered the extreme situations of all joints either continuous either simples. For the other cases, the steel joints and steel-to-concrete joints are semi-continuous. In all calculations, the column bases joints were assumed simples. In Table III.5 are listed the executed simulations identifying the joint properties considered in each case. Although the focus of the present is on the steel-to-concrete joints, the steel joints were also semi-continuous so that the structural system was consistent. The several cases presented in the Table III.5 considered the combination of different values of joint initial rotational stiffness and resistance capacity. In terms of rotation capacity, it was assumed that unlimited rotation capacity was available. A total of 10 cases were foreseen for each load combination.

Table III.5: Definition of the cases for each load combination and each sub-structure

Case	Initial Rotational Stiffness			Bending Moment Resistance		
	Steel-to-concrete joint	Steel joint	Col. bases	Steel-to-concrete joint	Steel joint	Col. bases
1	R	R	P	FS	FS	P
2	R	SR: 0,5 (R/SR+SR/P)	P	FS	FS	P
3	SR: 2/3 (R/SR+SR/P)	SR: 0,5 (R/SR+SR/P)	P	FS	FS	P
4	SR: 1/3 (R/SR+SR/P)	SR: 0,5 (R/SR+SR/P)	P	FS	FS	P
5	SR: 2/3 (R/SR+SR/P)	SR: 0,5 (R/SR+SR/P)	P	PS: 2/3 (FS/PS+PS/P)	PS: 2/3 (FS/PS+PS/P)	P
6	SR: 1/3 (R/SR+SR/P)	SR: 0,5 (R/SR+SR/P)	P	PS: 2/3 (FS/PS+PS/P)	PS: 2/3 (FS/PS+PS/P)	P
7	SR: 2/3 (R/SR+SR/P)	SR: 0,5 (R/SR+SR/P)	P	PS: 1/3 (FS/PS+PS/P)	PS: 1/3(FS/PS+PS/P)	P
8	SR: 1/3 (R/SR+SR/P)	SR: 0,5 (R/SR+SR/P)	P	PS: 1/3 (FS/PS+PS/P)	PS: 1/3 (FS/PS+PS/P)	P
9	P	SR: 0,5 (R/SR+SR/P)	P	P	PS: 0,5 (FS/PS+PS/P)	P
10	P	P	P	P	P	P

R-Rigid; SR-Semi-rigid; P-Pinned; FS-Full-strength; PS-Partial-strength

### III.2.2.3 Description of the structural models

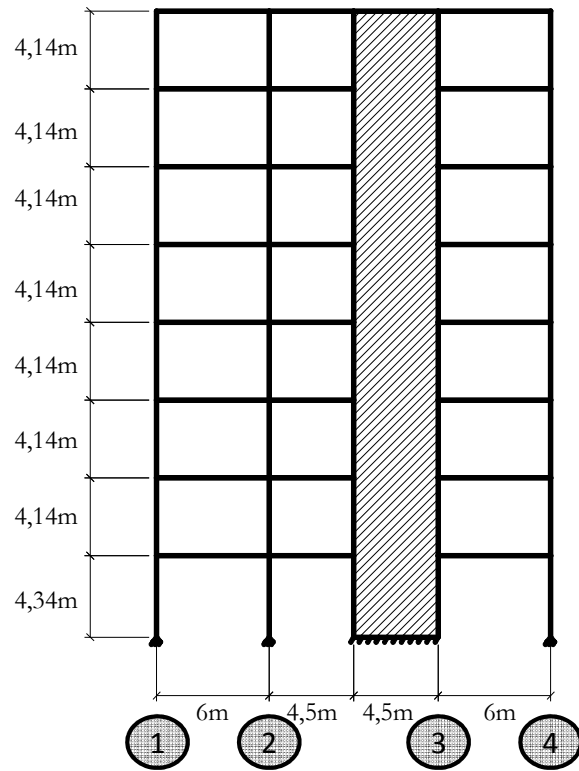
#### III.2.2.3.1 Geometric and mechanical properties of members

The three sub-structures selected for the structural calculations are illustrated in Fig. III.6. The members' geometric dimensions and material properties are given in Table III.6. For the bare steel cross-sections, the material behaviour was considered elastic-perfectly-plastic.

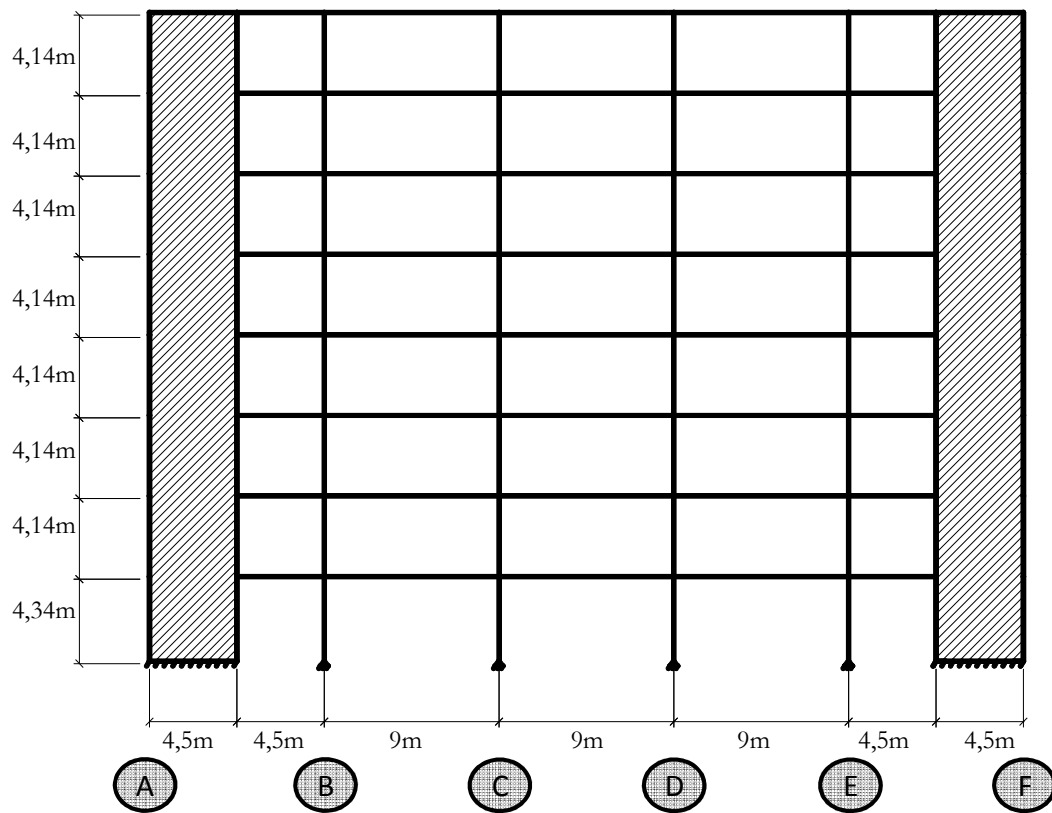
Table III.6: Sub-structures members' geometric and material properties

Sub-structure	Members	Geometric	Material
I	Columns: AL-1 and 4	Bottom to 2 <sup>nd</sup> floor: HEB320 2 <sup>nd</sup> floor to Top: HEB260	S355 S355
	AL-2	Bottom to 2 <sup>nd</sup> floor: HEB340 2 <sup>nd</sup> floor to Top: HEB320	S355 S355
	Beams*	IPE360+Composite slab ( $h_{slab}=130mm$ ) #Φ6//200mm	S355 LC35/38
	Walls	$t_w=300mm$ vertical reinforcement Φ20//30cm horizontal Φ10//30cm	C30/37 S500
II	Columns	Bottom to 2 <sup>nd</sup> floor: HEB 340 2 <sup>nd</sup> floor to Top: HEB 320	S355 S355
	Beams*	IPE360+Composite slab ( $h_{slab}=130mm$ ) #Φ6//200mm	S355 LC35/38
	Walls	$t_w=300mm$ vertical reinforcement Φ20//30cm horizontal Φ10//30cm	C30/37 S500
III	Columns	Bottom to 2 <sup>nd</sup> floor: HEB 550 2 <sup>nd</sup> floor to 4 <sup>th</sup> floor: HEB 400 4 <sup>th</sup> floor to 6 <sup>th</sup> floor: HEB 300 6 <sup>th</sup> floor to 8 <sup>th</sup> floor: HEB 220	S460 S460 S460 S460
	Beams*	IPE450+Composite slab ( $h_{slab}=120mm$ ) #Φ8//200mm	S355 C25/30
	Walls	$t_w=400mm$ # Φ20//20cm	C30/37 S500

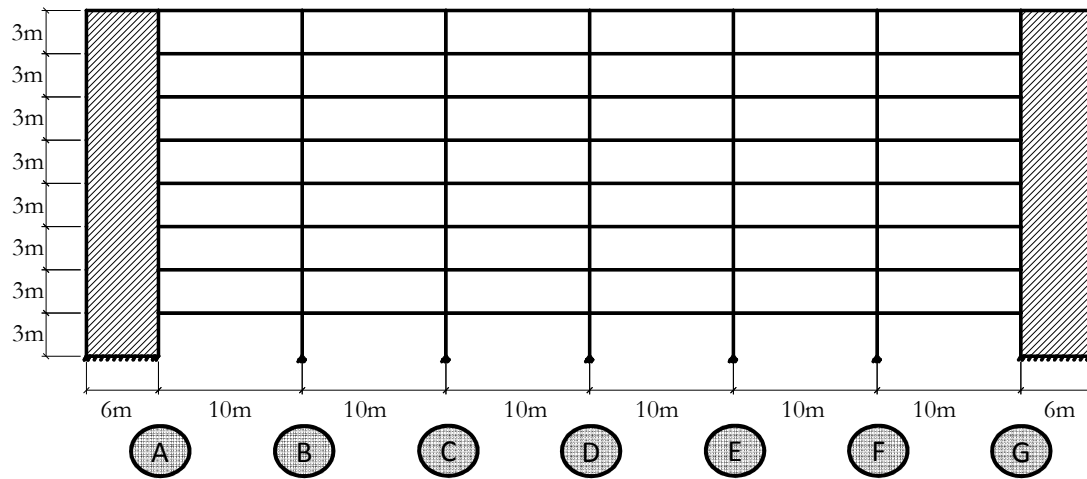
\*In all composite beams full interaction was assumed between composite slab and steel profile



a) Sub-structure I (Office building alignment A)



b) Sub-structure II (Office building alignment 3)



c) Sub-structure III (Car park building alignment 2)

Fig. III.6: Geometry of each sub-structure selected for calculation

In order to simplify the structural modelling, the composite beams cross-section was replaced by equivalent rectangular cross-sections (see Table III.7). Because of the different behaviour of the composite section under sagging and hogging bending moments, the equivalent beams cross-section (*EqCS*) varies within its length, as identified in Fig. III.7. In terms of material properties, equivalent yield strength was also determined so that the equivalent cross-section attained a maximum bending moment equal to the resistance of the real composite cross-section.

Table III.7: Properties of the equivalent cross-sections replacing the real composite cross-sections

Sub-structure I				
EqCS-1	EqCS-2	EqCS-3	EqCS-4	EqCS-5
$I=1,59 \times 10^8 \text{ mm}^4$	$I=3,885 \times 10^8 \text{ mm}^4$	$I=1,63 \times 10^8 \text{ mm}^4$	$I=5,4975 \times 10^8 \text{ mm}^4$	$I=1,58 \times 10^8 \text{ mm}^4$
$A=7034,56 \text{ mm}^2$	$A=14512,67 \text{ mm}^2$	$A=7087,57 \text{ mm}^2$	$A=12633,20 \text{ mm}^2$	$A=7024,62 \text{ mm}^2$
<i>Equivalent rectangular cross-section dimension</i>				
$h=520,08 \text{ mm}$	$h=566,78 \text{ mm}$	$h=525,23 \text{ mm}$	$h=580,67 \text{ mm}$	$h=519,09 \text{ mm}$
$b=13,53 \text{ mm}$	$b=25,61 \text{ mm}$	$b=13,49 \text{ mm}$	$b=21,76 \text{ mm}$	$b=13,53 \text{ mm}$
<i>Yield strength (<math>f_y</math>) of the equivalent rectangular cross-section to obtain the maximum bending moment (<math>M_{cb,max}</math>) of the composite beam cross-section</i>				
$M_{cb,max}$ $=351,41 \text{ kN.m}$	$M_{cb,max}$ $=605,00 \text{ kN.m}$	$M_{cb,max}$ $=358,94 \text{ kN.m}$	$M_{cb,max}$ $=565,00 \text{ kN.m}$	$M_{cb,max}$ $=349,98 \text{ kN.m}$
$f_y=576,30 \text{ N/mm}^2$	$f_y=441,31 \text{ N/mm}^2$	$f_y=578,52 \text{ N/mm}^2$	$f_y=462,12 \text{ N/mm}^2$	$f_y=575,88 \text{ N/mm}^2$

<b>Sub-structure II</b>				
EqCS-1	EqCS-2	EqCS-3	EqCS-4	EqCS-5
$I=1,14 \times 10^8 \text{ mm}^4$ $A=6012,32 \text{ mm}^2$	$I=2,74 \times 10^8 \text{ mm}^4$ $A=11207,20 \text{ mm}^2$	$I=1,20 \times 10^8 \text{ mm}^4$ $A=6101,78 \text{ mm}^2$	$I=3,38 \times 10^8 \text{ mm}^4$ $A=16431,90 \text{ mm}^2$	$I=1,23 \times 10^8 \text{ mm}^4$ $A=6141,54 \text{ mm}^2$
<i>Equivalent rectangular cross-section dimension</i>				
$h=476,37 \text{ mm}$ $b=12,62 \text{ mm}$	$h=541,42 \text{ mm}$ $b=20,70 \text{ mm}$	$h=486,39 \text{ mm}$ $b=12,54 \text{ mm}$	$h=496,74 \text{ mm}$ $b=33,08 \text{ mm}$	$h=490,57 \text{ mm}$ $b=12,52 \text{ mm}$
<i><math>f_y</math> of the equivalent rectangular cross-section to obtain the <math>M_{max}</math> of the composite cross-section</i>				
$M_{max}=274,86 \text{ kN.m}$ $f_y=575,81 \text{ N/mm}^2$	$M_{max}=470 \text{ kN.m}$ $f_y=464,75 \text{ N/mm}^2$	$M_{max}=286,85 \text{ kN.m}$ $f_y=579,90 \text{ N/mm}^2$	$M_{max}=631 \text{ kN.m}$ $f_y=463,83 \text{ N/mm}^2$	$M_{max}=292,05 \text{ kN.m}$ $f_y=581,62 \text{ N/mm}^2$
<b>Sub-structure III</b>				
EqCS-1	EqCS-2	EqCS-3		
$I=6,72 \times 10^8 \text{ mm}^4$ $A=13192,32 \text{ mm}^2$	$I=1,42 \times 10^9 \text{ mm}^4$ $A=27012,63 \text{ mm}^2$	$I=7,23 \times 10^8 \text{ mm}^4$ $A=13600,91 \text{ mm}^2$		
<i>Equivalent rectangular cross-section dimension</i>				
$h=781,66 \text{ mm}$ $b=16,88 \text{ mm}$	$h=794,22 \text{ mm}$ $b=34,01 \text{ mm}$	$h=798,44 \text{ mm}$ $b=17,00 \text{ mm}$		
<i><math>f_y</math> of the equivalent rectangular cross-section to obtain the <math>M_{max}</math> of the composite cross-section</i>				
$M_{max}=988,86 \text{ kN.m}$ $f_y=575,37 \text{ N/mm}^2$	$M_{max}=1338,00 \text{ kN.m}$ $f_y=374,20 \text{ N/mm}^2$	$M_{max}=1057,61 \text{ kN.m}$ $f_y=584,00 \text{ N/mm}^2$		

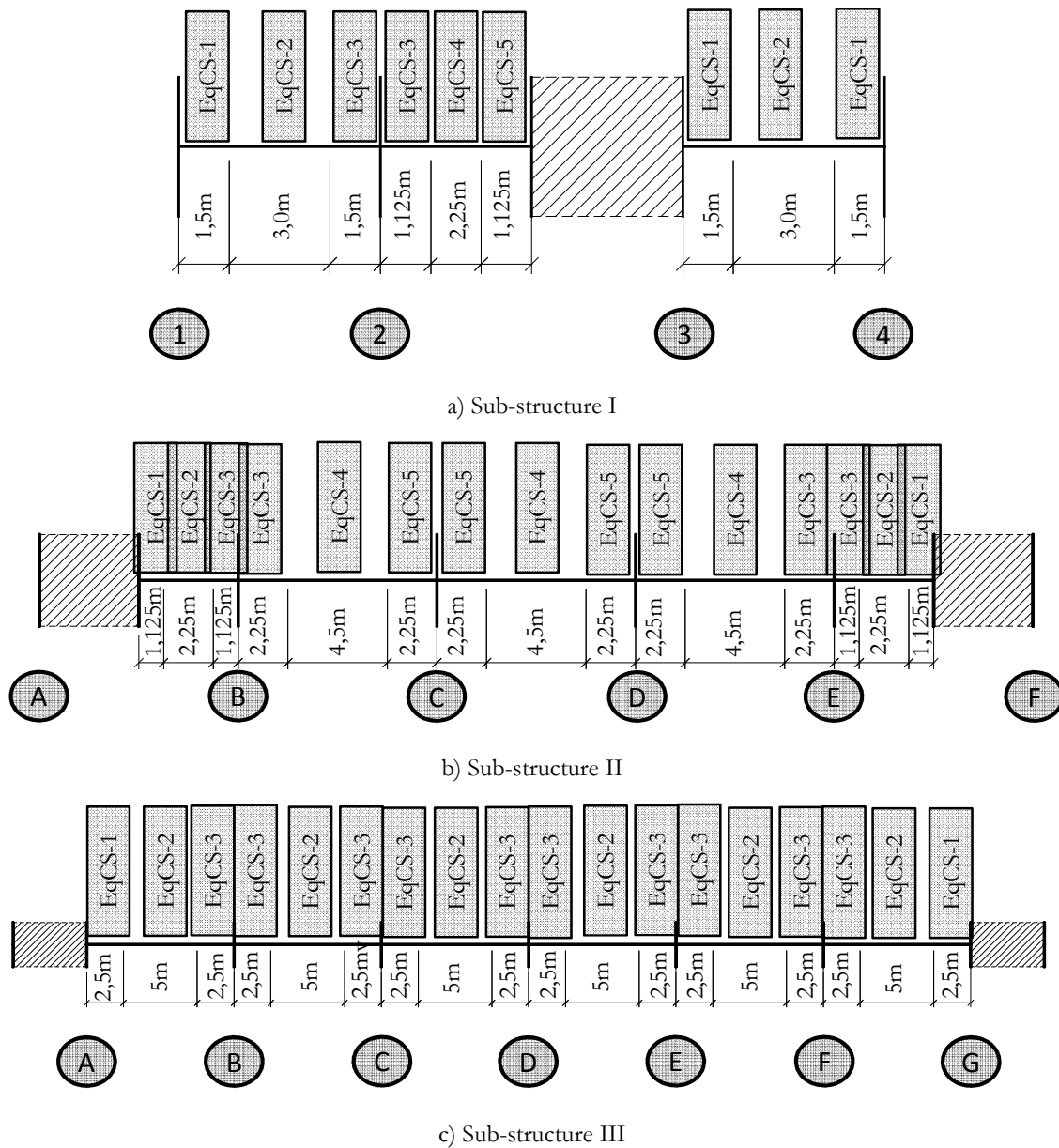


Fig. III.7: Identification of the equivalent cross-sections of the beams in each sub-structure

### III.2.2.3.2 Joint properties

The boundary values for classification of the joint in terms of rotational stiffness and resistance are listed in Table III.8 for the three sub-structures. The values were obtained applying the expressions given in Table III.1. The joints were included in the structural models using concentrated flexural springs. For the partial-strength joints, a tri-linear behaviour was assigned (Fig. III.8). The initial joint rotational stiffness is considered up to  $2/3$  of  $M_{j,Rdb}$  and then the joint rotation at  $M_{j,Rd}$  is determined using the secant joint rotational stiffness. The latter is determined using a stiffness modification coefficient ( $\eta$ ) equal to 2.

Table III.8: Quantification of the boundary values for classification of the joints in each sub-structure

	Joints	Rotational Stiffness		Bending Moment Resistance	
		R-SR [kN.m/rad]	SR-P [kN.m/rad]	FS-PS [kN.m]	PS-P [kN.m]
Sub-structure I	AL-1-right	108780,0	2782,5	351,4	87,9
	AL-2-left	108780,0	2782,5	358,9	89,7
	AL-2-right	205340,0	3710,0	358,9	89,7
	AL-3-left	205240,0	3710,0	345,0	87,5
	AL-3-right	108780,0	2782,5	351,4	85,9
	AL-4-left	108780,0	2782,5	351,4	87,9
Sub-structure II	AL-A-right	102293,3	2660,0	274,9	68,7
	AL-B-left	102293,3	2660,0	286,9	71,7
	AL-B-right	94640,0	2100,0	286,9	71,7
	AL-C-left	94640,0	2100,0	292,1	73,0
	to				
	AL-D-right	94640,0	2100,0	286,9	71,7
	AL-E-left	102293,3	2660,0	286,9	71,7
	AL-E-right	102293,3	2660,0	274,9	68,7
AL-F-left	238560,0	7056,0	988,9	247,2	
Sub-structure III	AL-B-left	238560,0	7056,0	As below	As below
	AL-B-right	238560,0	7591,5	b-6 <sup>th</sup> : 1058,1	b-6 <sup>th</sup> : 264,3
	to			6 <sup>th</sup> -T:380,4	6 <sup>th</sup> -T: 95,1
	AL-F-left	238560,0	7056,0	As above	As above
	AL-F-right	238560,0	7056,0	As above	As above
	AL-G-left	238560,0	7056,0	988,9	247,2

R-Rigid; SR-Semi-rigid; P-Pinned; FS-Full-strength; PS-Partial-strength

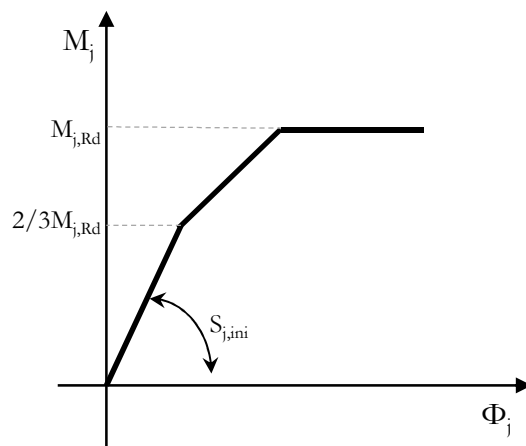


Fig. III.8: Partial strength joint mechanical behaviour



### III.2.2.3.3 Loading conditions

The loading considered in each sub-structure was determined for each load combination and varies with the structural conception and building occupancy. The loads and load combinations were defined according to: (EN 1990, 2002), (EN 1991-1-1, 2002) and (EN 1991-1-4, 2005). Note that for Sub-structure I and II, the wind action was also considered while for Sub-structure 3 no lateral action was assumed (this action was not quantified in (Demonceau *et al.*, 2012) and it was considered that the stiffness of the wall will “absorb” it).. In the office building structure, the slab works in the transverse direction, therefore the beams in the Sub-structure II are loaded with uniform distributed loads. For the other two sub-structures, the represented beams are the main beams so the loads are transmitted as concentrated loads, at the intersection of the secondary beams. In all cases the self-weight is considered.

Finally, in what concerns the Accidental Combination, the exceptional event of loss of a column is assumed. In the present study, as the focus is on the steel-to-concrete joints, the column loss was considered near the RC wall, occurring at the bottom floor.

### III.2.2.3.4 Sub-structures finite element models

The structural calculations were performed in the finite element software (Abaqus, 2011). A brief description of this numerical tool has been given in Part II. In Table III.9 are listed the types of elements used to reproduce each component of the structural system (members and joints): i) beam elements for beams and columns, ii) shell/plate elements for the RC walls, and iii) spring elements to connect the structural members, in the different degrees of freedom.

Table III.9: Types of finite elements attributed to each component (members and joints)

Structural Model Component	Type of finite element	Description
Beams and Columns	Beam element	2-node linear beam element B31
Shear Walls	Shell element	4-node shell element S4R (general-purpose) with reduce integration and hourglass control
Beam-to-column and Beam-to-Wall Joints	Spring element	Non-linear spring element with single degree of freedom

Amongst the different possibilities to include the joint behaviour described in §III.2.1, the concentrated joint modelling was selected, where a flexural spring was used to represent the connection at each side of the column. As the parametric study was performed varying the properties of this flexural spring, it was assumed that this spring was already integrating the deformation of the column web panel and was already affected by the transformation parameter ( $\beta$ ), so that an iterative calculation was avoid. As the main goal is to analyse the influence of the joint and to obtain some structural requirements to the steel-to-concrete joints, the joint springs are located at the axis of the columns, and the eccentricity

associated to the height of this member is neglected. . In what concerns the other degrees of freedom, namely axial and shear direction of the beam, translation springs are used to connect the members. In this way, in each connection, between structural members, three springs are used, one for each relevant degree of freedom.

The use of the above described types of elements was previously validated against academic problems (Simões da Silva *et al.*, 2010). Simultaneously, the calibration of the required mesh refinement was performed. Table III.10 summarizes the mesh refinement to consider in the different members of the structural models simulated and discussed in the next section.

Table III.10: Summary of the mesh refinement for each member of the structural model

Member	Number of elements or mesh size
Beams	40
Columns	10
Shear walls	400mmx400mm

The performed numerical calculations are 2 dimensional; therefore, no out-of-plane deformations occur. Both material and geometrical non-linearities are taken into account. Furthermore, the analysis neglects any possible in-plane buckling phenomena. The structural capacity is in this way only limited by the maximum resistance of the members and joints cross-sections. Finally, in what concerns to the simulation of the column loss, the procedure consisted in replacing the support of the relevant column by the reactions forces obtained in a previous calculation during the application of the real loading, and then to reduce them to zero.

## III.3 Analysis and discussion of results

### III.3.1 Calculation results

#### III.3.1.1 Load combination for Service Limit State (SLS)

The structure under service limit state has to guarantee the comfort of the users. If in terms of loading this limit state is less demanding, in terms of deformation requirements it is often the most limiting state, and therefore, design guiding. For this load condition, the analysis of the steel-to-concrete joint properties is performed using the two following parameters: beams deflection and structure lateral deformation. For the latter, only Sub-structures I and II are considered, as no horizontal load (namely wind load) was considered in the analysis of Sub-structure III.

In Fig. III.9 is illustrated how the beams deflection was considered. In Table III.11 are listed the maximum values obtained for each case, in a beam connected to a RC member (columns in grey) and in a beam only supported by steel columns. According (NP EN 1993-1-1, 2010) the limit value ( $\delta_{max} = L/300$ ) was calculated and is included in the table. It can be observed that in Sub-structures I and II, the values are distant from this limit, even if the beams deformation achieves 20 mm in the sub-structure II with simple joints (the value is still 33% below the limit)., The beam deformations in sub-structure III are closer to the limit value but still, this value is not exceeded for any of the cases. In Fig. III.10 are represented the beams deformations for the cases corresponding to the maximum and minimum deflections, for the beams implementing steel-to-concrete joints. These can be seen as the envelope of the beams deformation, as these cases consider the two extreme situations in what respects the joint properties: i) continuous (Rigid + Full Strength); and ii) simple (Pinned). Using the beam deformation mode corresponding to the maximum beam deflection, the deformation corresponding to the code limit was extrapolated and is also included in the figure. The figure illustrates the above observations, confirming Sub-structure III closer to the limit.

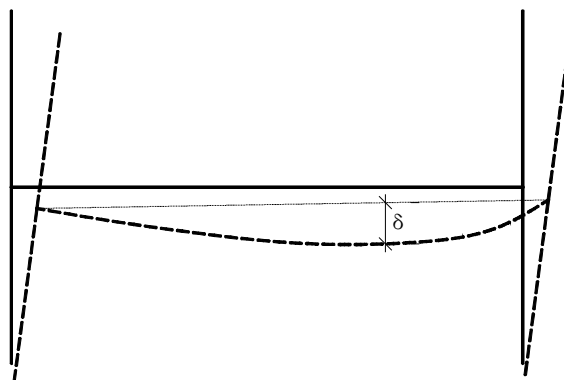


Fig. III.9: Representation of the considered beams deflection

Table III.11: Maximum beams deformation under service limit state

Case	Sub-structure I		Sub-structure II		Sub-structure III		Joint Properties	
	Beam 1-2	Beam 3-4	Beam C-D	Beam A-B	Beam C-D	Beam F-G		
1	2,62	3,00	5,58	0,33	21,79	7,69	R	FS
2	3,32	3,27	7,80	0,37	22,93	12,65	↓	↓
3	3,31	3,51	7,80	0,40	23,39	12,62		
4	3,31	3,67	7,80	0,43	23,75	12,60		
5	3,31	3,51	7,80	0,40	23,73	14,07		
6	3,31	3,67	7,80	0,43	24,11	14,06		
7	3,31	3,51	7,80	0,40	24,79	18,78		
8	3,31	3,67	7,80	0,43	25,21	18,78		
9	3,28	4,63	7,80	0,66	28,10	15,11	P	P
10	6,16	6,14	20,54	1,55	31,37	27,07		
$\delta_{max}$ [mm]	20	20	30	15	33,33	33,33		

R-Rigid; P-Pinned; FS-Full-strength

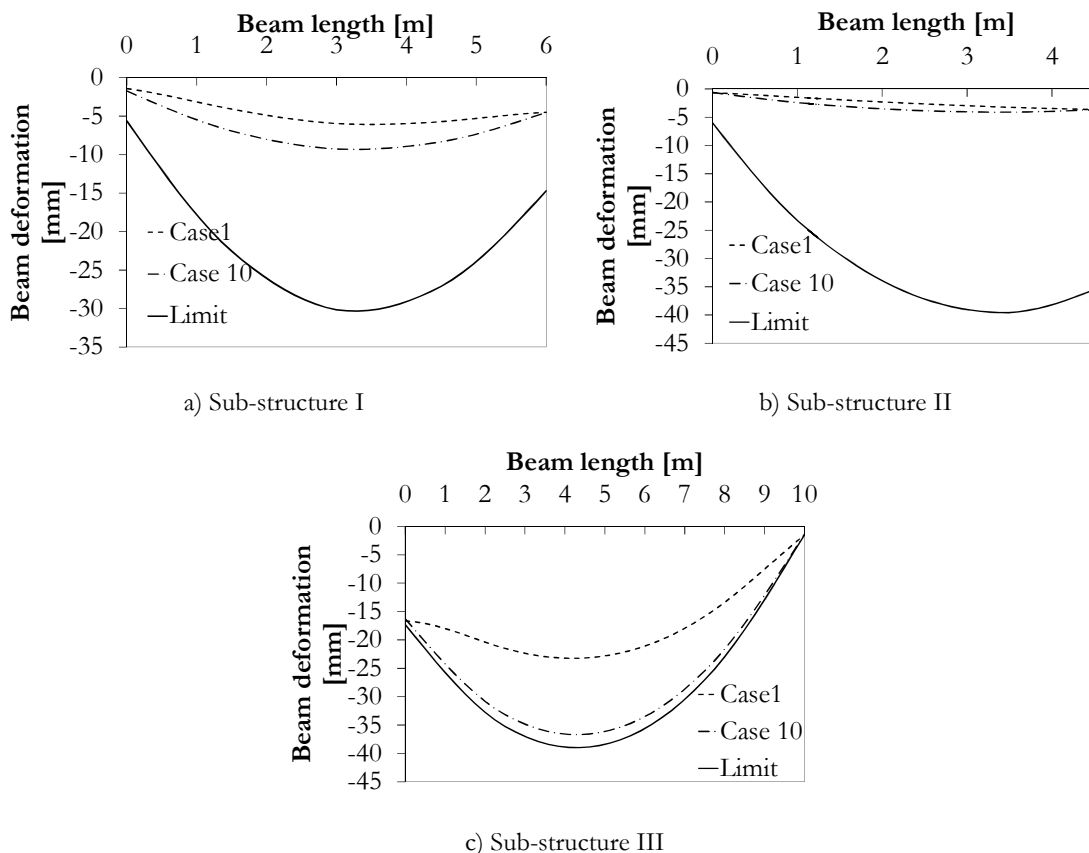


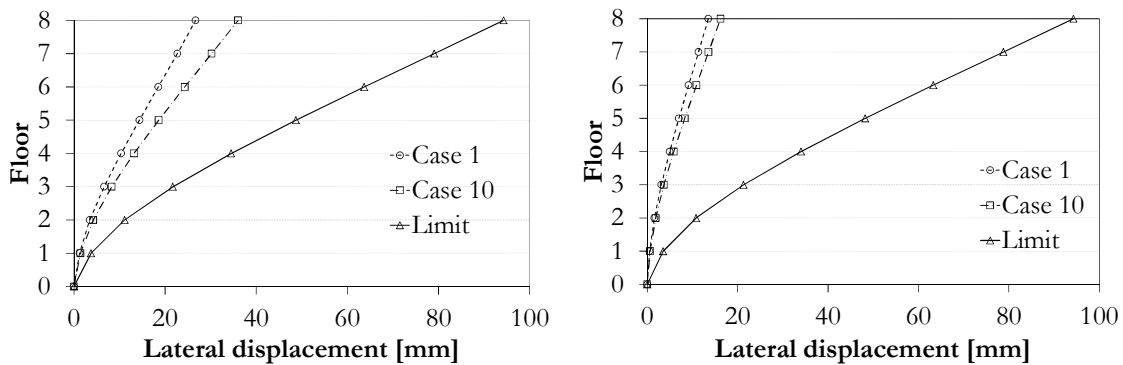
Fig. III.10: Beam deformations envelop and limit according to (NP EN 1993-1-1, 2010) (supported by a steel-to-concrete joint)

Besides the beams deformation, the lateral stiffness of the sub-structures is also affected by the joint properties. In Table III.12 are listed the maximum top floor displacements obtained for each case and for Sub-structures I and II. The design limit ( $d_{b,top,limit}$ ) according to (NP EN 1993-1-1, 2010) is also included. As for the beams deflections, it can be observed that the observed values are distant from the code limit. Note that as long as the joints are continuous or semi-continuous, the top floor displacement suffers small variations. This is due to the dominant contribution of the RC wall to the lateral stiffness of the sub-structures. In Fig. III.11 are represented the sub-structures lateral displacement envelopes and the code limit. In Sub-structure II, because two RC walls contribute to the lateral stiffness of the sub-structure, the variation between minimum and maximum is quite reduced.

Table III.12: Top floor lateral displacement for Sub-structures I and II

Case	Sub-structure I	Sub-structure II	Joint Properties	
			R	FS
1	26,69	13,50	↓	↓
2	27,91	13,95		
3	28,29	14,09		
4	28,60	14,19		
5	28,29	14,09		
6	28,60	14,19		
7	28,29	14,09		
8	28,60	14,19		
9	31,43	14,81		
10	36,01	16,22		
$d_{b,top,limit}$ [mm]	94,29	94,29	P	P

R-Rigid; P-Pinned; FS-Full-strength

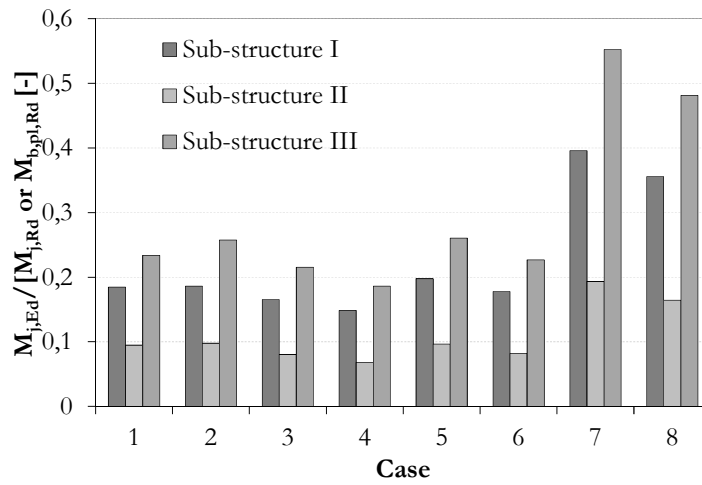


a) Sub-structure I

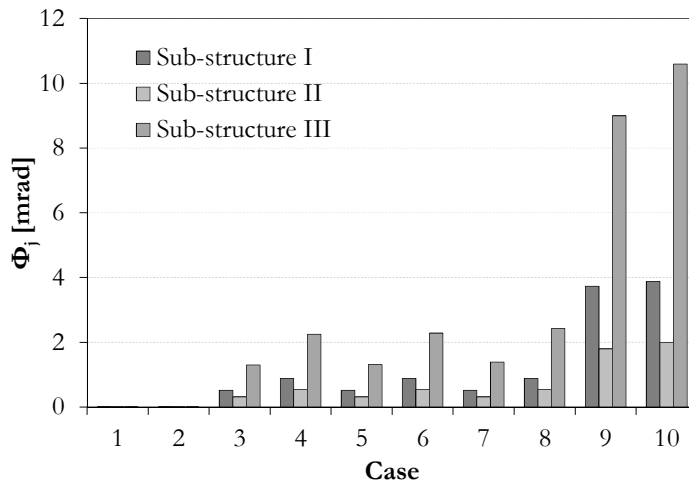
b) Sub-structure II

Fig. III.11: Sub-structures I and II lateral displacements envelopes

In what concerns the steel-to-concrete joints, under service limit state, the bending moment developed in the joints and the required joint rotation are represented in Fig. III.12. In Fig. III.12-a), the ratio between the bending moment developed in the joints and the joint or beam bending moment capacity is represented. For none of the cases, the joints under SLS attained the maximum bending moment resistance of the joint. As for the deformations, Sub-structure III is the most demanding to the joints. In case 7, almost 70% of the joint bending moment capacity is activated. Because the assumed joint resistance is lower, in case 7 and 8 the percentage of bending moment activated is higher. In Fig. III.12-b) is shown the maximum joint rotations observed for each sub-structure and for each case. For the cases where the joints are modelled as pinned, the joint rotation required is naturally higher, but never greater than  $11\text{ mrad}$ . In the other cases, the joint rotation is quite low, below  $3,2\text{ mrad}$ , which is expectable as not plastic deformation of the joints occurs.



a) Ratio between acting bending moment and bending moment capacity of joint or beam



b) Joint rotation

Fig. III.12: Joint structural demands under SLS

### III.3.1.2 Load combination for Ultimate Limit State (ULS)

At ULS, joints should perform so that the structural integrity is not lost. This requires to the joints either resistance either deformation capacity, allowing the redistribution of internal forces within the structure. In order to quantify such structural demands to the steel-to-concrete joints, calculations considering the load combinations of this limit state are performed. In Table III.13 are summarized the maximum loads obtained on these joints ( $M_j$ ,  $N_j$ ,  $V_j$ ). In all cases, hogging bending moment and the axial compression are reported. Though, it should be referred that axial tension is observed in bottom floors of the sub-structures; however, in average, the maximum value does not exceed 10kN. Fig. III.13 shows the ratio between acting bending moment and the bending moment capacity of the steel-to-concrete joints or of the beams, in the case of full strength joints. As expected, for this limit state the ratio increases in comparison to the service limit state though, in none of the cases the full capacity of joints is activated. The higher ratios are observed in Sub-structures I and III, for the cases with lower bending moment resistance. In Fig. III.14 are plotted the maximum joint rotations observed in the different calculations. The maximum required joint rotation is approximately  $20\text{mrad}$  for the case studies where the steel-to-concrete joints are modelled as simple joints.

Table III.13: Maximum loads in the steel-to-concrete joints at ULS

Joint Location	Sub-structure I			Sub-structure II			Sub-structure III			Joint Properties			
	AL-3-L	AL-3-R	AL-3-L	AL-F-L	AL-A-R	AL-F-L	AL-G-L	AL-A-R	AL-A-L				
Case	$M_j$ [kN.m]	$N_j$ [kN]	$V_j$ [kN]	$M_j$ [kN.m]	$N_j$ [kN]	$V_j$ [kN]	$M_j$ [kN.m]	$N_j$ [kN]	$V_j$ [kN]	↓	↓		
1	169,02	68,52	181,11	64,56	31,77	72,88	441,06	387,58	345,80			R	FS
2	170,00	61,66	183,25	65,67	33,40	73,85	539,46	406,36	371,42				
3	151,21	62,34	178,26	54,22	31,47	70,80	406,44	392,56	362,28				
4	136,23	62,83	174,30	46,16	30,07	68,65	350,42	382,13	355,60				
5	151,20	62,34	178,26	54,22	31,47	70,80	432,08	384,00	381,60				
6	136,25	62,83	174,30	46,16	30,07	68,65	376,06	372,48	376,12				
7	137,99	62,07	174,82	54,75	32,98	71,33	401,93	381,33	394,54				
8	121,74	62,35	170,51	46,62	31,58	69,17	344,744	371,89	388,89				
9	0	65,93	138,86	0	20,97	56,47	0	282,44	346,48				
10	0	43,28	133,95	0	51,71	59,39	0	346,66	370,90	P	P		

AL-Alignment; L – Left hand side; R- right hand side; R – Rigid; P – Pinned; FS – Full Strength

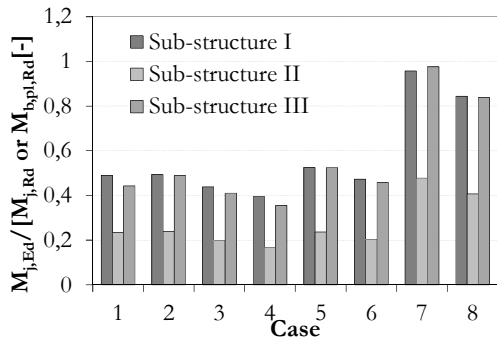


Fig. III.13: Ratio between acting bending moment and bending moment capacity of joints, and beam at ULS

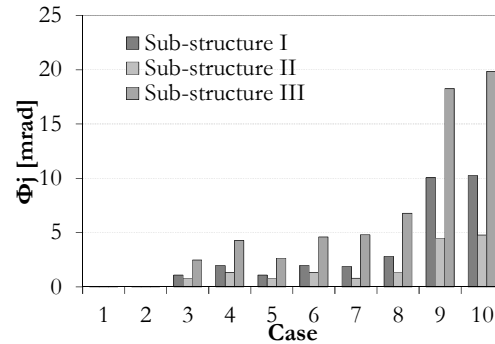


Fig. III.14: Maximum joint rotation at ULS

### III.3.1.3 Load combination for Accidental Action: exceptional event of loss of a column

The robustness requirements to the steel-to-concrete joints were determined by performing again the calculations of the 10 cases for each sub-structure, as before. The loading conditions considered the accidental combination defined according to (EN 1990, 2002) and the column loss. The simulation of the column loss was considered adjacent to a steel-to-concrete joint in order to obtain the most demanding situation. The calculation procedure is illustrated in Fig. III.15, using the Sub-structure I, and is divided into three steps:

- Step 1: The sub-structure is calculated with a loading resultant from the load combination for accidental actions, and the vertical reaction load  $R_v$  of the target column is obtained;
- Step 2: A new model is performed with the same loading conditions and where the support of the target column is replaced by a vertical load equal to the vertical reaction load  $R_v$  obtained in the preceding step;
- Step 3: Using the model defined in step 2, a subsequent step is added to the calculation where a vertical load is applied to the target column base having the opposite direction of the reaction load  $R_v$  applied in the previous step. The goal of this calculation is to obtain no reaction load on the bottom of the target column and therefore, have completed the simulation of the column loss.



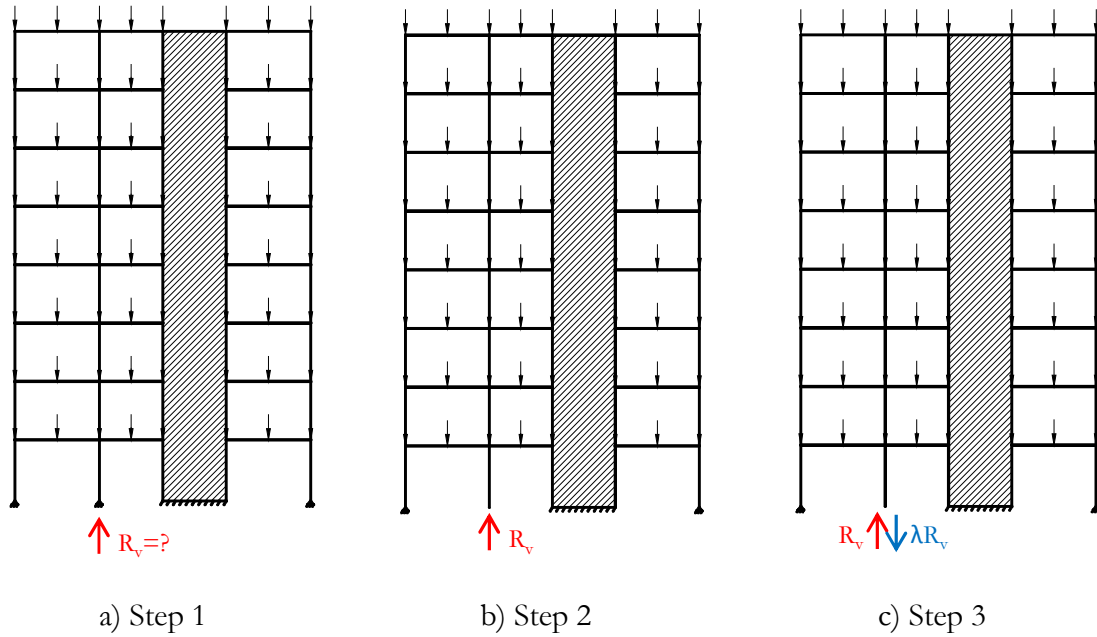


Fig. III.15: Procedure for simulation of the column loss

In such conditions, the structural demands to the steel-to-concrete joints increase in terms of bending moment and deformation capacity. Because of the column loss, in the directly affected part of the structure, plastic hinges may form in the joints or in the beams, depending on the weakest (Fig. III.16). Subsequently, a significant increase of the vertical displacements of the failing column occurs due to the loss of the bending stiffness of the joints or of the beams. As the displacements increase, the second order effects become significant. As a consequence of these deformations, considerable tension forces develop in the bottom floor beams. Due to the magnitude of these tension loads, joints have now to perform under combined bending moment and tension load. This can be a limitation to the joint, as the joints may fail before the complete column loss, and consequently the sub-structure collapses. In that case, the structure is classified as not robust to the loss of the column. In the performed calculations, the joints have no limitations of deformation capacity or of load interactions. Thus, structural failure could only occur due to a beam or column failure. In Table III.14 are given the load factors  $\lambda$  for the three sub-structures and for all the 10 cases. Load factors equal to 1 mean that the column loss is supported; load factors smaller than 1 show that the collapse of the sub-structure was attained before the complete removal of the target column reaction. The target column to simulate the column loss for Sub-structures I, II and III, was column of alignment 2, B and B, respectively.

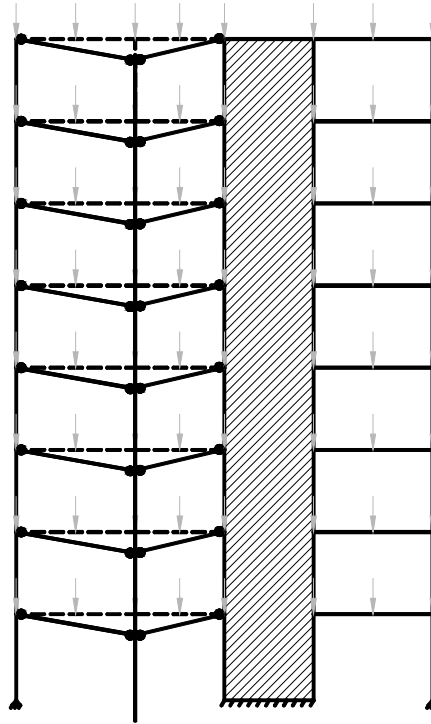


Fig. III.16: Beam plastic mechanism in the directly affected part of the sub-structure

The load factors presented in Table III.14 show that Sub-structures II and III are capable of losing the target column without losing the structural integrity for all the considered cases. In what respects to Sub-structure I, for four cases the complete removal of the column reaction was not possible. Fig. III.17 shows the evolution of the vertical displacement  $v$  at the top of the failing column versus the load factor  $\lambda$  for case 9. It can be noticed that the sub-structure becomes unstable before the column reaction has been completely removed.

Table III.14: Load factors for column loss

Case	Sub-structure I	Sub-structure II	Sub-structure III	Joint Properties	
1	1	1	1	R	FS
2	1	1	1	↓	↓
3	1	1	1		
4	1	1	1		
5	1	1	1		
6	1	1	1		
7	0,72	1	1		
8	0,72	1	1		
9	0,79	1	1	P	P
10	0,04	1	1		

R – Rigid; P – Pinned; FS – Full Strength

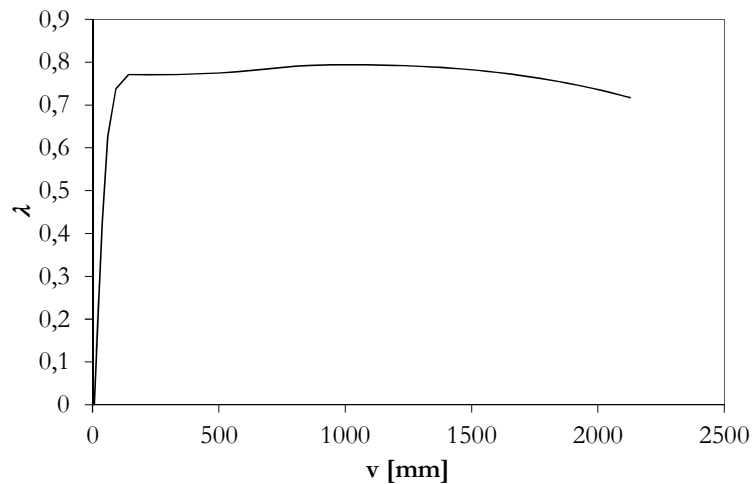


Fig. III.17: Load factor *versus* vertical displacement at the top of the failing column for Sub-structure I, case 9

In Fig. III.18 are presented the maximum ratios between acting and resistant bending moment of the steel-to-concrete joints or the beams (in the case of full-strength joints). As observed in the previous sections, Sub-structure III is the most demanding. For all cases including steel-to-concrete joints with bending moment resistance, the joints or the beam capacity is fully used. For the other sub-structures, only for cases 7 and 8, the loss of the column fully activates the steel-to-concrete joints adjacent to the column loss. As seen in Table III.14, for these two cases, Sub-structure I is not robust under the column loss.

As the maximum capacity of the joints is achieved, in order to redistribute the internal forces, joint rotation capacity is required. In Fig. III.19 are presented the maximum joint rotations required to the steel-to-concrete joints for each sub-structure and analysed case. Note that the results for Sub-structure I, cases 7 to 10, are not included because the sub-structure does not support the loss of the column. The maximum joint rotation required to redistribute the internal forces is naturally demanded to the cases where the joints are modelled without bending moment capacity. In such conditions, the maximum value is approximately  $128\text{mrad}$ . In what respects the cases with moment resisting joints, the maximum joint rotation required to the steel-to-concrete joints is approximately  $94\text{mrad}$ . Logically, this is obtained for the case with lower joint bending moment capacity. Fig. III.19 shows that whenever the joint resistance is fully activated, the joint rotation required is above  $40\text{mrad}$ . For cases 1 to 4, in Sub-structure III, the distribution of internal forces is obtained with plastic hinges in the beam instead of the joints; therefore the joint rotation is considerably reduced in comparison to the other cases.

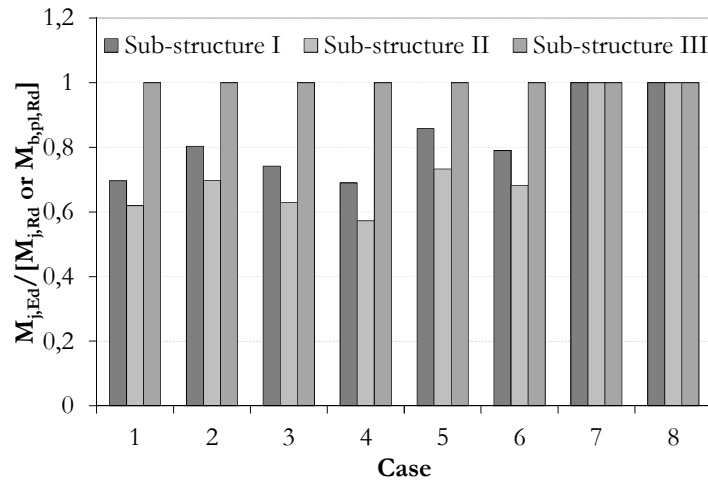


Fig. III.18: Ratio between acting bending moment and bending moment capacity of joints or beam for the exceptional event of loss of a column

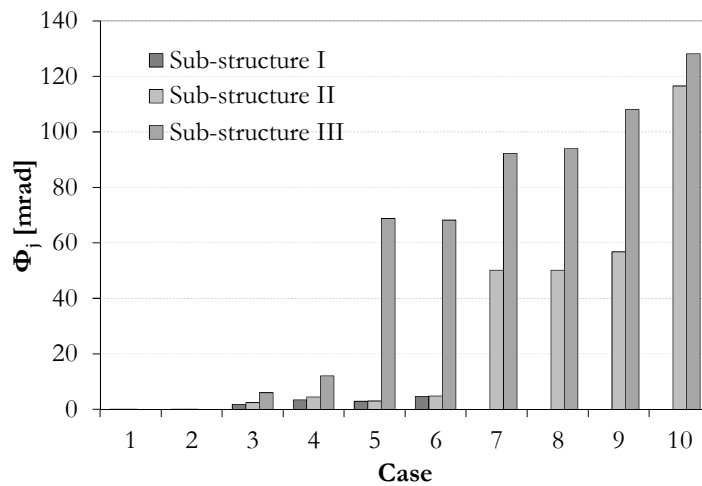


Fig. III.19: Maximum joint rotation for the exceptional event of loss of a column

In what concerns the axial loads, as referred the loss of the column leads to the development of high tension loads, especially at the bottom floor where the loss of the column was simulated. In Table III.15 are listed the maximum tension loads obtained in the calculations. In addition the bending moments acting simultaneously are included. The tension loads obtained confirm that this type of load only develops when the joint bending moment capacity is attained and therefore high rotations develop. In Fig. III.1 is shown the evolution of the axial load in a steel-to-concrete joint with load factor. It is clear that the sub-structure “recovers” load capacity when the so-called catenary actions develop.

Table III.15: Maximum tension loads developed on the steel-to-concrete joints for the exceptional event of loss of a column

Case	Sub-structure I		Sub-structure II		Sub-structure III		Joint Properties	
	M <sub>i</sub> [kN.m]	N <sub>i</sub> [kN.m]	M <sub>i</sub> [kN.m]	N <sub>i</sub> [kN.m]	M <sub>i</sub> [kN.m]	N <sub>i</sub> [kN.m]		
1	237,57	7,86	170,29	23,60	988,9	3429,44	R	FS
2	262,71	4,6	191,75	27,01	988,9	3740,81	↓	↓
3	243,75	4,26	172,81	28,97	988,9	3720,05		
4	227,43	3,97	157,40	30,77	988,9	3469,84		
5	239,71	4,38	167,85	30,17	824,05	4619,02		
6	222,42	4,52	15,28	31,76	824,05	4541,99		
7	145,83	235,88	114,53	449,54	412,03	5692,1		
8	145,83	268,77	114,53	449,38	412,03	5853,27		
9	0	273,75	0	415,27	0	5543,75	P	P
10	0	335,44	0	1891,75	0	5864,05		

R – Rigid; P – Pinned; FS – Full Strength

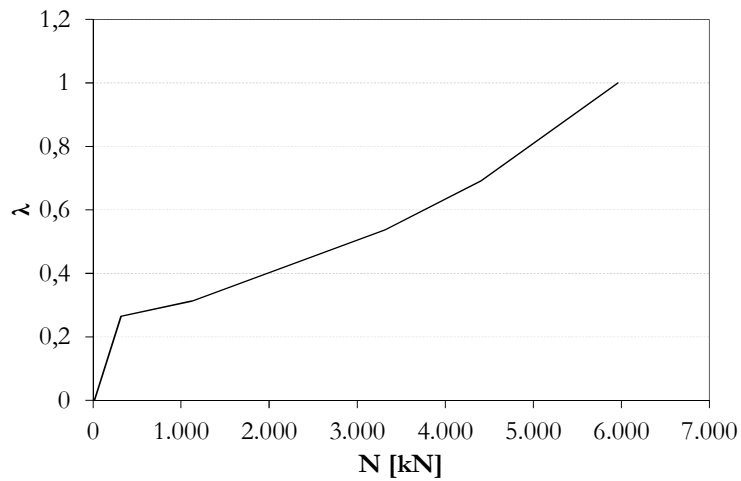


Fig. III.20: Load factor *versus* axial load on the steel-to-concrete joint for Sub-structure III, case 7

## III.4 Comparative analysis with the studied steel-to-concrete joints

### III.4.1 General Considerations

In the present chapter, a comparative analysis between the results of the structural calculations and the joint properties of the steel-to-concrete joints discussed in Part II is performed. In this way, an evaluation of the joint configurations regarding the structural demands is provided. Then, the joint configurations are commented foreseeing the improvement of performance for specific loading situations. In order to make simpler the analysis, the results of numerical calculations and experimental tests are summarized. In Table III.16 and Table III.17 is presented a summary of the results of the calculations presented in this part of the thesis. Note that the values in Table III.17 gather the maximum values for each analysis and for each type of building occupancy. In Table III.18 are summarized the experimental results of the simple and the semi-continuous joint solutions tested within the RFCS research project *InFaSo* (Kuhlmann *et al.*, 2012).

Table III.16: Summary of the joint classification: maximum and minimum values

Type of building structure	Strength [ $kN.m$ ]		Stiffness [ $kN.m/rad$ ]	
	FS/PS	PS/P	R/SR	SR/P
Office	359	69	205340	2100
Car park	1058	95	238560	7056

R-Rigid; SR-Semi-rigid; P-Pinned; FS-Full-strength; PS-Partial-strength

Table III.17: Summary of the results of the structural calculations: maximum values

Analysis		Type of joint			
		Moment Resisting		Pinned	
		$M_j$ [ $kN.m$ ]	$\Phi_j$ [ $mrad$ ]	$V_j$ [ $kN$ ]	$\Phi_j$ [ $mrad$ ]
SLS	Office	64,30	0,88	139,40	3,88
	Car Park	254,69	2,42	171,1	10,59
ULS	Office	170,00	2,87	183,25	10,24
	Car Park	539,46	6,78	371,88	19,84
Accidental: Exceptional event of loss of a column		Office: 262,71	Office: 50,14	Office: 247,61	Office: 116,60
		Car Park: 988,9	Car Park: 94,00	Car Park: 891,23	Car Park: 128,18
		$N_{j,tens}$ [ $kN$ ]		$N_{j,tens}$ [ $kN$ ]	
		Office: 449,54		Office: 1891,75	
		Car Park: 5853,27		Car Park: 5864,04	

Table III.18: Summary of the results from the experimental investigations within WP 4.1 and WP 4.3

"Envelope"	Type of joint				
	Moment resisting			Pinned	
	$M_j$ [ $kN.m$ ]	$S_j$ [ $kN.m/rad$ ]	$\Phi_j$ [ $mrad$ ]	$V_j$ [ $kN$ ]	$\Phi_j$ [ $mrad$ ]
Maximum	330,77	$\approx 37390,62$	65,35	822,80	163,50
Minimum	178,93	$\approx 10540,33$	33,46	201,00	6,87

### III.4.2 Comparison and discussion of results

A global comparison between numerical and experimental results exhibit that, for the office type of building and for normal design conditions (SLS and ULS), the joint configurations studied accomplish the structural demands. In what concerns Robustness requirements, the required joint rotation capacity and joint tension resistance may be a limitation for the structural capacity. Though, in some cases, giving the higher resistance of the joints, the sub-structures were able to redistribute loads because of the column loss without developing plastic hinges. In what concerns the car park building structure, the structural demands are higher and therefore, the studied joint configurations are limited. However, it must be taken into account that the dimensions of the joints in such structural systems would be of bigger size and therefore, the properties (especially resistance) would also be improved. Based on the values obtained at SLS and ULS and on the experimental results of the tested joint configurations, one can expect that the studied steel-to-concrete joints can also perform adequately. On the other hand, in the exceptional event of loss of a column, it appears to be difficult to avoid a premature failure of the steel-to-concrete joint, as the tension loads developed are considerable. Considerations concerning the improvement of the joint properties are provided in the next section. A deeper analysis of the results is performed hereafter for each joint configuration.

- Moment resisting joint

In what concerns the classification of the joint, only for the joint stiffness, the value defining the boundary between Rigid and Semi-rigid joint seems not possible to be obtained with the joint under study. The difference is significant, the ratio calculation/test is around 5,5. Such increase of stiffness seems difficult with this joint configuration. The main source of deformability is the longitudinal reinforcement, as the bottom part is already very rigid. The increase of stiffness can only be achieved in this component, though, as the simulation with two rows of reinforcement bars performed in Part II, the increase is not sufficient to attain such values. Thus, this joint should always present semi-rigid behaviour. In terms of resistance, the difference between the test resistance and the boundary for full-strength classification is smaller. The possible actions to improve the resistance are of greater number and with higher impact; if required, this classification is expected to be obtained.

Then, in terms of ULS and SLS, the joint properties are perfect within the structural demands. The accidental action (robustness – loss of a column) demonstrates the weaknesses of the joint configuration which is the resistance to tension actions. These properties have not been tested directly, but considering the joint configuration, it is unlikely that the joint, with the defined geometry, is able to develop such tension capacity. The tension capacity of the bottom part is very dependent of the capacity of the “nose” in the steel bracket; therefore, its resistance is expected to be limited. Finally, the maximum rotation required in this type of analysis exceeds the joint rotation capacities. Though, this maximum was obtained for the cases where the joint capacity is considerably low; therefore, this issue may be overcome increasing the joint resistance.

- Simple (pinned) joint

At service and ultimate limit states, this joint solution is capable to fulfil the structural demands for all types of structures. For the exceptional event of loss of a column, as in the case of the moment resisting joint configurations, the problem appears with tension load capacity that can be limited. In terms of rotation, the steel part of this joint, which was not the target of this investigation, should provide the required rotation in order to avoid the development of high bending moments. Though, it should be noticed that using hanger reinforcement in the tests allowed obtaining high rotation which from themselves are sufficient to redistribute the structural loads.

### III.4.3 Improvement of the joints performance

In order to overcome some of the “weaknesses” of the joint configurations identified in the previous section, several considerations regarding the improvement of the joints performance are here provided. These mainly focus on the moment resisting joint. For the pinned joint, the comparison of results demonstrated that no special action should be required. In fact, regarding the latter, only the following should be remarked: in the case of seismic action, the shear capacity of the joint should be achieved in both directions. Thus, when considering the inclusion of special reinforcement, it should be provided in both anchor rows, so that the joint presents equivalent resistances in both shear load directions (upwards and downwards). Thus, in Table III.19 are described the potential improvements for the joint configurations which have been tested within the *InFaSo* experimental programme (Kuhlmann *et al.*, 2012). The requirements are provided for the different joint components.



Table III.19: Proposals to improve the joint properties

Component	Requirements
Longitudinal reinforcement	<p>Higher deformation capacity is obtained increasing the distance of the first shear stud to the joint face;</p> <p>For ductility, the reinforcement used should be class C (according to (EN 1992-1-1, 2004))</p>
Concrete slab in compression	<p>The resistance of this component is clearly dependent on the concrete class used;</p> <p>According to (Stuttgart University, 2008), the concrete crushing is important to enable a ductile behaviour for sagging bending moment but the influence of the concrete compressive strength seems to have minor importance;</p> <p>(This component is relevant for the sagging bending moment capacity of the joint, not analysed in this thesis)</p>
Steel bracket	<p>The tension capacity of the joint is very dependent of this part of the joint; increasing the height and the thickness of the “nose” should increase the tension resistance of the bottom part of the joint</p>
Anchor Plate	<p>The anchor plate resistance, for tension load, should be increased with the use of anchorage reinforcement, as tested in (Kuhlmann <i>et al.</i>, 2012)</p>
Contact Plate	<p>Using wider and thicker contact plates increase the effective area (projection at 45°) for transmission of the compression forces from the beam bottom flange to RC wall</p>

### III.5 Concluding remarks

In the present part, the analysis of the steel-to-concrete joints has been extended to the structural analysis. These regarded not only the expected influence of the joint properties in the structural analysis but mainly the structural requirements to the steel-to-concrete joints. The implementation of mixed steel-reinforced concrete structural foresees mainly two type multi-storey buildings: offices and car parks. Thus, amongst the available information in the literature, (British Steel plc, 1999) and (Demonceau *et al.*, 2012), one structure of each type was selected as reference structures. Then, as a simplification, the analysis was limited to 2D sub-structures selected from the reference structures. A total of 3 sub-structures were used to perform several calculations: two from the office building and one from the car park. The structural models developed in finite element software (Abaqus, 2011) included the rotational behaviour of the joints. These were incorporated using flexural springs. For the other degrees of freedom, full continuity was assumed. Then, for each of the referred sub-structures, the joints rotational properties were varied from continuous to simple and several cases were defined. In order to define a variation of the joint properties, the joints were classified in terms of resistance and stiffness. In the absence of an approach for the classification of the steel-to-concrete joint, the approach in (EN 1993-1-8, 2005) was applied. This seems an appropriate procedure as the philosophy of the method should be similar. In addition to the joint properties variations, the analyses considered three load combinations: service limit state, ultimate limit state and accidental action (exceptional event of the loss of a column). The parametrical variations performed allowed to evaluate the joint requirements in terms of resistance, stiffness and deformation capacity. In addition, the impact on the structural response was analysed.

A comparison between numerical calculations and experimental investigations was performed. Subsequently, the joint configurations tested within the experimental programme of the research project *InFaSo* (Kuhlmann *et al.*, 2012) were comparatively evaluated. At service and ultimate limit state, the performed comparison outputs that for the simple joint, the configuration fulfils the structural requirements without requiring any relevant modification. The maximum resistance observed in the tests is considerably greater than structurally required. In what respects to the moment resisting joints, the quality of the joint depends on the type of building. For the office type, the joint properties are within the structural demands. For the car park type, improvements are required. However, the robustness analysis performed, demonstrate that capacity to develop tension axial load is also necessary. In this case, the joint capacities are limited. Some considerations, regarding the improvement of this joint configuration to this type of action were provided in a final section. However, their quantification was not included. Though, in what concerns Accidental Combination (exceptional event of loss of a column), it should bear in mind that the calculations performed assumed unlimited deformation capacity of the member and therefore the presented results are influenced by this simplification. Nevertheless, they represent an upper limit.

## References

- (Abaqus, 2011) Abaqus 6.11, Theory Manual and Users Manuals, Dassault Systèmes Simulia Corp., 2011.
- (British Steel plc, 1999) British Steel plc, Swinden Technology Centre (1999). The behaviour of multi-storey steel framed buildings in fire. European Joint Research Programme, South Yorkshire, United Kingdom, 1999.
- (Demonceau, 2008) Demonceau, J-F. Steel and composite building frames: sway response under conventional loading and development of membrane effects in beams further to an exceptional action. PhD Thesis, University of Liège, Liège, 2008.
- (Demonceau *et al.*, 2012) Demonceau, J-F, Huvelle, C, Comelieu, L, Hoang, L V, Jaspert, J-P, Fang, C, *et al.* Robustness of car parks against localised fire. European Commission, Grant Agreement Number RFSR-CT-2008-00036, Final Report, Brussels, 2012. (to be published)
- (EN 1990, 2002) European Committee for Standardization – CEN. EN 1990. Eurocode 0: Basis of structural design. Brussels, 2002.
- (EN 1991-1-1, 2002) European Committee for Standardization – CEN. EN 1991-1-1. Eurocode 1: Actions on structures – Part 1.1: General actions – Densities, self-weight, imposed load for buildings. Brussels, 2002.
- (EN 1991-1-4, 2005) European Committee for Standardization – CEN. EN 1991-1-4. Eurocode 1: Actions on structures – Part 1.4: General actions – Wind actions. Brussels, 2005.
- (EN 1992-1-1, 2004) European Committee for Standardization – CEN. EN 1992-1-1. Eurocode 2: Design of concrete structures. Part 1-1: General rules and rules for buildings. Brussels, 2004.
- (EN 1993-1-8, 2005) European Committee for Standardization – CEN. EN 1993-1-8. Eurocode 3: Design of steel structures. Part 1-8: Design of joints. Brussels, 2005.
- (EN 1992-1-1, 2004) European Committee for Standardization – CEN. EN 1994-1-1. Eurocode 4: Design of composite steel and concrete structures. Part 1-1: General rules and rules for buildings. Brussels, 2004.
- (Fang *et al.*, 2011) Fang, C, Izzuddin, B A, Elghazouli, A Y, Nethercot, D A. Robustness of steel-composite building structures subject to localised fire. *Fire Safety Journal*, 46, pp. 348-363, 2011.
- (Huber and Tschemmerneegg, 1998) Huber, G, Tschemmerneegg, F. Modeling of Beam-to-Column Joints: Test evaluation and practical application. *Journal of Constructional Steel Research*, 45(2), pp. 119-216, 1998.
- (Jaspert, 1991) Jaspert, J-P. Étude de la semi-rigidité des nœuds poutre-colonne et son influence sur la résistance des ossatures en acier. PhD Thesis (in French), University Liège, Liège, 1991.

(Jaspart and Vandegans, 1998) Jaspart, J-P. Recent advances in the field of steel joints - column bases and further configurations for beam-to-column joints and beam splices. Professorship Thesis, Department MSM, University of Liège, Belgium. 1997.

(Jaspart, 2002) Jaspart, J-P. Design of structural joints in building frames. *Prog. Struct. Engng Mater.*, 4, pp. 18–34, 2002.

(Kuhlmann *et al.*, 2012) Kuhlmann K, Hofman J, Wald F, da Silva L, Krimpmann M, Sauerborn N *et al.*, New market chances for steel structures by innovative fastening solutions BETWEEN STEEL AND CONCRETE (INFASO). Final report, Report EUR 25100 EN, European Commission, 2012.

(Maquoi and Chabrolin, 1998) Maquoi, R, Chabrolin, B. Frame Design Including Joint Behaviour. ECSC, Report 18563. Luxembourg. Office for Official Publications of the European Communities, 1998.

(NP EN 1993-1-1, 2010) Instituto Português da Qualidade – IPQ. Eurocódigo 3: Projecto de estruturas de aço. Parte 1-1: Regras gerais e regras para edifícios. Caparica, 2010.

(Simões da Silva *et al.*, 2010) Simões da Silva, L, Simões, R, Gervásio, H. Design of Steel Structures, Eurocode 3: Design of steel structures, Part 1-1 General rules and rules for buildings. ECCS Eurocode Design Manuals, 1<sup>st</sup> Edition, 2010.

(Stuttgart University, 2008) Stuttgart University. Robust structures by joint ductility. Final report of the RFCS project N° RFS-CR-04046, Stuttgart, 2008.

(Weynand *et al.*, 1996) Weynand, K., Jaspart, J.-P. Steenhuis, M. The Stiffness Model of Revised Annex J of Eurocode 3. in Bjorhovde R. Colson A. Zandoninni R. (eds.) *Connections in Steel Structures III*, Pergamon, Oxford and New York, pp. 441-452, 1996.

(Zoetemeijer, 1974) Zoetemeijer, P. A design method for tension side of statically loaded bolted beam-to-column joints. *Heron*, 20(1), pp. 1-59, 1974.

## *IV. General conclusions and perspectives*



## IV.1 Conclusions

In order to overcome the absence of standardized design models and practical solutions for steel-to-concrete joints; the RFCS research project *InFaSo* (Kuhlmann *et al.*, 2012) was launched in 2007. The project focussed on two main topics:

- Development of practical solutions for three types of joints: steel beam to reinforced concrete wall; composite beam to reinforced concrete wall; and column bases. Amongst the collected joint configurations, one of each type, considered of easy fabrication and erection, was selected to be studied.
- Development of design models, for each type of joint, able to characterize the joint behaviour.

The developments presented in this thesis are directly linked and grounded on the author's contribution to this research project. The main focus of the presented work has been the proposal of a design model for the joint configuration considering the connection between a composite beam and a reinforced concrete wall. Two main objectives have been achieved:

- Characterization of the behaviour of the joint components and complete joint in terms of force/moment-deformation/rotation curves;
- Proposal of analytical component based model to determine the response of the activated components and of the complete joint.

In addition to the above, and in order to provide comprehensive approach on steel-to-concrete joints, beam to wall configurations, the discussion included two other sub-topics: i) the behaviour of simple joint, for steel beam to reinforced concrete wall joint, which can be seen as a variant of the complete joint configuration for the composite beam to reinforced concrete wall joint; and ii) the structural analysis including the joint behaviour, where the structural demands to this type of joints have been analysed. These two sub-topics are already by themselves considerably ample to be the main subject. Consequently, their approach has been minimized. Furthermore, in what concerns the behaviour of the simple joint, detail analysis is being performed at University of Stuttgart.

To achieve the above objectives, numerical and analytical investigations were conducted and validated with the experimental tests on steel-to-concrete beam-to-wall joints performed within the RFCS research project *InFaSo* (Kuhlmann *et al.*, 2012). In Part II, the developments concerning the joint behaviour have been presented and in Part III, the structural calculations including the joint behaviour analysed. In both parts detail conclusions were already given. Accordingly, in the present chapter only the main accomplishments of the thesis are summarized.

- a) Characterization of the anchor plate connection under the loading conditions within the composite beam to reinforced concrete wall joint

The anchor plate with headed anchors is used at the bottom part of the composite beam to reinforced concrete wall joint to perform the connection between steel beam and wall. In

the absence of specific experimental tests on this part of the joint, numerical models were developed to study the behaviour of this connection under similar loading conditions as in the complete joint. Under such conditions, it was observed that the shear load transferred through this part of the joint had a residual effect and therefore it was neglected in the analysis. A previous validation of the numerical tool was performed using experimental tests on T-stub in compression (Sokol and Wald, 1997) and in tension (Bursi and Jaspart, 1997). The behaviour of the connection was expressed in terms of load to deformation curves. The load was applied at the level of upper anchor row and deformation measured also at this level, in the loading direction. The out of plane deformation of plate was affected by the presence of a bottom anchor row which increased the plate-concrete contact surface and consequently, the resistance of the connection when compared to a case without this anchor row. The behaviour of the connection, shape of the force-deformation curve, was governed by the concrete response presenting a non-linear response. Though, plastic deformations developed in the plate at the edges of the contact plate (loading zone). Understandably, the level/extend of these plastic deformations depend on the ratio between the concrete and steel strengths, and on the plate dimensions, especially the thickness. Furthermore, as the focus of the study was on the concrete part, no limitations to the plastic strains on the steel plate were considered. These numerical observations grounded the analytical models proposed.

- b) Analytical models to predict the response of the anchor plate subjected only to compression

For the anchor plate subjected only to compression two analytical models were proposed within the thesis. Given the similarities, both were based on the T-stub in compression approach prescribed by the (EN 1993-1-8, 2005) for column bases. The first model, based on the (Guisse *et al.*, 1996) model for column bases, is a sophisticated model which requires more effort in its application. However, the approximation obtained can provide an more optimized solution. The second model, consisting in a modification of the T-stub in compression model for column bases (EN 1993-1-8, 2005) where the effect of the anchor row on the non-loaded side is included, is more suitable for a daily design though, more conservative than the first. A parametric study validated analytical models for a range of geometrical and material properties within practical values for these type of joints.

- c) Numerical model developed to reproduce and characterize the simple joint between steel beam and reinforced concrete wall using an anchor plate connection

In the simple joint only subjected to shear load, the dimension of the eccentricity governs the response of the anchor plate. In the case of high eccentricity, failure is governed by the tension capacity of the upper row and lower shear resistance of the connection is obtained. In the case of low eccentricities, the shear capacity of the anchorage controls the ultimate capacity and higher shear resistance of the connection is observed. In both, the response of the connection, limited by the concrete components, is characterized by extensive cracking of the concrete increasing considerably the numerical difficulties to simulate the complete load-deformation response. Within this thesis, only the ascending range of the load-



deformation curve of the anchor plate connection subjected to shear load was accomplished. The complete reproduction of the load-deformation curve of the anchor plate under the referred load conditions demonstrated to be an extensive task, out of the scope of the thesis. Therefore, in order to characterize the anchor plate connection within the design range (initial load-deformation range up to maximum load), the referred numerical simulations were compared with experimental tests showing an satisfactory accuracy. From these numerical simulations, the joint load path was identified and characterized providing additional basis for the analytical developments.

- d) Analytical prediction of the response of the simple joint between a steel beam and reinforced concrete wall joint

The analytical model for anchor plate subjected only to shear load developed within the RFCS research project *InFaSo* (Kuhlmann *et al.*, 2012) has been described. The model is an extension of the component method to steel-to-concrete joints. Consequently, as in the experimental tests performed in the referred project, the focus of the application of the model was on the concrete part of the connection. Thus, “new” joint components were identified requiring a characterization in terms of force-deformation curve which was accomplished within the project. The application of the model to two of the test specimens demonstrated the potential of the model, predicting resistance and deformation of the connection with good approximation. The influence of several parameters, e.g. edge of the concrete member, were not included yet limiting the range of validation of the model. Though, the introduction of such parameters, performed at the component level, should not limit its accuracy.

- e) Numerical analysis of the anchor plate connection subjected to combined loading (compression + shear)

The anchor plate under combined compression and shear loading are the real load conditions within the semi-continuous joint presented in §II.1. The experimental tests on this joint configuration did not focus on the anchor plate under such load conditions. An extensive study of the problem was not in the main scope of the presented work. Thus, an simplified numerical approach was performed. Several numerical simulations were performed allowing the idealization of an interaction curve. It was clear that the presence of compression load on the anchor plate, also subjected to shear, increased the shear capacity of the connection. The first reason is because the friction component of the shear resistance increases. The second reason relies in the fact that the compression applied at the upper anchor row diminishes the effect of the tensions forces induced by the shear load applied with eccentricity. The proposed interaction curve lacks of experimental evidence thought it provides an insight of the behaviour of the anchor plate under such conditions.

- f) Numerical characterization of the behaviour of part of the wall contributing to the joint response between composite beam and reinforced concrete wall and identified as joint link

The experimental data produced in RFCS research project *InFaSo* (Kuhlmann *et al.*, 2012) did not focussed on the wall zone adjacent to the connection between the composite beam and the reinforced concrete wall. The design of the test specimens avoided the failure of this part considering the thickness of the wall and providing significant reinforcement in this region. Consequently, this part of the joint was neglected in the joint behaviour. In order to include this part of the joint, as new joint component, in the global behaviour of the joint, a numerical model regarding only the wall, under similar conditions of the complete joint, was developed. As result of this numerical study, the behaviour of the joint component was characterized in terms of force-deformation, as required by the component method. A small parametric study was then performed varying several geometrical properties, as wall thickness, bend radius of the reinforcement bars and height of the composite beam. This study allowed concluding that mainly the resistance of this component was affected by the geometrical variations while deformation pattern of this curves was unaffected.

- g) Analytical prediction of the joint link response in terms of force-deformation curve

The analytical model developed for characterization of the joint link component should be divided in two parts: resistance and deformation. For the resistance, a STM based model was derived and validated against the numerical calculations. The proposed model is simplified and consists in a single strut model connecting tension and compression zones. Given the dimension of the wall, no influence of edges, and the different dimensions of the loading zones, tension and compression, the concrete strut was identified to have a bottle shape. Consequently, the resistance of this strut is obtained from the nodes resistance. The model demonstrated to be suitable for the range of parametric variations performed in the numerical analysis of the component. In terms of deformation, according to the low influence of the geometrical variations and the complexity of the strain field within the strut, a mathematical expression was derived from the case where higher resistance was obtained. The analytical model for the joint link was in this way completed. From the comparison with numerical simulations, it was concluded that considering a single concrete strut to represent the joint link within the complete joint model is satisfactory and safe, if within the range of strut angle considered in this study ( $45^\circ \leq \theta \leq 70^\circ$ ).

- h) Validation of numerical model developed in ABAQUS (Abaqus, 2011) to predict the response of the composite beam to reinforced concrete wall joints tested within the RFCS research project *InFaSo* (Kuhlmann *et al.*, 2012)

The numerical model developed to predict the response of the composite beam to reinforcement wall joint was a laborious task involving many complex phenomena. The development of this model may be divided in two stages: i) calibration stage of the different joint components; and ii) validation of the complete model. In the first stage, the different joint components numerical models were calibrated through benchmarking. In

the second stage, the complete joint model was validated against the experimental tests performed in (Kuhlmann *et al.*, 2012). Given the accuracy of the approximation obtained for global and local phenomena, was concluded that the numerical model developed in (Abaqus, 2011) can be used with good confidence to simulate the response of the composite beam to reinforced concrete wall joints.

- i) Analytical prediction of the composite beam to reinforced concrete wall joint response

The analytical model for the complete joints is an extension of the component method. The model predicts the moment-rotation behaviour of a composite beam to reinforced concrete wall joint. The model may be divided in three group of components: i) tension components; ii) compression components; and iii) the joint link. According to the level of sophistication desired by the designer, two options were proposed: sophisticated and simplified. These options differentiate mainly in the model of two joint components: the anchor plate in compression and the longitudinal reinforcement bar in tension. With the first, an optimized solution may be obtained while the second provides safe and conservative approach. From the application of to the test specimens of the RFCS research project *InFaSo* (Kuhlmann *et al.*, 2012) and from the comparison of the corresponding experimental results was concluded that the model is adequate.

- j) Evaluation of the structural demands to the steel-to-concrete joints

The structural calculations considering different type of structures (office and car park), structural configurations and loading situations allowed having an insight on the structural demands for the steel-to-concrete joints. It was concluded that under normal design situations, SLS and ULS, the joint configurations developed within the RFCS research project *InFaSo* (Kuhlmann *et al.*, 2012) are deemed to accomplish the structural requirements. In the case of special loading situation, as the exceptional event of loss of a column, depending on the relative members/joint properties, the joints may not accomplished the structural demands. In these situations, it was observed the necessity of the joints to perform under combined bending and tension loads. In particular for the composite beam to reinforced concrete wall, limited tension capacity is expected, because of the joint detail at the bottom part, and therefore premature failure may be observed. Thus, for these load conditions, improvement of the joint or development of other joint configurations should be required.

## IV.2 Open questions and further research interests

The work presented in this thesis dealt with the behaviour of steel-to-concrete joints under monotonic loading focussing on a moment resisting solution to connect a composite beam to a reinforced concrete wall. In detail numerical and analytical modelling aspects were covered. In the course of this research, several topics were identified as requiring further examination. These issues include the following:

- a) The very limited number of experimental tests performed for the composite beam to a reinforced concrete wall joint is a clear lack on the presented study. A much more extensive experimental programme is required which could provide with better confidence mean values of the moment-rotation behaviour of the joint configuration. This should include: i) the execution of more than one test for the same type of specimen in order to eliminate mainly the uncertainty related to variations of the materials properties and the execution errors; ii) other geometries, as eccentric beam-to-wall joint; iii) other type of loading, as sagging bending moment and cyclic loading. Furthermore, the range of the experimental studies should cover situations where the failure of other parts of the joint, as the anchor plate in compression and the joint link may occur. This should characterize the type of response the joint present if other failure modes govern the joint behaviour. Also specific tests on these components (components tests) should be performed to further validate the analytical and numerical components models proposed within this thesis.
- b) The analysis of the steel-to-concrete joints presented in the thesis and within the RFCS research project *InFaSo* disregarded the influence of close edges. Though in most practical situations, the proximity of one or more edges should be frequent. This fact requires that the behaviour of the joints, in such conditions, is characterized and the proposed analytical models extended. The latter should be easily achieved; as the influence of the edges should be mainly integrated at the component level. This is already taken into account in the existing resistance models for the anchorage in concrete using different type of anchors. This influence should now be extended to the deformation models. For the other components, namely the longitudinal reinforcement bars and the joint link, the influence of the edges is also related to the eccentricity introduced in the joint configuration. The response of these components and of the joint in such conditions needs to be characterized.
- c) The joint configurations covered in this thesis, either simple or semi-continuous solution, were developed mainly for monotonic loading design situations. In what concerns the semi-continuous solution, the configuration foreseen was idealized for the general loading situations found in a non-seismic region, and therefore the behaviour presented is appropriate for hogging bending moment loading. Though, it is of interest a solution that can cover other design demands, as seismic regions require. Consequently, the behaviour of this joint should be analysed, first to

sagging bending moment and then to cyclic loading. The first type of loading, should already reveal the limitations of the joint configuration to transfer tension load through the bottom part. This study should reveal the need to improve/adapt the proposed joint configuration or to develop a new configuration for use in such demanding design situations.

- d) The influence of the structure load on the joint behaviour was disregarded in the study. This may have a favourable or unfavourable influence. For example: i) the compression load on the wall from the above floors should increase the tension resistance of the anchor plate to high eccentric shear loads; ii) the ordinary reinforcement of the wall should be needed for the wall loading and therefore cannot be accounted in the equilibrium of the joint link components (namely upper node). This influence should be assessed.
- e) The numerical simulation of the anchor plate subject to shear has been demonstrated to be complex and requiring extensive work, as the numerical simulation of the behaviour of the concrete in crack state is complex. In the particular case of (Abaqus, 2011), the use of “Explicit” algorithm, tool experimented within the course of the thesis but not exploited, may overcome these numerical difficulties. This is an important tool which may allow to further analysing the behaviour of the anchor plate connection. And as consequence, exploit the individual components, improving and extending the analytical models proposed within the RFCS research project *InFaSo* (Kuhlmann *et al.*, 2012).
- f) The analytical models for the anchor plate subjected to shear load demonstrated a good accuracy in reproducing the experimental tests. Though, these specimens were focussed on the concrete part. It was an important step to overcome the lack of “interaction” between the design of the concrete and steel composite parts. Though, a more general analysis is now required where the plate behaviour may also play a relevant role influencing the connection response, if plastic deformation occur at some components. Furthermore, and to generalize the developed model it is also interesting to introduce more rows of anchors (common situation) where distribution of loads has to be performed. This distribution is influenced by the type of component governing the joint behaviour, if it will be brittle (concrete) or ductile (steel), requiring an elastic or allowing an plastic analysis.
- g) The numerical and analytical models for the moment resisting joint between a composite beam and a reinforced concrete wall should be used in larger parametric studies covering a wider range of situations as: i) beam sizes; ii) % of longitudinal reinforcement and number of reinforcement layers; iii) materials; iv) type of loading; v) beam eccentricity in relation to the supporting member; vi) different type of failure modes governing the joint. This type of study allows characterizing the joint in terms of resistance, stiffness and deformation capacity for a larger range of geometrical and material properties. Together with a structural analysis, as presented in Part III of this thesis, the range of applications of such joints can be clearly identified.

- h) In mixed steel-concrete structural solutions, one of the problems engineers are faced is the combination of the different levels of tolerances used in the two type of materials achieving their maximum importance in the joints. Thus, the use of post-installed solutions for connection of the different parts between steel/composite beam and reinforced concrete wall may be seen as more efficient. For the joint configuration covered in the thesis, the following options may be analysed: i) use of rebar threaded connectors to connect the reinforcement bar in the slab of the composite beam to the extended part in the wall ; ii) use post-installed anchors in the anchor plate. These options should provide efficient solutions for the compatibility of tolerances and simplify the execution of the joint in the construction site. The influence of these different connection elements on the joint behaviour should be evaluated and integrated in the design models.

The work developed within this thesis aimed at contributing to perform the bridge between reinforced concrete and steel/composite design, at the “meeting point”, the joints. As seen, in the list of research interests presented above, this is an extensive subject. The approach started in the RFCS research project *InFaSo* and continued in this thesis, along with the extensive studies developed and in development at the Universities of Stuttgart and Prague, are the starting points on the process of unification of the methods for the simple and efficient design of steel-to-concrete joints, beyond the work developed in the past decades on column bases which remained always on the “steel side”.

## IV.3 Personal contributions

The main personal contributions to the presented investigations are listed here below:

- a) Calibration and validation of FE model developed in the software ABAQUS to reproduce the behaviour of the anchor plate in compression (§ II.3.1.2);
- b) Development of analytical models for anchor plate in compression, based on the extension of existing models for column bases, calibration and validation through comparison with numerical results (§ II.3.1.3 and § II 3.1.4);
- c) Development of numerical model to reproduce the anchor plate subjected only to shear load (§II.3.2.)
- d) Realization of series of numerical simulations considering the anchor plate subjected to combined shear and compression load allowing the derivation of an interaction curve (§II.3.3)
- e) Realisation of numerical study to characterize the behaviour of the reinforced concrete wall zone adjacent to the joint, denominated as joint link, complemented with small parametric study (§ II.4.2);
- f) Derivation of simplified STM model to reproduce behaviour of the joint link component in terms of resistance and adjustment of mathematical equation to evaluate the contribution of the component deformation (§ II.4.3)
- g) Contribution to the design of the composite beam to reinforced concrete wall joint specimens tested within the RFCS research project *InFaSo* at the University of Stuttgart and at the Technical University in Prague, and interpretation of the experimental results (§ II.2.3.3);
- h) Validation of FE software ABAQUS for the investigation of the behaviour of composite beam to reinforced concrete wall joint (§ II.5.2.2 and § II.5.2.3);
- i) Realisation of small sensitivity study to extend the parametric variations performed within the experimental tests on composite beam to reinforced concrete wall joints (§ II.5.2.4)
- j) Development and validation of component based model for composite beam to reinforced concrete wall joints (§ II.5.3);
- k) Numerical investigations on mixed steel-concrete structural system identifying structural demands for the steel-to-concrete joints (§ III.3);
- l) Comparative analysis between properties of the steel-to-concrete beam-to-wall joints covered within the RFCS research project and the joint structural demands, identifying the weak points of the joints and suggesting possible improvements for better performance (§ III.4.3).

Finally, here below are listed the author publications within the course of this thesis.

a) International journals (ISI)

Henriques, J, Raposo, J M, Simões da Silva, L, Costa Neves, L. Tensile resistance of steel reinforced anchorages: experimental evaluation. *ACI Structural Journal*, 110(2) March-April, pp. 329-250, 2013.

Henriques, J, Simões da Silva, L, Valent, I. Numerical modeling of composite beam to reinforced concrete wall joints Part I: Calibration of joint components. *Engineering Structures*, 52, pp. 747-761, 2013.

Henriques, J, Simões da Silva, L, Valent, I. Numerical modeling of composite beam to reinforced concrete wall joints Part II: Global behavior. *Engineering Structures* 52, pp. 734-746, 2013.

b) Other journals/magazines

Henriques, J, Ozbolt, A, Zizka, J, Kuhlmann, U, Simões da Silva, L, Wald, F. Behaviour of steel-to-concrete joints: moment resisting joint of a composite beam to reinforced concrete wall. *Steel construction: Design and Research* (Ed. Ernst & Sohn), 4(3), pp. 161-165, 2011.

Ozbolt, A, Kuhlmann, U, Henriques, J, Simões da Silva, L. Behaviour of steel-to-concrete joints. *Steel construction: Design and Research* (Ed. Ernst & Sohn), 3/2012, pp. 145-150, 2011.

Henriques, J, Simões da Silva, L, Valente, I. Design model for composite beam-to-reinforced concrete wall joints. *Steel construction: Design and Research* (Ed. Ernst & Sohn), 1/2013, pp. 19-26, 2013.

c) International and national conferences

Henriques, J, Simões da Silva, L, Valente, I. Numerical evaluation of mixed steel-concrete structures including joint behaviour. *Proceedings of the Twelfth International Conference on Civil, Structural and Environmental Engineering Computing*, B.H.V. Topping, L. F. Costa Neves, R. Barros (Editors), Civil-Comp Press, Stirlingshire, Scotland, Madeira, Portugal, paper 206, 1-4 Septmeber 2009.

Henriques, J, Simões da Silva, L, Valente, I. Ligações Aço-Betão: Modelação Numérica de Componentes Envolvendo Betão. *Actas do VII Congresso de Construção Metálica e Mista*, LNEC, Lisboa, pp. 501-510, 19 e 20 de Novembro, 2009.

Ozbolt, A, Berger, W, Henriques, J, Kuhlmann, U, Eligehausen, R, Simões da Silva, L. Behaviour of steel-to-concrete joints I: Pinned joint of a steel beam to a reinforced concrete wall. *Proceedings of the 6th European Conference on Steel and Composite Structures* (Eds.: L. Dunai, M. Iványi, K. Jármai, N. Kovács, L. Gergely Vigh), Budapest, Hungary, Volume A, pp. 471-476, 2011.

Henriques, J, Ozbolt, A, Žižka, J, Kuhlmann, U, Simões da Silva, L. Behaviour of steel-to-concrete joints II: Moment resisting joint of a composite beam to reinforced concrete wall. in L. Dunai, M. Iványi, K. Jármai, N. Kovács, L. Gergely Vigh (eds.), *Proceedings of the*



6th European Conference on Steel and Composite Structures, Budapest, Hungary, Volume A, pp. 477-482, 2011.

Henriques, J, Simões da Silva, L, Ozbolt, A, Kuhlmann, U. Innovative beam-to-wall joints in steel-concrete structural solutions. Actas do VIII Congresso de Construção Metálica e Mista, Centro Cultural Vila Flor, Guimarães, pp. II-211 a II-220, 24 e 25 de Novembro, 2011.

Henriques, J, Simões da Silva, L, Valente, I. Modelo numérico de ligação entre viga mista e parede de betão armado: Calibração e estudo paramétrico. Actas do VIII Congresso de Construção Metálica e Mista, Centro Cultural Vila Flor, Guimarães, pp. II-221 a II-234, 24 e 25 de Novembro, 2011.

Henriques, J, Simões da Silva, L, Valente, I. Design model for composite beam-to-reinforced concrete wall joints. VII International workshop on connections in steel structures, Timisoara, 30 May - 02 June, 2012.

Ozbolt, A, Henriques, J, Kuhlmann, Simões da Silva, L. Behaviour of steel-to-concrete joints. Nordic Steel Construction Conference, Oslo, Norway, pp. 561-570, September 5-7, 2012.

## References

- (Abaqus, 2011) Abaqus 6.11. Theory Manual & Users Manuals. Dassault Systèmes Simulia Corp., 2011.
- (Bursi and Jaspart, 1997) Bursi, O, Jaspart, J-P. Benchmarks for Finite Element Modelling of Bolted Steel Connections. *Journal of Constructional Steel Research*, 43(1-3), pp.17-42, 1997.
- (EN 1993-1-8, 2005) European Committee for Standardization – CEN. EN 1993-1-8. Eurocode 3: Design of steel structures. Part 1-8: Design of joints. Brussels, 2005.
- (Guisse *et al.*, 1996) Guisse, S, Vandegans, D, Jaspart, J-P. Application of the component method to column bases: Experimentation and development of a mechanical model for characterization. Research Centre of the Belgian Metalworking Industry, MT195, Liège, 1996.
- (Kuhlmann *et al.*, 2012) Kuhlmann K, Hofman J, Wald F, da Silva L, Krimpmann M, Sauerborn N *et al.*, New market chances for steel structures by innovative fastening solutions BETWEEN STEEL AND CONCRETE (INFASO). Final report, Report EUR 25100 EN, European Commission, 2012.
- (Sokol and Wald, 1997) Sokol Z, Wald F. Experiments with T-stubs in tension and compression. Research report, Czech Technical University in Prague, Prague, 1997.